WET GAS FLOW METERING TECHNIQUE USING A VENTURI WITH CONDUCTANCE SENSORS

Abdurazzaq Abdulla Musbah

A thesis submitted to the University of Huddersfield in partial fulfilment of the requirements for the degree of Doctor of Philosophy

The University of Huddersfield

April 2015

Copyright statement

i. The author of this thesis (including any appendices and/or schedules to this thesis) owns any copyright in it (the "Copyright") and s/he has given The University of Huddersfield the right to use such copyright for any administrative, promotional, educational and/or teaching purposes.

ii. Copies of this thesis, either in full or in extracts, may be made only in accordance with the regulations of the University Library. Details of these regulations may be obtained from the Librarian. This page must form part of any such copies made.

iii. The ownership of any patents, designs, trademarks and any and all other intellectual property rights except for the Copyright (the "Intellectual Property Rights") and any reproductions of copyright works, for example graphs and tables ("Reproductions"), which may be described in this thesis, may not be owned by the author and may be owned by third parties. Such Intellectual Property Rights and Reproductions cannot and must not be made available for use without the prior written permission of the owner(s) of the relevant Intellectual Property Rights and/or Reproductions

Abstract

Wet gas metering is becoming an increasingly important problem to the oil and gas industry. Much research has been done to measure the water and gas flow rates of two-phase flows using a Venturi meter. The Venturi meter is a favoured device for metering of unprocessed wet natural gas production flows. In this thesis, various combinations of techniques have been employed in annular gas-liquid two phase flows to measure the flow parameters (e.g. liquid film thickness, gas volume fraction and gas and water flow rates). One of the most useful techniques which was used and which has proven attractive for many previous multiphase flow applications is the electrical conductance technique used in conjunction with the Venturi.

In this thesis, research has been done on designing a novel wet gas flow metering technique, which combines a Venturi with conductance sensors at the inlet and throat to measure the gas and the water flow rates and gas mass flow rate in vertical annular (wet gas) flows. Two ring conductance sensors at the inlet of the Venturi were used to measure the film velocity by cross correlation, one of the inlet ring conductance sensors was used to measure the film thickness and the inlet gas volume fraction. A ring conductance sensor at the throat was used to measure the gas volume fraction at the Venturi throat. A digital level sensor was also used to measure the film thickness (and the gas volume fraction) at the inlet of the Venturi. The reason for measuring the film thickness, the film velocity, the gas volume fraction at the inlet and the throat of the Venturi was to determine the gas and water flow rate and the gas mass flow rate in annular wet gas two phase flow using a variety of mathematical models of Venturis.

This work included both static ‘bench’ and flow loop experiments. In the flow loop experiments, which were limited to air-water two-phase flow, the test section included a Venturi meter with a 50mm inlet diameter with conductance sensors at inlet and the throat. Reference measurements of the water and air were made with a turbine flow meter and a variable area flow meter respectively. A Honeywell DP cell sensor was used to measure the differential pressure between the inlet and the throat of the Venturi.

A NI USB 6009 data acquisition device was used to integrate the system measurements and to control the operation of the overall Venturi system. A program was created using Labview software to read the input signals from the throat conductance ring sensor; the inlet conductance ring sensors; the digital level sensor; the DP cell sensor; the variable area flow meter and the turbine meter. From these measurements the gas volume fraction at the Venturi inlet and the throat, the differential pressure between the inlet and the throat of the Venturi, the film thickness and the film velocity at the Venturi inlet were calculated and were used with appropriate mathematical models to calculate the gas volumetric rate; gas mass flow rate; and the water mass and volumetric flow rates. Reference values of the gas a water flow rates were also calculated from the turbine meter and variable area flow meter outputs.

Table of Contents

List of Tables

Table of Figures

Declaration

No portion of the work referred to in this thesis has been submitted in support of an application for another degree or qualification of this or any other university or other institute of learning.

Acknowledgments

First and foremost, all thanks and praises are due to God the Almighty for his blessing that made this work possible and to be completed on time.

Secondly,
Completion of this research work has only been made possible through the valuable contributions of a number of people over the past three years. The following list is by no means exhaustive.

I would like to thank my supervisor Professor Gary Lucas who has been a constant source of guidance, support and ideas throughout the duration of this PhD program at the University of Huddersfield.

I would like to thank the technicians at the University of Huddersfield Mr. Steve Goldstein and Mr. Philip Holdsworth, for their help in manufacturing and modification of the flow loop.

A big thank you to all those in the flow measurements research group for their many and interesting conversations

Many thanks to my family in Libya especially my father and my mother God's mercy upon here and my brothers and sisters, for their support and substantial encouragements from the time I was in my primary school till now. By no means least, my special thanks to my wife: Omima Abo Ababdalla and my princess daughter Alia, for their support, encouragement and patience over the last years. I promise you to make amends for the past years with much fun in the coming years.

Nomenclature

Acronyms

CVM	Conductance Venturi Meter
DLFLS	Digital Liquid Film Level Sensor
dp	Differential Pressure
GVF	Gas Volume Fraction
I/V	Current-to-Voltage
PCB	Printed Circuit Board

Symbols

A	Cross sectional area
A_{ste}	Steven constant; Equation (2.60)
A_t	Area at the contraction
(BF)	Blockage factor
B_{ste}	Steven constant; Equation (2.61)
C	Capacitance
C_{ste}	Steven constant; Equation (2.62)
C_{dg}	Gas discharge coefficient
C_{dw}	Water discharge coefficient
C_{dm}	Homogenous mixture discharge coefficient
D	Diameter
$\mathrm{D_{rod,i}}$	Diameter of the i^{th} nylon rod used in bench tests
$\mathrm{D_{inlet}}$	Venturi inlet diameter
$\mathrm{D_t}$	Venturi throat diameter
D_{ste}	Steven constant; Equation (2.63)
E	Entrainment fraction in annular flow
Fr	Froude number
fq	Rotation frequency in turbine flow meter

g	Acceleration of gravity
G_{mix}	Conductance of the mixture
h_c	Heights defined in Figure 3-2
h_i	Heights defined in Figure 3-2
h_{tt}	Heights defined in Figure 3-2
K	Flow coefficient
K_{Lin}	Corrective coefficient in the Lin correlation (Equation (2.44))
L	Distance between two sensors (Figure 2-7)
$\dot{m}$	Mass flow rate
n	de Leeuw number (Equation (2.53) and (2.54))
P	Static pressure
P_{at}	Atmospheric pressure
$\hat{P}$	Pressure ratio (Equation (3-26))
Q	Volume flow rate
$Q_{g,\tilde{\emptyset}}$	Correct gas flow rate using a homogenous model
$Q_{m,\tilde{\emptyset}}$	Correct mixture homogenous flow rate
$Q_{w,ref}$	Reference water volumetric flow rate
$Q_{w,c}$	Water droplet volumetric flow rate in the gas core
R	Resistance
γ	Specific gas constant
$R_{xy}(\tau)$	Cross-correlation function
S	Slip ratio
T	Time period
U	Velocity
U_f	Film velocity
$U_{f,xc}$	Liquid film velocity by cross-correlation technique
$\widehat{U}_{f,xc}$	The correct film velocity
Vol	Volume occupied by the phase
V	Dc output voltage
V_{1B}	Output voltage, Figure 4-17
$V_{e,\boldsymbol{B}}$	Input voltage from the switching mechanism circuit, (Figure (4-17))

V_{in}	Input voltage
V_{out}	Output voltage in a fluid conductance circuit, (Figure (5-17))
V_{off}	Dc offset.
V_{VAF}	Dc output voltage from Variable Area Flowmeter.
$V(\alpha_1)$	Dc output voltage from channel B conductance circuit
$\mathrm{V}^{\mathrm{t}}(\alpha_2)$	Dc output voltage from throat conductance circuit
V_{off}	Dc offset from the conductance circuit channel B
V_{off}^{t}	Offset voltage of the throat conductance circuit
$K(\alpha_1)$	Cell constant for conductance ring sensor B
$\overline{K}(\alpha_1)$	Simplifying cell constant for conductance ring sensor B
$\overline{K}^{t}(\alpha_2)$	Cell constant for the ring conductance sensor C
x	Mass flow quality
X_{mod}	Modified Lockhart-Martinelli parameter
ΔP	Differential pressure drop
ΔP_H	Magnitude of the hydrostatic head loss between the inlet and the throat of the CVM in annular (wet gas) flow
ΔP_{TP}	Two phase pressure drop

Greek symbols

α	Gas volume fraction
α_W	Water volume fraction
τ	Variable time delay in cross-correlation technique
τ_p	Time shift between the maximum similarities in the two measurement signals
ρ	Fluid density
$\emptyset$	Angle
γ	Specific heat ratio
β	Diameter ratio
ω	Excitation frequency
c_p	The specific heats at constant pressure
c_v	The specific heats at constant volume

$\bar{\alpha}$	Mean gas volume fraction (Equation (3.48))
δ	Water film thickness measured by ring sensor
$\tilde{\delta}$	Water film thickness measured by digital level sensor
$\delta_{\mathrm{i,sim}}$	Simulated liquid film thickness at the Venturi inlet
$\delta_{i,t,\mathrm{sim}}$	Simulated liquid film liquid film thickness at the Venturi throat
σ_w	Water conductivity measured by a proprietary conductivity meter
$\sigma_{w,m}$	Measured water conductivity using a conductance ring sensor with digital level sensor
$\sigma_{w,ref}$	Reference water conductivity for calibration experiments
α_{ns}	The no-slip gas volume fraction in homogenous model
$\alpha_{1,mean}$	The actual value of the gas volume fraction α_1
$\alpha_{1,i,sim}$	Gas volume fraction at the inlet of the Venturi in simulated annular flow
$\alpha_{2,i,sim}$	Gas volume fraction at the Venturi throat in simulated annular flow
$\tilde{\alpha}_2$	The correct value of the gas volume fraction $\alpha_{2,rs}$
ɣ	Scaling factor to give the actual value of the gas volume fraction at the Venturi inlet α_1
Ψ	Scaling factor to give the correct film velocity
$\widetilde{\Psi}$	Scaling factor taking entrainment into account
$\widetilde{\emptyset}$	Scaling factor to give a correct gas volume fraction at the throat

Subscripts

1	inlet of the Venturi
2	throat of the Venturi
Chisholm	Chisholm correlation
de Leeuw	de Leeuw correlation
dls	digital level sensor
f	liquid (water) film
g	gas phase
i,sim	simulating annular flow at the inlet of the Venturi
t,sim	simulating annular flow at the throat of the Venturi

hom	Homogenous
l	liquid phase
Lin	Lin correlation
m	mixture
Murdock	Murdock correlation
ns	No slip
pipe	Pipeline.
rod	nylon rod
ref	reference
rs	ring sensor
U_{gs}	gas superficial velocity
U_{ws}	Superficial water velocity
t	Thtoat
wc	water at the gas core

Chapter 1 Introduction

Introduction

The main objective of the study described in this thesis is the design of a novel wet gas flow metering technique which combines a Venturi with conductance sensors at the inlet and throat, and which is capable of measuring the gas and the water flow rates in annular two phase flow. Various combinations of techniques have been employed in annular wet gas flow to measure the gas and the water flow rates parameters (e.g. liquid film thickness, gas volume fraction and the phase flow rates) they have been used successfully.

1.1 What is Wet Gas?

The term wet gas has no official definition, however the companies in the field of natural gas exploration and production generally agree that the term denotes a relatively small amount of liquid in a production natural gas flow. In fact, the amount of liquid can vary from small to substantial amounts of water or liquid hydrocarbons. The amount and nature of the liquid, as well as the temperature and pressure of the flow stream will impact the selection and accuracy of the measurement system [1]. To date there has been no agreed definition of wet gas and several definitions have been proposed. Some researchers adopt the definition that wet gas is a flow with gas volume fraction greater than 95% [2]. Other authors set the gas volume fraction at greater than 90% [3]. For the purpose of this work the definition of wet gas flow is simply a *gas-liquid* two phase flow, or to be specific, an *air-water* two phase flow in the annular flow regime. The main flow regimes found in vertical liquid-gas flows are described in Section 2.2.

1.2 Wet Gas Metering

Wet gas metering is becoming increasingly important in natural gas exploration and thus for the Oil and Gas and Chemical industries. Wet gas flows are becoming more common for two reasons.

1:- The gas industry wants to increase production from off-shore platforms. Many natural gas producers are developing new fields that produce two phase flows of natural gas with sea water or natural gas condensate. These marginal fields are having their wet natural gas production flows combined with dry flows or other wet natural gas production flows upstream of the separator facilities. Thus wet gas metering is becoming increasingly important.

2:-Over time as dry natural gas wells age, changes in flow conditions including a reduction in line pressure may result in the heavier hydrocarbon gases condensing in flow-lines and transportation pipelines may have wet gas flow [4]. Because many gas wells world-wide are now coming to the later stages of their production life there has been an increased demand for wet gas metering.

Hence the applications of wet-gas metering have increased in recent years and wet natural gas metering is becoming an increasingly important technology to the operators of natural gas producing fields. However, there have been additional pressures for accurate wet gas metering, particularly in allocation, monitoring of production and the moves towards fiscal metering for newly developed marginal and large gas fields. .

Measurement of the gas and the liquid flow rates in wet gas flow is of critical importance and the Venturi meter is a favoured device for the metering of such flows. A number of other metering technologies are also currently available, including separation type meters, a combination of throttling devices, ultra-sonic meters and conventional single-phase flow meters. This chapter briefly describes wet gas metering of multiphase flows and defines such terms as multiphase flows, flow regimes, vertical flow regimes, and then introduces some wet gas measurement terms.

The Aims and Objectives of the current study are given and finally the structure of thesis is presented.

International trade in natural gas increased by 9% in 2004 (BP Review, 2005). Natural gas production increased by 2.4% in 2007, in 2009 the United States became the world's largest gas producer as measured by the International Energy Agency. The gas produced is mixed with liquid hydrocarbons and water that may be present in the same zone as the oil and gas. Also there will be condensed water in the wellbore and at the surface as flow pressure and temperature drop. Thus the techniques used for metering dry gas metering cannot be employed for all flows.

A number of wet gas metering technologies have been developed and some are currently available commercially, but most metering technologies are still being tested, analysed and validated. Venturi flow meters are widely used by the oil companies and much work has been carried out on wet gas metering using advanced Venturi flow meters which are simple and reliable, contain no moving parts, have a low and permanent pressure loss, low operating cost, accurate, repeatable and cost effective. These characteristics have led the author to choose the Venturi flow meter for this project.

1.3 Multiphase flow meters (MPFMs)

For the reasons given above the development, evaluation and use of multiphase flow meter systems has been a major focus for the Oil and Gas industry worldwide over the last two decades. So far, many alternative metering systems, including both established and novel technologies, have been developed but none of them can be referred to as generally applicable or universally accurate for the measurement of gas, water and oil flow rates in all of the different types of two or three-phase flows.

The first commercial multiphase flow meter appeared about twenty years ago, as a result of several multiphase metering research projects that took place in the early 1980's [5]. The multiphase flow meter is becoming more accepted in the field and is starting to be considered among the primary metering solutions for new field developments, the recent commercial available multiphase flow meters such as

Schlumberger VenturiX meter technology, Roxar multiphase meter, Framo multiphase flow meter and NetOil&Gas measuring skid. The universities, research centres and oil companies that contributed to that development are carrying out further studies on the subject.

1.3.1 What are multiphase flows?

The term 'Multiphase flow' is used to refer to any fluid flow consisting of more than one phase or component flowing simultaneously in a pipe. A multiphase flow is the flow of a mixture of phases such as liquid-liquid (e.g. water in oil), or liquid droplets in gases, or gases in a liquid (e.g. natural gas bubbles in oil) [6, 7]. In this research, the multiphase flow under consideration is air-water two phase flow.

1.4 Wet Gas Measurement Terms

The Wet Gas Measurement Group use specific definitions and terms to describe wet gas flow and its effects on metering. The following are some of those commonly used today, not all of the terms are used in the current study, but these are presented for the purpose of general knowledge and overview.

- **Gas Superficial Velocity** U_{gs}

  In a gas-liquid flow, this term refers to the gas velocity in the pipe that would exist if there were no liquid present in the gas flow. If liquid is present in the pipe, the actual gas velocity will be higher due to the reduction in available pipe area caused by the liquid present taking space in the pipe. The superficial gas velocity is defined as the gas volumetric flow rate divided by the total pipe cross sectional area. Mathematically, the superficial velocity of gas, U_{gs} can be expressed as:

$$U_{gs} = \frac{Q_g}{A}$$

Equation 1.1

where Q_g is the gas volumetric flow rate and A the cross sectional area of the pipe.

- **Water Superficial Velocity** U_{ws}

  In a gas-water flow, the term water superficial velocity refers to the water velocity that would exist if there were no gas present in the gas flow. The superficial water velocity is defined as the water volumetric flow rate divided by the total pipe cross sectional area. Mathematically, the superficial velocity of water, U_{ws} can be expressed as:

$$U_{ws} = \frac{Q_w}{A}$$

Equation 1.2

  where Q_w is the water volumetric flow rate and A the cross sectional area of the pipe.

- **Gas Volume Fraction** α_g

  In-situ gas volume fraction, is defined as the ratio of the area occupied by the gas to the total flow area as shown in Figure 1-1.

$$\alpha_g = \frac{A_g}{A_t}$$

Equation 1.3

  where A_g is the area of the pipe cross section containing gas and A_t is the total cross sectional area.

- **Water Volume Fraction** α_w

  In-situ water volume fraction, is defined as the ratio of the cross-sectional area of the water film (and entrainment water droplets if they are present) to the total cross-sectional area of the pipe as shown in Figure 1-1.

$$\alpha_w = \frac{A_w}{A_t}$$

Equation 1.4

where A_w is the area of the liquid film and A_t is the total cross-sectional area of the pipe. The sum of these phase volume fractions is equal to one.

$$\alpha_w + \alpha_g = \frac{A_g + A_w}{A_t} = 1$$

Equation 1.5

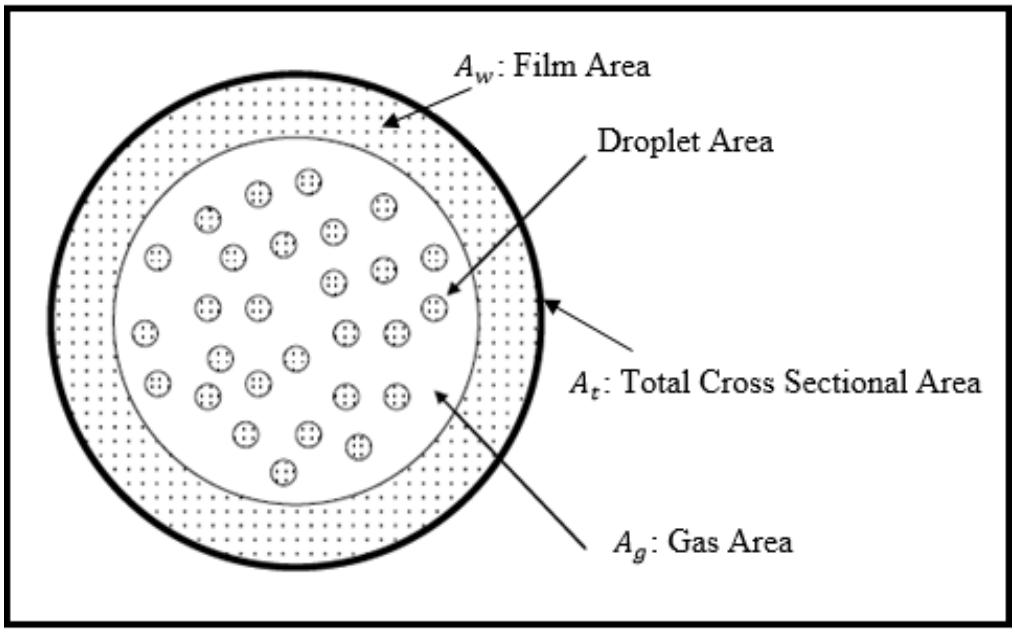

Figure 1-1: Schematic of flow phases distribution in annular flow

- **Liquid Load**

  Liquid load, or mass ratio is used to define the amount of liquid in the two-phase gas-liquid flow. This term is generally defined as the ratio of the liquid mass flow-rate to the gas mass flow-rate and is commonly expressed and used in calculations as a percentage value.

- **Martinelli & Lockhart Parameter**

The term Martinelli Lockhart number X is a dimensionless parameter that is used to correlate gas and liquid flow in a pipe. It was derived by two engineers Martnelli and Lockhart who worked on steam flow measurement and is used by wet gas researchers in wet gas calculations. The [8] parameter X defined as:

$$X^2 = \frac{\left(\frac{dP}{dZ}\right)_l}{\left(\frac{dP}{dZ}\right)_v}$$

Equation 1.6

where $\left(\frac{dP}{dZ}\right)_l$ is frictional pressure gradient, assuming that liquid alone is flowing in the pipe and $\left(\frac{dP}{dZ}\right)_v$ frictional pressure gradient, assuming that vapor alone is flowing in the pipe

- **Measurement Over or Under Reading**

  Over reading measurement occurs when the flow measurement device operating in a wet gas environment reports a higher flow-rate than is actually occurring. Under reading measurement occurs when a flow measurement device reports a lower flow-rate than is actually occurring.

- **Conductivity**

  The capability of a material to conduct or transmit electricity, sound or heat. Its units are Siemens/m or S/m

- **Mass flow rate**

  Mass flow rate is defined as the rate of movement of fluid mass through a unit area.

- **Wet gas flow patterns in vertical flows**

  In vertical gas-liquid flows, as the superficial gas velocity increases the multiphase flow will change between different regimes, bubble - slug - churn and annular (see Figure 2-2). Note that for high superficial gas velocity, the

multiphase flow is annular for all superficial liquid velocities (refer to chapter 2 section 2.2 and Figure 2-2). The flow that are relevant to this work are annular flows (see Figure 2-2) with and without entrained liquid droplets.

- **Wet gas flow patterns in horizontal flows**

  The wet-gas flow regimes in a horizontal pipe are affected by gravity which causes the gas phase to flow at the upper side of the horizontal pipe (see Figure 1-2). In horizontal flows, the transitions are functions of factors such as pipe diameter, interfacial tension and density of the phases. However horizontal gas-liquid flows are not relevant to the present study.

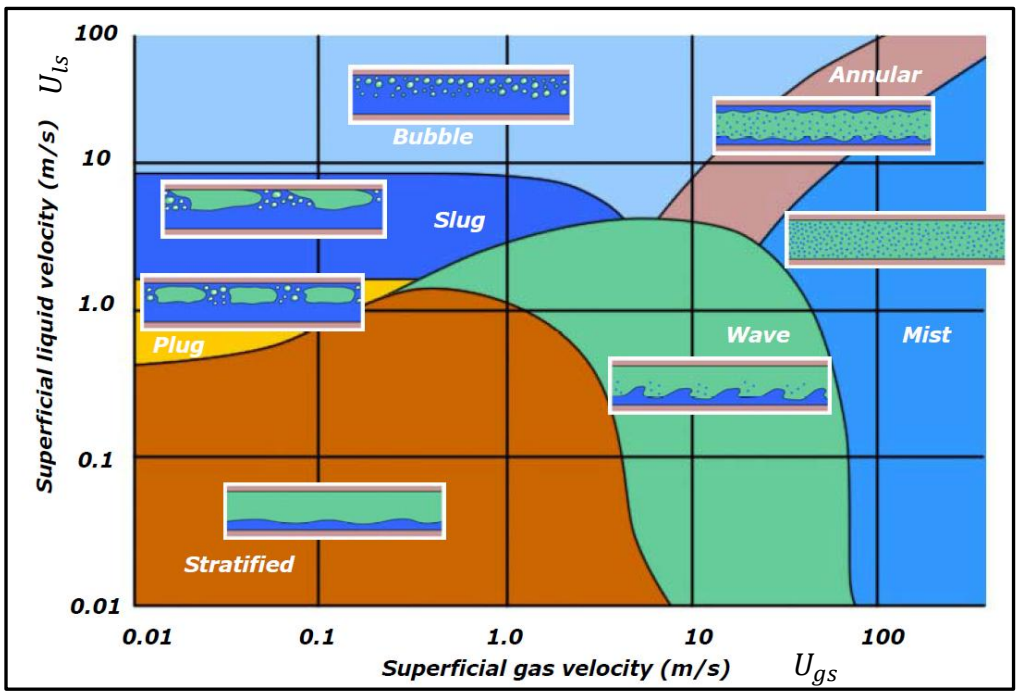

Figure 1-2: Generic map of two-phase flows for horizontal pipe geometry [9]

1.5 Overall Research Aim

The overall aim of this research is to measure phase volumetric flow rates in wet-gas annular flows to an accuracy of 1% on each phase. In order to do this the use of a

Venturi tube with conductance sensors was decided upon after extensively reviewing previous literature as described in chapter 2.

1.6 Structure of thesis

This thesis is organised in nine chapters describing the work that was done to achieve the aims and objectives of this work. This thesis is laid out as follows:

CHAPTER 2 A literature review of the subject area is presented encompassing traditional test separators, measurements techniques in multiphase flow and previous correlations on Venturis and orifice meters used for two-phase flow measurements (e.g. Murdock, Chisholm, Smith and Leang, Lin, de Leeuw and Steven correlations) are also discussed in this chapter.

CHAPTER 3 This chapter introduces the measurements and mathematical model, employed is this thesis the measurements needed, and how these measurements will be integrated into the mathematical model to give the liquid and gas flow rates which enable the gas and mass flow rate to be determined.

CHAPTER 4 The design and construction of: a Venturi meter, conductance electronic circuits for two upstream ring sensors, for the throat ring sensor and for the digital level sensor are all described in this chapter

CHAPTER 5 This chapter describes bench tests on the Venturi with conductance sensors at inlet and the throat. To simulate the film thickness (and hence the liquid volume fraction) in annular flow through the Venturi meter, different diameter nylon rods were inserted through the inlet and the throat sections of the

Venturi whilst the gap between the outer surface of the nylon rod and the inner surface of the Venturi was filled with water, representing the water film in a real annular flow situation. Also the calibration of the digital level sensor at the Venturi inlet is presented.

CHAPTER 6 This chapter presents the experimental devices and flow loop procedures used to carry out flow measurement of two phase flows using a Venturi meter in the annular vertical flow regime. The calibration procedures for the reference equipment are also described in this chapter.

CHAPTER 7 This chapter presents the experimental results obtained using the Venturi meter with conductance sensor at inlet and throat for vertical annular (wet gas) flow. Most results are presented in a graphical format. Predicted gas and water flow rates in a annular gas-water two phase flow were obtained from the Venturi with conductance sensors flow meter and compared with reference gas and water flow rates. The results of the current study were used to test the Abbas model and homogenous model, and also used with the de Leeuw and Murdcuk correlations models.

CHAPTER 8 The main conclusions drawn from the research work, and proposals for future work, are presented.

Chapter 2 Literature Review

Introduction

In the petroleum industry, gas water two phase flows are widely encountered in production processes such as exploration and transportation. The accurate measurement of the flow rate of gas-water two-phase flows is necessary in industrial processes. Many methods have been proposed for this, such as single-phase flow meters, ultrasonic methods, conductance techniques, tomography and capacitance methods. Among them the differential pressure (DP) meters play a significant role and have been widely used as two phase flow meters.

At present, the application of differential pressure flow meters in multiphase flow measurement is of increasing research interest, (e.g. Venturi and orifice meters) and a number of correlations have also been developed for multiphase flow measurements with differential pressure devices for example by; [10], [11, 12], [13], [14], [15, 16] and [2].

In this chapter, the test separator as traditional solution employed in multiphase flow applications is presented in Section 2.1, vertical pipe flow regimes is presented in Section 2.2, a review of existing techniques for measuring multiphase flows is presented in Section 2.3. Following this, previous correlations associated with Venturis and orifice meters used for two-phase flow measurements are presented Section 2.4 finally measurement techniques for film thickness in annular flows are presented in Section 2.5.

2.1 Traditional test separators

In the field, accurate flow metering has traditionally involved the separation of multiphase flows into component phases (gas and liquid e.g. oil and water) using dedicated test separation equipment [17]. Such a process then allows the measurement

of the individual flow rates using proven single phase flow measurement techniques such as turbine meters, orifice plates and positive displacement meters. However, the development of unmanned and sub-sea installations highlights the expense and complexity of this approach and so other technologies have been developed to eliminate the necessity of phase separation [18].

While a new generation of multiphase flow meters offers the potential of capital and operational advantages, no single technique has yet been found to be effective over all multiphase metering conditions [19]. Indeed, routine multiphase measurements at production facilities exist as a test separator combined with instrumentation to form a multiphase flow meter [20]. Figure 2-1 shows a schematic of a traditional three phase separator with its associated instrumentation. The test separator consists of the following major parts:

1. Inlet emergency shutdown (ESD) valve.
2. Three ESD valves - one each at the outlets for water, gas and oil.
3. The vessel.
4. Level control valves for oil and water (LCV).
5. Pressure control valves.

In general, the feed to the separator is a mixture of gas, oil and water. Due to the difference in density, the oil sits on top of the water and flows over a weir from compartment A into a separate compartment B. In the latter, the oil level is maintained by means of the outlet LCV activated by a level controller (LC). In a similar way, a constant oil/water interface is maintained by a second LC that adjusts the water output from compartment A. In order to ensure that the gas leaving the separator is free of liquid droplets, the gas section is fitted with a set of baffles to promote the separation. A gas control valve is used to maintain the pressure of the separator. Following the phase separation, each phase flow rate may then be metered separately.

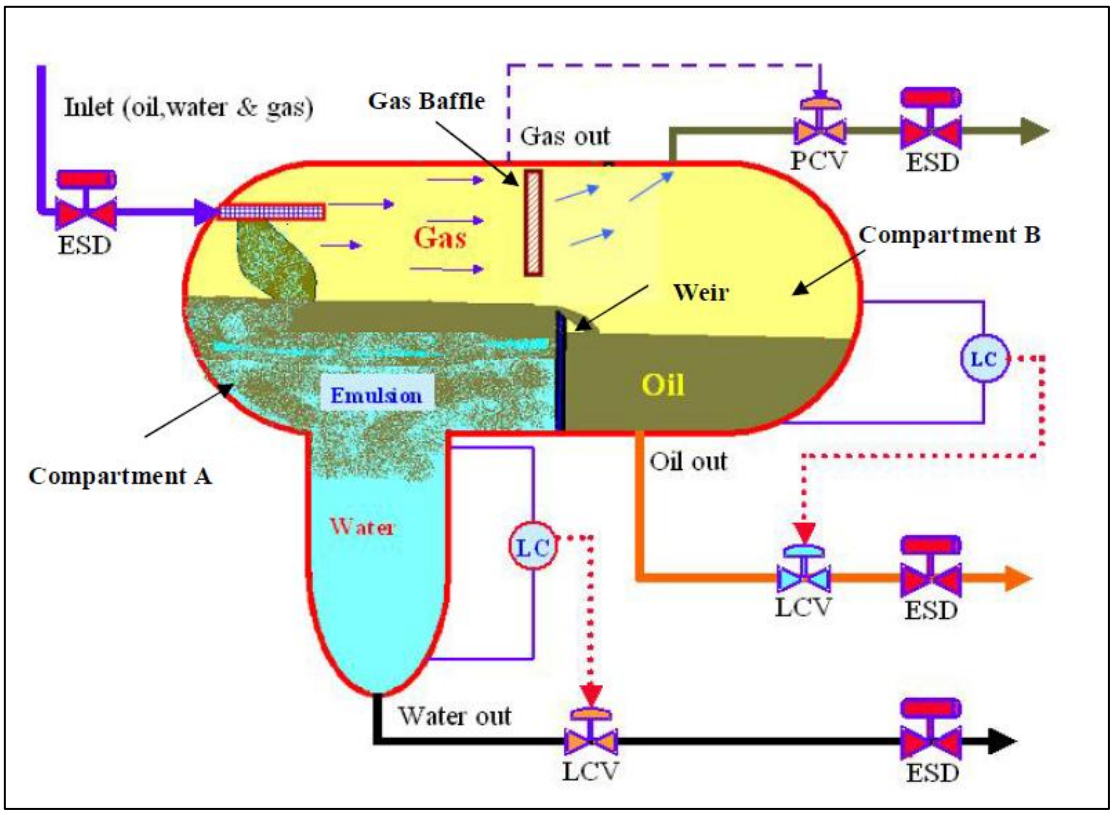

Figure 2-1 Simplified oil well separator [21]

This form of multiphase treatment with a test separator is today used mainly for production testing and so such measurement is performed only periodically to determine performance by establishing the flow rates of oil, water and gas per well under prevailing conditions of pressure and temperature. Where a number of wells exist at a facility, combined production flows into a production separator via the test header, and in general only one well at a time may be routed to the test separator.

Once taken, these measurements can then be correlated either to a dedicated flow device, e.g. a Venturi wet gas meter, or to well-head valve conditions. While the relationships are well understood, both in theory and practice, for wet gas flows, for other regimes, e.g. slug flows, the correlations are more approximate and empirical. The aim remains, however, to replace test separators with flow meters that can discriminate between the various phases with sufficient accuracy in a continuous, on-line, real time fashion.

Replacement of the conventional test separator with a multiphase measurement system has a number of advantages. Some of the advantages of using multiphase flow meters in multiphase flow applications include;

(i) Multiphase flow meters (MPFMs) are suited for offshore applications because a MPFM is lighter and more compact than a test separator.
(ii) For an accurate MPFM, real-time measurements of oil, water and gas flows can be made simultaneously without separation of the phases.
(iii) MPFMs can be cheaper than test separators because they eliminate the need for test lines, separators and separate flow meters.
(iv) MPFMs can work under a wide range of temperatures and different pressures.

These are the disadvantages of a test separator.

(i) Test separator is very expensive.
(ii) It is not practical in many sub-sea applications because it needs large space for the equipment and facilities.
(iii) It takes a long time to test the oil or gas well compared with a MPEM. The reaction time of a separator could be hours while for a MPEM it could be minutes [2].
(iv) Maintenance work of the test separator is very difficult particularly in sub-sea applications.

The ideal technical solution would involve the elimination of the separator (and its disadvantages) and the use of a multiphase flow meter to monitor continuously the flow rates of the different phases on each well. To be able to view production variations in real time would enhance reservoir management, reduce costs and increase the ultimate recovery, especially of the condensate. These advantages are further enhanced for isolated or sub-sea facilities. However, such a multiphase flow meter must combine a relatively low cost, whilst being robust, reliable and reasonably accurate.

2.2 Vertical pipe flow regimes

It is common to find multiphase flow in oil well pipelines; the pressure drop experienced by the oil as it is transported from the bottom of the well to the surface can result in gas release from the liquid oil phase. The flow regimes in vertical risers are usually fully developed and essentially axial-symmetrical and the multiphase flow features seen are dependent on the age of the well with a larger gas vapour fraction found in older wells. Figure 2-2 shows a generic map of two-phase flows in vertical pipes issued by the Norwegian Society for Oil and Gas Measurement [22], based on gas and liquid superficial velocities, for upward multiphase flow in a vertical pipeline.

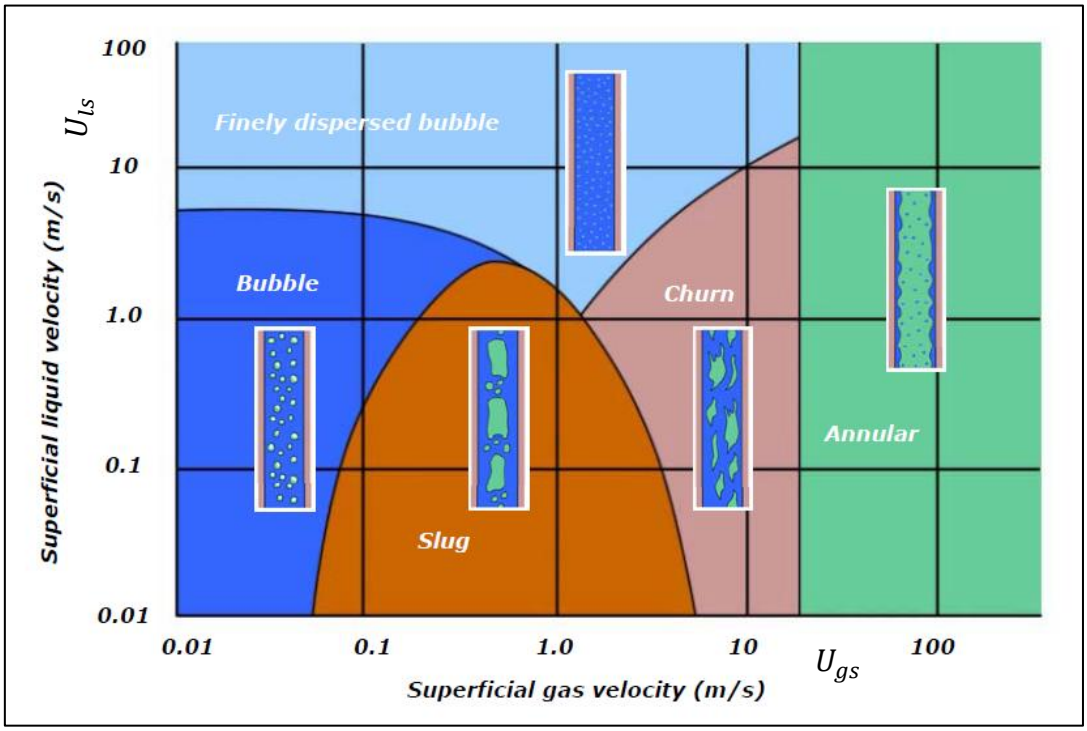

Figure 2-2 Generic map of two-phase flows for vertical pipe geometry [9]

The vertical flow regimes are commonly categorised into four main classifications:

Bubble (including finely dispersed bubble): At low gas flow rates, a continuous liquid phase is formed with the gas phase producing discrete bubbles within the continuum. The gas bubbles may coalesce to form larger bubbles or slugs.
Slug: Increased gas flow rates increase bubble coalescence until the bubble diameter eventually approaches that of the pipe diameter. The resulting flow alternates between high-liquid and high-gas composition.

Churn: This is somewhat similar to slug flow, but more chaotic in nature owing to the larger gas flow rates. The slug bubbles have become distorted to form longer, narrow structures and the flow adopts a random oscillatory nature. The liquid flow occurs mainly at the pipe wall but a significant proportion is vigorously mixed with the gaseous core.

Annular: At very high gas flow rates, the liquid phase is forced to flow up the pipe wall as a liquid film while the gas flows in the centre. The interface between the phases is typically wavy. The wavy interface enables liquid entrainment in the gaseous core. When the quantity of entrained liquid becomes significant, the flow is described as being in the annular mist regime. This is the regime of interest in the present study.

2.3 Annular flow

Annular flow in a vertical upward pipe is a very common two-phase flow pattern and its structure is quite complicated. It is a two-phase flow (gas-liquid) configuration, in which some of the liquid travels as a film on the pipe walls and the remainder is carried as drops by the gas in the centre of the pipe. Figure 2-3 shows a schematic plot of a typical annular flow regime. The fraction of liquid travelling as drops is considered as the entrained fraction and this may vary from zero to a value close to one.

Annular flow occurs at high or low gas and low to medium liquid flow rates and at all pipe orientations. At high liquid flow rates, roll or disturbance waves appear on the

film [23]. Disturbance waves are the most obvious feature of the liquid film in annular two-phase flows [24].

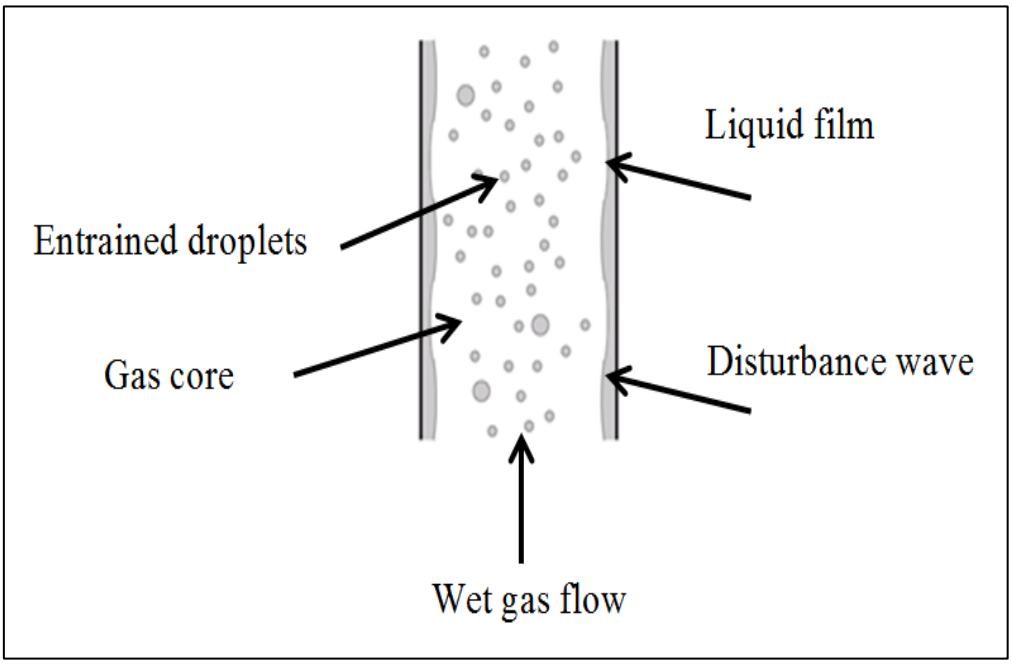

Figure 2-3 Vertical annular flow

In annular vertical flow the film is fairly uniform around the pipe circumference but for inclined and horizontal pipes, gravity causes a significant asymmetry of the film, and the liquid film thickness is found to be much thicker on the lower side than on the upper side of the pipe. In this research, annular flow is the principal regime of the wet gas flows studied. In the flow loop experiments described in this thesis the gas at large enough flow rate to support a liquid film on the wall of the pipe and so the annular flow regime occurs, in which a liquid film flows at the pipe wall while gas core flows at the centre of the pipe with some entrained liquid droplets. The liquid film thickness δ, the liquid film velocity U_f and the entrainment fraction E of the annular flow regime were all studied in this study.

2.3.1 Film thickness in annular flow

Two-phase flow is commonly encountered in many industrial processes. Due to its practical interest, extensive experimental and theoretical studies have described two-

phase flows in the last decades [25-28]. In the analysis of gas–liquid two-phase flow systems, especially for annular flows, the liquid film thickness is treated as one of the key parameters [29, 30]. Once the liquid film thickness is determined, it becomes easier to estimate the two-phase parameters, such as the volume fraction and the gas and liquid velocities. The general trend is for the mean film thickness to decrease with an increase in the gas flow rate or with a decrease in the liquid flow rate [31].

The measurement of liquid film thickness has been an essential subject in two-phase annular flow and the importance of the field is reflected in the many techniques that have been developed for it. Given the wide range of possible flow conditions it is difficult to make a single recommendation and thus it is more appropriate to consider a technique's suitability depending on the type of film and the thickness measurements required [32]. In the present study, the conditions used involved vertical annular flow and the conductance method was chosen to measure the film thickness at the Venturi inlet (refer to Sections 3.2.1 and 4.2.3). However, a description of the alternative methods is appropriate and these can be classified into four groups according to their measurement principles: 1) acoustic, 2) Interface detection methods and 3) electrical methods.

2.3.2 Measurement techniques for film thickness

2.3.2.1 Acoustic methods

Acoustic methods are based on ultrasonic waves and have been used by many researchers to measure liquid film thickness in two-phase flow. A measurement method with considerable advantages in industrial applications is the Ultrasonic Pulse-Echo Method [33]. The ultrasonic technique is based on the fact that ultrasound waves are attenuated and reflected when crossing discontinuities of a medium such as a liquid–gas interface. Therefore, reflection can be used to measure the film thickness based on the transit time.

[34] measured liquid film thicknesses of the organic working fluids R113 and FC-72 to generate power (electricity). R113 and FC-72 working fluids condensing inside a horizontal rectangular channel of 40x25 mm^2. Ultrasonic transducers were fixed at five different locations along the tube bottom. The measurement method was based on the delay time between a pulse emission and its return after reflection from the liquid–vapour interface. The film thickness was then calculated as the product between the delay time and the sound velocity in the liquid phase.

2.3.2.2 Interface detection methods

These methods are based on the detection of the liquid–gas and liquid–solid interfaces. Light emitted by each phase should present different characteristics (colour or intensity) in such a way that light gradients are generated at the interfaces. The two phase flow image is recorded using high-speed video and photographs and the film thickness determined by a pixel counting procedure. Various techniques are employed to produce the light gradient at the interface, e.g., induced fluorescent dye, shadowgraph and seeding particles. Stratified air–water film thicknesses were measured by [35] in rectangular hydrophilic channels by using an optical fluorescence imaging technique. A video camera and a 10x objective lens were used to capture the flow images and film thicknesses down to 20 μm were measured.

2.3.2.3 Electrical methods

2.3.2.3.1 The needle-contact method

One of the earliest and most straightforward methods used in the measurement of thin liquid films is the needle-contact method. Several investigators have employed this method, which is based on the conductivity of water ([36]; [37]; [38]; [39]).
The probe consists of a needle, the body of which is electrically insulated, mounted on a moveable rod. An electrode is inserted flush to the wall over which the film flows. The needle and moveable rod are placed directly opposite the electrode. The rod is gradually moved forward until the conducting tip of the needle just makes contact with the surface of the film. A conduction path now exists between the needle and the

electrode and a current flows. The distance moved by the rod will give, by subtraction, the thickness of the film.
Due to its simplicity and its physically intuitive operation, the needle contact method is often used as a standard measurement with which other methods are compared. Limiting errors have been associated with the mechanical positioning apparatus [40].

2.3.2.3.2 Conductance-based methods

Of all film thickness measurement methods, electrical conductance is perhaps the most used. The method consists of imposing an electrical potential difference between electrodes and measuring the resulting current. The conductance between the electrodes is directly related to the amount of fluid between them. A thicker liquid film decreases the electrical conductance which can be measured in terms of either current or potential (or voltage) through the electrodes. One problem related to this method is the fact that the output from the electrodes is saturated if the distance between the sensor electrodes is small in comparison with the film thickness [41].

In the current research the electrical conductance technique is used to measure the film thickness at the Venturi (refer to Sections 4.2.1 and 4.2.3) and the gas volume fraction at inlet and the throat of the Venturi (refer to Section 4.2.1).

2.3.2.3.3 Capacitance-based methods

Methods based on electrical capacitance have attracted the interest of several researchers since they were proposed by [42]. This technique is based on the fact that when two metal plates subjected to an electric current face each other, a capacitance is created the value of which will depend on the plate area, the distance of the plates, and the dielectric constant of the medium between them. If the dielectric medium is composed of liquid and gas, the capacitance will vary according to the two-phase morphology. Then, the capacitance can be measured and correlated with the film thickness. [43] used a parallel-plate capacitance sensor to measure liquid film thickness for horizontal, vertical upward and downward two-phase flows in a square

cross-section channel which was 12.7 mm on each side. The capacitance was measured with a commercial instrument with a resolution of 0.1 fF and accurate to 0.1% of full scale.

2.4 Direct measurement techniques in multiphase flow

2.4.1 Phase volume fraction measurement

2.4.1.1 Electrical conductance technique

This technique has proven attractive for measuring the phase volume fraction in many industrial applications with water-continuous multiphase flows due to its fast response and its relative simplicity in operation.

Early work using electrical conductance methods was reported by [44] and [45] who studied the method and the design of electrodes. It was found [44] that ring electrodes were preferable to those which interfered with the flow for fixed field applications. Extensive reviews of the electrical conductance technique in multiphase flows have been provided, for example, by [46], [47], [48], [49], [50].

In multiphase flows, electrical conductance is dependent on the concentration and distribution of the phases, and in particular on the gas volume fraction in the water in gas-water two phase flows. The conductance is typically measured by passing a known electrical current through the flow and then measuring the voltage drop between two electrodes in the pipe. Once the current and the voltage drop are obtained, the conductance (or resistance) of the mixture can be calculated [51].

The operation of the electrical conductance technique in water-gas two phase flows relies on the fact that the conductance of the mixture depends on the gas volume fraction in the water. The conductance of the mixture, G_{mix}, can be calculated using an inverting amplifier circuit as shown in Figure 2-4. The inverting amplifier output V_{out} is proportional to the conductance, $G_{mix} = \frac{1}{R_{mix}}$, between the ring sensor A electrodes 1 and 2. The output voltage of this stage is given by:

$$V_{\text{out}} = -\left(\frac{R_{fb}}{R_{mix}}\right) V_{in}$$

Equation 2.1

where R_{fb} is the reference feedback resistance, V_{out} is the output voltage, and V_{in} is the input voltage. The conductance *G* is the reciprocal of the resistance. Therefore, Equation (2.1) can be re-written as:

$$V_{out} = -\frac{G_{mix}}{G_{fb}} V_{in}$$

Equation 2.2

where G_{mix} is the conductance of the mixture.

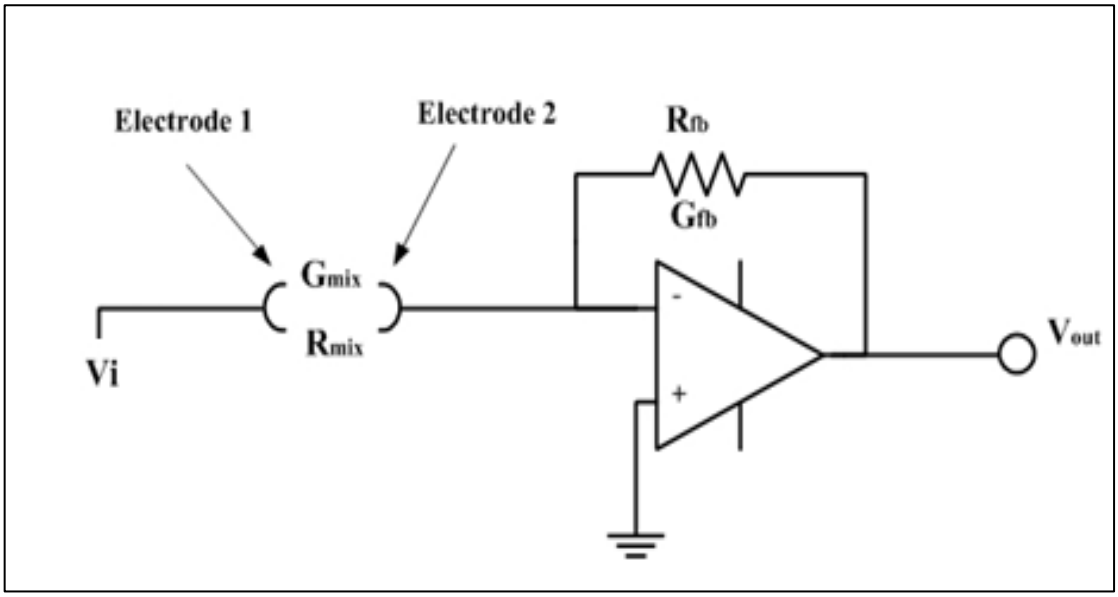

Figure 2-4 Fluid electronic conductance circuit

Thus any variation in the fluid between electrodes 1 and 2 of the ring sensor A which changes the conductance of the mixture, G_{mix}, is reflected in a change in the inverting amplifier circuit output voltage V_{out}. The conductance of the mixture, increases with increasing water volume fraction and decreases with increasing gas volume fraction.

The relationship between conductivity and the gas volume fraction from Maxwell's work [52] is given by:

$$\alpha_s = \frac{2\sigma_w - 2\sigma_m}{\sigma_m + 2\sigma_w}$$

Equation 2.3

where α_s is dispersed phase (non-conducting volume fraction), σ_w is the water conductivity and σ_m is the mixture conductivity.

Using Maxwell equation [52] the mixture conductivity σ_m can be easily determined. Therefore;

$$\sigma_m = \sigma_w \frac{2 - 2\alpha_s}{2 + \alpha_s}$$

Equation 2.4

Once the mixture conductivity is obtained using Equation (2.4) then as it is well known that the conductance of the mixture is given by;

$$S_m = K\sigma_m$$

Equation 2.5

where S_m is the conductance of the mixture and K is the cell constant.

The conductance technique forms the basis of one of the techniques used in the current research. Specifically, this technique was used to measure the gas volume fractions at the inlet and throat of a Venturi, together with the film thickness and the liquid film velocity at the Venturi inlet in vertical annular (wet gas) flows. In other words, the gas volume fractions at the inlet (and hence the film thickness) and the throat of the Venturi meter in vertical annular (wet gas) flows were measured using a sensor made from two ring electrodes flush mounted with the inner surface of the Venturi inlet, and a sensor made from two ring electrodes flush mounted with inner surface of the Venturi throat (see Sections 4.2.1 and 4.2.2). The film thickness was also measured by a conductance digital level sensor at the Venturi inlet (see Section 4.2.3).

The liquid film velocity was measured using a cross correlation technique between two conductance ring sensors at the Venturi inlet, (see Chapter 4 for more details). The design and calibration of the Venturi with conductance sensors at inlet and the throat investigated in this thesis is described, in detail, in Chapters 4, and 5.

2.4.1.2 Electrical impedance methods

Electrical impedance tomography (EIT) is a non-intrusive phase fraction measurement technique. It depends on measurements of the variation in electrical properties (e.g. capacitance and resistance) to provide an image of the pipe contents for measuring liquid and gas volume fractions in a multiphase flow. The concept of EIT is to reconstruct an image of a component based on its spatial distribution of electrical properties [53], [54]. This enables the phase fractions to be measured. Relying on the properties of the flow more simple, non-imaging apparatus can determine the capacitance, resistance or complex impedance of the flow to find the liquid and gas volume fractions. The basic operation of the impedance method of component fraction measurement is shown in Figure 2-5.

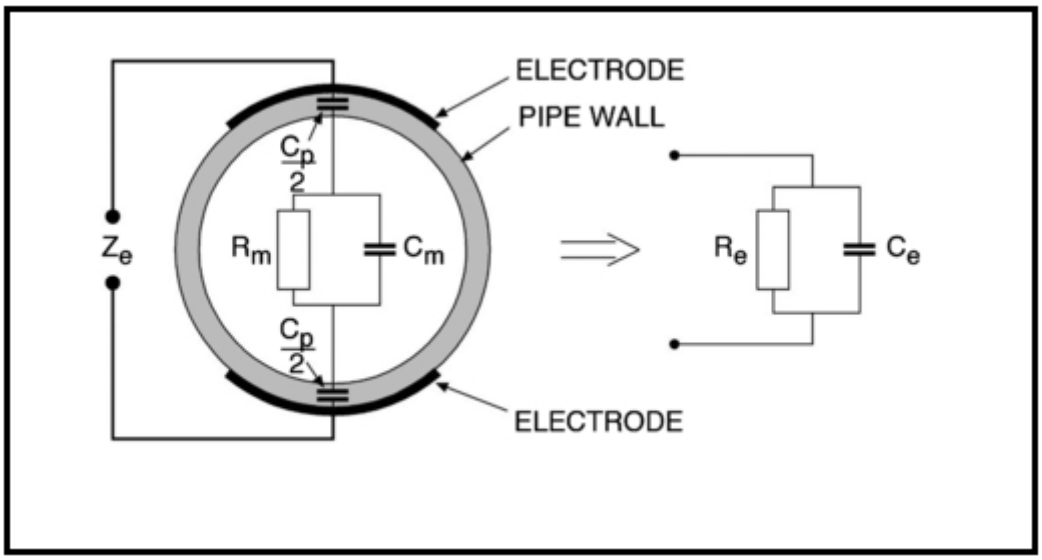

Figure 2-5 The impedance method of component fraction measurement [55].

If the electrical impedance (Z_e) is measured across two electrodes, between which an oil-water-gas mixture is flowing, then the effective or measured resistance (R_e) and capacitance (C_e) [56] are given by:

$$R_e = \frac{1 + \omega^2 R_m^2 (C_m + C_P)^2}{\omega^2 R_m C_P^2}$$

Equation 2.6

$$C_e = \frac{[1 + \omega^2 R_m^2 C_m (C_m + C_P)] C_P}{1 + \omega^2 R_m^2 (C_m + C_P)^2}$$

Equation 2.7

The resistance (R_m) and capacitance (C_m) of the mixture flowing through the pipe depend on the permittivity and the conductivity of the oil, water and gas components, the gas void fraction and the water fraction of the flow, and the flow regime. The resistance and capacitance measured across the electrodes will in turn depend upon R_m, C_m and the excitation frequency ω of the detection electronics, the geometry and material of the sensor. For a particular sensor geometry (and hence the capacitance of the electrode-pipe coupling C_p is fixed) and flow regime, the measured impedance will be a direct function of the flow's component ratio [56].

Such impedance methods have two important limitations, however: they cannot be used over the full component fraction range and are flow regime dependent. If the continuous phase is aqueous then a short circuiting effect will occur caused by the conductive water and so the measured C_e will remain constant even when the water fraction in the flow varies [57]. More information regarding EIT and other impedance methods can be found in [58], [59], [60] and [61].

2.4.1.3 Gamma radiation attenuation

Gamma radiation attenuation techniques can be used to resolve two-component phase fractions using a single-energy gamma source, or three-component mixtures using a dual-energy source [62]. A collimated gamma ray beam is directed at the pipe with a

sensor placed diametrically opposite the source (refer to Figure 2-6). The intensity of the radiation decays in an approximately exponential fashion as it passes through material flowing in the pipe measurement section.

The attenuation of the gamma ray beam is dependent on both the material density and the energy of the beam itself.

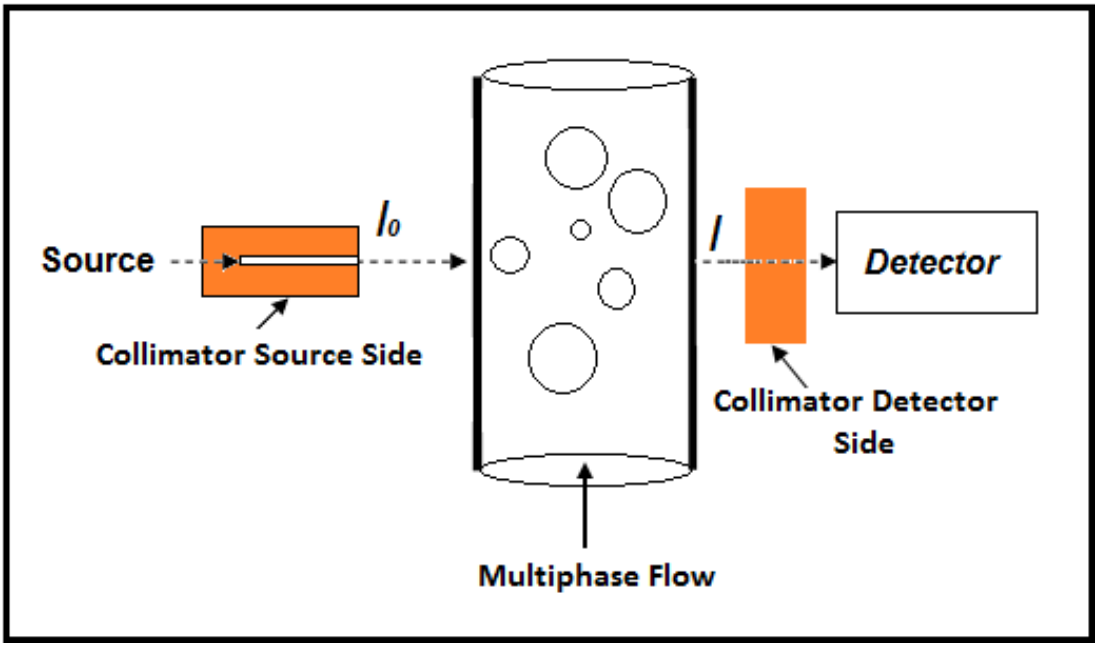

Figure 2-6 Gamma attenuation measurement

For a homogenous medium, the intensity I, of the received beam at the detector is given by;

$$I = I_0 e^{-\mu z}$$

Equation 2.8

where I_0 is the initial radiation intensity, μ is the total attenuation coefficient per unit of length of the fluid and z is the gamma ray path length through the medium.

[63] studied how the distribution of the phases within the flow effects the measurement of the void fraction. In this study, two hypothetical flows were studied as described below.

(i) In the first case, they proposed a hypothetical flow where the phases (i.e. gas and liquid) are arranged in layers at right angles to the radiation beam as shown in Figure 2-7 (see also [64]).

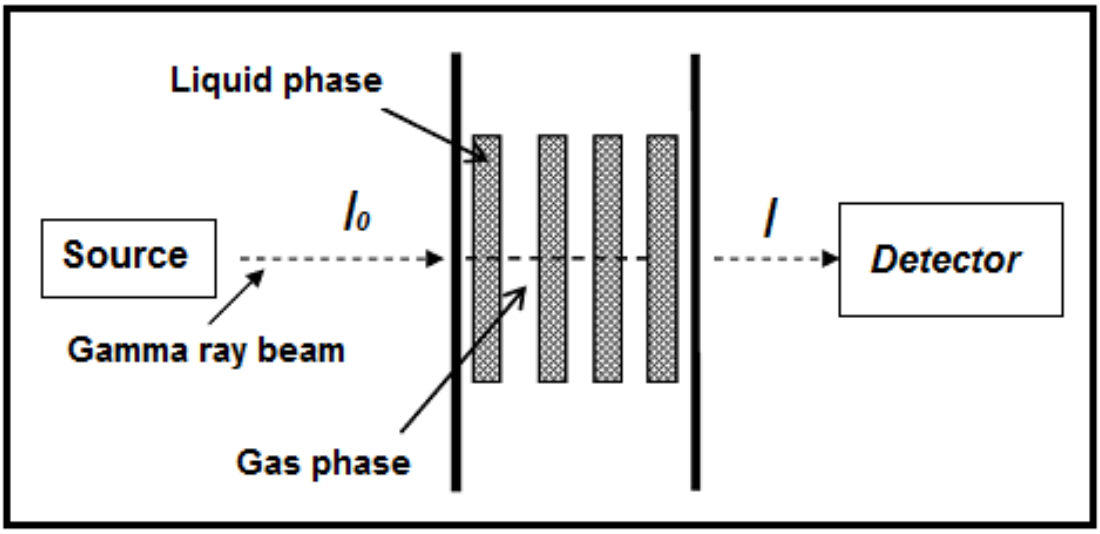

Figure 2-7: Gamma ray densitometer: A hypothetical flow where the liquid and gas phases are in Layers perpendicular to the radiation beam

For the above case, the gas void fraction α is given by;

$$\alpha = \frac{\ln\left(\frac{I}{I_{liq}}\right)}{\ln\left(\frac{I_g}{I_{liq}}\right)}$$

Equation 2.9

where I is the intensity of the received beam at the detector in the presence of the homogeneous mixture, I_{liq} is the intensity of the received beam at the detector with the pipe full of liquid only and I_g is the intensity of the received beam at the detector with the pipe full of gas only.

(ii) In the second case, they considered a hypothetical flow where the phases are arranged in layers parallel to the beam as shown in Figure 2-8.

If the beam applied is horizontal to the fluid layers then the gas void fraction α is given by;

$$\alpha = \frac{I - I_{liq}}{I_g - I_{liq}}$$

Equation 2.10

Equations (2.9) and (2.10) shows that the gamma radiation attenuation from method is highly dependent upon the arrangement of the phases in the flow.

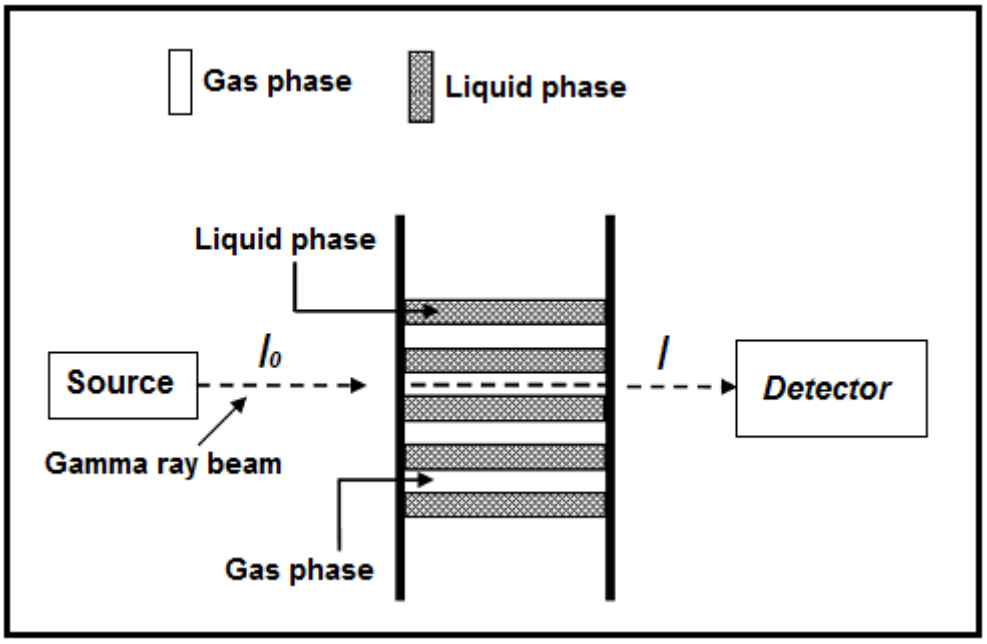

Figure 2-8: Gamma ray densitometer: A hypothetical flow where the phases are arranged in Layers parallel to the radiation beam

2.4.2 Phase velocity measurement

2.4.2.1 Differential pressure measurements

Where a multiphase flow is sufficiently mixed, and flows as a single homogenous fluid, differential pressure-based flow measurement techniques, such as Venturis and orifice plates, can be utilised to determine both the flow velocity and also the mixture flow rate [65], [66]. [Note: - this assumption of a homogenous mixture is different to the flows considered later in section 2.4 where differential pressure devices are again discussed]. The fluid flow rate across these sections can be expressed as a function of

the measured pressure drop. For homogenous mixture and single-phase flows measurement, the operating principles of Venturis and orifice meters are well understood and full descriptions of their technical designs are detailed in ISO 5167:2003. However, the equations described by the ISO standard for the Venturi under these conditions cannot be applied directly to multiphase flows without correction.

Several theoretical and experimental studies have described mathematical models of Venturi meters in multiphase flow applications including their use in vertical and horizontal configurations. The study of multiphase flow through Venturi and orifice meters is described for example by [10], [11], [67], [68], [15], [2] and [69] (see Section 2.4).

Figure 2-9 shows the geometry of both Venturi and orifice inserts and their characteristic flow profiles. In the Venturi, the reduction in the flow area results in increased fluid velocity, and consequently reduced fluid pressure. Frictional losses are minimised by the small angle of the downstream cone that allows good pressure recovery. In contrast, the abrupt reduction in flow diameter in the orifice plate hinders downstream pressure recovery due to the creation of regions of fluid recirculation [70].

If the region between the upstream and throat sections of a Venturi are well designed, then the relationship between the differential pressure across the Venturi meter and the velocity of the fluid (and hence the mass/volume flow rate) can be derived from the Bernoulli's equation.

For the single phase and hence homogenous flows, the Bernoulli equation can be written as;

$$P_{ph1} + \frac{1}{2}\,\rho_{ph1}\,U_{ph1}^2 = P_{ph2} + \frac{1}{2}\,\rho_{ph2}\,U_{ph2}^2$$

Equation 2.11

where P is the static pressure, ρ is the density and U the velocity. The subscript 1 refers to the inlet of the Venturi, the subscript 2 refers to the throat of the Venturi and subscript ph refers to the single phase fluid (liquid or gas).

While the use of orifice plates tends to be restricted to wet gas measurements (due to their poor pressure recovery properties) the Venturi method has many advantages, including low cost, good pressure recovery, familiarity, and simple operation. The Venturi is at the heart of the current research in which a conductance Venturi meter was used in vertical annular (wet gas) flows; the design of the Venturi is described in Chapter 4.

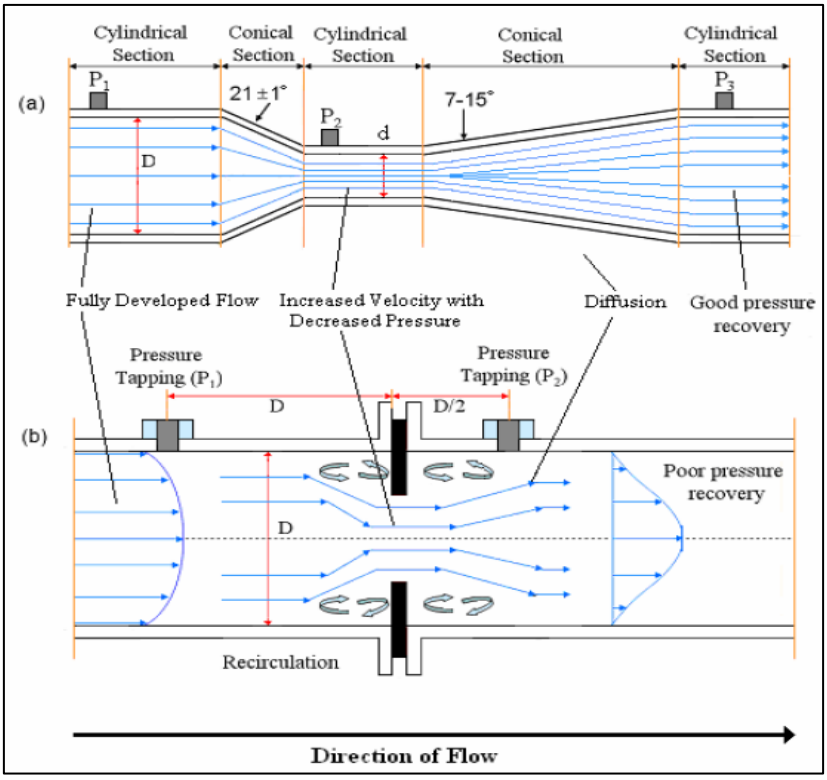

Figure 2-9 Differential pressure measurement systems (a) Venturi, (b) orifice [70]

2.4.2.2 Cross-correlation technique

The use of the cross-correlation technique for velocity measurement of multiphase flows has been extensively described by [71]. The principle of technique is shown in

Figure 2-10. Two sensors are used to monitor the flow, one being positioned downstream of the other.

These sensors are used to detect variations in some property of the flow with time such as density, permittivity or conductivity. The time delay between the output signals of the two sensors can be found by computing the cross-correlation function of these signals $x(t)$ and $y(t)$ over a measurement period, T. The cross-correlation function is given by:

$$R_{xy}(\tau) = \frac{1}{T}\int_{0}^{T} x(t-\tau).y(t)dt$$

Equation 2.12

where: $R_{xy}(\tau)$ is defined as the cross-correlation function between the outputs from the two sensors which are referred to as $x(t)$ (from the upstream sensor) and $y(t)$ (from the downstream sensor). T is the total time period for which data was acquired, see Figure 2-11.

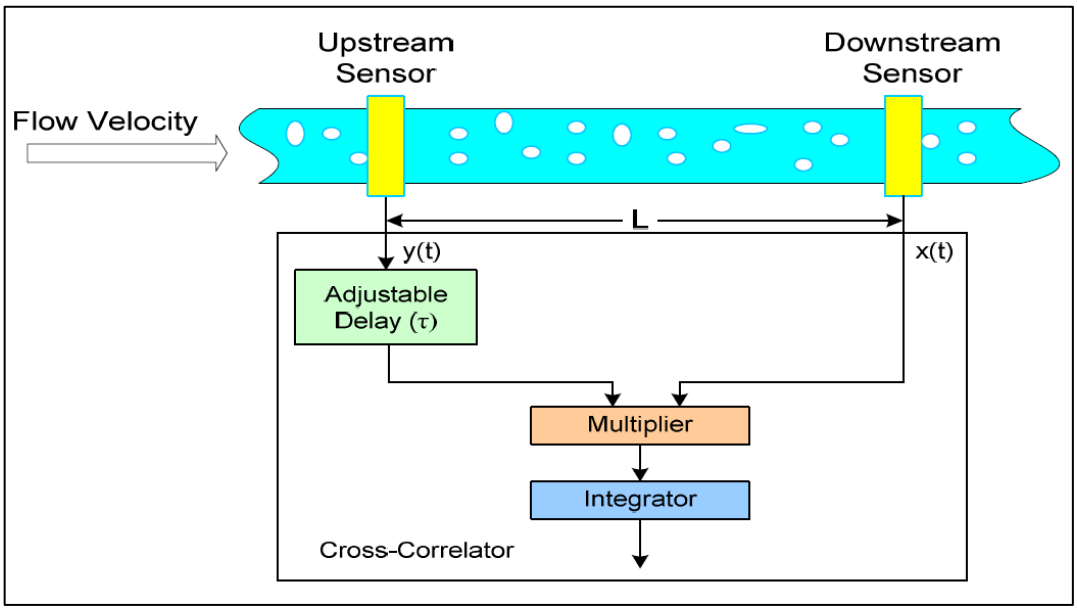

Figure 2-10 A schematic diagram of a cross-correlation flow meter

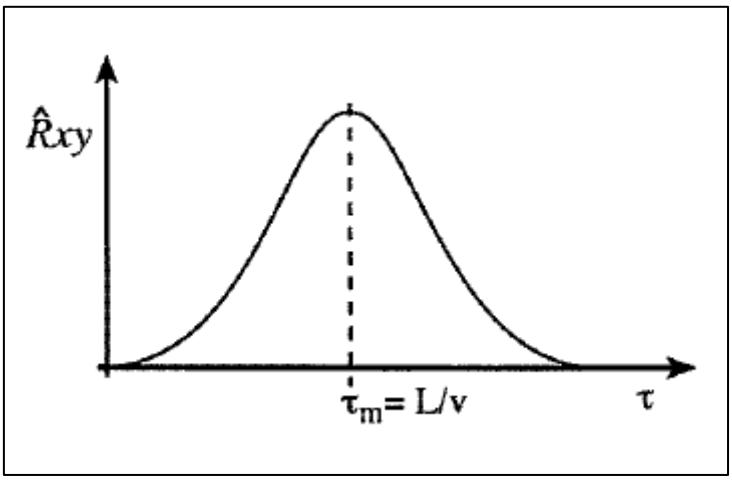

Figure 2-11 Cross-correlation function [56]

The transit time of the flow between the two sensors is usually found by observing the time lag τ_m at which the cross-correlation function is a maximum. A characteristic flow velocity $\overline{U}$ can then be calculated, as:

$$\overline{U} = \frac{L}{\tau_m}$$

Equation 2.13

where: L is the axial separation distance between the pair of identical sensors.

In this study a conductance cross-correlation technique has been used. Two sensors are designed to measure the film velocity by cross-correlating signals at the inlet of a Venturi.

2.4.2.3 Turbine flow meters

The turbine flow meter is one of the most important fluid flow rate techniques used in the process industries. A typical turbine flow meter (see Figure 2-12) can be used to measure the volumetric flow of a flowing single phase fluid (liquid or gas). These devices have been fully described by [72] who also discuss the problems associated with their use for flow metering.

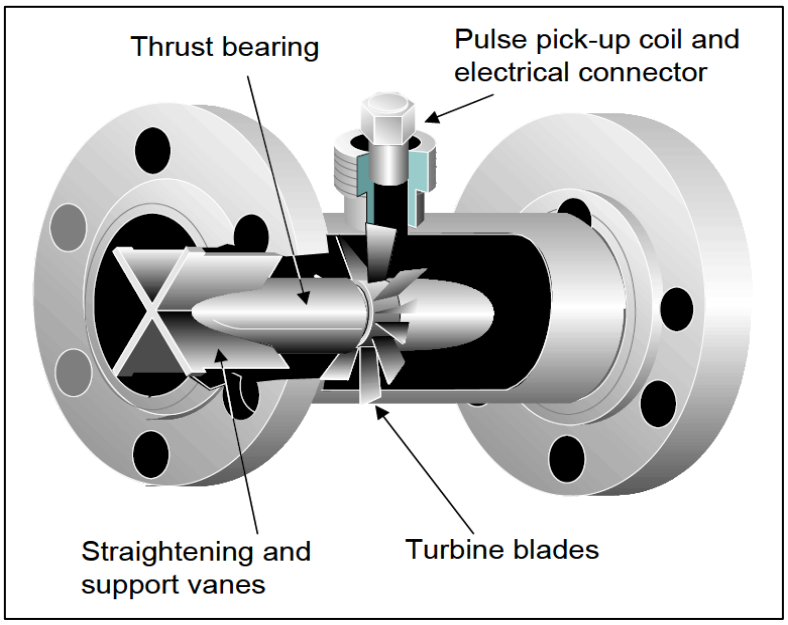

Figure 2-12 Turbine meter [73]

The unit consists of a multi-bladed rotor housed in a non-magnetic body, mounted with a pipe perpendicular to the liquid flow. As the fluid passes through the blades, the rotor spins and the rotational speed (which is a direct function of flow rate) can be sensed by magnetic pick-up, photoelectric cells, or gears. For an ideal linear turbine flow meter, the angular speed of the rotor is proportional to the mean liquid velocity U through the turbine meter. Therefore:

$$f_{turbine} = k_{turbine}\, U$$

Equation 2.14

where $f_{turbine}$ is the frequency in revolutions per second, U is the mean liquid velocity in ms^{-1} and $k_{turbine}$ is the constant of proportionality.

The volumetric flow rate Q is given by;

$$Q = AU$$

Equation 2.15

where A is the 'effective' cross sectional area of the turbine meter.

Combining Equations (2.14) and (2.15) gives;

$$f_{turbine} = KQ$$

Equation 2.16

where K is the meter constant (or K-factor) and is given by;

$$K = \frac{k}{A}$$

Equation 2.17

In two-phase flow the output signal of turbine flow meter is proportional to the combination of the liquid fraction velocity and the gas fraction velocity [74].

In two-phase conditions there is no agreement about an analytical expression which relates the flow rates of the individual phases to the turbine output. The presence of the slip between the two phases, the different flow regimes, the influence of the gas flow rate and of the liquid flow rate strongly affect the output from the turbine flowmeter [74].
[75], [76] and [77] have all proposed models to enable the use of turbine flow meters in two-phase flows. These three analytical models have been proposed to relate the two-phase velocity measured by a turbine meter with the actual gas velocity U_G and the actual liquid velocity U_L, based on different assumptions.

Rouhani model [75] is based on the assumption that the change in momentum (impulse) of the turbine flowmeter blades, due to the flow stream, is negligible as follows:

$$\alpha U_G \rho_G (U_G - U_{turbine}) - (1-\alpha) U_L \rho_L (U_L - U_{turbine}) = 0$$

Equation 2.18

Rouhani derived a model for the turbine velocity $U_{turbine}$ as follows;

$$U_{turbine} = U_L \frac{\alpha \rho_G S^2 + (1-\alpha)\rho_L}{\alpha \rho_G S + (1-\alpha)\rho_L}$$

Equation 2.19

Based on the single phase meter constant k (or meter factor), $U_{turbine}$ can be obtained from Equation (2.14).

$$U_{turbine} = \frac{f_{turbine}}{k_{turbine}}$$

Equation 2.20

where U_L is the liquid velocity, U_G is the gas velocity, S is the slip ratio, ρ_L and ρ_G are the liquid and gas densities respectively and α is the gas volume fraction.

Aya model [76] is based on a momentum balance on a turbine blade due to velocity differences between the two phases and the turbine blade. It typically describes dispersed flow with gas velocity higher than the liquid one.

$$\alpha\rho_G C_{TG}(U_G - U_{turbine})^2 = (1-\alpha)P_L C_{TL}(U_{turbine} - U_L)^2$$

Equation 2.21

where C_{TG} and C_{TL} are the drag coefficients of a turbine blade for the gas and liquid phases respectively.
Aya derived a model for the turbine velocity $U_{turbine}$ as follows;

$$U_{turbine} = U_L \frac{\sqrt{\rho_L(1-\alpha)} + S\sqrt{\rho_G\alpha}}{\sqrt{\rho_L(1-\alpha)} + \sqrt{\rho_G\alpha}}$$

Equation 2.22

Volumetric model [77] assumes that the measured velocity $U_{turbine}$ represents the volumetric flow rate per unit flow area, which gives;

$$Q = A(\alpha U_G + (1-\alpha)U_L)$$

Equation 2.23

The turbine velocity $U_{turbine}$ as follows;

$$U_{turbine} = \frac{Q}{A} = \alpha U_G + (1-\alpha)U_L = U_L\big(S\alpha + (1-\alpha)\big)$$

Equation 2.24

2.4.2.4 Vortex flow meters

Vortex shedding flow meters are widely used for measuring the single phase fluid flow rate in applications such as processed natural gas and steam. The phenomenon of vortex shedding occurs when a fluid (gas or liquid) meets a non-streamlined obstacle termed a bluff body. In this situation, the flow is unable to follow the defined contours of the obstacle and the peripheral layers of the fluid separate from the obstacle's surfaces to form vortices in the low pressure area behind the body (see Figure 2-13). These vortices are shed alternately from either side of the bluff body (and are swept downstream to form a so-called Karman vortex street) at a frequency that, within a given Reynolds number range, is proportional to the mean flow velocity in the pipe.

In two phase gas-liquid flows Vortex shedding meters are used too and the operation of the vortex shedding flow meter is complicated because the frequency of shedding is dependent on the gas void fraction. [78] investigated the vortex shedding flow meter which can be used in two phase flows. They established that the application of vortex shedding becomes very difficult at low velocities and higher gas void fraction. They advise that the mixture velocity should be higher than 0.45ms^{-1} and the gas void fraction should be less than 10%.

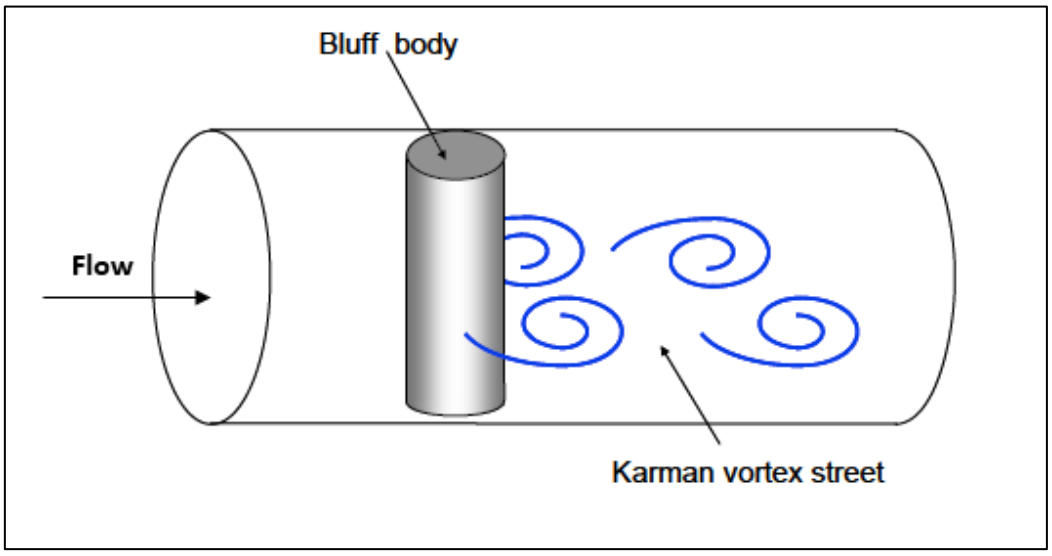

Figure 2-13 The Karman vortex street – with vortices formed on alternate sides in the low pressure area of a bluff body [73]

2.4.2.5 Ultrasonic flow meters

Ultrasonic flowmeters (USFM), suitable for both liquids and gases, have shown promise in both single-phase and two-phase flow metering tests [79].

The principle of these devices is that the required information about the measured medium can be obtained by from the reflection, absorption, and scattering effects of the medium on incident ultrasonic waves that are transmitted and received using a number of transducers. The transducers are able to convert an acoustic signal into an electrical signal (voltage pulse) and vice-versa. Figure 2-14 shows a schematic diagram of a common ultrasonic flow meter configuration.

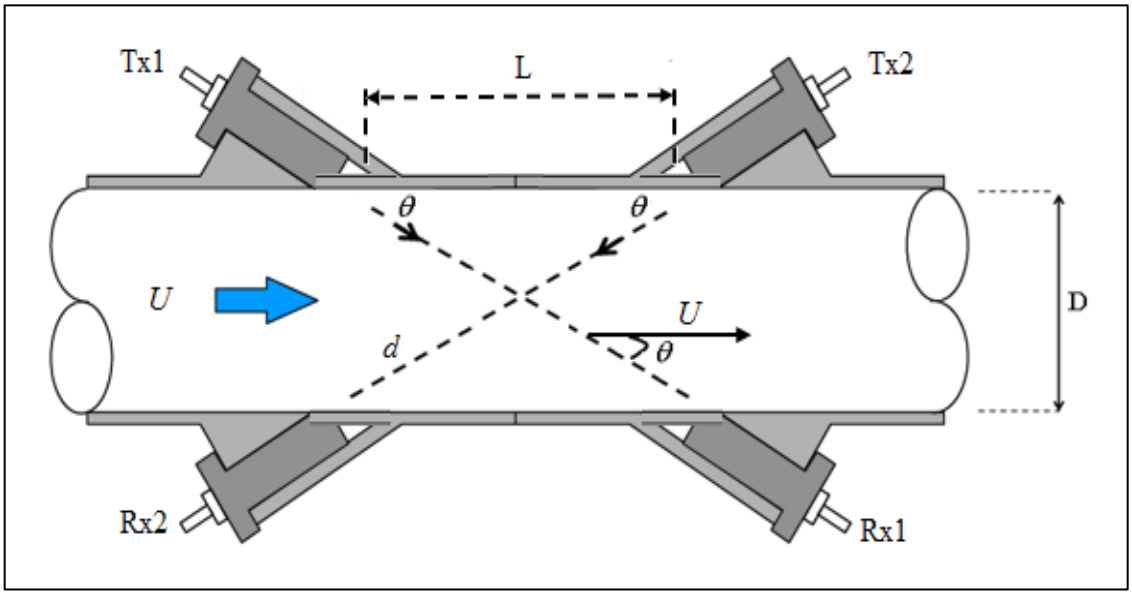

Figure 2-14 A schematic diagram of ultrasonic flow meter configuration

In Figure 2-14, U is the velocity of the fluid (ms^{-1}), D is the inside pipe diameter (m), L is the axial separation (m) between the transmitters (Tx1 and Tx2) and receivers (Rx1 and Rx2), d is the length (m) of the acoustic path and θ is the angle (in degrees) between the acoustic path and a vector representing the direction in which the medium moves.

Ultrasonic meters can measure the velocity of the gas flowing through the meter body. By knowing the velocity and the cross-sectional area, uncorrected volumetric flow rates can be found.

To determine fluid velocity U in a flow using the ultrasonic technique, some assumptions are made, including constant path length d, constant speed of sound c and a mean velocity profile for a coordinate system. The acoustic distance travelled by the ultrasonic beam can be expressed as:

$$d = \frac{D}{\sin\theta}$$

Equation 2.25

The velocity U_d of the ultrasonic beam along the downstream path from Tx1 to Rx1 U_d can be expressed as:

$$U_d = c + U\cos\theta$$

Equation 2.26

The velocity of ultrasonic along the upstream path from Tx2 to Rx2 U_u is given by:

$$U_u = c - U\cos\theta$$

Equation 2.27

where U is the fluid velocity, U_d and U_u are downstream and upstream fluid velocities respectively and θ is the angle shown in Figure 2-14.

Moreover, the application of the ultrasonic technique was also found in gas-liquid flow to determine the gas velocity and gas volumetric flow rate in annular flow. Q. Al-Yarubi [21] designed a successful ultrasonic flow meter with a novel transducer configuration to measure the gas velocity in annular flow.

[21] did calibration tests of the USFM with gas only flowing only in the pipe, the USFM seemed to be very promising. When gas-water flow flowed in the pipe, the transducers could be covered with liquid film thicknesses of up to about 0.5mm thickness and the device still responded. However if the film thickness was more than about 0.5mm, the device stopped responding due to changes in gas velocity. To overcome this problem, the transducers were positioned so that they intruded into the

pipe i.e. they passed though liquid film as shown in Config. B, see Figure 2.15. This action it solved the problem of measuring the gas flow rate Q_g [21].

[21], has reported how to measure the gas flow rate in gas-water flow, as follows.
The phase difference between upstream and downstream signals is given by:

$$\phi = \hat{c}U_g$$

Equation 2.28

where U_g is the gas velocity (m/s) and $\hat{c}$ is a constant.

The mean volumetric gas flow rate is usually the quantity required:

$$Q_g = AU_g$$

Equation 2.29

where: $Q_g$is the gas volumetric flow rate (m^3/s), U_g is the gas velocity (m/s) and A is the pipe cross-sectional area of the pipe (m^2).

The electronic circuit output when calibrated which was designed by [21] and used in his investigation is given by:

$$V_{out} = \hat{a}\cos(\phi) + \hat{b}$$

Equation 2.30

where: $\hat{a}$ and $\hat{b}$ are to be found from a calibration curve and ϕ is the phase-shift angle.

Substituting Equation (2.28) into Equation (2.30) gives:

$$V_{out} = \hat{a}\cos(\hat{c}U_g) + \hat{b}$$

Equation 2.31

From Equation (2.31) the gas velocity U_g is given by:

$$U_g = \frac{\cos^{-1}\left[\frac{V_{out} - \hat{b}}{\hat{a}}\right]}{\hat{c}}$$

Equation 2.32

Substituting Equation (2.32) into (2.29) gives the gas volumetric flow rate.

The USFM technique can be used in wet gas flow to measure the gas flow rate only if the transducers are not covered by the liquid film (the transducers should be intruded into the pipe) as shown in the Figure 2-15 Config. B.

Most ultrasonic flow meters are bi-directional, and sense flow in either direction. The advantages of ultrasonic flow meters are their suitability for large diameter pipes, fast response, no moving parts, long operating life and immunity to fluid properties. The disadvantages are that the fluid must be acoustically transparent, they are expensive and the pipeline must be full.

The reason behind not considering using the ultrasonic flow meter technique in this work because when the transducers are covered with liquid film thickness, the device stopped responding to changes in gas velocity as shown in Config. A, see Figure 2-15, Config. B , see Figure 2-15 the transducers will introduce a disturbance to the liquid film thickness of the annular flow.

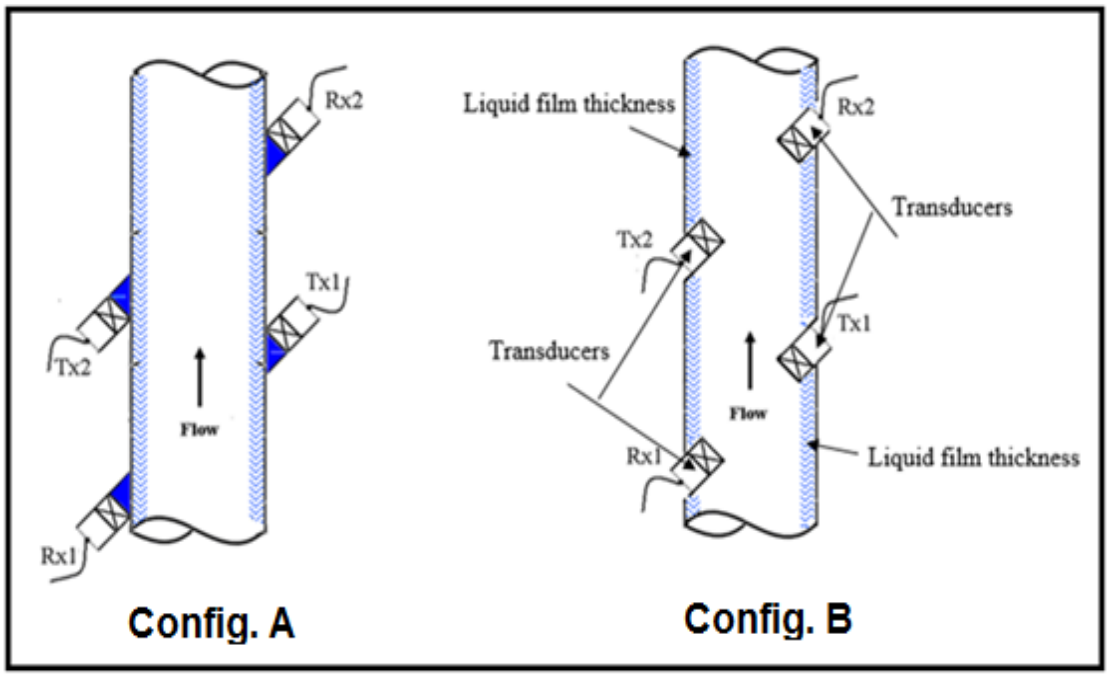

Figure 2-15: Transducers configurations to measure the gas flow rate in annular flow.

2.5 Previous correlations on Venturis and orifice meters used for two-phase flow measurements

Correlations for the use of orifice plates in two-phase flow conditions have existed since the 1960s: the most commonly used correlations are those of Murdock and Chisholm. As well as orifice plates, wedges, Venturi and nozzles have been used as two-phase flow meters and different correlations have been obtained to compute the mass flow rates of the gas and water in two-phase flow.

2.5.1 The Murdock correlation

A paper published by [10] considered gas-water two-phase flow through an orifice plate meter. The correlation Murdock offered was formed from a wide range of data points and therefore it was not restricted only to wet gas flows and it was valid for a wide range of flow conditions. Murdock's method was to consider the two-phase flow to be separated (stratified flow). In this way, the total mass flow rate was computed using an experimentally obtained constant M=1.26, assuming that the mass flow x is known (the quality is the mass flow rate of the gas divided by the total mass flow rate, see Equation (2.39). He stated that the two phase flow might be computed with a tolerance of 1.5 percent. The limits that he established were:

- The diameter ratio (β): 0.25 and 0.5.
- The standard taps locations of radius: (1D and 1/2D).
- minimum liquid Reynolds number of 50,
- minimum gas Reynolds number of 10,000,
- maximum liquid weight fraction of 0.9,
- minimum volume ratio gas to liquid of 100:1 and
- minimum gas expansion coefficient of 0.98.

The gas mass flow rate in the Murdock correlation is given by;

$$\dot{m}_g = \frac{A_t K_g \sqrt{2\Delta P_{TP}\, \rho_g}}{1 + 1.26 \frac{1-x}{x} \frac{K_g}{K_w} \sqrt{\frac{\rho_g}{\rho_w}}} = \frac{\left(\dot{m}_g\right)_{apparent}}{1 + 1.26 X_{mod}}$$

Equation 2.33

where $\left(\dot{m}_g\right)_{apparent}$ is the gas mass flow rate under two phase differential pressure $\left[\left(\dot{m}_g\right)_{apparent} = A_t K_g \sqrt{2\Delta P_{TP}\, \rho_g}\right]$ and X_{mod} is a modified version of the Lockhart–Martinelli parameter as it is the ratio of the superficial flows' momentum pressure drops and not the friction pressure drops as in the original definition by [8]. The Murdock definition is:

$$X_{mod} = \sqrt{\frac{\Delta P_w}{\Delta P_g}} = \left(\frac{\dot{m}_w}{\dot{m}_g}\right)\left(\frac{K_g}{K_w}\right)\sqrt{\frac{\rho_g}{\rho_w}} = \left(\frac{1-x}{x}\right)\left(\frac{K_g}{K_w}\right)\sqrt{\frac{\rho_g}{\rho_w}}$$

Equation 2.34

ΔP is the pressure drop, $\dot{m}$ is the mass flow rate, K is the flow coefficient (including the respective product of the velocity of approach, the discharge coefficient and the net expansion factor), ρ is the density and x is the mass flow quality. The subscripts w and g refer to the water and gas phases flowing alone respectively.

It is known that:

$$\frac{1-x}{x} = \frac{\dot{m}_w}{\dot{m}_g}$$

Equation 2.35

$$\therefore (1-x)\dot{m}_g = x\dot{m}_w$$

Equation 2.36

$$\therefore \dot{m}_g = x\left(\dot{m}_g + \dot{m}_w\right)$$

Equation 2.37

$$\therefore \dot{m}_g = x\dot{m}_T$$

Equation 2.38

$$\therefore x = \frac{\dot{m}_g}{\dot{m}_T}$$

Equation 2.39

The water mass flow rate $\dot{m}_w$ in the Murdock correlation can be obtained by the following equation:

$$\dot{m}_w = \frac{A_t K_w \sqrt{2\Delta P_{TP} \rho_w}}{1.26 + \frac{1}{X_{mod}}}$$

Equation 2.40

2.5.2 The Chisholm correlation

The [12] is a function of pressure and the modified Lockhart-Martinelli parameter, X_{mod} in which equations could be developed to predict pressure drop over sharp-edged orifices during the passage of incompressible two-phase flow. Chisholm reported that, when the Lockhart-Martinelli parameter $X_{mod} < 1$, then the slip ratio, S, is given by:

$$S = \left(\frac{\rho_w}{\rho_h}\right)^{\frac{1}{2}}$$

Equation 2.41

where ρ_h is the homogenous density, and when $X_{mod} > 1$, then the slip ratio is given by:

$$S = \left(\frac{\rho_w}{\rho_g}\right)^{\frac{1}{4}}$$

Equation 2.42

The gas mass flow rate given by [12] is:

$$\dot{m}_g = \frac{A_t K_g \sqrt{2\Delta P_{TP}\, \rho_g}}{1 + \left[\left(\frac{\rho_w}{\rho_g}\right)^{\frac{1}{4}} + \left(\frac{\rho_g}{\rho_w}\right)^{\frac{1}{4}}\right] X_{mod} + X_{mod}^2}$$

Equation 2.43

2.5.3 The Lin correlation

The [14] is applicable to general stratified two phase flows through Orifice Plate meters. Like Chisholm, Lin includes the effect of shear between the phases and his correlation allows for the independent effects of pressure and liquid mass content. He also uses the modified Lockhart-Martinelli parameter. The corrective coefficient K_{Lin} in the Lin correlation is given by:

$$K_{Lin} = 1.48625 - 9.26541\left(\frac{\rho_g}{\rho_w}\right) + 44.6954\left(\frac{\rho_g}{\rho_w}\right)^2 - 60.6150\left(\frac{\rho_g}{\rho_w}\right)^3 - 5.12966\left(\frac{\rho_g}{\rho_w}\right)^4 - 26.5743\left(\frac{\rho_g}{\rho_w}\right)^5$$

Equation 2.44

The gas mass flow rate in the Lin correlation is given by:

$$\dot{m}_g = \frac{A_t K_g \sqrt{2\Delta P_{TP}\, \rho_g}}{K_{Lin}\left(\frac{\dot{m}_w}{\dot{m}_g}\right)\sqrt{\frac{\rho_g}{\rho_w} + 1}} = \frac{A_t K_g \sqrt{2\Delta P_{TP}\, \rho_g}}{K_{Lin} X_{mod} + 1}$$

Equation 2.45

The water mass flow rate in Lin correlation can be obtained by the following equation:

$$\dot{m}_w = \frac{A_t K_w \sqrt{2\Delta P_{TP}\, \rho_w}}{K + \left(\frac{1}{X_{mod}}\right)}$$

Equation 2.46

2.5.4 The Smith & Leang correlation

The [13] is applicable to Orifice Plate and Venturi meters using the concept of a blockage factor (*BF*) to determine the gas mass flow rate. Equation (2.48) can be altered to take account of the liquid presence by introducing a parameter that accounts for the partial blockage (*BF*) of the pipe area by the liquid.

The *BF* is given by:

$$BF = 0.637 + 0.4211x - \frac{0.00183}{x^2}$$

Equation 2.47

where *x* is the mass flow quality.
It is well known that, the single gas mass flow rate $\dot{m}_g$ through a Venturi/orifice is given by;

$$\dot{m}_g = A_t K_g \sqrt{2\,\rho_g \Delta P_g}$$

Equation 2.48

where A_t is the area at the constriction, $K_g$is the gas flow coefficient, $\Delta P_g$is the gas pressure drop and $\rho_g$is the gas density.

The Smith and Leang correlation resolves for the single phase flow rate directly (i.e. introducing the (*BF*) directly into Equation (2.48) and taking into accounts the gas flow area A_t). Therefore; the gas mass flow rate in Smith & Leang correlation is given as:

$$\dot{m}_g = A_t K_g (BF) \sqrt{2\,\rho_g \Delta P_g}$$

Equation 2.49

The water mass flow rate in Smith & Leang correlation can be obtained by the following equation:

$$\dot{m}_w = \frac{A_t K_w (BF)\sqrt{2\,\rho_w \Delta P_w}}{x\sqrt{1-\beta^4}}$$

Equation 2.50

where A_t is the area at the constriction, K_w is the water flow coefficient, $\Delta P_w$is the water pressure drop, $\rho_w$is the water density and β is is the diameter ratio.

2.5.5 The de Leeuw correlation

The [15] and [16] uses a Venturi in wet gas applications. De Leeuw claims the liquid induced error in the gas flow prediction is not only dependent on the pressure and the Lockhart–Martinelli parameter but also the gas and liquid densiometric Froude numbers Fr_g and Fr_l:

$$Fr_g = \frac{U_{sg}}{\sqrt{gD}}\sqrt{\frac{\rho_g}{\rho_w - \rho_g}}$$

Equation 2.51

$$Fr_l = \frac{U_{sw}}{\sqrt{gD}}\sqrt{\frac{\rho_g}{\rho_w - \rho_g}}$$

Equation 2.52

where *D* is the pipe diameter, g=9.81ms^{-2}, U_{sg} is the superficial gas velocity and U_{sw} is the superficial liquid (water) velocity.

De Leeuw's correlation is given in the form of Chisholm correlation (Equation 2.43) with the constant of 1/4 replaced by a parameter denoted as *n*. De Leeuw claims that *n* is solely a function of the gas Froude number (Fr_g) as shown in Equations (2.53) and (2.54):

$$n = 0.41 \quad \text{for} \quad 0.5 \leq Fr_g \leq 1.5$$

Equation 2.53

$$n = 0.606(1 - e^{-0.746Fr_g}) \quad \text{for} \quad Fr_g \geq 1.5$$

Equation 2.54

De Leeuw used a simplified definition X_{simp} of the modified Lockhart–Martinelli parameter X by assuming the superficial flow coefficients to be equal, hence substituting $K_g = K_w$ in Equation (2.34). Therefore:

$$X_{simp} = \sqrt{\frac{\Delta P_w}{\Delta P_g}} = \left(\frac{\dot{m}_w}{\dot{m}_g}\right)\sqrt{\frac{\rho_g}{\rho_w}} = \left(\frac{1-x}{x}\right)\sqrt{\frac{\rho_g}{\rho_w}} = \frac{Fr_l}{Fr_g}$$

Equation 2.55

According to the Shell Expro two-phase flow pattern map [16], the gas densiometric Froude number value of 1.5 which divides Equations (2.29) and (2.30) is on the boundary of two different flow patterns. Hence, de Leeuw claims that the flow pattern plays an important part in the magnitude of the error caused by the gas being wet. The gas mass flow rate in the de Leeuw correlation is given by:

$$\dot{m}_g = \frac{A_t K_g \sqrt{2\Delta P_{TP}\,\rho_g}}{1 + \left[\left(\frac{\rho_w}{\rho_g}\right)^n + \left(\frac{\rho_g}{\rho_w}\right)^n\right] X_{simp} + X_{simp}^2}$$

Equation 2.56

where $K_g$is the gas flow coefficient, A_t is the area at the constriction, ΔP_{TP} is the two phase pressure drop and *n* is defined by Equations (2.29) and (2.30).

The water mass flow rate in the de Leeuw correlation is given by:

$$\dot{m}_w = \frac{A_t K_w \sqrt{2\Delta P_{TP}\, \rho_w}}{1 + \left[\left(\frac{\rho_w}{\rho_g}\right)^n + \left(\frac{\rho_g}{\rho_w}\right)^n\right] X_{simp} + X_{simp}^2}$$

Equation 2.57

where K_w is the water flow coefficient.

2.5.6 The Steven correlation

[2] introduced a further correlation in Venturis for wet gas metering. His study considered new independent data from the NEL (NEL is a leading provider of measurement services to the world's Oil and Gas Industry, and is the custodian of the UK's Standard for Flow Measurement, [80]) wet gas loop for a 6 inch Venturi and 0.55 diameter ratio geometry β, at pressures of 20, 40 and 60 bar at gas flow rates between 400 m^3/h and 1000 m^3/h: this correlation is also based on the Froude number (Equation (2.34)):

$$\sqrt{\frac{\Delta P_{TP}}{\Delta P}} = f\left(X, Fr_g\right)$$

Equation 2.58

Steven also undertook a detailed analysis of all previous correlations and their suitability for predicting the over-readings obtained in his work. He found that the de Leeuw correlation, based on a Venturi with 4 inch diameter and β = 0.40, was not suitable for the NEL wet gas loop. Steven correlation is given by:

$$\sqrt{\frac{\Delta P_{TP}}{\Delta P}} = \frac{1 + A_{Ste} X_{mod} + B_{Ste} Fr_g}{1 + C_{Ste} X_{mod} + D_{Ste} Fr_g}$$

Equation 2.59

where A_{Ste}, B_{Ste}, C_{Ste} and D_{Ste} are gas and liquid density ratios dependent on empirical constants and are given respectively by:

$$A_{Ste} = 2454.51\left(\frac{\rho_g}{\rho_w}\right)^2 - 389.568\left(\frac{\rho_g}{\rho_w}\right) + 18.146$$

Equation 2.60

$$B_{Ste} = 61.695\left(\frac{\rho_g}{\rho_w}\right)^2 - 8.349\left(\frac{\rho_g}{\rho_w}\right) + 0.223$$

Equation 2.61

$$C_{Ste} = 1722.917\left(\frac{\rho_g}{\rho_w}\right)^2 - 272.92\left(\frac{\rho_g}{\rho_w}\right) + 11.752$$

Equation 2.62

$$D_{Ste} = 57.387\left(\frac{\rho_g}{\rho_w}\right)^2 - 7.679\left(\frac{\rho_g}{\rho_w}\right) + 0.195$$

Equation 2.63

The gas mass flow rate in the Steven correlation can be expressed as:

$$\dot{m}_g = A_t K_g \sqrt{2\Delta P_{TP}\,\rho_g}\left(\frac{1 + C_{Ste}X_{mod} + D_{Ste}Fr_g}{1 + A_{Ste}X_{mod} + B_{Ste}Fr_g}\right)$$

Equation 2.64

The water mass flow rate in the Steven correlation is given by:

$$\dot{m}_w = \frac{C_{Ste}A_t\sqrt{2\Delta P_{TP}\,\rho_w}}{x\sqrt{1-\beta^4}\left(\frac{1 + A_{Ste}X_{mod} + B_{Ste}Fr_w}{1 + C_{Ste}X_{mod} + D_{Ste}Fr_w}\right)}$$

Equation 2.65

where Fr_w is the water densiometric Froude numbers.

2.5.7 Abbas model

[81] developed a new mathematical flow model for separated vertical (wet gas) flows through a Venturi meter. The new Abbas model for vertical annular (wet gas) flow through a Venturi meter depends on the measurements of the gas volume fractions at the inlet and the throat of the Venturi rather than relying on prior knowledge of the mass flow quality. This model is based on the fact that each phase flows separately and can be used to determine the gas mass flow rate and the water mass flow rate in annular (wet gas) flow. The gas mass flow rate $\dot{m}_g$ in the Abbas model is given by:

$$\dot{m}_g = C_{dg} \frac{\left[2\rho_{g1}\left(\left(\Delta P_{TP,wg} - \Delta P_H\right)\right)\right]^{\frac{1}{2}} A_1 A_2 \alpha_1 \alpha_2}{\left[\hat{P}^{-\frac{1}{\gamma}} (A_1\alpha_1)^2 - (A_2\alpha_2)^2\right]^{\frac{1}{2}}}$$

Equation 2.66

where C_{dg} is a gas discharge coefficient, ρ is the density, $\Delta P_{TP,wg}$ is the differential pressure in annular (wet gas) flow measured by a DP cell, ΔP_H is the magnitude of the hydrostatic head loss between the inlet and the throat of the Venturi, A is the cross sectional area, α is the gas volume fraction. The subscript 1 refers to the inlet of the Venturi, the subscript 2 refers to the throat of the Venturi and subscript g refers to the gas phase.

The water mass flow rate in Abbas model is given by:

$$\dot{m}_w = C_{dw}\sqrt{2\rho_w\left(\Delta P_{TP,wg} - \Delta P_H\right)} \frac{A_1(1-\alpha_1)A_2(1-\alpha_2)}{\sqrt{(1-\alpha_1)^2 A_1^2 - (1-\alpha_2)^2 A_2^2}}$$

Equation 2.67

where C_{dw} is a water discharge coefficient in annular (wet gas) flow. ρ_w is the water density. The Abbas model will be discussed in more details in chapter 3 because it is of significance regarding the work undertaken is this thesis.

2.6 Research Methodology

The aim was achieved by the following staged work plan. Again this work was decided upon the light of the literature reviews given in chapter 2.

- Design and build a Venturi meter to enable measurement of the gas volume fraction at the inlet and the throat of the Venturi using electrical conductance techniques.
- Design and build a digital liquid level sensor to measure the liquid film thickness at the inlet of the Venturi in vertical annular gas water flows.
- Design and build three separate electronic conductance circuits:-
  1. Two upstream ring sensors, designed to measure the film velocity by cross correlating signals between two ring sensors at the inlet of the Venturi.
  2. A digital level sensor, designed to measure the liquid film thickness in annular flow (and hence the gas volume fraction at the Venturi inlet).
  3. A throat ring sensor, designed to measure the gas volume fraction at the throat.
- Design and build a flow loop to establish annular two phase flows.
- Develop a mathematical model for annular two phase flow, predicting the gas and the water flow rates.
- Use a data acquisition device to integrate the system measurements and to control the operation of:-
  1. The throat conductance ring sensor.
  2. The digital level sensor.
  3. The inlet conductance ring sensors.
  4. The differential pressure sensor.

  Then to calculate gas volumetric rate; gas mass flow rate; gas volume fraction at inlet and the throat of the Venturi; and water flow rate).
- Undertake an experimental program of testing of the novel wet gas flow meter on the flow loop.
- Investigate the film thickness measurement measured by a conductance sensor and digital level sensor at the Venturi inlet
- Analyse the accuracy of the measurement technique.

- Characterise and calibrate the integrated system.

Summary

The aim of this research is to measure the gas and water volumetric flow rates in wet-gas annular flows to an accuracy of 1% on each phase.

A review of existing techniques for measuring two phase flows has been presented in Section 2.4. Including phase fraction measurements (such as, electrical conductance technique, electrical impedance technique and gamma radiation attenuation) and the phase velocity measurements (such as, a differential pressure measurements, cross-correlation technique, turbine flow meter, vortex flow meter and ultrasonic flow meter).
Previous models on Venturis and orifice meters used for two-phase flow measurements such as, Murdock, Chisholm, Lin, Smith and Leang, de Leeuw, Steven correlations and Abbas model were presented in Section 2.5.

These previous models (Murdock, Chisholm, Lin, Smith and Leang, de Leeuw, Steven models) are not good enough to achieve the aim of this research because they require a-prior knowledge of the mass flow quality *x*. Generally a- prior knowledge of the mass flow quality is required. In fact, online measurement of the mass flow quality is difficult and not practical in wet gas metering applications. Abbas model depends on the measurement of the gas volume fraction at the inlet and the throat of the Venturi and does not require a-prior knowledge of the mass flow quality *x* and so it will be investigated as a means of measuring the gas and water flow rates and developed if necessary.

In the current investigation, the design of Venturi tube with conductance sensors placed at the inlet and throat which (refer to Chapter 4) will be used for the measurement of gas and water flow rates in vertical annular gas-water two phase flow.

The Venturi with conductance sensors flow meter consists of Venturi meter, two ring conductance sensors (A and B) flush mounted with the inner surface of the Venturi inlet, which is capable of measuring the liquid film velocity at the Venturi inlet, ring

sensor B is capable of measuring the gas volume fraction and liquid film thickness and at the inlet of the Venturi, the digital level sensor placed at the Venturi inlet which is capable of measuring the inlet liquid film thickness and ring sensor C flush mounted with the inner surface of the Venturi throat, which is capable of measuring the gas volume fraction at the throat of the Venturi.

Based on the previous research it was decided in the present study to investigate the use of the Venturi with conductance sensors over other common differential pressure devices (e.g. orifice plates) and measurement techniques because the Venturi Meter is a popular flow meter for wet gas flow and it has a smooth flow profile that decreases the frictional losses which in turn, increases the reliability, predictability and repeatability of the device. Also the reason for choosing the electrical conductance technique in the present study because this technique has proven attractive for many industrial applications due to its fast response and relative simplicity in operation.

Chapter 3 The Measurements and Mathematical Modelling

Introduction

The fact that wet gas metering is becoming an increasingly important problem to the oil and gas industry [2] was introduced in Section 1.2. The Literature Review in the previous chapter confirms that wet gas metering is becoming increasingly important to the Oil and Gas Industry and various suggestion have been made by various researchers as to how to tackle this problem. While the Venturi meter is the most common differential pressure device for the metering of the unprocessed wet natural gas production flows, orifice plates have also been widely used. The advantage of the Venturi meter over the orifice plate is that the use of the Venturi meter is much more predictable and repeatable than the orifice plate for a wide range of flow conditions. Further, the smooth flow profile in a Venturi meter reduces frictional losses which (i) increases the reliability of the device and (ii) improves the pressure recovery. This chapter describes a new advanced design of Venturi meter with conductance sensors, which is capable of measuring the gas volume fraction at the inlet and the throat of the Venturi in annular gas-water two phase flows.

The contents of this chapter are a description of the measurements and mathematical model which enable the gas and water flow rates and mass flow rate to be determined.

3.1 The measurements we need to take

Here the measurements that need to be made are described and how these measurements will be integrated into the mathematical model to give the water and gas flow rates in annular flow.

- Measuring the liquid film velocity in wet gas flow U_f.
- Measuring the liquid film thickness δ.

- Measuring the gas volume fraction at inlet α_1.
- Measuring the water conductivity $\sigma_{w,m}$.
- Measuring the gas volume fraction at the throat α_2.
- Differential pressure between the Venturi inlet and the throat in wet gas flow ΔP.

The reasons for measuring the liquid film thickness, the liquid film velocity, the gas volume fraction at the inlet and the throat of the Venturi and the differential pressure between the inlet and the throat of the Venturi are to determine the gas volumetric flow rate and the water volumetric flow rate in annular flow.

3.1.1 The film velocity measurement: U_f

The film velocity in wet gas flow can be measured by cross-correlating the conductance signals between two upstream ring sensors at the inlet of the Venturi, using the associated conductance electronic circuits of the two sensors.

3.1.2 The film thickness measurements $(\delta$ or $\tilde{\delta})$

The film thickness in wet gas can be measured using a digital level sensor (dls) at the inlet of the Venturi (upstream), once the film thickness is obtained the water volume fraction $\alpha_{W,1}$ at the Venturi inlet can be determined using the following equation:

$$\alpha_{W,1} = (1 - \alpha_1) = \frac{2\tilde{\delta}}{R} + \left(\frac{\tilde{\delta}}{R}\right)^2$$

Equation 3.1

where $\tilde{\delta}$ is the symbol used to represent the liquid film thickness measured using the digital level sensor, R is the pipe radius and α_1 is the gas volume fraction at the inlet of the Venturi. We make these measurements to estimate the water flow rate Q_f of the liquid in the film using the following equation:

$$Q_f = \pi\, R^2\, \alpha_{w,1}\, U_f$$

Equation 3.2

where U_f is the liquid film velocity in wet gas flow measured by the cross-correlation technique.

An alternative method to measure the liquid film thickness in two phase flows is by using one of the upstream conductance ring sensors at the inlet of the Venturi. When a conductance ring sensor is used, the symbol δ is used to represent liquid film thickness. The gas volume fraction at the inlet of the Venturi needs to be determined by a conductance ring sensor in order for the film thickness at the inlet to be obtained. By using a conductance ring sensor the gas volume fraction may be obtained from a calibration curve (see Sections 5.1 and 3.1.4). Once the inlet gas volume fraction α_1 is obtained, the film thickness δ can then be easily determined using the following equation;

$$\delta \cong \frac{R(1-\alpha_1)}{2}$$

Equation 3.3

Once the gas volume fraction α_1 at the Venturi inlet obtained using a conductance ring sensor, the water volume fraction can be determined using the following equation;

$$\alpha_{W,1} = (1-\alpha_1)$$

Equation 3.4

Then the water flow rate Q_f of the liquid in the film can be determined by using Equation (3.2). It should be noted that in order to obtain the gas volume fraction α_1 at the Venturi inlet using a conductance ring sensor, the water conductivity is required. The water conductivity can be measured using proprietary conductivity meter. Alternatively if proprietary conductivity meter is not available, the water conductivity can be measured by using the digital level sensor in conjunction with one of the upstream conductance ring sensors. The water conductivity $\sigma_{w,m}$ measured in this

way can then be used to enable the gas volume fraction α_2 at the Venturi throat to be determined using the conductance ring sensor at the Venturi throat.

3.1.3 The Gas volume fraction measurement α_1

One of the upstream conductance sensors needs to be calibrated in order for its cell constant to be determined. This is done using a bench calibration system for one upstream ring sensor (see Section 5.1.1). Nylon rods are inserted through the inlet of the Venturi meter. The gap between the outer surface of the rod and the inner surface of the pipe wall is filled with water of conductivity $\sigma_{w,ref}$, representing the water film that would occur in a real annular flow. From the conductance electronic circuit channel B as shown in Figure 4-18 we know the feedback resistance R_{fb} and the excitation voltage V_{in}. The voltage measurement equation is

$$V(\alpha_1) = V_{in}\, R_{fb}\, \sigma_{w,ref}\, K(\alpha_1)$$

Equation 3.5

where $\sigma_{w,ref}$ is the known water conductivity and $K(\alpha_1)$ is the ring sensor cell constant. Therefore the cell constant is given by:

$$K(\alpha_1) = \frac{V(\alpha_1)}{V_{in}\, R_{fb} \sigma_{w,ref}}$$

Equation 3.6

where $V(\alpha_1)$ is the output voltage from the measurement conductance circuit at the Venturi inlet (see Section 5.1.1). Hence we can find the relationship between the cell constant $K(\alpha_1)$ and the gas volume fraction α_1 at the inlet to the Venturi (refer to Figure 5-5 of calibration curve $K(\alpha_1)$ vs α_1).

If V_{in} and R_{fb} are known constants and we also measure the offset voltage V_{off} when water conductivity equals zero($\sigma_w = 0$), when the pipe is full of air only then we may simplify the definition of the cell constant to $\overline{K}(\alpha_1)$.

where

$$\overline{K}(\alpha_1) = \frac{V(\alpha_1) - V_{off}}{\sigma_{w,ref}}$$

Equation 3.7

where $V(\alpha_1)$ is the value of the output voltage from the conductance measurement circuit at the inlet of the Venturi and V_{off} is a dc offset. This cell constant $\overline{K}(\alpha_1)$ can be used either (i) to determine the inlet gas volume fraction α_1, if proprietary conductivity meter is used or (ii) to enable measurement of the water conductivity, when used in conjunction with the digital level sensor, if a proprietary conductivity meter is not used.

3.1.4 The water conductivity measurements

We now need to know how the conductivity sensor will be used with the digital level sensor in a real application to find the water conductivity. The film thickness $\tilde{\delta}$ is obtained from the digital level sensor. Then the following equation is used to determine the inlet gas volume fraction α_1.

$$\alpha_1 = 1 - \frac{2\tilde{\delta}}{R} + \left(\frac{\tilde{\delta}}{R}\right)^2$$

Equation 3.8

From the gas volume fraction α_1 at the Venturi inlet we may use the corresponding cell constant value $\overline{K}(\alpha_1)$ from the calibration data (see Section 5.1). Then the actual water conductivity $\sigma_{w,m}$ can be determined under the actual flowing conditions by using the following equation:

$$\sigma_{w,m} = \frac{V(\alpha_1) - V_{off}}{\overline{K}(\alpha_1)}$$

Equation 3.9

If the water conductivity σ_w in annular air-water flow is already known e.g. by using a proprietary conductivity sensor then we may write cell constant $\overline{K}(\alpha_1)$ from Equation (3.7):

$$\overline{K}(\alpha_1) = \frac{V(\alpha_1) - V_{off}}{\sigma_w}$$

Equation 3.10

Consequently the gas volume fraction at the Venturi inlet α_1 can be directly obtained (without the need for a digital level sensor) from the known relationship between $\overline{K}(\alpha_1)$ and α_1 (obtained from calibration see Section 5.1.5). The value of α_1 obtained in this way is denoted $\alpha_{1,rs}$ which represents the gas volume fraction measured using a conductance ring sensor B at the Venturi inlet in Chapter 7.

3.1.5 The Gas volume fraction measurement at the throat α_2

The conductance ring sensor C at the throat of the Venturi flow meter needs to be calibrated in order for its cell constant to be determined. This is done using a bench calibration system for ring sensor C at the throat of the Venturi (see Section 5.1.3). Nylon rods are inserted through the throat of the Venturi meter. The gap between the outer surface of the rod and the inner surface of the pipe wall is filled with water of known conductivity $\sigma_{w,ref}$, representing the water film that would occur in a real annular flow. From the conductance electronic circuit for the throat as shown in Figure 4-20 we know the output voltage and the dc offset therefore the cell constant at the throat is given by:

$$\overline{K}^t(\alpha_2) = \frac{V^t(\alpha_2) - V^t_{off}}{\sigma_{w,m}}$$

Equation 3.11

where $V^t(\alpha_2)$ is the output voltage from the conductance measurement circuit at the throat of the Venturi (refer to Figure 4-20) and V^t_{off} is a dc offset measured when the pipe is full of air only and hence the water conductivity α_w was effectively zero.

The water conductivity $\sigma_{w,m}$ has been obtained from Equation (3.9) and the relationship between the cell constant $\overline{K}^t(\alpha_2)$ of the throat conductance sensor and the gas volume fraction α_2 at the throat is known from calibration (see Section 5.1.5).

Therefore we can determine the gas volume fraction α_2 at the throat of the Venturi using the value of $\overline{K}^t(\alpha_2)$ and the known relationship between $\overline{K}^t(\alpha_2)$ and α_2 (see Section 5.1.5). Alternatively, if the water conductivity in known from a proprietary conductivity meter Equation (3.11) may also be used to the gas volume fraction α_2 at the Venturi throat.

3.1.6 Differential pressure in wet gas flow ΔP

The differential pressure will be measured using the DP cell sensor. From Figure 3-1, given that the lines connected to the pressure tapping of the throat and the inlet of the Venturi to the DP cell sensor are filled with water, the gas-water two phase differential pressure drop across the Venturi in annular (wet gas) flow can be written as:

$$\Delta P_{TP,wg} = (P_1 - P_2)$$

Equation 3.12

where P_1 and P_2 are the static pressures at the inlet and the throat of the Venturi.

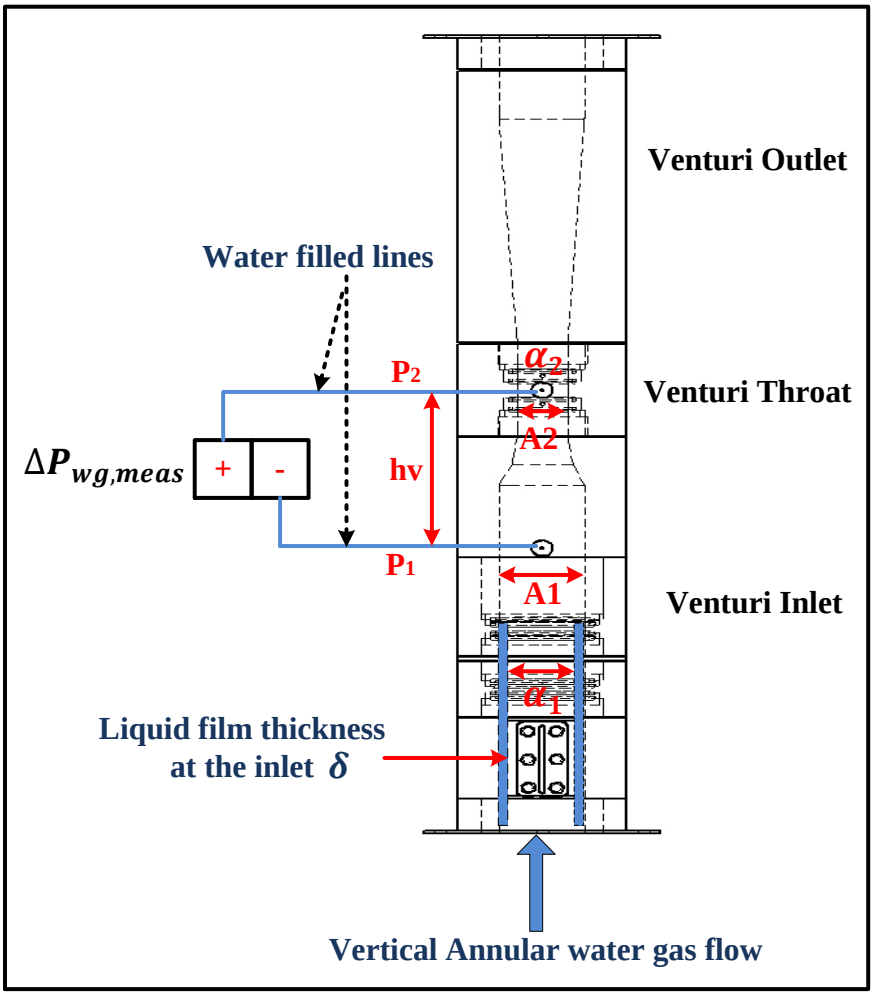

Figure 3-1 Vertical annular gas-water flow through a Venturi

The differential pressure cell (DP cell) used in the present study cannot read negative differential pressure drops between two points (i.e. DP cell cannot read a differential pressure if the pressure at the 'high side +' input is lower than the pressure at the 'low side -' input (refer to Figure 3-1)). In two phase air-water flow through a Venturi flow meter, the pressure drop across the Venturi flow meter may change its sign from positive to negative. In other words, in a two phase flow through a Venturi flow meter, the inlet and throat of the Venturi are connected to the DP cell through water filled lines, because the mixture density is less than the water density the pressure at the high (sign +) input of the DP cell can be lower than the pressure at the low (sign -) input (refer to Figure 3-1).

This section describes when the high and low sides of the DP cell are alternately sensor connected to the inlet and throat of the Venturi flow meter. As described above the high pressure must always be connected to the high (sign +) of the DP cell for a correct differential pressure to be measured. If the high pressure is not connected to the high (sign +). Experimentally we do ensure that the high pressure is always connected to the high (sign +) input by measuring the voltage of the DP cell, the output voltage from the DP cell must be always above 1 Volt.

With reference to Figure 6.3 when the high side of the DP cell sensor is connected to throat then

$$\Delta P_{wg,meas} = \rho_w g h_v + P_2 - P_1$$

Equation 3.13

where $\Delta P_{wg,meas}$ is the differential pressure in annular water-gas flow measured by the DP cell sensor, ρ_w is the water density, g is the acceleration due to gravity and h_v is the pressure tapping separation between inlet and throat of the Venturi. The subscripts *w* and *g* refer to the water and gas phases.

By rearranging Equations (3.12) and (3.13)

$$\Delta P_{wg,meas} = \rho_w g h_v - \Delta P_{TP,wg}$$

Equation 3.14

where $\Delta P_{TP,meas}$ is given in terms of $\Delta P_{wg,meas}$

Equation (3.14), when the high side of the DP cell sensor is connected to the throat, can be written as:

$$\Delta P_{TP,wg} = \rho_w g h_v - \Delta P_{wg,meas}$$

Equation 3.15

With reference to Figure 6.3 when the low side of the DP cell sensor is connected to throat then

$$\Delta P_{wg,meas} = (P_1 - P_2) - (\rho_w g h_v)$$

Equation 3.16

By rearranging Equations (3.12) and (3.16)

$$\Delta P_{wg,meas} = \Delta P_{TP,wg} - \rho_w g h_v$$

Equation 3.17

$$\Delta P_{TP,wg} = \Delta P_{wg,meas} + \rho_w g h_v$$

Equation 3.18

The voltage of $\Delta P_{TP,wg}$ obtained using either Equation (3.15) or Equation (3.18) can then be combined with the Abbas model (2010) [81] described below in Section 3.2 to enable prediction of the gas mass and volumetric flow rate in annular two phase flow.

3.2 Vertical annular wet gas flow model

It should be noted here that the mathematical model described in this section for vertical annular (wet gas) flow through a Venturi meter is based on a model by[81].

Measuring the gas flow rate in annular wet gas flow

For the gas phase, the Bernoulli equation can be written as;

$$P_{g1} + \frac{1}{2}\,\rho_{g1}\,U_{g1}^2 = P_{g2} + \frac{1}{2}\,\rho_{g2}\,U_{g2}^2$$

Equation 3.19

where P is the static pressure, ρ is the density and U the velocity. The subscript 1 refers to the inlet of the Venturi, the subscript 2 refers to the throat of the Venturi and subscript g refers to the gas phase.

The differential pressure relevant to the Bernoulli equation is

$$\Delta P_{TP,wg} - \Delta P_H$$

Equation 3.20

where ΔP_H is the magnitude of the hydrostatic head loss between the inlet and the throat of the Venturi. ΔP_H (from Equation (3.69) [81]) is given by:

$$\Delta P_H = gh_i\{\rho_w(1-\alpha_1) + \rho_{g1}\alpha_1\} + gh_c\{\rho_w(1-\bar{\alpha}) + \bar{\rho}_g\bar{\alpha}\} + gh_{tt}\{\rho_w(1-\alpha_2) + \rho_{g2}\alpha_2\}$$

Equation 3.21

Refer to Figure 3-2 the hydrostatic head loss term ΔP_H in Equation (3.39) can be calculated by making the assumption that the mean gas volume fraction in the converging section of the Venturi is $\bar{\alpha}$ (refer to Figure 3-2) where:

$$\bar{\alpha} = \frac{\alpha_1 + \alpha_2}{2}$$

Equation 3.22

However, if the gas density $\rho_g \cong 0$ then Equation (3.21) can be written as:

$$\Delta P_H = gh_i\,\rho_w\,(1-\alpha_1) + gh_c\,\rho_w\left(1 - \left(\frac{\alpha_1+\alpha_2}{2}\right)\right) + gh_{tt}\,\rho_w\,(1-\alpha_2)$$

Equation 3.23

where $h_i, h_c,$ and h_{tt} are the heights defined in Figure 3-2 and ρ_w is the water density.

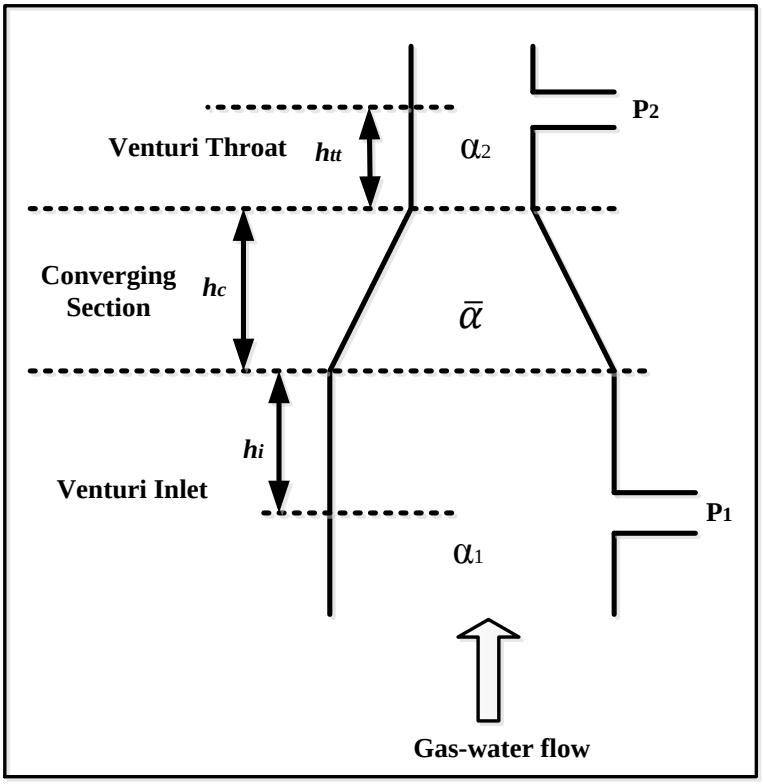

Figure 3-2 Venturi Inlet, converging and throat sections

From Equation (3.34) in [81] for the gas phase the continuity equation of the gas phase is given by:

$$U_{g1}A_1\alpha_1\rho_{g1} = U_{g2}A_2\alpha_2\rho_{g2} = \dot{m}_g$$

Equation 3.24

where A_1 is the cross sectional area at the inlet of the Venturi, A_2 is the cross sectional area at the throat of the Venturi and $\dot{m}_g$ is the gas mass flow rate.

From equation (3.36) in [81].

$$\rho_{g2} = \rho_{g1}\left(\hat{P}\right)^{1/\gamma}$$

Equation 3.25

where

$$\hat{P} = \frac{P_2}{P_1}$$

Equation 3.26

where γ is the specific heat ratio for air at atmospheric pressure given by $\left(\gamma = \frac{C_p}{C_v} = 1.401\right)$ where c_p and c_v are the specific heats at constant pressure and volume respectively.

Equation (3.24) can be re-arranged to give:

$$U_{g1}A_1\alpha_1 = U_{g2}A_2\alpha_2\left(\hat{P}\right)^{1/\gamma}$$

Equation 3.27

Therefore $$\left(U_{g2}\right)^2\left[\hat{P}\right]^{2/\gamma} = \left(U_{g1}\right)^2\left[\frac{A_1\alpha_1}{A_2\alpha_2}\right]^2$$

Equation 3.28

Equation (3.28) can be re-arranged to give:

$$\left(U_{g2}\right)^2 = \left(U_{g1}\right)^2\left[\frac{A_1\alpha_1}{A_2\alpha_2}\right]^2\left[\hat{P}\right]^{-\frac{2}{\gamma}}$$

Equation 3.29

From the Bernoulli Equation (3.20) and Equation (3.25)

$$P_1 - P_2 = \frac{1}{2}\,\rho_{g1}\left[\hat{P}^{-\frac{1}{\gamma}}\,{U_{g2}}^2 - {U_{g1}}^2\right]$$

Equation 3.30

The pressure should be different for the gas phase compared with the water phase because it might come from the fact that the gas phase is compressible while the water phase is an incompressible.

From Equation (3.29) and Equation (3.30)

$$P_1 - P_2 = \frac{1}{2}\,\rho_{g1}\left[\hat{P}^{-\frac{1}{\gamma}}\;\hat{P}^{-\frac{2}{\gamma}}\;{U_{g1}}^2\;\left[\frac{A_1\alpha_1}{A_2\alpha_2}\right]^2 - {U_{g1}}^2\right]$$

Equation 3.31

$$P_1 - P_2 = \frac{1}{2}\,\rho_{g1}{U_{g1}}^2\left[\hat{P}^{-\frac{1}{\gamma}}\;\;\left[\frac{A_1\alpha_1}{A_2\alpha_2}\right]^2 - 1\right]$$

Equation 3.32

Refer to Figure 3-1

$$P_1 - P_2 \equiv \Delta P_{TP,wg} - \Delta P_H$$

Equation 3.33

Combining Equations (3.31) and (3.33) gives:

$$\Delta P_{TP,wg} - \Delta P_H = \frac{1}{2}\,\rho_{g1}{U_{g1}}^2\left[\hat{P}^{-\frac{1}{\gamma}}\;\;\left[\frac{A_1\alpha_1}{A_2\alpha_2}\right]^2 - 1\right]$$

Equation 3.34

From Equation (3.34) U_{g1} is given by:

$$U_{g1} = \sqrt{\frac{2\left(\Delta P_{TP,wg} - \Delta P_H\right)}{\rho_{g1}}}\;\sqrt{\frac{1}{\left(\hat{P}^{-\frac{1}{\gamma}}\right)\left[\frac{A_1\alpha_1}{A_2\alpha_2}\right]^2 - 1}}$$

Equation 3.35

From Equation (3.24) we have:

$$\dot{m}_g = \rho_{g1}U_{g1}A_1\alpha_1$$

Equation 3.36

where $\dot{m}_g$ is the predicted gas mass flow rate in annular (wet gas) flow through the Venturi.

Combining Equations (3.35) and (3.36) gives:

$$\dot{m}_g = \sqrt{2\rho_{g1}\left(\Delta P_{TP,wg} - \Delta P_H\right)} \sqrt{\frac{A_1^2\alpha_1^2}{\left(\hat{P}^{-\frac{1}{\gamma}}\right)\left[\frac{A_1\alpha_1}{A_2\alpha_2}\right]^2 - 1}}$$

Equation 3.37

Now from Equation (3.37)

$$\sqrt{\frac{A_1^2\alpha_1^2}{\left(\hat{P}^{-\frac{1}{\gamma}}\right)\left[\frac{A_1\alpha_1}{A_2\alpha_2}\right]^2 - 1}} = \sqrt{\frac{(A_1\alpha_1)^2}{\hat{P}^{-\frac{1}{\gamma}}\left((A_1\alpha_1)^2\right) - (A_2\alpha_2)^2}{(A_2\alpha_2)^2}}$$

$$= \sqrt{\frac{(A_1\alpha_1)^2(A_2\alpha_2)^2}{\hat{P}^{-\frac{1}{\gamma}}(A_1\alpha_1)^2 - (A_2\alpha_2)^2}}$$

$$= A_1A_2\alpha_1\alpha_2 \sqrt{\frac{1}{\hat{P}^{-\frac{1}{\gamma}}(A_1\alpha_1)^2 - (A_2\alpha_2)^2}}$$

Equation 3.38

Combining Equations (3.37) and (3.38) gives:

$$\dot{m}_g = \frac{\left[2\rho_{g1}\left(\left(\Delta P_{TP,wg} - \Delta P_H\right)\right)\right]^{\frac{1}{2}} A_1A_2\alpha_1\alpha_2}{\left[\hat{P}^{-\frac{1}{\gamma}}(A_1\alpha_1)^2 - (A_2\alpha_2)^2\right]^{\frac{1}{2}}}$$

Equation 3.39

which agrees with Equation (3.66) of [81], where $\dot{m}_g$ is the predicted gas mass flow rate in annular (wet gas) flow through the Venturi.

The gas mass flow rate in annular (wet gas) flow through the Venturi can be determined from Equation (3.39). If the reference gas mass flow rate in annular (wet gas) flow is known, it is possible to define a discharge coefficient C_{dg} for the gas phase as follows:

$$\dot{m}_{gref} = C_{dg}\dot{m}_g$$

Equation 3.40

where $\dot{m}_{gref}$ is the reference gas mass flow rate in annular (wet gas) flow and C_{dg} is the gas discharge coefficient which can be expressed as:

$$C_{dg} = \frac{\dot{m}_{gref}}{\dot{m}_g}$$

Equation 3.41

The gas volumetric flow rate Q_g can be obtained using the following equation:

$$Q_g = \frac{\dot{m}_g}{\rho_{g1}}$$

Equation 3.42

where the gas mass flow rate in annular (wet gas) flow $\dot{m}_g$ is given by Equation (3.39) and where the gas density ρ_{g1} in Equation (3.42) is given by:

$$\rho_{g1} = \frac{P_1}{\gamma T_1}$$

Equation 3.43

Where P_1 and T_1 are the absolute pressure and absolute temperature at the inlet section respectively.

Measuring the mass flow rate of water in annular (wet gas)

Measuring the mass flow rate of water in the film of an annular (wet gas) flow Q_w also can be obtained from Equation (3.2):

$$\dot{m}_w = \rho_w \, Q_w$$

Equation 3.44

where ρ_w is the water density and the volumetric flow rate $Q_w$is given by Equation (3.2). It should be noted that for a given phase (gas or water), the mass flow rate, $\dot{m}$ is related to the volumetric flow rate, Q by:

$$\dot{m} = \rho \, Q$$

Equation 3.45

where ρ is the density of the phase in question. Hence, the gas and water volumetric flow rates can be calculated using Equations (3.42) and (3.2).

3.3 Vertical homogenous gas-water two phase flow model

In the previous section the mathematical a model of [81] for vertical annular (wet gas) flow through a Venturi flow meter was described and will be used to determine the gas and water flow rates in the present study. An alternative model is also described in this section. This model is a homogenous model for gas water two phase flow through a Venturi when the slip between the gas and water is assumed to be zero. The mixture density at the Venturi throat and the mixture density at the inlet of the Venturi can be assumed equal.

The assumption of the homogeneous flow model is that the two phases are mixed well and both phases travel at the same velocity; therefore, they can be treated as if there is only one phase. Figure 3-3 shows homogenous gas-water two phase flow for the general case of a vertical Venturi meter.

From Equations (3.15) and (3.18) the Venturi differential pressure relevant to Bernoulli's equation is ΔP_B

$$\Delta P_B = \Delta P_{TP,wg} - \Delta P_H$$

Equation 3.46

where ΔP_H is given by Equation (3.23) and where $\Delta P_{TP,wg}$ is given using either Equation (3.15) or Equation (3.18).

One method for defining the homogenous mixture density is using the relationship:

$$\rho_m = \rho_w(1 - \bar{\alpha})$$

Equation 3.47

The mixture density in the homogenous model defined by Equation (3.47) will be used in Section 7.9 for measuring the homogenous mixture volumetric flow rate and the gas volumetric flow rate in homogenous model.

The term $\bar{\alpha}$ in Equation (3.47) is the mean gas volume fraction in the converging section of the Venturi, which can be obtained using the following equation:

$$\bar{\alpha} = \frac{\alpha_1 + \alpha_2}{2}$$

Equation 3.48

From Bernoulli's equation, it is possible to write that:

$$\Delta P_B = \frac{1}{2}\rho_m(U_2^2 - U_1^2)$$

Equation 3.49

where ρ_m is the mixture density and U is the fluid velocity. The subscripts 1 and 2 refer to the inlet and the throat of the Venturi respectively.

Assuming constant mixture density the mass conservation equation is given by:

$$U_1 = U_2\frac{A_2}{A_1}$$

Equation 3.50

where $A_1$and A_2 are the cross sectional areas at inlet and the throat of the Venturi.
From Equations (3.49) and (3.50), it is possible to write:

$$U_2^2 = \frac{2A_1^2}{\rho_m(A_1^2 - A_2^2)}\Delta P_B$$

Equation 3.51

It is well known that the volumetric flow rate of the homogenous mixture, Q_m can be expressed as:

$$Q_m = (U_2 A_2)$$

Equation 3.52

Combining Equations (3.51) and (3.52) gives:

$$Q_m = \left\{\frac{2\,\Delta P_B}{\rho_m}\right\}^{\frac{1}{2}} \frac{A_2}{\left[1 - \left(\frac{A_2}{A_1}\right)^2\right]^{\frac{1}{2}}}$$

Equation 3.53

where Q_m is the homogenous (mixture) volumetric flow rate.
ΔP_B is given by Equation 3.46 and ρ_m is given by Equation (3.47). It is clear from Equation (3.53) that, in order to determine Q_m, the mean gas volume fraction in the converging section of the Venturi, $\bar{\alpha}$ must be known.
The reference homogenous volumetric flow rate can be obtained from the following equation:

$$Q_{m,ref} = Q_{g,ref} + Q_{w,ref}$$

Equation 3.54

where $Q_{g,ref}$ and $Q_{w,ref}$ are the reference gas and water volumetric flow rates respectively.

The homogenous mixture discharge coefficient C_{dm} is given by:

$$C_{dm} = \frac{Q_{m,ref}}{Q_m}$$

Equation 3.55

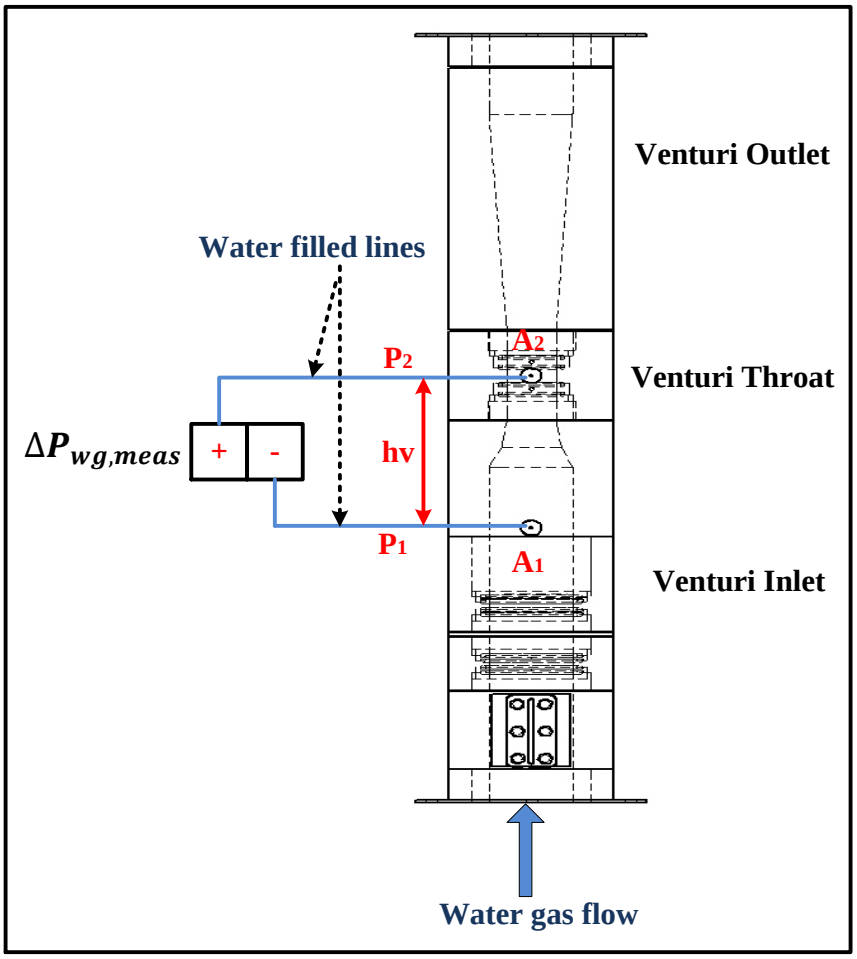

Figure 3-3: Vertical homogenous wet gas flow in a Venturi meter

3.4 Homogenous model assuming no slip between water and air in wet gas flow

An alternative method for defining the homogenous mixture density is given below. Since then is no slip between the gas and liquid, the gas volume fraction in the homogenous model α_{ns} can be defined as:

$$\alpha_{ns} = \frac{Q_{g,ref}}{Q_{g,ref} + Q_{w,ref}}$$

Equation 3.56

where α_{ns} is the no-slip gas volume fraction, $Q_{g,ref}$ is the reference gas flow rate and $Q_{w,ref}$ is the reference water flow rate. The mixture density in the homogenous model, assuming no slip gas volume fraction, is given by:

$$\rho_{m,ns} = p_w(1 - \alpha_{ns})$$

Equation 3.57

The mixture density in the homogenous model ρ_m defined by Equation (3.47) will be used in Section 7.9 to determine the predicted mixture volumetric flow rate and predicted gas volumetric flow rate where the gas volume fraction at the inlet α_1 and the throat α_2 of the Venturi are measured values obtained using the conductance Venturi system described in Chapter 4. The mixture density in the homogenous model $\rho_{m,ns}$ defined by Equation (3.57) and while assumes the no slip gas volume fraction will be used in Section 7.10 for measuring the homogenous mixture volumetric flow rate and the water and gas volumetric flow rates.

The magnitude of the hydrostatic head loss ΔP_H between the inlet and the throat of the Venturi in the homogenous model when the no slip gas volume fraction is assumed is given by:

$$\Delta P_H = g\ (h_i + h_c + h_{tt})\ \rho_w(1 - \alpha_{ns})$$

Equation 3.58

where $h_i, h_c,$ and h_{tt} are the heights defined in Figure 3-2 and ρ_w is the water density.

The gas and water flow rates in the homogenous model when the no slip gas volume fraction is assumed can be obtained using Equations (3.59) and (3.60) respectively:

$$Q_{g,ns} = \alpha_{ns} Q_{m,ns}$$

Equation 3.59

$$Q_{w,ns} = (1 - \alpha_{ns})\, Q_{m,ns}$$

Equation 3.60

where

$$Q_{m,ns} = \left\{\frac{2\,\Delta P_B}{\rho_{m,ns}}\right\}^{\frac{1}{2}} \frac{A_2}{\left[1 - \left(\frac{A_2}{A_1}\right)^2\right]^{\frac{1}{2}}}$$

Equation 3.61

It is clear from Equation (3.61) that, in order to determine the mixture volumetric flow rate $Q_{m,ns}$ from the homogenous Venturi model assuming the no slip gas volume fraction, the differential pressure ΔP_B defined using Equation (3.46) and Equation (3.58) and either Equation (3.15) or (3.18) must be known. Furthermore, the homogenous mixture density $\rho_{m,ns}$ assuming the no slip gas volume fraction must be known.

Summary

The measurements of (liquid film velocity, liquid film thickness, gas volume fraction at inlet, the gas volume fraction at the throat, water conductivity and differential pressure between the Venturi inlet and the throat) and how these measurements will be integrated into the mathematical model which enable the volumetric gas and water flow rates and mass flow rate in annular flow to be determined has been described (see Section 3.1).

The mathematical a model of Abbas for vertical annular flow through a Venturi flow meter was described and Abbas model will be used in the present study to determine the gas and water flow rates in vertical annular flow (see Section 3.2).

An alternative model is also has been described in this Chapter. This model is a homogenous model for gas water two phase flow through a Venturi when the slip between the gas and water is assumed to be zero (see Section 3.3).

Also an alternative method for defining the homogenous mixture density is described. The mixture density in the homogenous model $\rho_{m,ns}$ defined by Equation (3.57) and while assumes the no slip gas volume fraction will be used in Section 7.10 for measuring the homogenous mixture volumetric flow rate and the water and gas volumetric flow rates (see Section 3.4).

Chapter 4 Design and Construction of a Conductance Venturi Meter

Introduction

Wet gas metering is becoming an increasingly important problem to the oil and gas industry. The Venturi meter is a favoured device for the metering of the unprocessed wet natural gas production flows. Various combinations of techniques have been employed in annular gas-liquid two phase flows to measure the flow parameters (e.g. liquid film thickness, gas volume fraction and the phase flow rates). One of the most useful methods which has proved attractive for many multiphase flow applications is the electrical conductance technique.

The Venturi designed for this work is a Conductance Venturi Meter that is capable of measuring the gas volume fractions at the inlet and the throat of the Venturi meter using a conductance technique. Annular flow in such a device is highly complex and therefore, in order to determine the gas and water flow rates in vertical annular flow using Equations (3.42) and (3.2), measurement of gas volume fraction α_1 at the inlet, the gas volume fraction α_2 at the throat of the Venturi, the film thickness δ and the film velocity $U_{f,xc}$, must all be achieved. To do this, a new novel Venturi meter with conductance sensors was designed and constructed.

This device enables gas volume fraction measurements to be made in vertical gas-water flow. Two upstream conductance ring sensors (A and B ring sensors) at the inlet were used to measure the film velocity $U_{f,xc}$ by cross correlating signals between ring sensor A and ring sensor B at the inlet of the Venturi. One of the upstream conductance ring sensors (ring sensor B) could also used to measure the film thickness δ in annular two phase flow (and hence the gas volume fraction α_1) at the Venturi inlet if used in conjunction with a proprietary conductivity meter. Conductance ring sensor C at the throat of the Venturi was used to obtain the gas volume fraction α_2 at the throat of the Venturi.

A digital liquid film level sensor was designed and constructed at the inlet of the Venturi to measure the liquid film thickness $\tilde{\delta}$ in annular water-gas two phase flows (and hence the gas volume fraction α_1) at the inlet of the Venturi. It should again be mentioned if the water conductivity σ_w in annular air-water flow is known by using a proprietary conductivity sensor then we do not need the digital level sensor in order to obtain the inlet gas volume fraction α_1. The digital level sensor is only really needed if the water conductivity σ_w is not known however it also provides a useful "check" on the value of α_1 obtained from upstream conductance ring sensor B.

Section (4.1) of this chapter presents the design and construction of the Conductance Venturi Meter with sensors capable of measuring the gas volume fraction at the inlet and the throat of the Venturi in vertical gas-water two phase flows. This chapter also presents the design and construction of the conductance electronic circuits for upstream ring sensors A and B, for the throat ring sensor C and for the conductance electronic circuit for the digital level sensor in sections (4.2.1), (4.2.2) and (4.2.3) respectively.

4.1 Design of the Venturi meter with inlet and throat conductance sensors

The Venturi meter was designed and constructed at the University of Huddersfield to study the wet gas measurements in vertical annular gas-water two phase flows; Figure 4-1 shows the dimensions of the Venturi meter with conductance sensors at the inlet and throat. The internal diameter of the Venturi inlet is equal to 50mm and the internal diameter of the Venturi throat is equal to 30mm. The Venturi meter and its 2D drawing were designed using a SolidWorks application and constructed by University technicians.

In order to determine the gas volumetric flow rate Q_g and water volumetric flow rate Q_w using Equations (3.42) and (3.2) respectively, the following must all be obtained:

- The film velocity $U_{f,xc}$ in wet gas flow.
- The film thickness δ at the inlet.

- The gas volume fraction α_1 at the Venturi inlet.
- The gas volume fraction α_2 at the throat of the Venturi.
- Measurements of the differential pressure $\Delta P_{TP,wg}$.
- The Appropriate densities of the air and water.

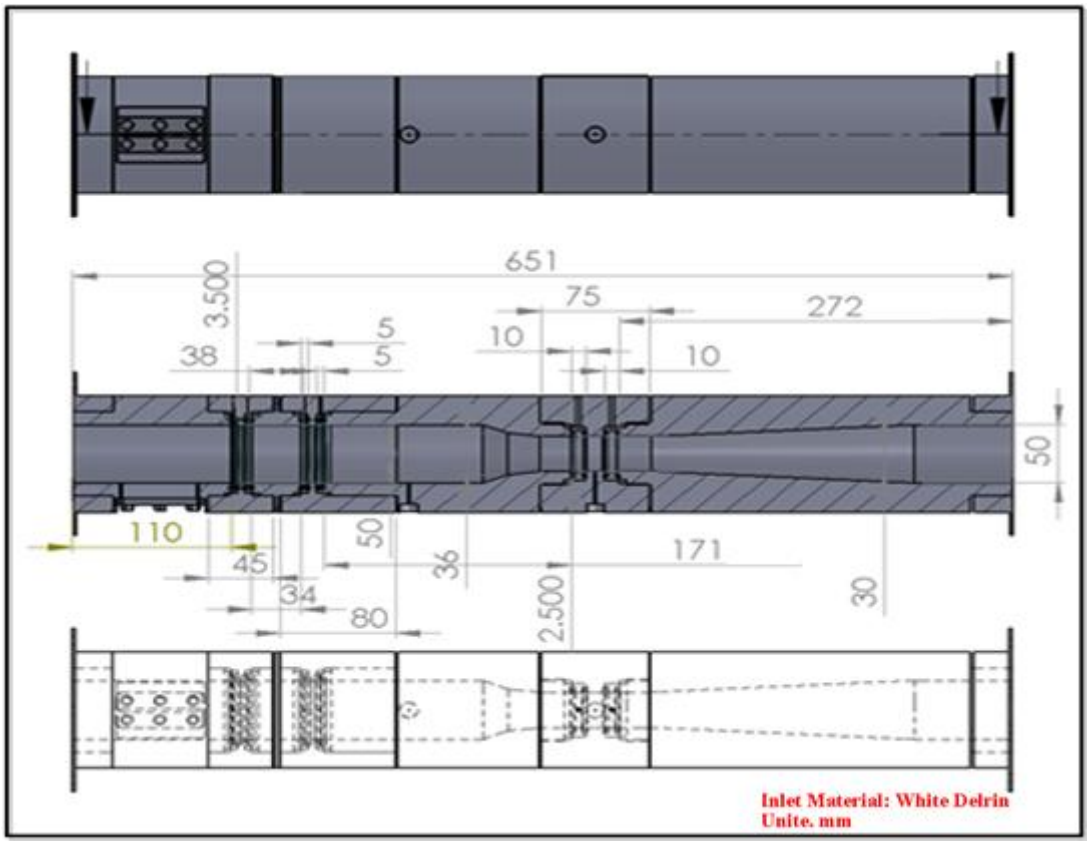

Figure 4-1: The design of the conductance Venturi meter

The differential pressure was measured by a Honeywell differential pressure transmitter. The DP cell sensor was connected between the inlet and throat of the Venturi meter via water filled lines. Atmospheric pressure was measured from a barometer.

A schematic diagram of the Venturi meter with conductance sensors at the inlet and throat (which represents the test section used to investigate vertical gas-water two phase flows) is shown in Figure 4-2.

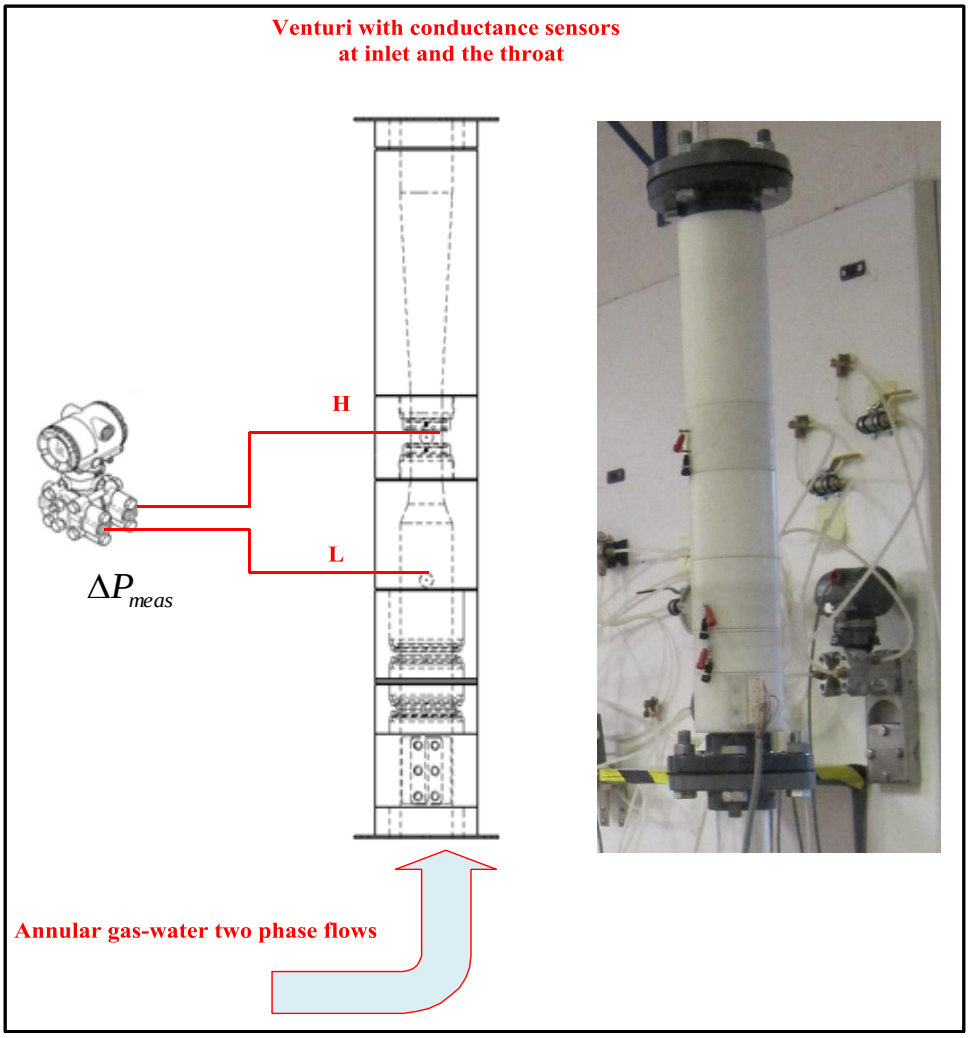

Figure 4-2: A schematic diagram of the Venturi meter with Venturi photograph

As shown in Figure 4-3, the components of the Venturi meter with conductance sensors consist of:

- Two threaded flanges at the inlet and outlet of the Venturi.
- Twelve O-rings.
- Six stainless steel ring sensors electrodes.
  - Ring sensor B comprising two ring sensors electrodes (1 and 2) at the inlet.
  - Ring sensor A comprising two ring sensors electrodes (3 and 4) at the inlet.
  - Ring sensor C comprising two ring sensors electrodes (5 and 6) at the throat.

- Digital level sensor head at the inlet.
- Throat and outlet sections.

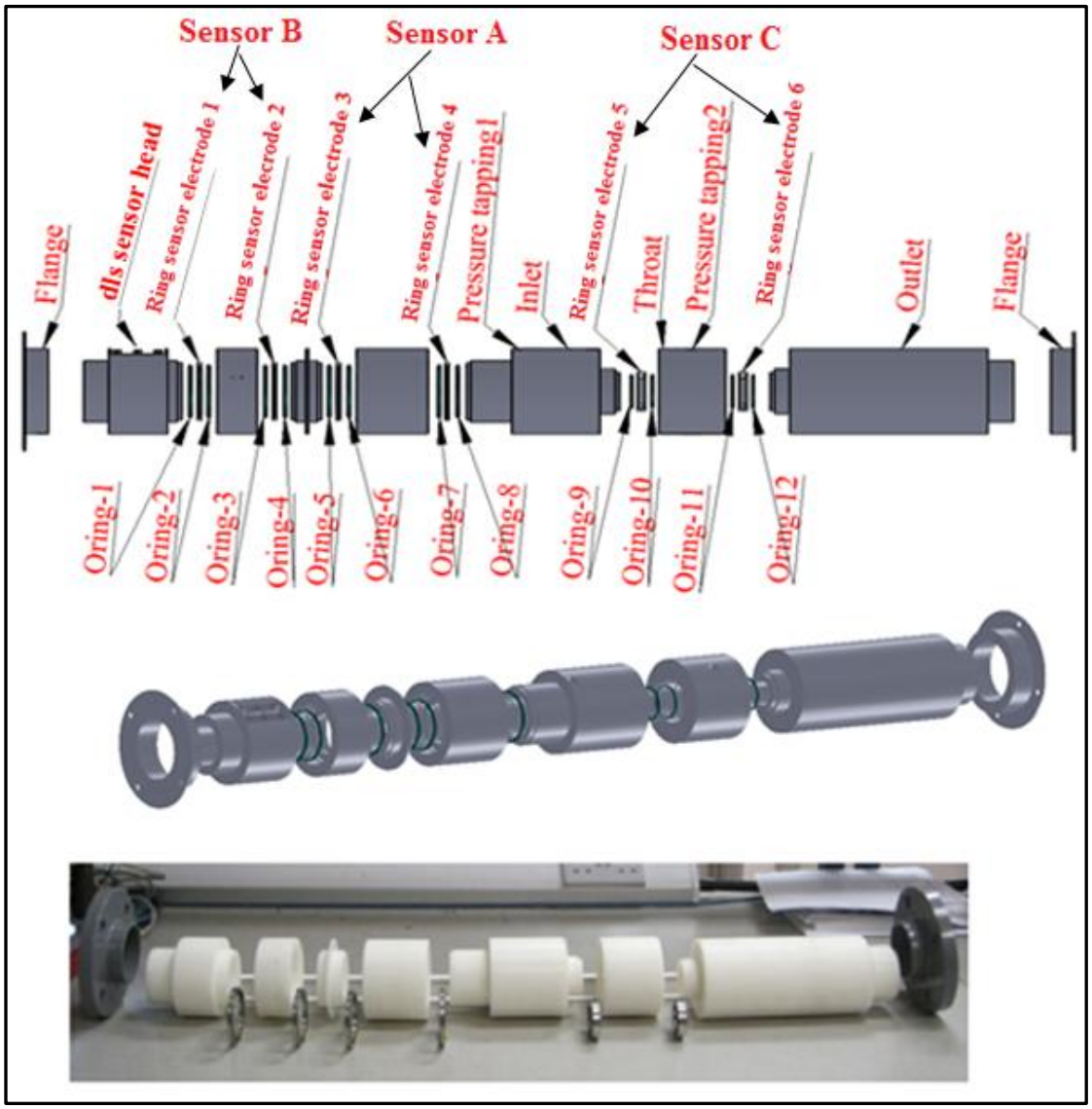

Figure 4-3: The assembly parts of the conductance Venturi meter (CVM)

An advanced feature of this design is that all parts of the Venturi flow meter can be assembled and disassembled for maintenance in a straightforward manner including the threaded flanges. The two ring sensors (A and B) are flush mounted with the inner surface of the Venturi inlet, the ring sensor C is flush mounted with the inner surface at the throat of the Venturi and the digital level sensor head is mounted at the inlet of the Venturi as shown in Figure 4-3.

The stainless steel ring sensor C flush mounted on the inner surface of the Venturi throat is used for determining the gas volume fraction α_2 at the throat by measuring the electrical conductance of the water-air flow at the throat of the Venturi. The two stainless steel ring sensors flush mounted with the inner surface of the Venturi inlet (sensors A and B) are used for measuring the film velocity $U_{f,xc}$ by cross correlating signals between the two ring sensors A and B at the inlet of the Venturi.

The digital level sensor mounted on the inner surface at the inlet of the Venturi is used to measure the film thickness $\tilde{\delta}$ of the liquid by means of the electrical conductance of the film flow in order to determine the water volume fraction $\alpha_{1w,}$ at inlet of the Venturi. Ring sensor B is used as alternative method for measuring the liquid film thickness δ (and hence the gas volume fraction) at the inlet of the Venturi in annular gas-water two phase flows, provided that the conductivity of the water σ_w is known, as measured using a proprietary conductivity meter.

2-D drawings of the Venturi inlet, electrode, Venturi throat, the Venturi outlet and digital level sensor head placed at the inlet of the conductance Venturi section are shown in Figures 4-4 to 4-10. The whole 2-D drawing of the conductance Venturi with all parts; the inlet, six electrodes with twelve O-rings, the throat, digital level sensor head, and the outlet sections are shown in Figure 4-11.

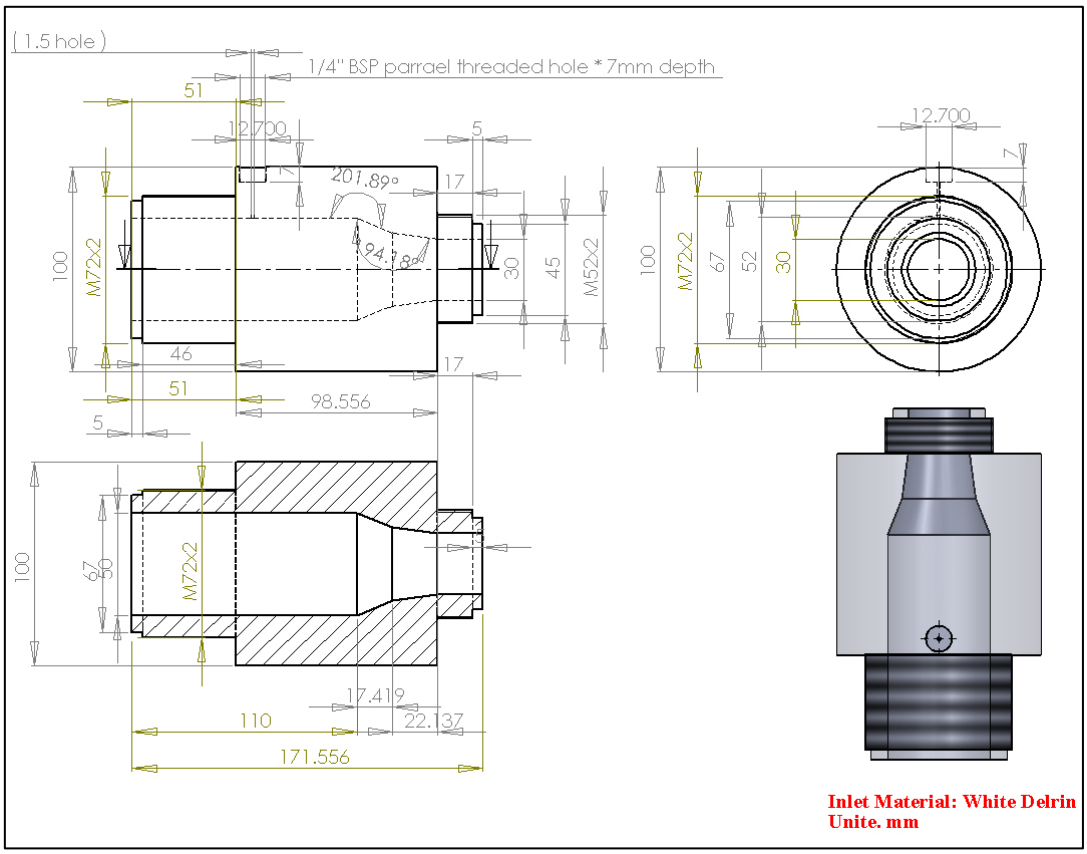

Figure 4-4: Inlet section of the Venturi

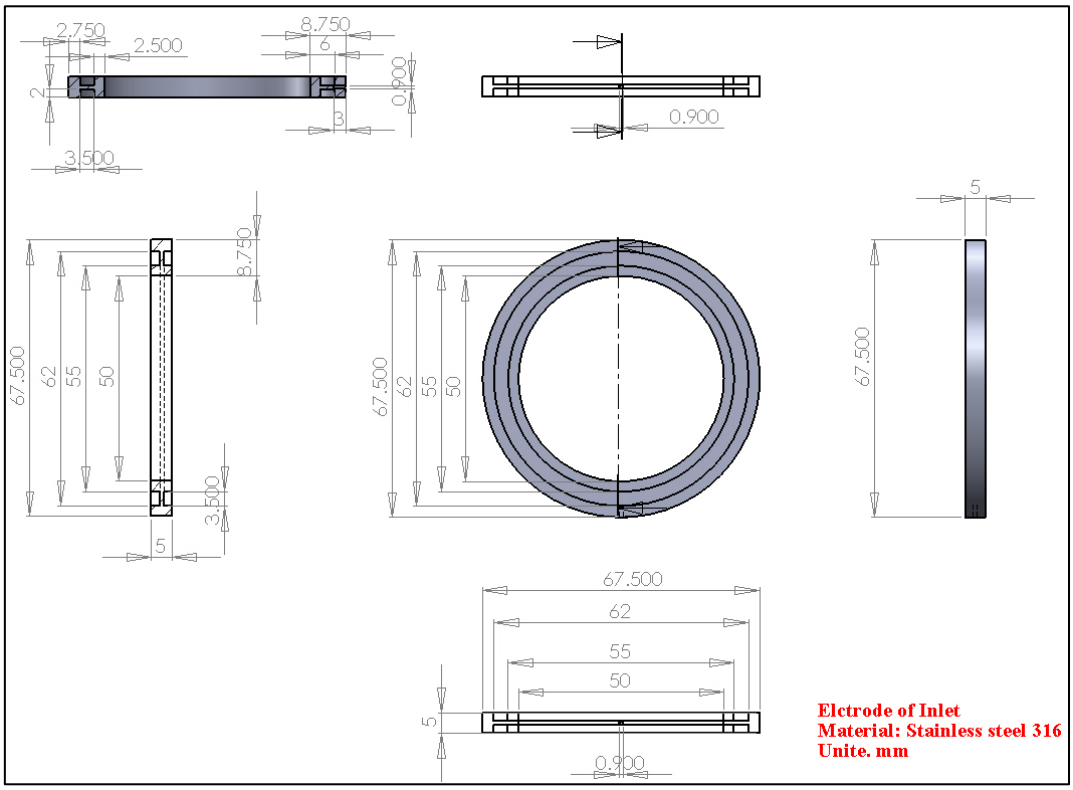

Figure 4-5: Design of the ring sensor electrodes for the inlet

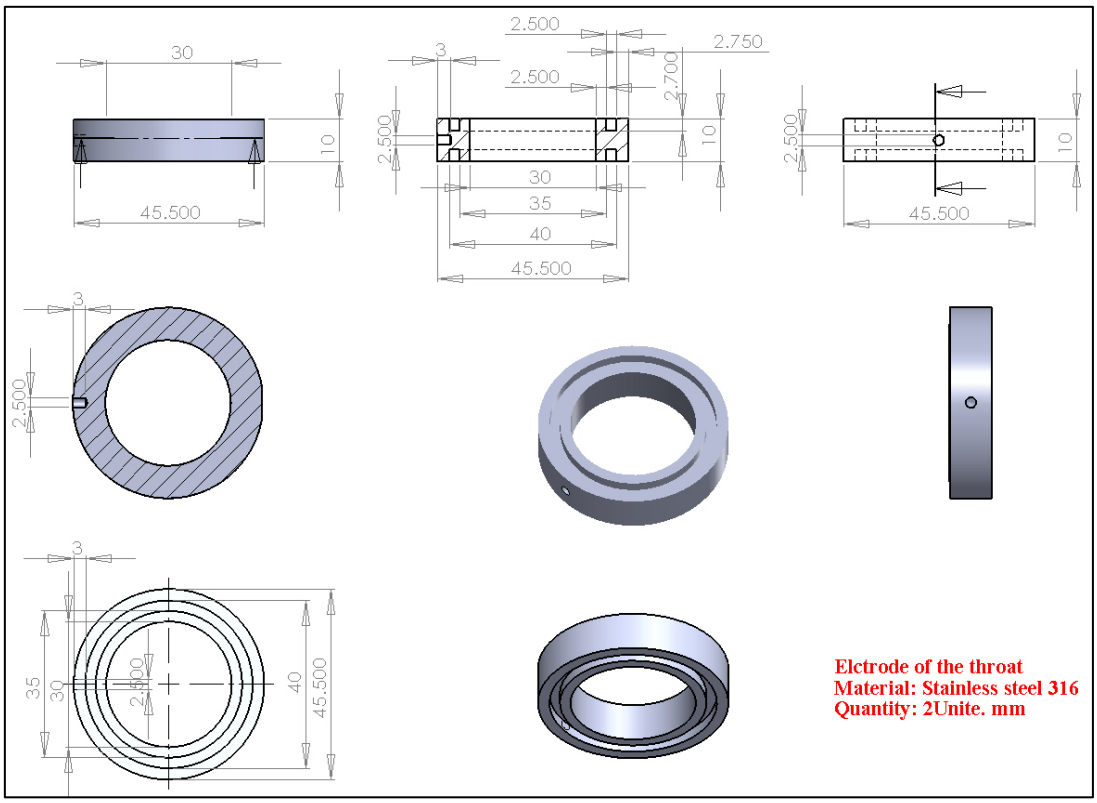

Figure 4-6: Design of the ring sensor elctrodes for the throat

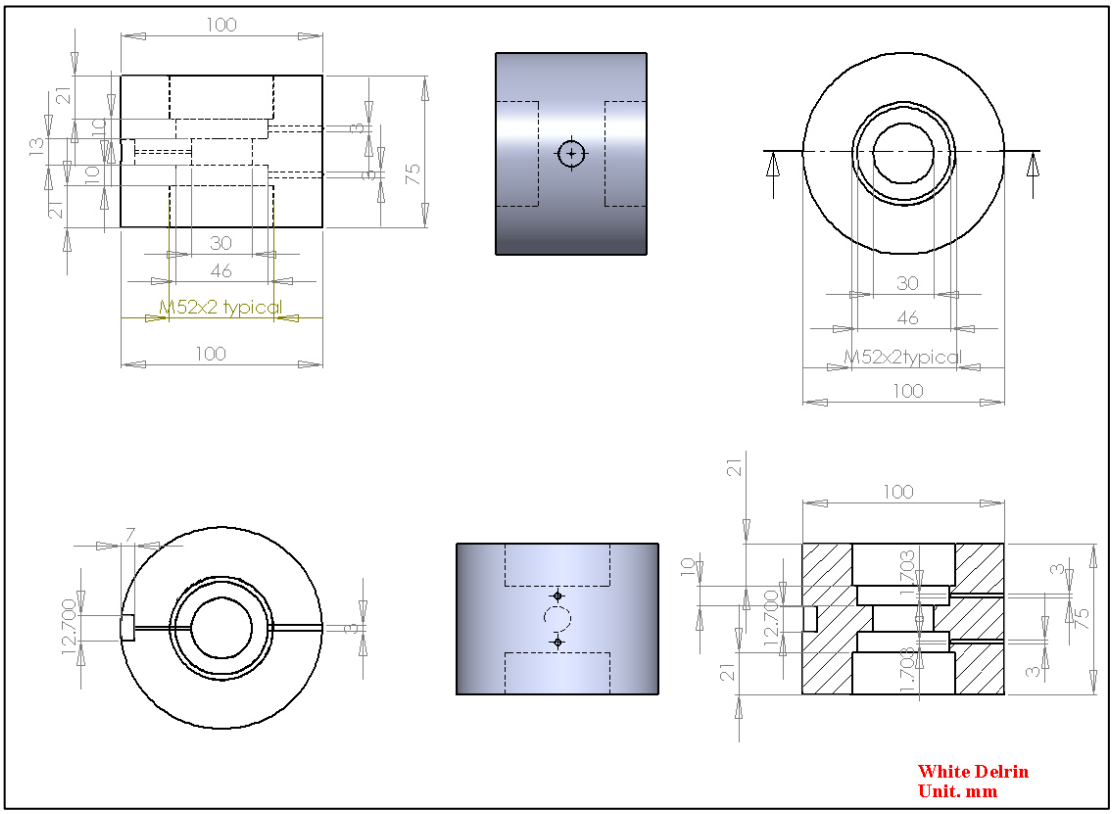

Figure 4-7: Design of the Venturi throat section

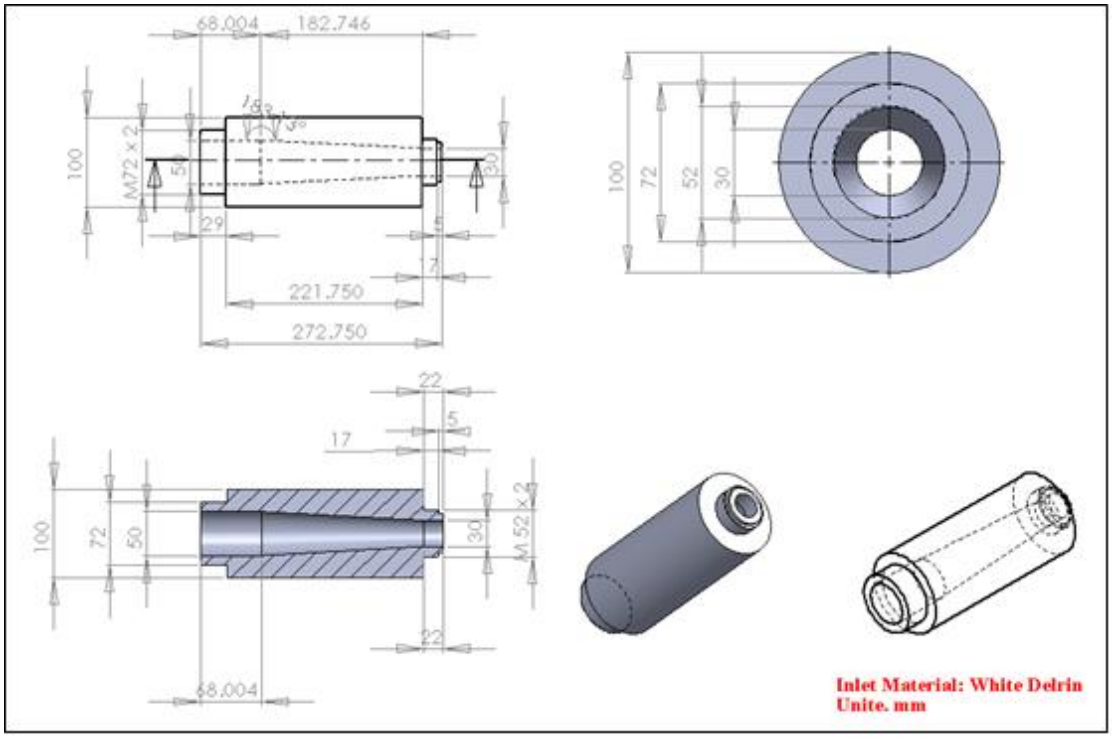

Figure 4-8: Design of the Venturi outlet section

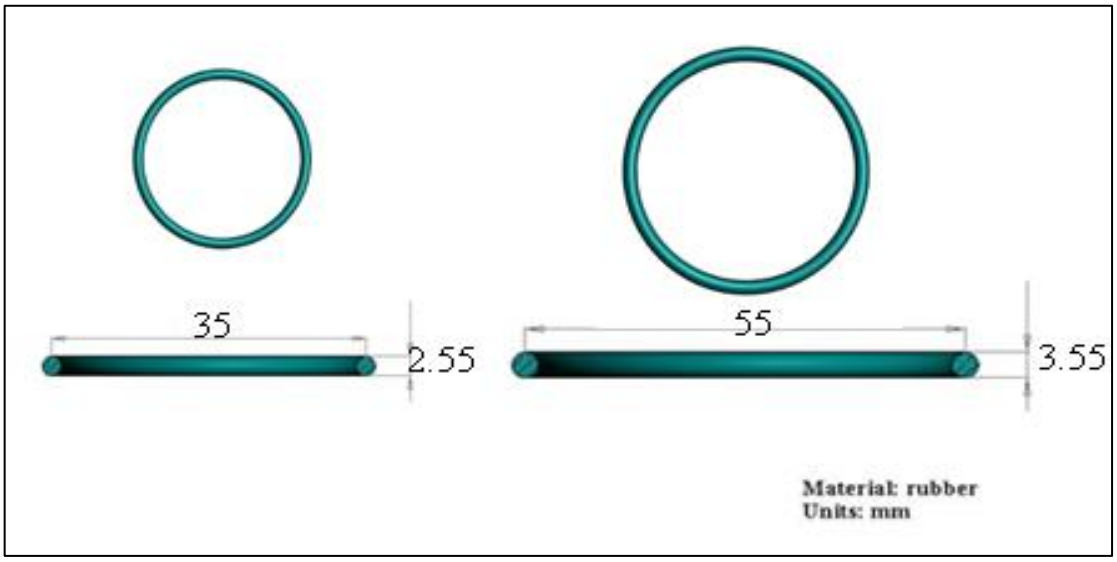

Figure 4-9: O-rings for the inlet and the throat ring sensors

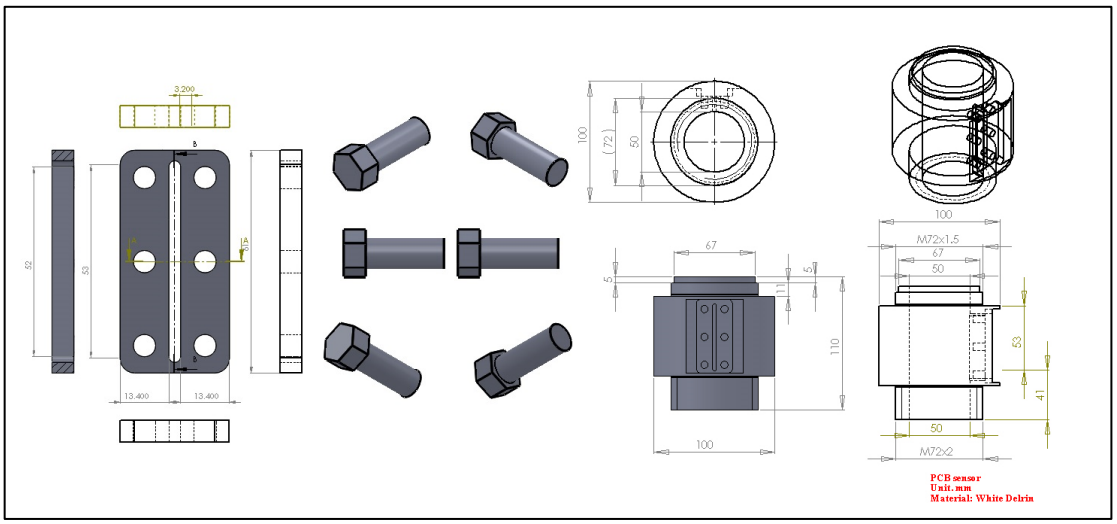

Figure 4-10: Design of the dls sensor head mounting bracket placed at the Venturi inlet

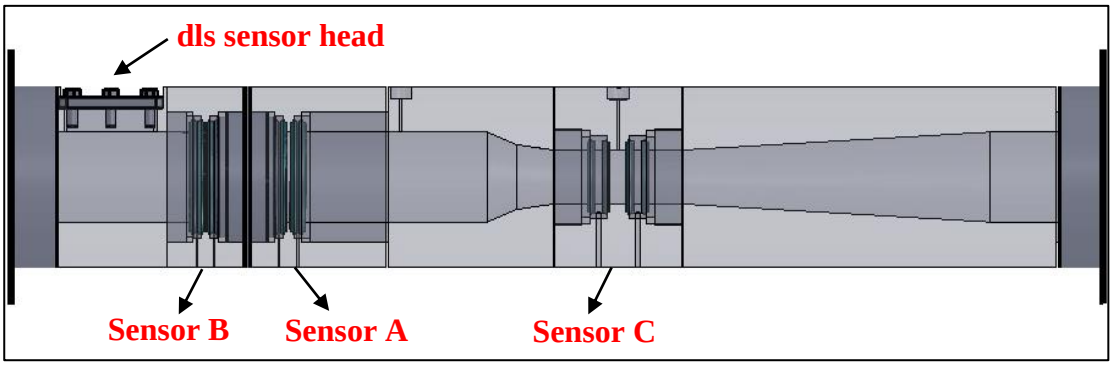

Figure 4-11: 2D drawing of the Venturi with conductance sensors after assembly

4.2 The measurement electronics system

The Venturi meter as designed has four sensors: the digital level sensor (dls), ring sensors A and B at the inlet of the Venturi and ring sensor C at the Venturi throat, as show in Figure 4-12. Conductance electronic circuits were built to enable the following measurements:

- The film velocity $U_{f,xc}$ by cross correlating signals at the Venturi inlet using ring sensors A and B.

- The gas volume fraction α_2 at the Venturi throat using sensor C.
- The water film thickness $\tilde{\delta}$ (and hence the gas volume α_1) using the digital level sensor at the inlet of the Venturi.
- The water film thickness δ (and hence the gas volume fraction α_1 at the inlet of the Venturi) using ring sensor B upstream of the Venturi.

The conductance electronic circuit for the inlet consists of two channels A and B. Channel A was connected to the ring sensor A while channel B was connected to the ring sensor B at the inlet of the Venturi in order to measure the film velocity $U_{f,xc}$ by cross correlating signals. The second conductance electronic circuit was connected to the ring sensor C at the Venturi throat by which the gas volume fraction α_2 at the throat of the Venturi be measured. The third electronic circuit was connected to the digital level sensor head in order to measure the film thickness $\tilde{\delta}$ (and hence the gas volume fraction α_1 at the inlet of the Venturi).

Channel B with ring sensor B was also used to measure the film thickness δ (and hence the gas volume fraction α_1 at the inlet of the Venturi) provided the water conductivity was σ_w already known. All the measurements were done in vertical annular gas-water two phase flows.

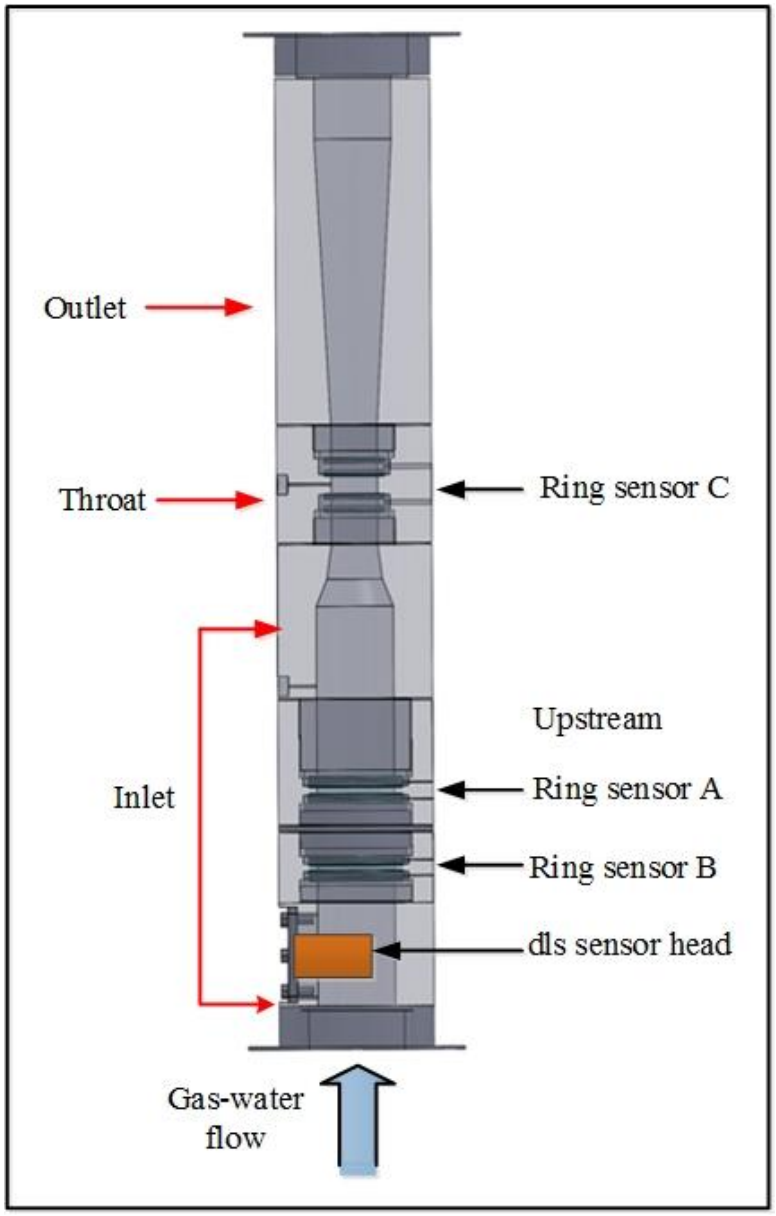

Figure 4-12: Venturi meter with all conductance sensors

4.2.1 The conductance electronic circuits for upstream ring sensors A and B

Two upstream ring sensors A and B at the inlet of the Venturi need to be used with the conductance electronic circuit in order to obtain the film velocity by cross correlating signals between ring sensors A and B in vertical annular gas-water two phase flows. To do this, an electronic conductance circuit was designed and built; the block diagram, Figure 4-13, shows the main components of the conductance circuit.

The circuit design was the same for both channels A and B and so only one description is necessary.

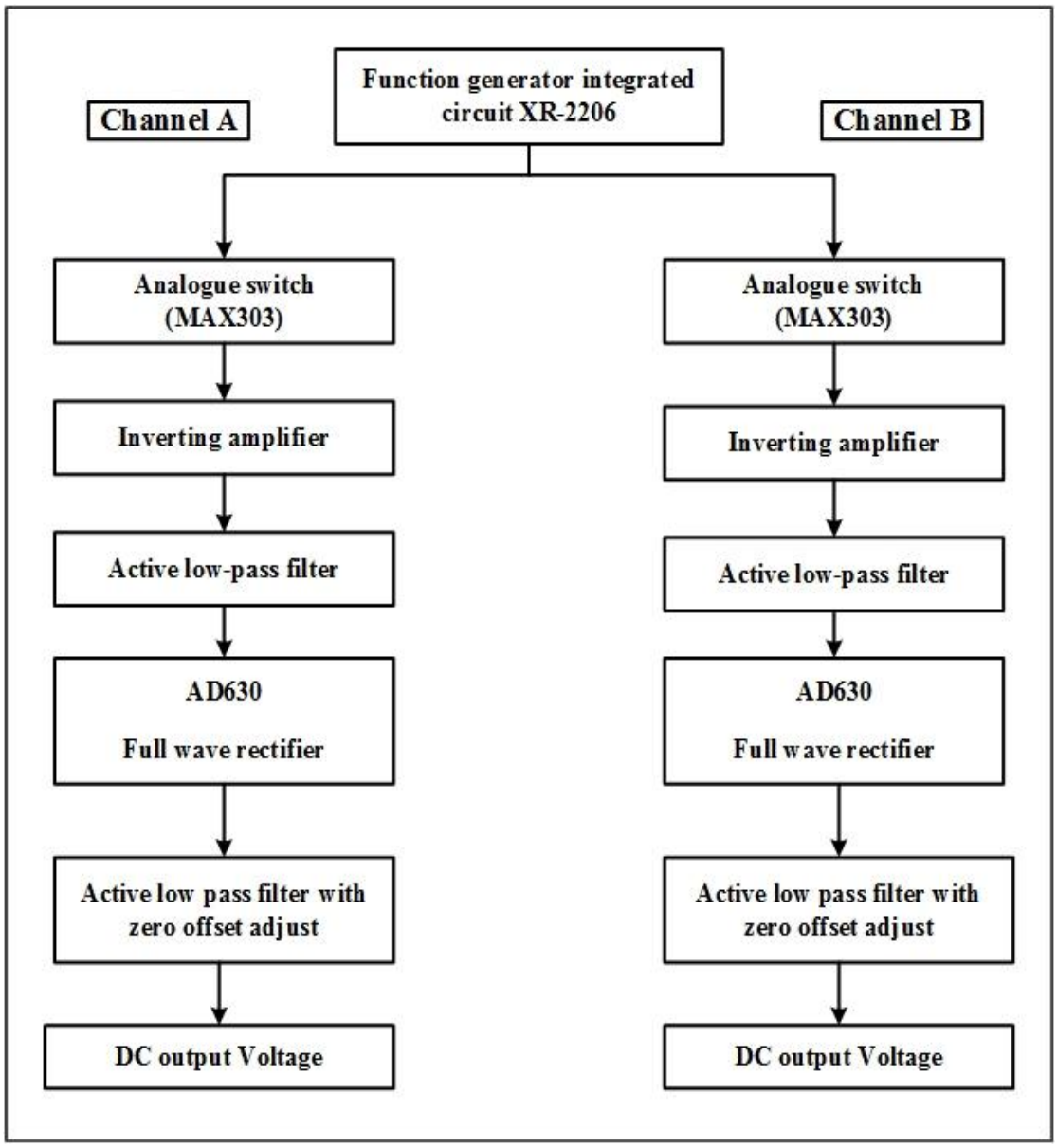

Figure 4-13: Block diagram of the measurement circuit for ring sensors A and B

Two circuits were built as channels A and B, channel A for conductance ring sensor A and channel B for conductance ring sensor B, each sensor having two electrodes, electrodes (1 and 2) for ring sensor A, electrodes (3 and 4) for ring sensor B (see Figure 4-3). The designed circuit consisted of parts **I** to **V** (refer to Figure 4-18): **(I)** function generator integrated circuit XR-2206 with analogue switches (MAX303A)

and (MAX303B), **(II)** inverting amplifiers, **(III)** active low-pass filters, **(IV)** full wave rectifiers, **(V)** active low-pass filters with zero offset adjustment.

Part (I) (from conductance electronic circuits for upstream ring sensors A and B).

As shown in Figure 4-18, the function generator, integrated circuit XR-2206, can produce pulse waveforms in two states low (0) and high (1) connected to the analogue switches (MAX303) A and B. Sensor A is connected to the analogue switch (MAX303 A), sensor B is connected to the analogue switch (MAX303 B); both switches are connected to an excitation source signal. As shown in Figure 4-14 when the function generator produces the high state (1) to the analogue switches (MAX303 A) and (MAX303 B) the results are:

For ring sensor A

Electrode 1 connected to the excitation source sine wave signal 2V peak to peak (V+). Electrode 2 connected to the measurement circuit (refer to Figures 4-14 and 4-17 for the measurement circuit).

For ring sensor B

At this time ring sensor B (electrode 3 and 4) is isolated (refer to Figure 4-14).

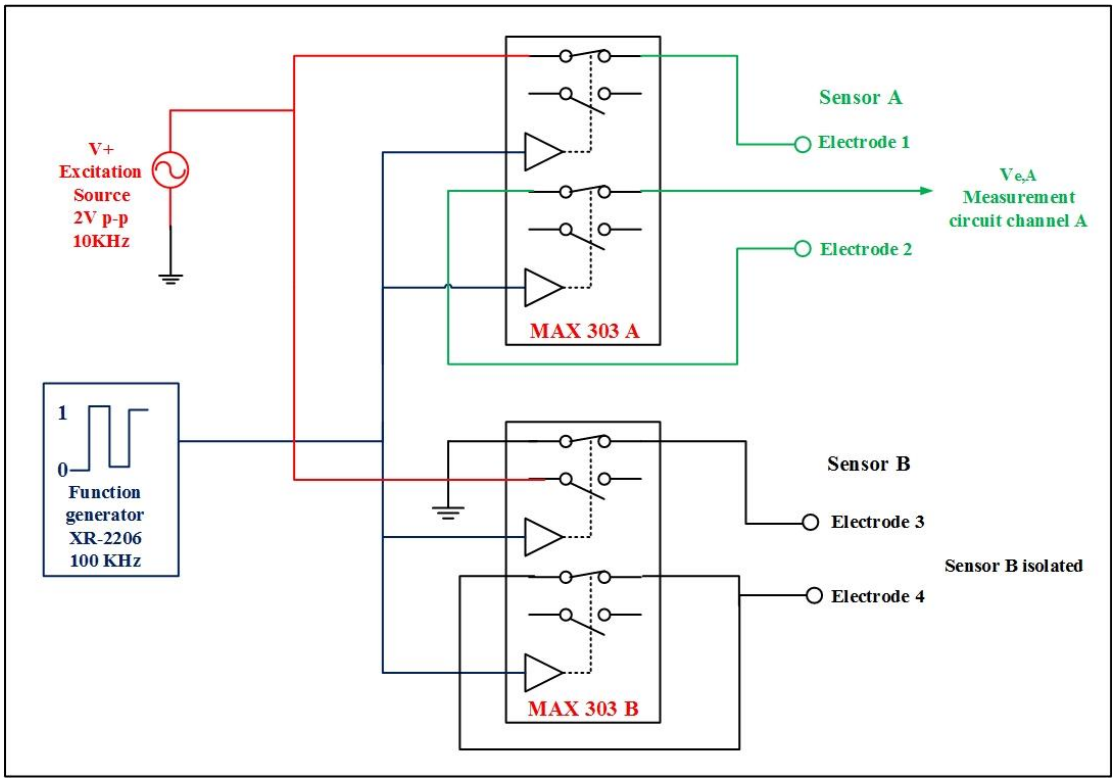

Figure 4-14: Switching mechanism and function generator producing high state (1)

As shown in Figure 4-15. When the function generator produces the low state (0) to the analogue switches (MAX303 A) and (MAX303 B) the results are:

For ring sensor B

Electrode 3 connected to the excitation source sine wave signal 2V peak to peak (V+). Electrode 4 connected to the measurement circuit (similar to measurement circuit for ring sensor A as showing in Figure 4-17).

For ring sensor A

At this time ring sensor A (electrode 1 and 2) is isolated (refer to 4-15)

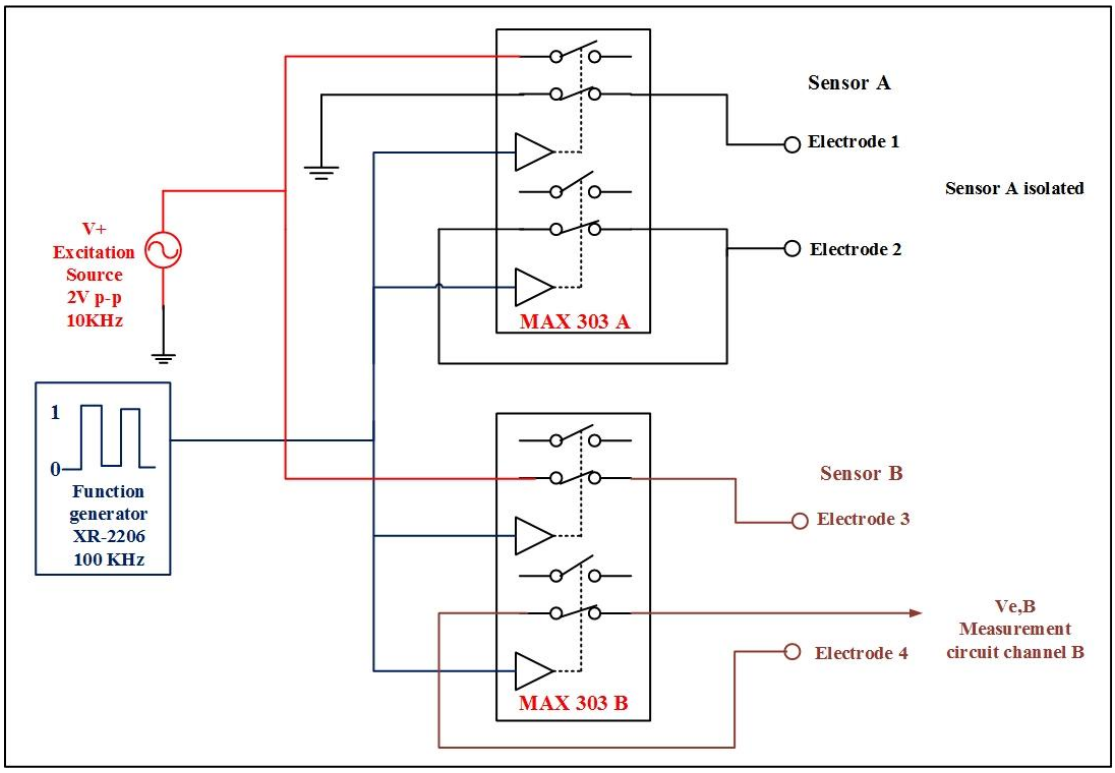

Figure 4-15: Switching mechanism and function generator produce low state (0)

The reason for using the function generator XR-2206 is to guarantee that the ring sensor A and ring sensor B were connected alternately to the excitation source signal (V+). In this way ring sensor A and ring sensor B were never working at the same time and so cross-talk was prevented between the two sensors.

The switching frequency was 100 kHz and the excitation source signal was 2 volts peak-to-peak with a frequency of 10 kHz applied alternately to ring sensor A (electrode 1) and ring sensor B (electrode 3) resulting in the signals $V_{e,A}$ and $V_{e,B}$ shown in Figure 4-16. It can be seen from Figure 4-16 that when ring sensor A is active, ring sensor B is not and when ring sensor B is active, ring sensor A is not, so cross-talk between the two ring sensors A and B is eliminated.

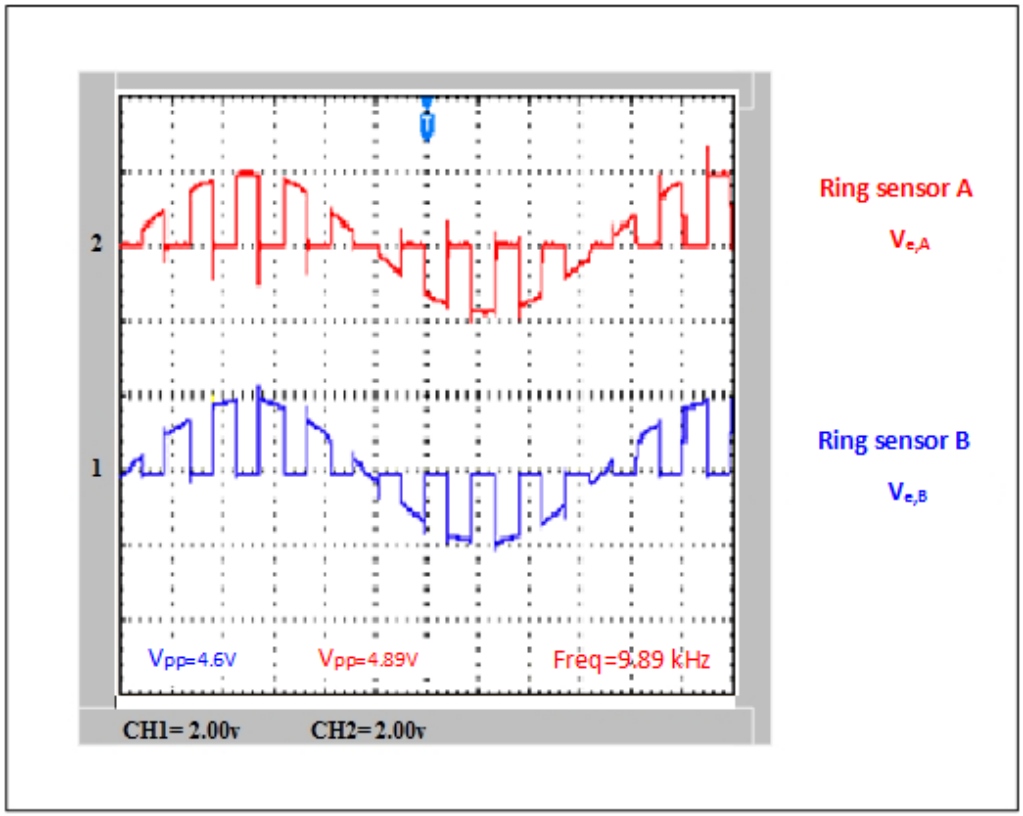

Figure 4-16: Excitation signals applied to ring sensors A and B

Part (II) (refer to Figure 4-18 for different parts of the conductance electronic circuit).

The operation of this part allows the conductance of the mixture G_{mix} at ring sensors A and B to be measured using the inverting amplifier stage as shown in Figure 4-18. For channel B the inverting amplifier circuit is also shown in Figure 4-17; the inverting amplifier output $V_{1,B}$ is proportional to the fluid conductance, $G_{mix} = \frac{1}{R_{mix}}$, between the ring sensor B electrodes 3 and 4. The output voltage of this stage is given by:

$$V_{1,B} = -\left(\frac{R_{fb}}{R_{mix}}\right) V_{e,B}$$

Equation 4.1

where R_{fb} is the reference feedback resistance, $V_{1,B}$ is the output voltage, and $V_{e,B}$ is the input voltage which is the output signal from the switching mechanism circuit. Conductance is the reciprocal of resistance and so. Equation (4.1) can be re-written as:

$$V_{1,B} = -\frac{G_{mix}}{G_{fb}} V_{eB}$$

Equation 4.2

where G_{mix} is the conductance of the fluid mixture.

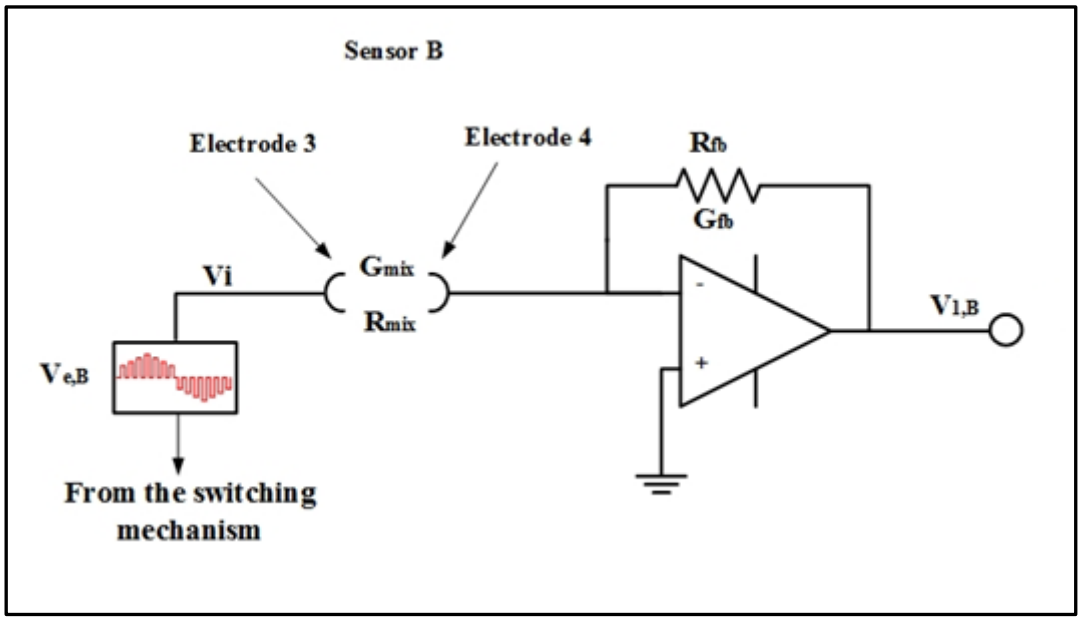

Figure 4-17: Part II of the electronic conductance circuit for upstream ring sensor B

Equation (4.1) can also be rewritten as:

$$V_{1,B} = -R_{fb} G_{mix} V_{e,B}$$

Equation 4.3

Thus any change in the water conductivity between the ring sensor B electrodes 3 and 4 which changes the conductance of the mixture G_{mix}, results in a change in the inverting amplifier circuit output voltage $V_{1,B}$.

Part (III) (refer to Figure 4-18 for different parts conductance electronic circuit).

For different parts of the circuit, as shown in Figure 4-18, The output voltage from part (II)**,** $V_{1,B}$, was fed into the second order low-pass filter with cut-off frequency of 150 kHz. This frequency was determined by repetition. Different many frequencies were tried and the best result found. Second order low pass filters [82] are easy to design and are used widely in many applications. The main purpose of the second order low pass filter shown in part (III) of Figure 4-18 is to remove any high frequency noise which is introduced by the high speed switching between the two ring sensors A and B. For channel B, the output voltage from part (III) is output the result as $V_{2,B}$.

Part (IV) (refer to Figure 4-18 for different parts conductance electronic circuit).

As shown in Figure 4-18, for channel B, the voltage $V_{2,B}$ was fed into an AD630 integrated circuit. The configuration of the AD630 makes it ideal for signal processing applications, such as balanced modulation and demodulation, square wave multiplication and precision rectification. It was configured as a precision rectifier. The main purpose of the AD630 was to achieve full wave rectification on the $V_{2,B}$ voltage signal and to output the result as $V_{3,B}$.

Part (V) (refer to Figure 4-18 for different parts conductance electronic circuit).

For channel B, as shown in Figure 4-18, this part of the circuit produces a final DC output voltage $V_{4,B}$. The signal $V_{3,B}$ was fed into an active low-pass filter with a cut-off frequency of 200 Hz. This cut the high frequency carrier wave content from the signal to give a DC output voltage, $V_{4,B}$.

The DC offset stage was adjusted to set V_{off} to zero (i.e. the output voltage $V_{4,B}$ is equal to zero) when no water is present in the pipe (air only) and hence the water conductivity σ_w was effectively zero. For no water present in the pipe, $V_{4,B}$ is equal to V_{off} in Equations (3.7) and (3.9) respectively.

The output signal from Channel B can be written as:

$$V_{4,B} = KV_{1,B}$$

Equation 4.4

where K represents the circuit gain, and so with reference to Equation (4.3), we may state that (for constant amplitude of $V_{e,B}$) the DC output voltage $V_{4,B}$ is proportional to the conductance of the air-water mixture at ring sensor B. With air and water at the inlet of the Venturi $V_{4,B}$ is equal to the voltage $V(\alpha_1)$ appearing in Equations (3.5) to (3.7) and (3.9) to (3.10). By the following arguments similar to these give above, the DC output voltage from channel A $V_{4,A}$ is proportional to the conductance of the air-water mixture at ring sensor A.

As the author mentioned earlier, two electronic conductance circuits were designed and built to serve the two ring sensors (A and B) at the inlet of the Venturi meter. However, the two ring sensors together in this study were used to measure the liquid film velocity by cross correlating signals and ring sensor B only was used to measure the film thickness at the Venturi inlet.

The choice of excitation frequency of the ring sensors is critical to their successful operation. At low frequencies a "double layer" effect might be found in which the conductance between the electrodes is affected by capacitance and resistive elements at the electrode-electrolyte interfaces [83]. Therefore, in the present work, to negate the double layer effect a sufficiently high excitation frequency was selected. The excitation source signal was a sine wave with an amplitude of 2V peak to peak and a wave frequency of 10 kHz as shown in Figure 4-16.

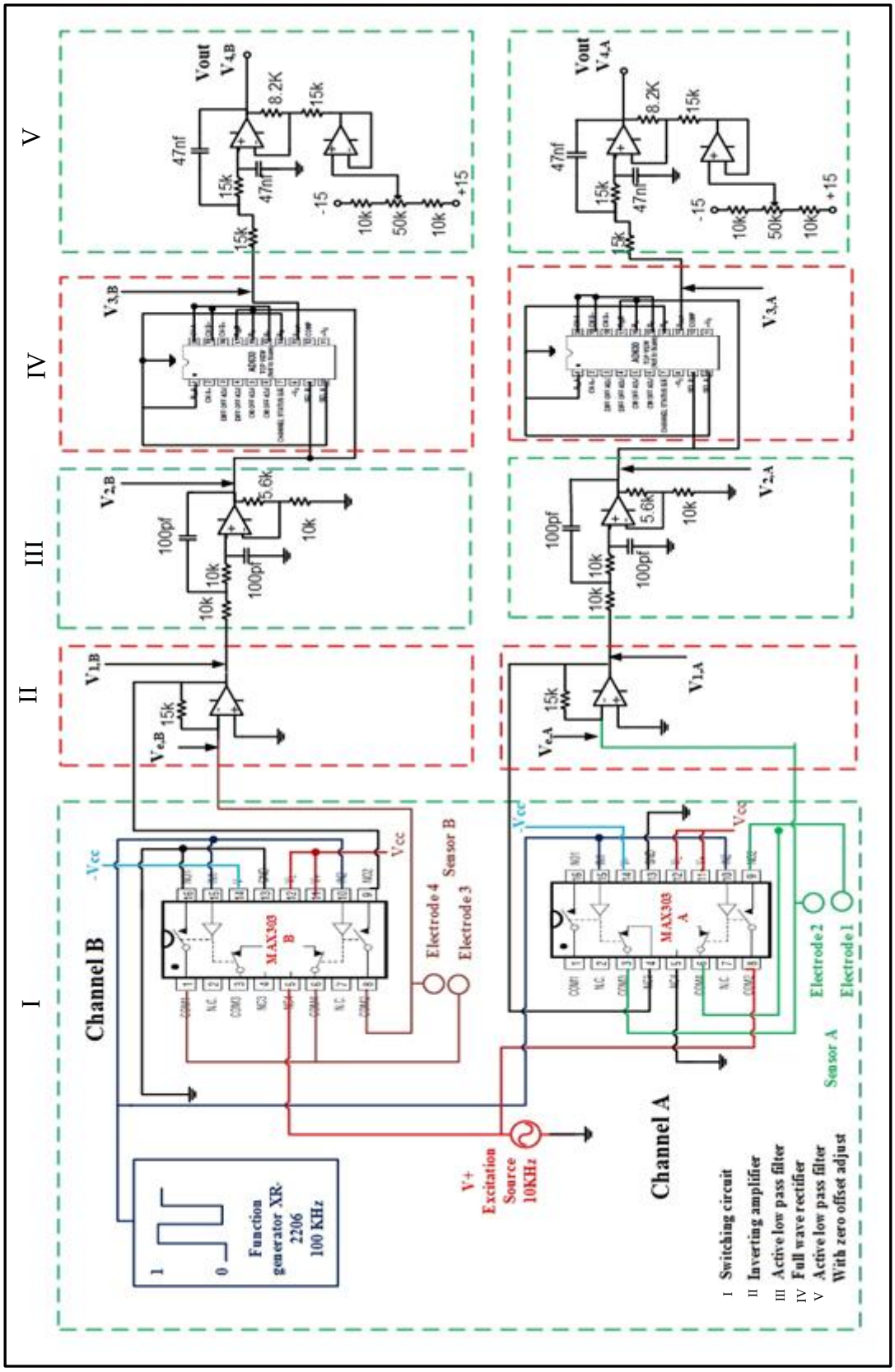

Figure 4-18: Schematic diagram of the conductance electronic circuits for upstream ring sensors A and B

4.2.2 The conductance electronic circuits for the throat ring sensor

A conductance electronic circuit was built to measure gas volume fraction α_2 at the throat of the Venturi in annular wet gas flow. The electronic circuit was connected to the stainless steel conductance ring sensor C at the throat of the Venturi in order to measure the gas volume fraction α_2 at the throat in vertical gas-water phase flow. The circuit was built to the same design as for channel A and B of the conductance electronic circuits for upstream ring sensors but without the switching mechanism. A block diagram of the measurement electronic circuit is shown in Figure 4-19; the designed circuit consisted of (refer to Figure 4.20): (i) inverting amplifier, (ii) active low-pass filter, (iii) full wave rectifier, (iv) active low-pass filter with zero offset adjustment. The excitation source signal used was a sine wave with amplitude 2V peak to peak and wave frequency 10 kHz.

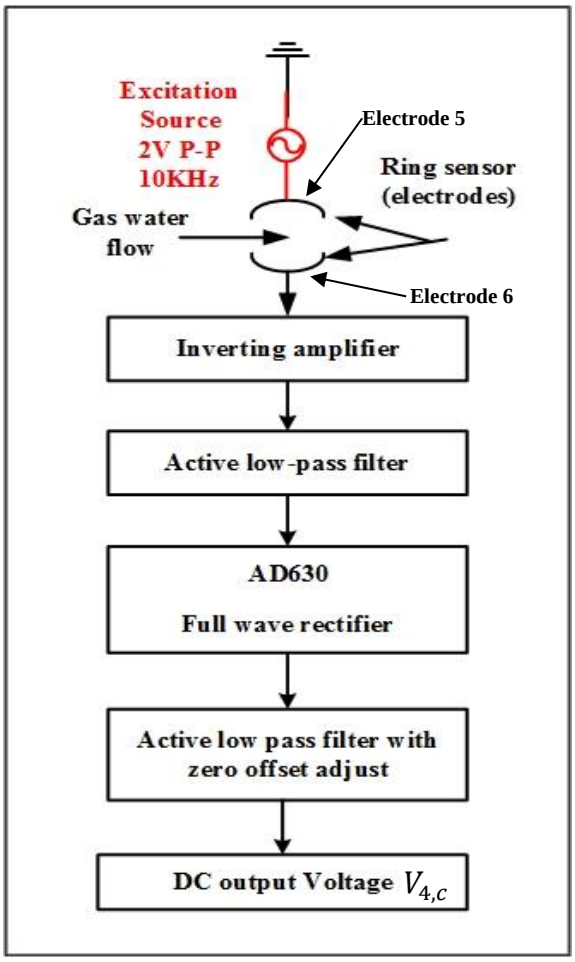

Figure 4-19: Block diagram of the measurement circuit for the throat ring sensor

To calibrate the Venturi flow meter with conductance sensor C at the throat in simulated annular flow, the zero offset stage was set to give a zero output value for $V_{4,c}$ when no water (air only) is present between the ring sensors (electrodes) at the throat of the Venturi. This equivalent to V_{off}^{t} in Equation (3.11) being equal to zero. For air and water present at the throat of the Venturi $V_{4,c}$ is equivalent to $V^{t}(\alpha_2)$ in Equation (3.11).

Part (i), the inverting amplifier gain (refer to Figure 4-20), could be adjusted by changing the feedback resistance to give a defined dc output voltage when the area between the ring sensors at the throat of the Venturi was completely filled with water. The gain of this amplifier for the throat ring sensor C was the same during the bench test described in Chapter 5 as during the subsequent flow loop tests.

The same procedure was followed for the inverting amplifier stage (part II in Figure 4-18) for conductance sensors A and B. The bench tests on the Venturi with conductance at the inlet and throat for simulated annular flow is fully described in Chapter 5.

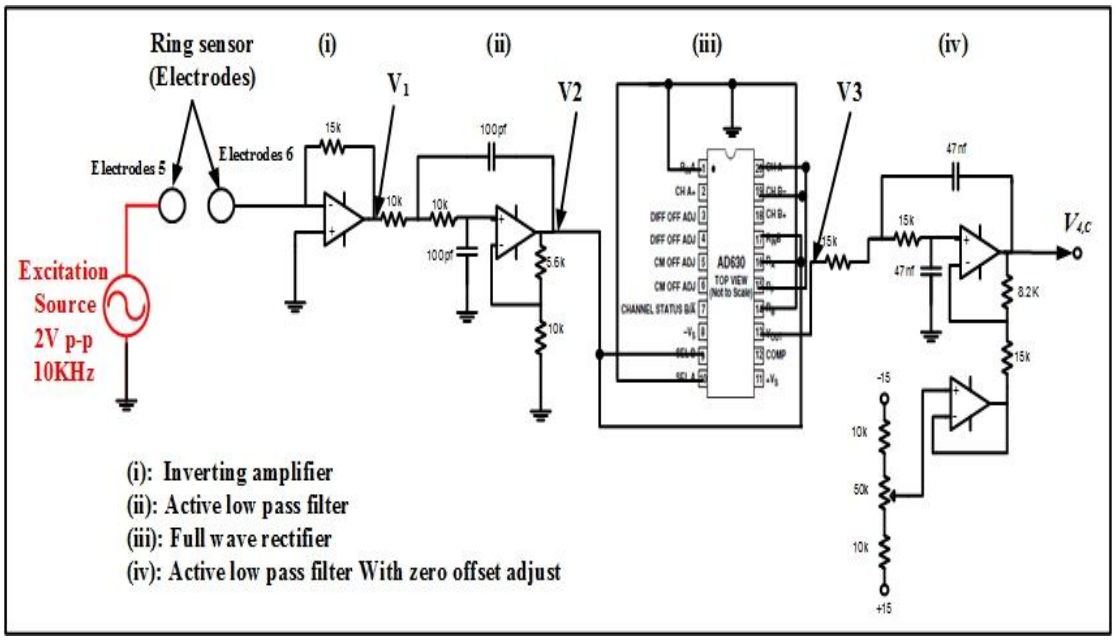

Figure 4-20: A circuit diagram of the conductance electronic circuit for the throat ring sensors

4.2.3 The conductance electronic circuit for the digital level sensor

A digital level sensor was used to measure the liquid film thickness $\tilde{\delta}$ of the film in annular gas-water two phase flow as shown in Figure 4-21. Conductance electronic circuits and a digital level sensor head were designed and built to measure the liquid film thickness $\tilde{\delta}$ (from which the gas volume fraction α_1 at the inlet can be derived) in vertical annular gas-water two phase flows at the inlet of the Venturi. The conductance electronic circuit was designed and built as 19 channels connected to the digital level sensor head which consisted of 19 electrodes to measure the film thickness in the range 0.5mm to 9.5mm in steps of 0.5mm at the inlet of the Venturi.

In order to measure the liquid film thickness, the conductance electronic circuit is needed to drive a DC output of 0 or 5 volts in order to send a signal to a BCD encoder.

Each conductance measurement circuit was connected to an electrode on the digital level sensor head. The digital level sensor head contains 19 electrodes capable of measuring the liquid level in the range 0.5mm to 9.5mm; the digital level sensor head electrodes were spaced at 0.5mm intervals as shown in Figure 4-24. 19 channels were built for the 19 electrodes of the digital level sensor head.

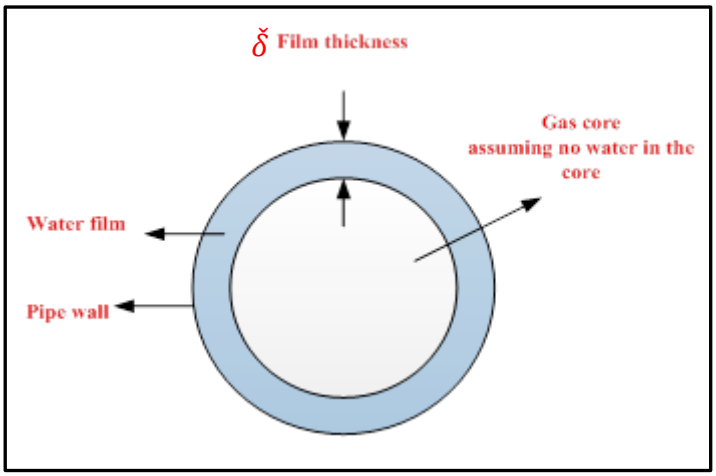

Figure 4-21: Liquid film thickness in vertical annular water-gas flows

The complete block diagram of the measurement electronic circuit for each channel is shown in Figure 4-22. It consists of three stages; (**A**) full wave rectifier, (**B**) a low-pass filter, (**C**) a non-inverting amplifier (refer to Figure 4-23); the excitation voltage is 2v peak to peak and the sine wave frequency is 10 kHz. The output voltage from the electronic circuit for all channels is 0 or 5 dc volt; the output of the electronic circuit for each channel was connected to a BCD priority encoder that features priority encoding of the inputs to ensure that the highest-order data line is encoded. Ten data input lines (0-9) are encoded to the four-line (8, 4, 2, 1) BCD. Since 19 channels were built, two BCD (CD401147B) encoders were used so that channels 1 to 10 were connected to the first BCD (encoder) and channels 11 to 19 were connected to the second BCD (encoder), the outputs from both BCD encoders are digital. All the outputs of the BCD encoders were connected to the digital input terminals of an NI USB 6009 data acquisition card. A program was written by the author using Labview (refer to Figure 4-27) to read the digital number from the BCD encoder via the NI USB 6009 card; refer to Figure (4-26) for a block diagram of the digital circuit.

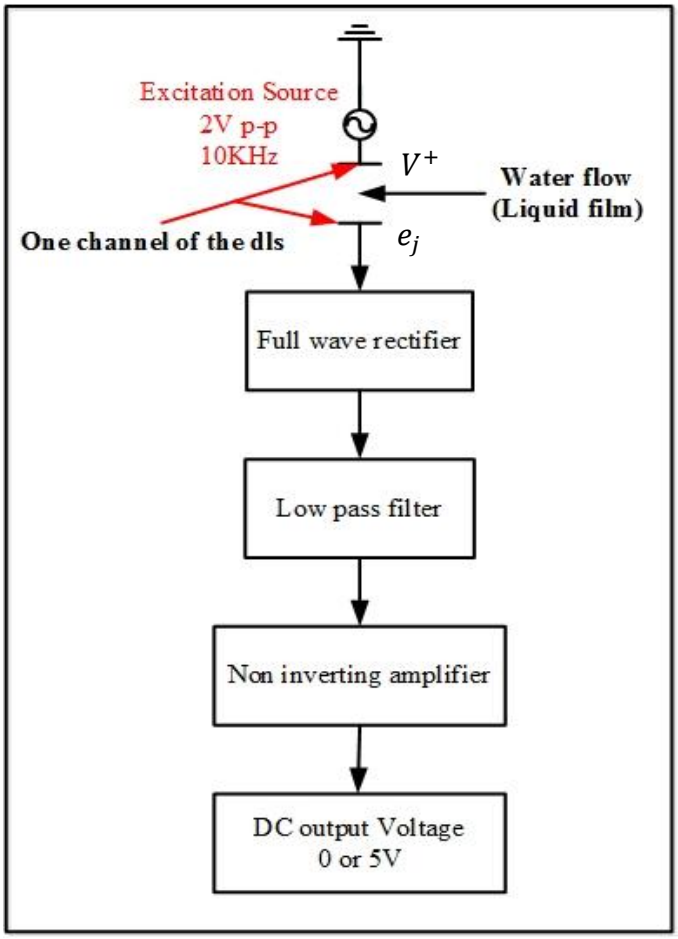

Figure 4-22: Block diagram of the measurement electronics

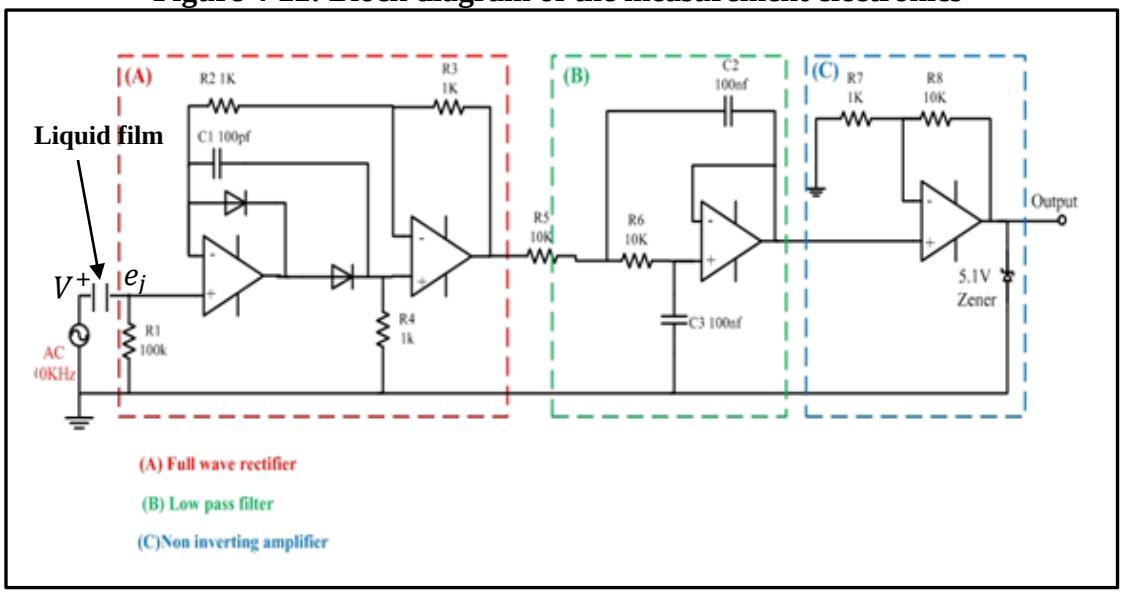

Figure 4-23: A schematic diagram of the conductance electronic circuit

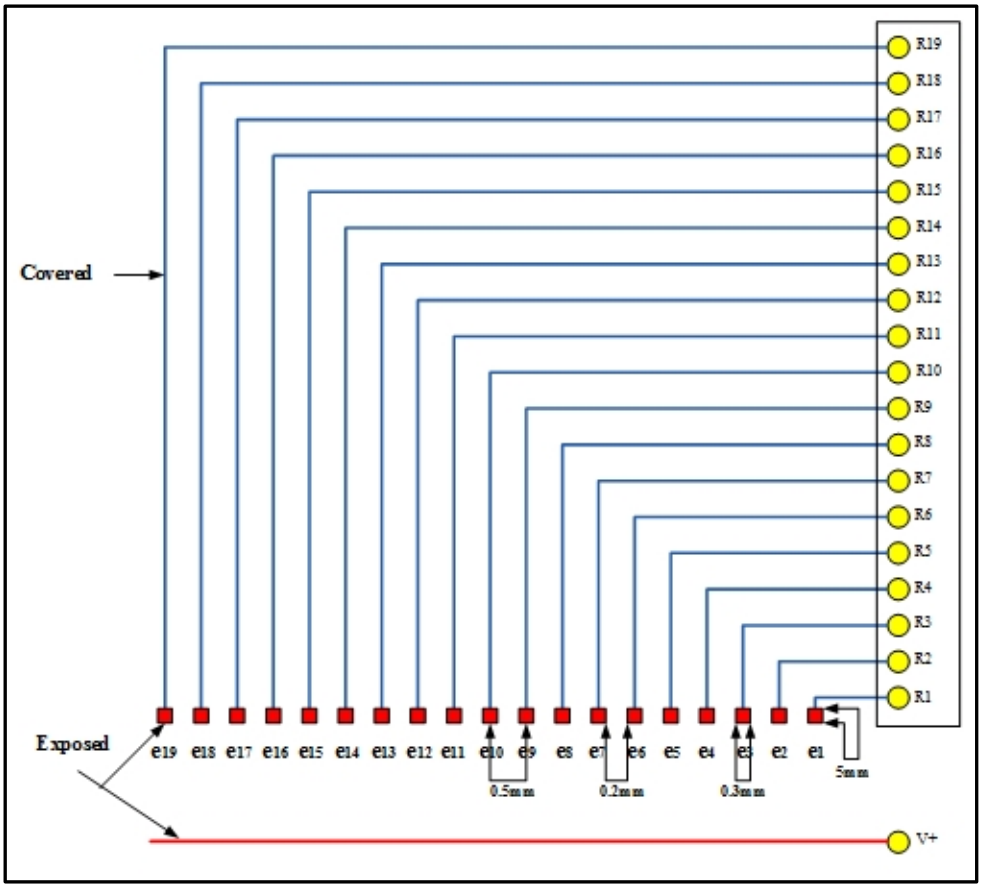

Figure 4-24: digital level sensor head design for measurement of the liquid film thickness in vertical annular flow

To measure the film thickness in annular flow, the digital level sensor head was mounted on the inner surface of the Venturi inlet and insulated to prevent water leaks during the experiments as shown in Figure 4-25.

The electrodes e_1 to e_{19}, shown in red on Figure 4-24, are either covered in water or exposed to air dependent upon the film thickness. For the electrodes covered by water, the corresponding output from the associated conductance circuit were high (refer to Figure 4-23). For the uncovered electrodes, the conductance circuit output were low. These high and low outputs were interpreted by the BCD encoder, the NI USB 6009 card and the Labview software, enabling the film thickness to be measured to a resolution of $\pm$ 0.5mm.

Figure 4-25: Photograph of the digital level sensor head mounted on the Venturi inlet

As shown in Figure 4-26. The digital level sensor has 19 channels with 19 LEDs which needs to be connected to the NI USB 6009 data acquisition card via two BCD priority encoders. The CD40147B encoders were and connected with the output of the digital level sensor conductance circuit (from channel 1 to 19), to drive low (0) or high (1) signal to the NI USB 6009 card.

The outputs from the conductance circuits of digital level sensor from ch1 to ch10 were connected to the BCD1 priority encoder (input 0 to input 9) respectively and from ch11 to ch19 of the digital level sensor circuit were connected to the BCD2 priority encoder (input 0 to input 8) respectively, input 9 from the BCD2 encoder was not needed because we have only 19 channels. The 19 LEDs functions in the circuit is to show when air is present the sensor channels 1 to 19 are all off and whenever water is present the sensor channel electrodes covered by water activate, indicating that water is present.

The CD40147B encoder features priority encoding of the inputs to ensure that only the highest-order data line is encoded. Ten data input lines (0-9) are encoded to four-line (8, 4, 2, 1) BCD. All inputs and outputs are buffered. The outputs from BCD1 encoder (A1 B1 C1 D1) and the outputs from BCD2 encoder (A2 B2 C2 D2) are connected to the digital input channel of NI USB 6009 data acquisition card as shown in Figure 4-26.

A Labview software program (see Figure 4-27) was created to read the digital input channels to the NI USB 6009 data card coming from the outputs of BCD encoders and this Labview software calculated converted the digital data to an equivalent decimal number to show the results of the measurement on a PC, (e.g. if the water covered the electrodes e1, e2, e3 and e4 of the dls head sensor, the corresponding output from the associated conductance circuit are high (refer to Figure 4-23), the Labview software will read from the BCD1 encoder a digital number (1100) and from BCD2 encoder a digital number (0000). Labview software will convert digital number to the equivalent number and show the results on PC as 2mm film thickness measured by digital level sensor). Table 4-1 and 4-2 shows the truth table of BCD encoders with equivalent numbers.

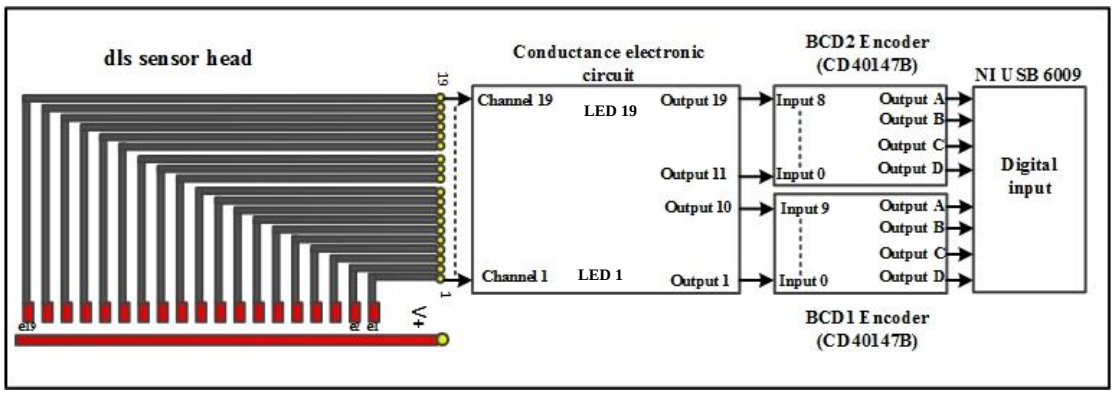

Figure 4-26: block diagram of the digital circuit for measuring the film thickness

BCD Encoder 2				BCD Encoder 1				Decimal number	Equivalent number mm
0	0	0	0	0	0	0	0	0	0
0	0	0	0	1	1	1	1	15	0.5
0	0	0	0	1	1	1	0	14	1

0	0	0	0	1	1	0	1	13	1.5
0	0	0	0	1	1	0	0	12	2
0	0	0	0	1	0	1	1	11	2.5
0	0	0	0	1	0	1	0	10	3
0	0	0	0	1	0	0	1	9	3.5
0	0	0	0	1	0	0	0	8	4
0	0	0	0	0	1	1	1	7	4.5
0	0	0	0	0	1	1	0	6	5

0=low 1=high x=don't care

Table 4-1: Truth table of BCD encoder 1 and equivalent number

BCD Encoder 2				BCD Encoder 1				Decimal number	Equivalent number mm
1	1	1	1	x	x	x	x	15	5.5
1	1	1	0	x	x	x	x	14	6
1	1	0	1	x	x	x	x	13	6.5
1	1	0	0	x	x	x	x	12	7
1	0	1	1	x	x	x	x	11	7.5
1	0	1	0	x	x	x	x	10	8
1	0	0	1	x	x	x	x	9	8.5
1	0	0	0	x	x	x	x	8	9
0	1	1	1	x	x	x	x	7	9.5

0=low 1=high x=don't care

Table 4-2: Truth table of BCD encoder 2 and equivalent number3

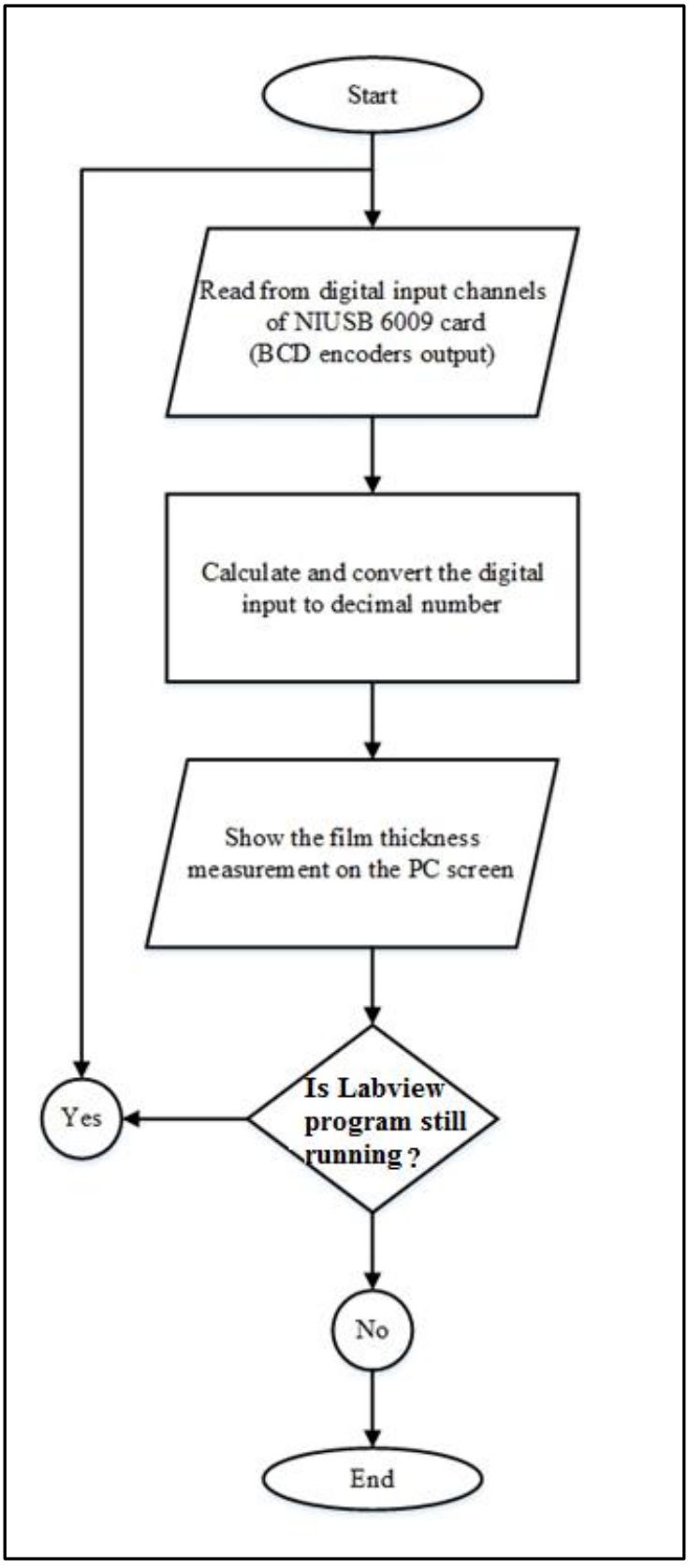

Figure 4-27: Flow chart of the digital level sensor Labview software

The Figure 4-28 shows the overall connection diagram used to make the digital sensor measurement. The bench test on the digital level sensor for measuring the film thickness in vertical annular flow is fully described in Chapter 5.

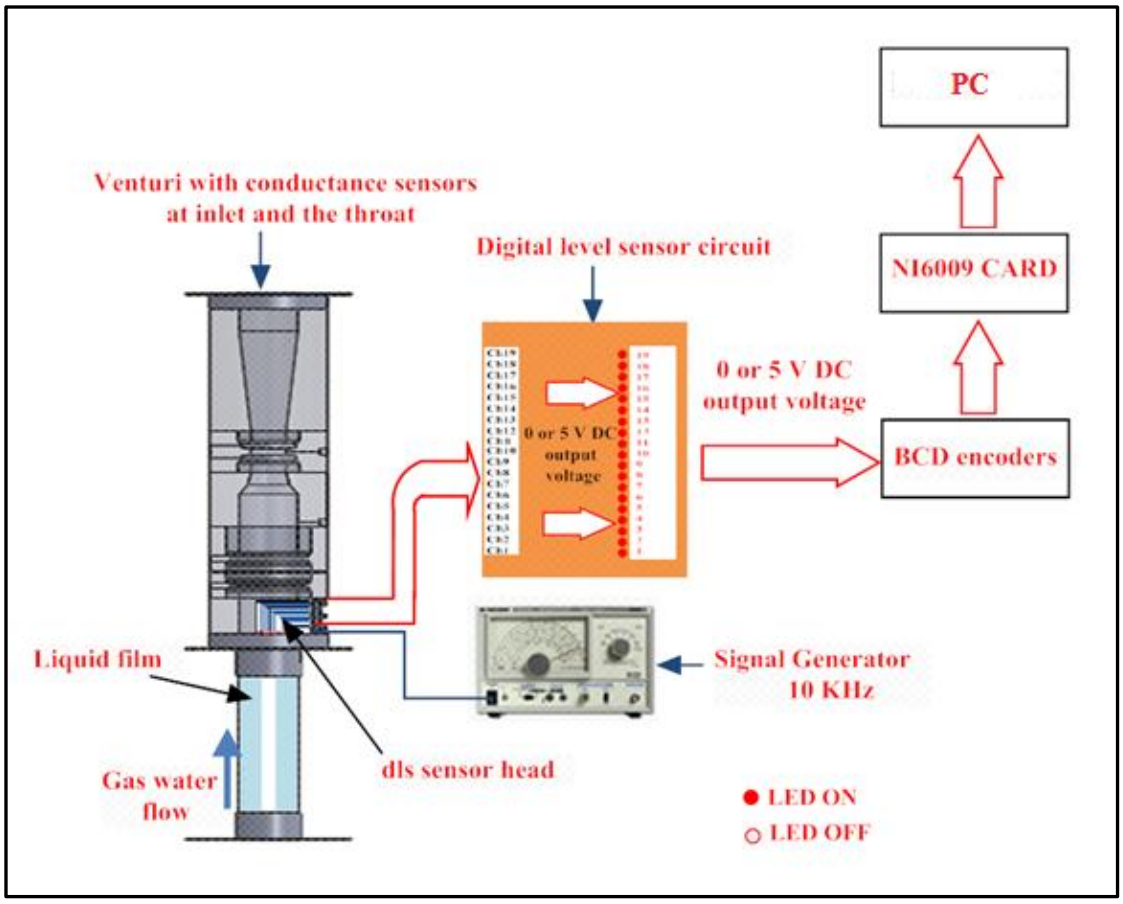

Figure 4-28: Overall connection diagram for the liquid film measurement

Summary

A Venturi meter with ring conductance sensors which can be used to measure the gas and water flow rates in vertical two phase flows was designed and constructed.
The Venturi meter was designed and constructed to measure the gas volume fraction at inlet and the throat of the Venturi in gas-water two phase flow (see Section 4.1). One of the most advanced features of this design is that all parts can be assembled and disassembled easily for maintenance. The Venturi meter with conductance sensors is also capable of measuring the gas volume fraction at the inlet and the throat of the Venturi.

The conductance Venturi meter consists of four sensors (see Section 4.1):

(i) the conductance ring sensor C in which two ring electrodes are mounted at the throat to measure the gas volume fraction at the throat of the Venturi.

(ii) the two conductance ring sensors A and B at the Venturi inlet in which four ring electrodes are mounted at the inlet. The sensors can be used to measure the film velocity of the liquid, and also to enable measurement of the gas volume fraction at the Venturi inlet.

(iii) digital level sensor at the Venturi inlet which is capable of measuring the film thickness (and hence the gas volume fraction) at the Venturi inlet.

The ring sensor B at the inlet of the Venturi was used as an alternative method of measuring the film thickness and hence the gas volume fraction at the inlet provided water conductivity σ_w is known.
The electronic circuits for the throat ring sensor, inlet ring sensors and digital level sensor at the Venturi inlet were built and calibrated to give appropriate dc output voltages. For sensors A,B and C their dc voltages are proportional to the local conductance of the mixture which can then be related to the local gas volume fraction at the relevant position in the Venturi.

Chapter 5 Bench Tests on the Venturi with the Conductance Sensors

Introduction

At the start of this chapter it should be reiterated that the Venturi with conductance sensors at the inlet and throat is capable of measuring the gas volume fraction at the inlet and the throat of the Venturi and the film thickness at the Venturi inlet in vertical annular water-gas flow as described in Sections 4.1 and 4.2. This work is based on the measurement of:

- The liquid film thickness at the inlet of the Venturi.
- The gas volume fractions at the inlet and the throat of the Venturi meter using electrical conductance technique.
- The film velocity.
- The water conductivity.
- The differential pressure between the inlet and the throat of the Venturi in wet gas flow.

The reasons for making these measurements are to determine the gas and water volumetric flow rates in annular flow, and the gas and water mass flow rates in vertical annular wet gas flow using Equations (3.42), (3.2), (3.3.39) and (3.44) respectively.

Before the Venturi with conductance sensors was used dynamically in the flow loop to take the measurement data in the vertical annular gas-water flow, a number of static experimental bench testing procedures were carried out. A bench test rig was designed and built in order to calibrate the conductance ring sensors at the inlet and the throat.

One of the conductance ring sensors at the inlet together with the conductance ring sensor at the throat of the Venturi needed to be calibrated in order for their cell constants to be determined. In addition, the digital level sensor that is used to measure the liquid film thickness at the inlet of the Venturi needed to be calibrated (before it is used in the flow loop) in order for the liquid film thickness and hence the gas volume

fraction at the inlet to be determined. This chapter presents the experimental bench testing procedures carried out on the Venturi with conductance ring sensors at the inlet and throat to simulate annular flow, and also the calibration of the digital level sensor at the Venturi inlet.

5.1 Bench tests on the Venturi with the conductnce sensors

Before the Venturi meter was used dynamically in the flow loop, a number of experimental bench testing procedures were carried out. A bench test rig was designed and built in order to calibrate the conductance measurements for one of the ring sensors at the inlet and the ring sensor at the throat. The static measurements were taken under laboratory conditions in which the temperature of the water was kept constant at 21^{o}C.

The simulation of the liquid film thickness and the gas volume fraction at the inlet of the Venturi is described in Section 5.1.1. The experimental setup of simulated annular two phase flow through a Venturi inlet is presented in Section 5.1.2. The simulation of the liquid film thickness and the gas volume fraction at the Venturi throat and the experimental setup of simulated annular flow through a Venturi throat are described in sections 5.1.3 and 5.1.4 respectively.

5.1.1 Simulation of the liquid film thickness and the gas volume fraction at the Venturi inlet in simulated vertical annular flow

To simulate the water film in the vertical Venturi meter, different diameters of nylon rods were inserted through the Venturi [84]. The gap between the outer surface of the rod and the inner surface of the Venturi inlet was then filled with water, representing the water film that would occur in a real annular flow (refer to Figure 5-1).

A nylon rod holder at the bottom of the Venturi was used to hold the different diameters of nylon rod in the static tests to ensure that the nylon rod was located at the exact centre of the Venturi. From the conductance circuit channel B (refer to Figure 4-

18) the cell constant of the upstream conductance sensors may be determined from the equation below:

$$V(\alpha_1) = \overline{K}(\alpha_1)\, \sigma_{w,ref} + V_{off}$$

Equation 5.1

$V(\alpha_1)$ corresponds to the output voltage $V_{4,B}$ from channel B conductance circuit in Figure 4.18. Note that for the research presented in this thesis the dc offset V_{off} adjusted to be zero.

In Equation (5.1) $\overline{K}(\alpha_1)$ is the cell constant for conductance ring sensor B and $\sigma_{w,ref}$ is the reference water conductivity. V_{off} is the value of $V_{4,B}$ when the Venturi is full of air only and hence the conductivity is zero, and, as stated above, was set to zero.

By rearranging Equation (5.1) $\overline{K}(\alpha_1)$ is given as:

$$\overline{K}(\alpha_1) = \frac{V(\alpha_1) - V_{off}}{\sigma_{w,ref}}$$

Equation 5.2

Hence we can find the relationship between the cell constant $\overline{K}(\alpha_1)$ and the gas volume fraction α_1 at the inlet to the Venturi. From Figure 5-5, the liquid film thickness $\delta_{i,sim}$ in simulated annular flow at the inlet of the Venturi is given by:

$$\delta_{i,sim} = \left(\frac{\mathrm{D_{inlet}} - \mathrm{D_{rod,i}}}{2}\right)$$

Equation 5.3

where $\delta_{\mathrm{i,sim}}$ is the simulated liquid film thickness at the Venturi inlet, $\mathrm{D_{inlet}}$ is the Venturi inlet diameter and $\mathrm{D_{rod,i}}$ is the diameter of the i^{th} nylon rod used in bench tests. The in situ gas volume fraction at the inlet of the Venturi is defined as the ratio of the area occupied by the gas to the total flow area. Therefore the gas volume

fraction at the inlet of the Venturi in simulated vertical annular flow $\alpha_{1i,sim}$ can be expressed as:

$$\alpha_{1,i,sim} = \left(\frac{D_{rod,i}}{D_{inlet}}\right)^2$$

Equation 5.4

$D_{rod,i}$ (mm)	$\delta_{i,sim}$ (mm)
46.05	1.975
40.92	4.54
36.64	6.68
32.72	8.64
28.74	10.63
25.55	12.225
22.55	13.725
20.55	14.725
16.55	16.725
10.21	19.895
6.2	21.9

Table 5-1: $D_{rod,i}$ and $\delta_{i,sim}$ used in the experiments

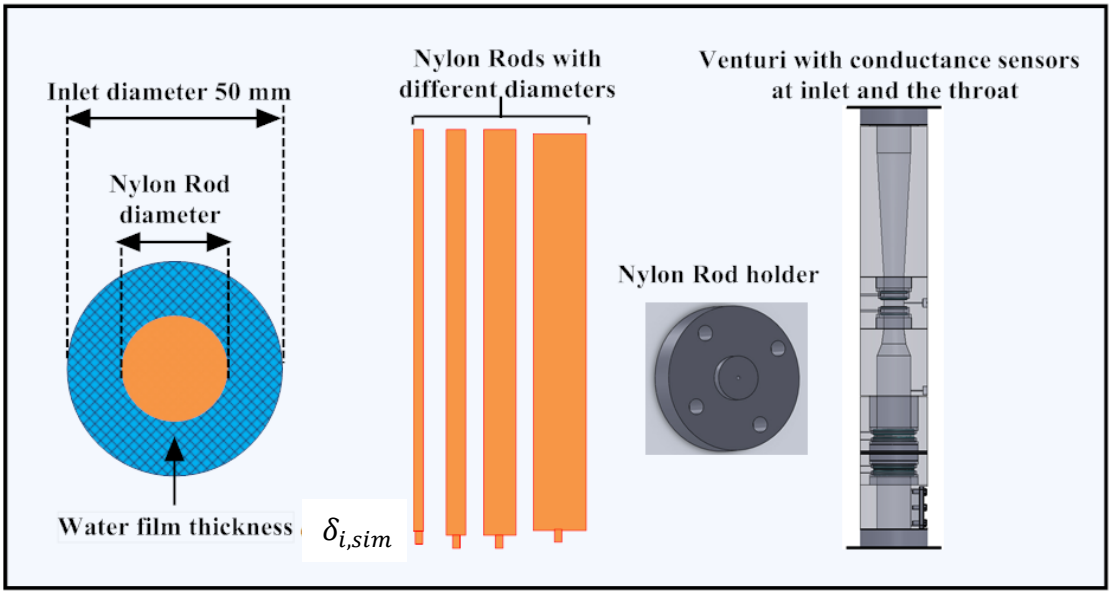

Figure 5-1: Configuration of the vertical simulated annular flow at the Venturi inlet

5.1.2 Experimental setup of simulated vertical annular two phase flow at the Venturi inlet

As mentioned earlier it is necessary to perform a number of experimental bench testing procedures before the Venturi meter may be used dynamically in the flow loop. Figure 5-2 shows the bench test experimental setup for vertical simulated water film through the inlet upstream conductance ring sensor B. Only one of the upstream conductance ring sensors, sensor B needed to be calibrated in order for its cell constant to be determined.

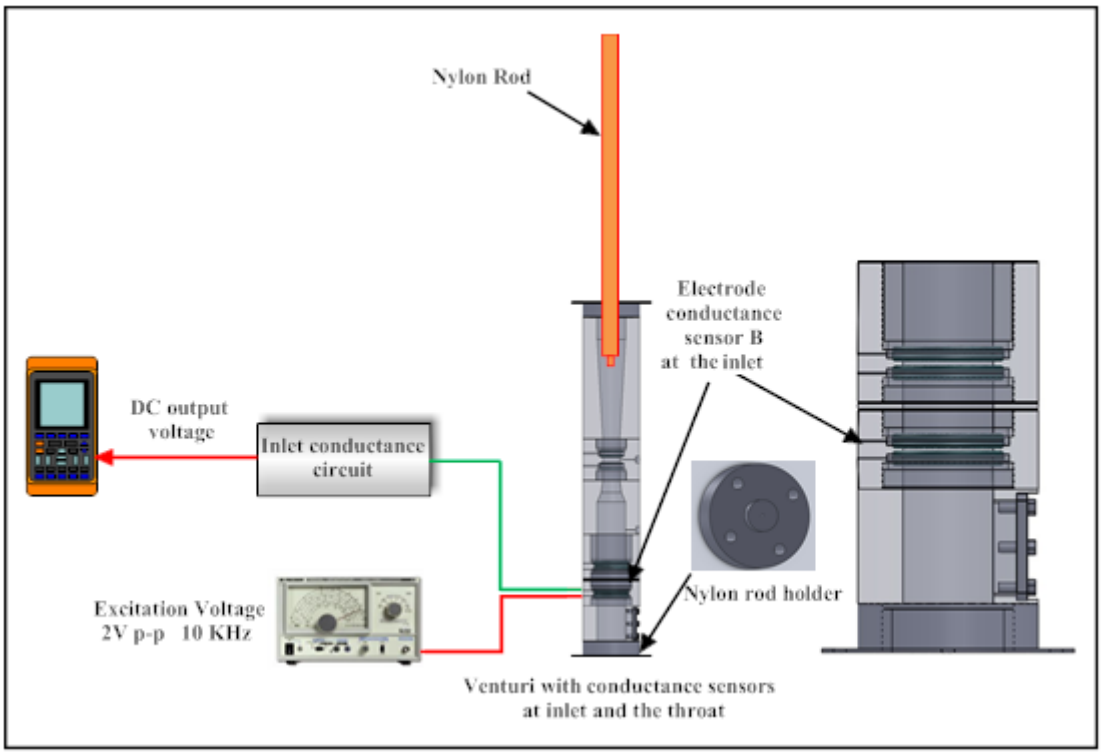

Figure 5-2: Bench test experimental setup of simulated vertical water film at the Venturi inlet

To do this, one electrode of the ring sensor B was connected to the signal generator in which the excitation voltage was 2V peak to peak and the sine-wave frequency was 10 kHz. The other electrode (measurement electrode) was then connected to the conductance circuit channel B (refer to Figure 4-18). The measurement circuit was

then adjusted to obtain zero output voltage when no water (only air) was present between the electrodes of the ring sensor B at the Venturi inlet.

The space between the electrodes of ring sensor B (which were flush mounted with the wall of the Venturi inlet) and the i^{th} nylon rod was then completely filled with water and the dc output voltage was obtained, the amplifier gain is the same during the calibration experiments as it is during the flow loop tests. Different diameters of nylon rods were successively inserted through the Venturi, the volume between the outer surface of the rod and the inner surface of the Venturi always being filled with water. The dc output voltages $V(\alpha_1)$ was recorded using the interfacing system (refer to Figure 5-2). The values of $V(\alpha_1)$ were dependent on the simulated liquid water film thickness at the inlet of the Venturi. Thees static measurements were taken under laboratory conditions in which the temperature of the water was kept constant at 21^{o}C. Different values of the water conductivity value were used and measured three times for each experiment using a conventional proprietary conductivity meter. Water conductivity values of 145μScm^{-1}, 175μScm^{-1} and 195.7μScm^{-1} were used, these different values being achieved by adding a different amount of salt to the water for each experiment.

5.1.3 Simulation of the liquid film thickness and the gas volume fraction at the Venturi throat in simulated vertical annular flow

A similar static procedure was used to calibrate the conductance measurement system at the throat of the Venturi (see Section 5.1.1) in which nylon rods with different diameters were inserted in the throat of the Venturi. The gap between the inner surface of the Venturi throat and the outer surface of the nylon rod throat was then filled with water representing the liquid film that would occur in a real annular gas-water two phase flow as shown in Figure 5-3. From the conductance circuit of the throat ring sensor (refer to Figure 4-20) the cell constant of the throat conductance sensor may be determined by the equation below:

$$V^t(\alpha_2) = \overline{K}^t(\alpha_2)\,\sigma_{w,ref} + V_{off}^t$$

Equation 5.5

where $V^t(\alpha_2)$ is the output voltage from throat conductance circuit, and corresponds to the output voltage $V_{4,c}$ in Figure 4.20, $\overline{K}^t(\alpha_2)$ is the cell constant for the ring conductance sensor C, $\sigma_{w,ref}$ is the reference water conductivity and V_{off}^t is the offset voltage of the throat conductance circuit when the Venturi was full of air only and hence the conductivity is zero. V_{off}^t was always set to zero for the work described in this thesis. The subscript t refers to the throat of the Venturi.

By rearranging Equation (5.5):

$$\overline{K}^t(\alpha_2) = \frac{V^t(\alpha_2) - V_{off}^t}{\sigma_{\mathrm{w,ref}}}$$

Equation 5.6

Hence we can find the relationship between the cell constant $\overline{K}^t(\alpha_2)$ and the gas volume fraction α_2 at the throat of the Venturi. From Figure 5-6, the liquid film thickness $\delta_{i,t,\mathrm{sim}}$ in simulated annular flow at the inlet of the Venturi is given by:

$$\delta_{i,t,sim} = \left(\frac{\mathrm{D_t} - \mathrm{D_{rod,i}}}{2}\right)$$

Equation 5.7

where $\delta_{i,t,\mathrm{sim}}$ is the simulated liquid film liquid film thickness at the Venturi throat, $\mathrm{D_t}$ is the Venturi throat diameter and $\mathrm{D_{rod,i}}$ is the rod diameter of the i^{th} nylon rod. The gas volume fraction at the throat of the Venturi in simulated vertical annular flow $\alpha_{2,i,sim}$ can be expressed as:

$$\alpha_{2,i,sim} = \left(\frac{\mathrm{D_{rod,i}}}{\mathrm{D_t}}\right)^2$$

Equation 5.8

$\mathbf{D_{rod,i}}$ **mm**	$\boldsymbol{\delta_{i,t,sim}}$ **mm**
28.74	0.63
25.55	2.225
22.55	3.725
20.55	4.725

16.55	6.725
10.21	9.895
6.2	11.9

Table 5-2: $D_{rod,i}$ and $\delta_{i,t,sim}$ used in the experiments

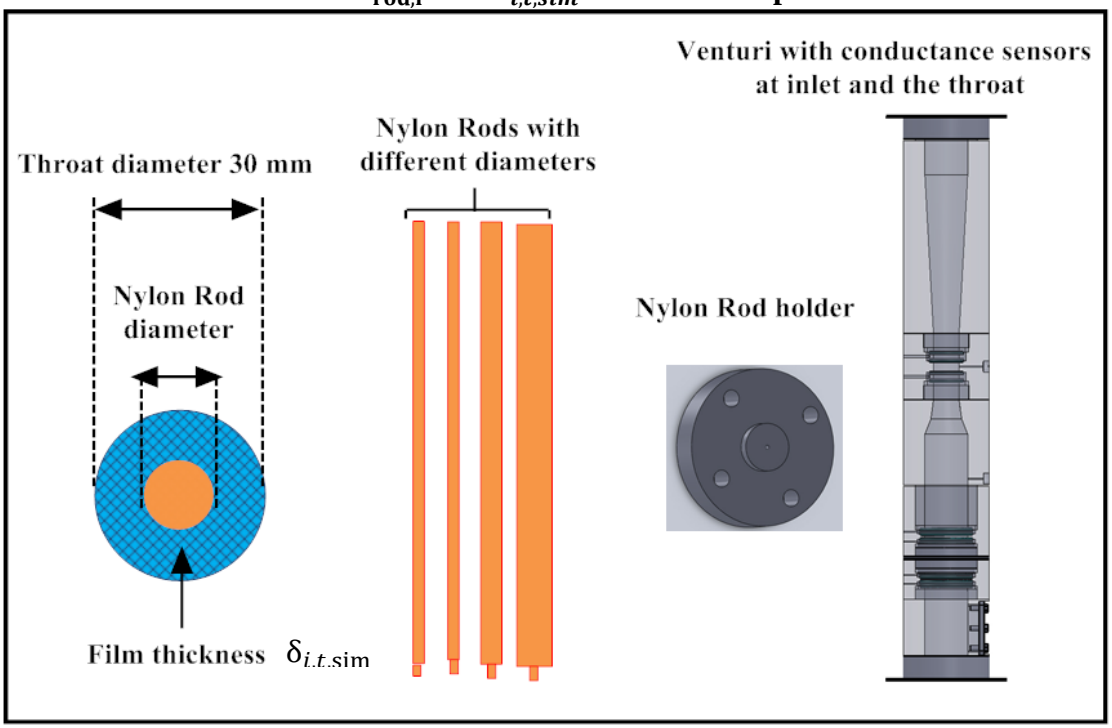

Figure 5-3: Configuration of the vertical simulated annular flow at the Venturi throat

5.1.4 Experimental setup of simulated vertical annular two phase flow at the Venturi throat

In a similar way to that for the inlet ring sensor, Figure 5-4 shows the bench test experimental setup for a vertical simulated water film at the throat of the Venturi. One electrode of the ring senor C at the throat was connected to the signal generator in which the excitation voltage was 2V peak to peak and the sine-wave frequency was 10 kHz. The other electrode (measurement electrode) was then connected to the throat conductance circuit (refer to Figure 4-20). The circuit dc offset adjusted to set V_{off} to zero when no water (only air) was present between the electrodes (ring sensor C) at the throat. Thus V_{off} in Equation (5.1) was always effectively zero.

The volume between the throat electrodes (ring sensor C) was then completely filled with water and dc output voltage was obtained, the gain of the amplifier for the throat ring sensor C was the same during the bench test as during the flow loop tests described in chapter 6 and 7. Note that the amplifier gain was set by adjusting the variable resistance in the amplifier part of the circuit shown in Figure 4-20. Different diameters of nylon rod were successively inserted through the Venturi with the gap between the inner surface of the Venturi and the outer surface of the nylon rod being filled with water. The dc output voltage $V^t(\alpha_2)$ was recorded using the interfacing system (refer to Figure 5-4). The dc output voltage of each test is a function of the volume fraction dependent cell constant $\overline{K}^t(\alpha_2)$, the water conductivity, the excitation voltage and the resistance feedback at the throat of the Venturi.

The static measurements were taken under laboratory conditions in which the temperature of the water was kept constant at 21^{o}C. Different values of the water conductivity value were used and measured three times for each experiment using a conventional conductivity meter. Water conductivity values of 64μScm^{-1}, 92.4μScm^{-1} and 166.5μScm^{-1} were used. It should be noted that the water conductivities were different in the two sets of experiments because of the difficulty in achieving a precise conductivity value by adding salt to water.

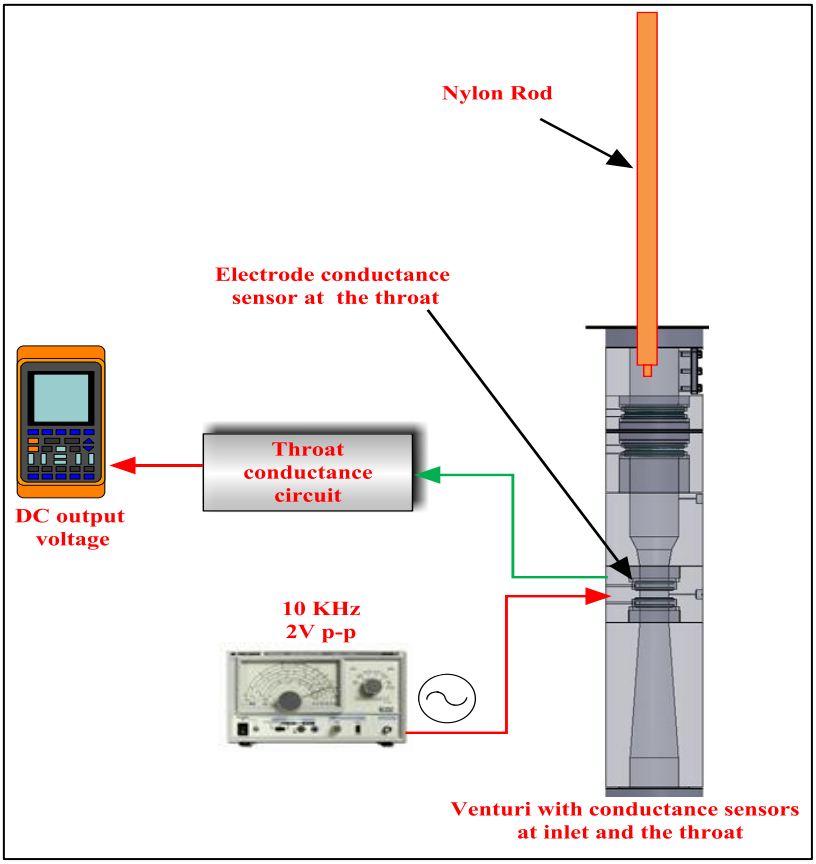

Figure 5-4: Bench test experimental setup of the simulated annular flow through the Venturi throat

5.1.5 Experimental results from the upstream ring sensor B at Venturi inlet and ring sensor C at the throat in simulated annular flow

As described previously, a bench test rig was designed and built in order to calibrate the conductance measurements at the inlet and the throat. Upstream conductance sensor B and the throat sensor (sensor C) were calibrated in order for their cell constants to be determined. Bench tests were performed by inserting non-conductive nylon rods with different diameters through the inlet and throat of the Venturi meter.

The dc output voltages from the electronic measurement circuits were recorded which are then related to the liquid water film at the inlet and the throat of the Venturi. Figure 5-5 shows the relationship between the gas volume fraction α_1 and the cell constant $\overline{K}(\alpha_1)$ obtained from the vertical simulated annular flow experiments at the inlet of the Venturi. Note that the relationship between $\overline{K}(\alpha_1)$ and α_1 is independent of the water conductivity, for the range of values of water conductivity investigated.

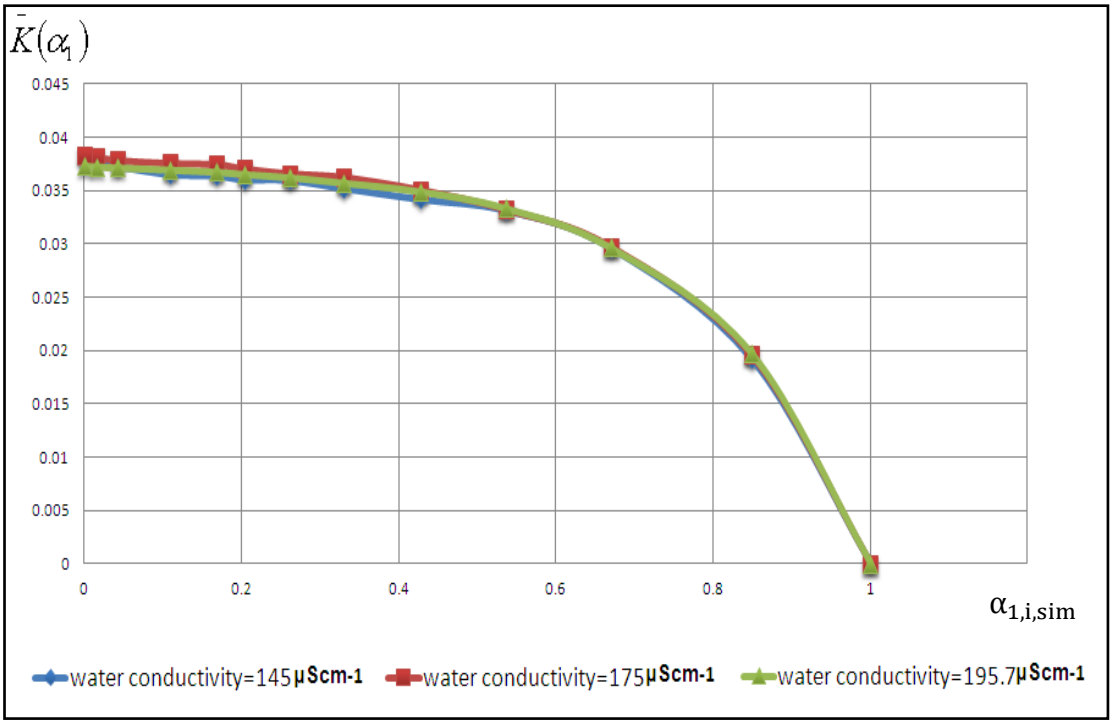

Figure 5-5: Calibration curve for upstream ring sensor at the Venturi inlet $\bar{K}(\alpha_1)$ *vs* $\alpha_{1,i,sim}$

Once the output voltage from the channel B conductance circuit $V(\alpha_1)$ at the Venturi inlet is measured, the dc offset is known and the reference water conductivity is known, then the cell constant $\bar{K}(\alpha_1)$ may be easily determined from Equation (5.2) in simulated annular flow. From Figure 5-5, plotting the cell constant on the vertical axis against the gas volume fraction on the horizontal axis, enables a more convenient best fit polynomial equation to be obtained (see Equations (5.9) and (5.10)).

$$\bar{K}(\alpha_1) = -0.1065(\alpha_{1,i,sim})^4 + 0.121(\alpha_{1,i,sim})^3 - 0.054(\alpha_{1,i,sim})^2 + 0.0024\alpha_{1,i,sim} + 0.038$$

Equation 5.9

For the flow loop tests described in chapters 6 and 7, Figure 5-5 can be used as follows.

I. Suppose that for a given flow condition $V(\alpha_1)$ is measured and V_{off} is known to be equal to zero. Then, if α_1 is known from digital level sensor, the corresponding value of $\overline{K}(\alpha_1)$ can be obtained from Figure 5-5 (or the polynomial fit to the data in Figure 5-5) to enable the conductivity $\sigma_{w,m}$ of the flowing water to be determined using Equation (3.9) or Equation (5.1).

II. Alternatively if the water conductivity σ_w is already known (e.g. by using proprietary conductivity sensor) then $\overline{K}(\alpha_1)$ can be determined from measurement of $V(\alpha_1)$, V_{off} and σ_w using Equation (3.9) (or Equation (5.1)). α_1 can then be determined from $\overline{K}(\alpha_1)$ using Figure 5-5 or the polynomial fit to the data in Figure 5-5.

Figure 5-6 shows the relationship between the gas volume fraction α_2 and the cell constant $\overline{K}^t(\alpha_2)$ obtained from the vertical simulated annular flow at the throat of the Venturi. Again, note that $\overline{K}^t(\alpha_2)$ vs α_2 is independent of the water conductivity.

In a real annular flow, once the output voltage from the throat ring sensor conductance circuit $V^t(\alpha_2)$ is measured, the cell constant $\overline{K}^t(\alpha_2)$ can be easily determined from Equation (5.6) since the water conductivity is known (see above) and the dc offset is also known.

Note that for the flow loop tests described in chapter 6 and chapter 7 the conductivity $\sigma_{w,m}$ of the flowing water can be obtained from inlet sensor B and the digital level sensor as described above. Alternatively, the water conductivity can be obtained using a proprietary conductivity meter.

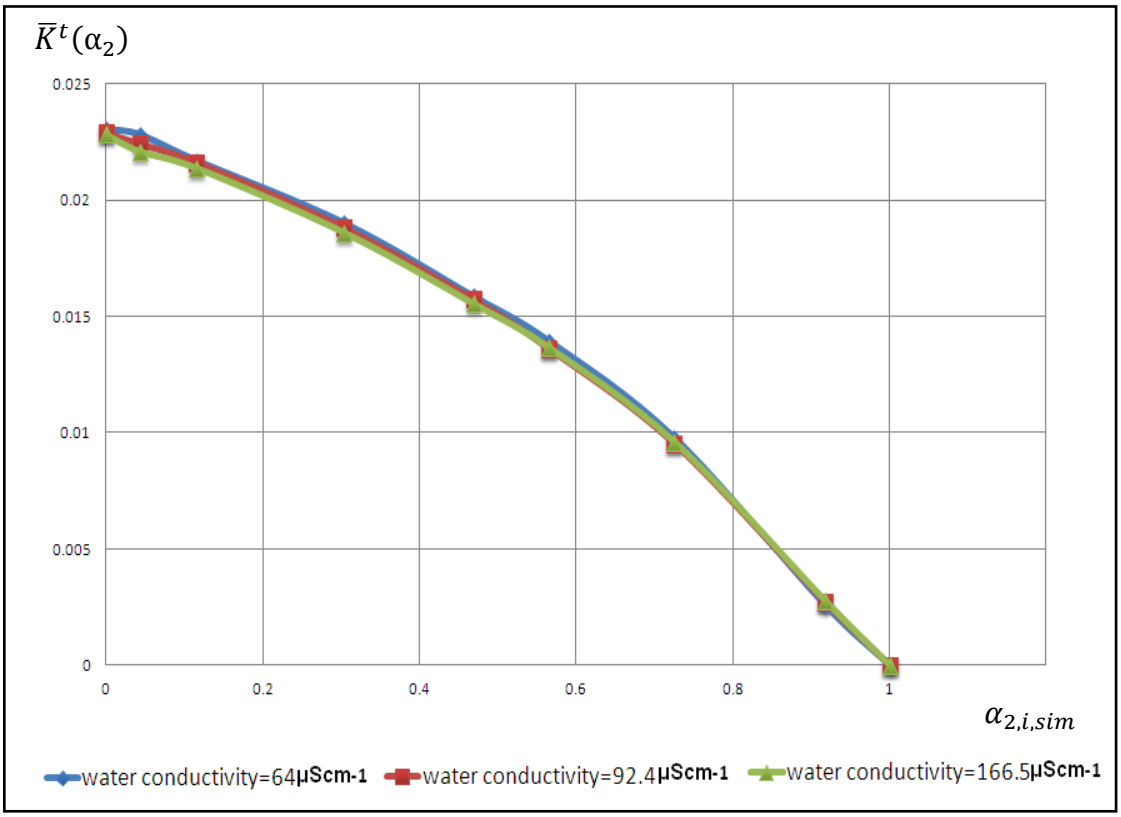

Figure 5-6: Calibration curve for ring sensor at the throat of the Venturi $\bar{K}^t(\alpha_2)$ vs α_2

$$\bar{K}^t(\alpha_2) = 0.0058(\alpha_{2,i,sim})^4 - 0.0162(\alpha_{2,i,sim})^3 - 0.0008(\alpha_{2,i,sim})^2 - 0.0119\alpha_{2,i,sim} + 0.023$$

Equation 5.10

5.2 Experimental setup and the results for the digital level sensor

Before the digital level sensor was used dynamically in the flow loop, an experimental bench testing procedure was carried out. A bench test rig was designed and built to test the digital level sensor at the Venturi inlet in order for the water film thickness $\tilde{\delta}$ to be measured enabling the water volume fraction $\alpha_{w,1}$ at the Venturi inlet to be determined in vertical annular water gas flow, using Equation (3.1).

The excitation electrode of the dls head sensor was connected to the signal generator in which the excitation voltage was 2 volt peak to peak and the sine-wave frequency was 10 kHz. The measurement conductance electrodes of the dls head sensor placed in a plastic rectangular box with a ruler. This allowed testing of the dls head sensor by adding an amount of water to the plastic box. The level of the water in the box (as measured by the ruler) was compared with the water level as indicated by the outputs from channels 1 to 19 of the digital level sensor conductance circuit (refer to Figure 4-23).

Figure 5-7, shows the experimental setup of the dls sensor head. The test results showed that whenever air is present the sensor channels 1 to 19 are all off and whenever water is present the sensor channel electrodes covered by water activate, indicating that water is present.

Figure 5-8 shows the outputs from the digital level sensor conductance circuit versus water height. This test showed that when the water is present LEDs successively turn ON as the water level rises and the effect of the test has shown that whenever the water level is increasing or decreasing, the LEDs turn ON or OFF correctly as expected. Using the digital level sensor, the water height in the range 0 to 9.5mm could be determined with an accuracy of $\pm$ 0.5mm.

The bench testing procedure was carried out to test the output from the channels 1 to 19 of the digital level sensor conductance circuit with the BCD encoders and NI USB 6009 data acquisition device.

Channels 1 to 19 of the dls conductance circuit were connected with the BCD encoders and NI USB 6009 device as shown in Figure 4-26. A Labview software was used during the bench test to read the data from the BCD encoders via NI USB 6009 card.

The Labview water level reading value was compared with the water level in the plastic box as measured by the ruler. The results agreed with each other e.g if the with water level in the box as measured by the ruler was 2mm, on the PC screen using the

Labview software (by reading the data from BCD encoders via NI USB 6009 card) showed 2mm as well. etc.

As mentioned earlier in section 4.2.3, for the flow loop experiments described in chapter 6 and 7 the digital level sensor head is mounted on the inner surface of the Venturi inlet and measures the liquid film thickness $\tilde{\delta}$ in annular wet gas flow. Measurement of $\tilde{\delta}$ enables the water volume fractions $\alpha_{w,1}$ to be determined using Equation (3.1). Once the the water volume fraction $\alpha_{w,1}$ at the Venturi inlet is obtained then the water flow rate can be determined using equation (3.2).

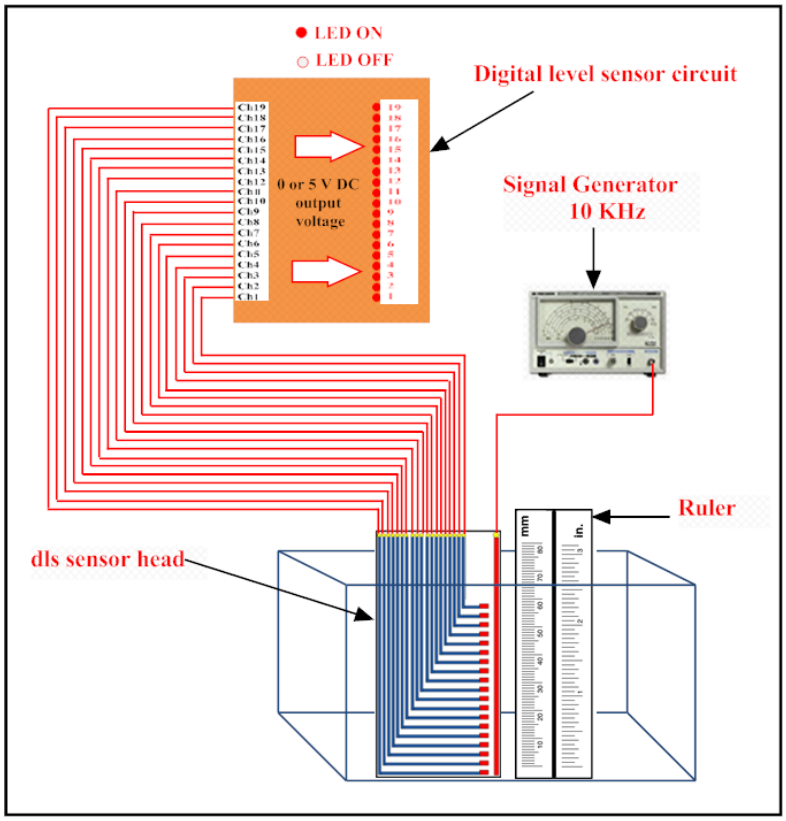

Figure 5-7: Calibration bench test of the digital level sensor

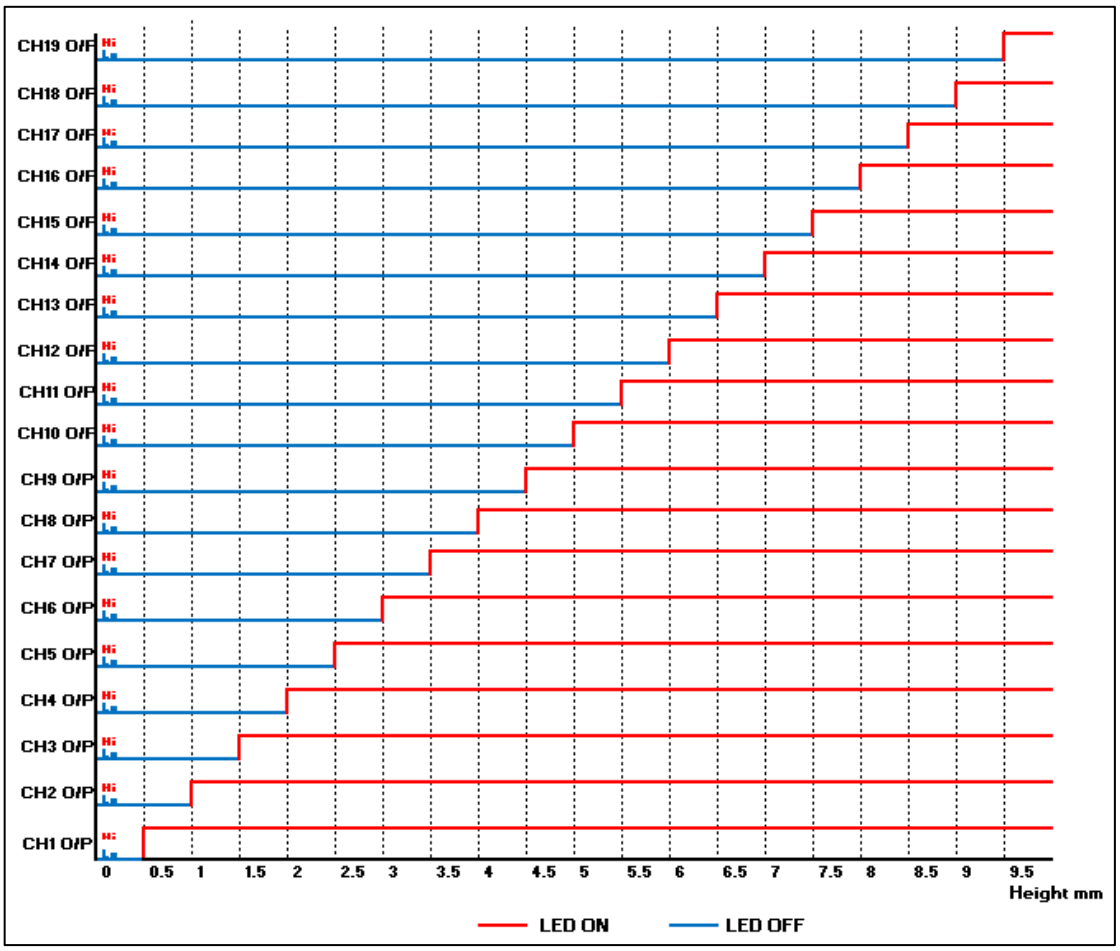

Figure 5-8: Outputs from the 19 channels of the digital level sensor verses water height

Summary

Before the Venturi meter was used dynamically in the flow loop, a number of experimental bench static testing procedures were carried out. Bench tests were designed and built to calibrate the one of the inlet ring sensors and to calibrate the ring sensor at the throat. The reason for carrying out the static tests on Venturi with conductance sensors at inlet and the throat was to find the relationships between the gas volume fractions α_1 and α_2 at the inlet and throat and the corresponding cell constants $\overline{K}(\alpha_1)$ and $\overline{K}^t(\alpha_2)$. This was achieved by using the dc output voltages measured from the throat and inlet electrical conductance circuits in simulated annular flow. These relationships enable the Venturi with conductance sensors to be used dynamically in real vertical annular water-gas two phase flows.

Calibration of the ring conductance sensors was achieved by inserting different diameters of nylon rod into the Venturi inlet and the throat, and filling the gap between the outer surface of the rod and the inner surface of the Venturi with water, thus representing the water film that would occur in a real annular flow. The dc output voltages from the electronic measurement circuits were recorded which were then related to the liquid water film thickness at the throat and inlet of the Venturi.

Chapter 6 The Annular Flow Rig and its Associated Measurement Instrumentation

Introduction

To carry out measurements in vertical annular gas-water two phase flows using the Venturi with conductance ring sensors at the inlet and throat, several items of equipment were required. The Venturi itself represents the device under test. Other instruments used in the flow loop included a DP (differential pressure) sensor, a variable area flow meter and a turbine flow meter which made up the reference measurement devices. In the current investigation, the flow loop was developed at the University of Huddersfield to enable vertical annular gas-water flows to be established. This flow loop has a 50 mm internal pipe diameter and a 2.5 meter long test section.

This chapter describes the experimental setup and the instrument devices used with annular gas-water two phase flows. An explanation of the instrumentation used on the flow loop, and the calibration of the reference measurement devices, is given in Section 6.2. These include:-

- A side blower (RT-1900) to provide the required high gas flow rates.
- A variable area flow meter to provide a reference measurement of the required gas volumetric flow rates.
- A turbine flow meter to provide a reference measurement of the water volumetric flow rates.
- Differential pressure devices, including a DP cell.

A change-over valve and flushing system used with the DP cell is described in Section 6.3. The NI USB data acquisition device is described in Section 6.4.

6.1 Two phase flow loop capabilities

An existing multiphase flow loops available at the University of Huddersfield was modified to produce gas and water flows in the annular flow regime. The gas phase is air with approximate density of 1.2kgm^{-3}. For the current investigation, the working section was composed of a 50mm internal diameter pipe, approximately 2.5m long. A photograph of the vertical annular flow gas-water two phase flow loop (see Section 6.1.1) used in the current research is shown in Figure 6-1. The configuration is described in detail below. Details of the reference measurement devices used in this configuration are given in Section 6.2.

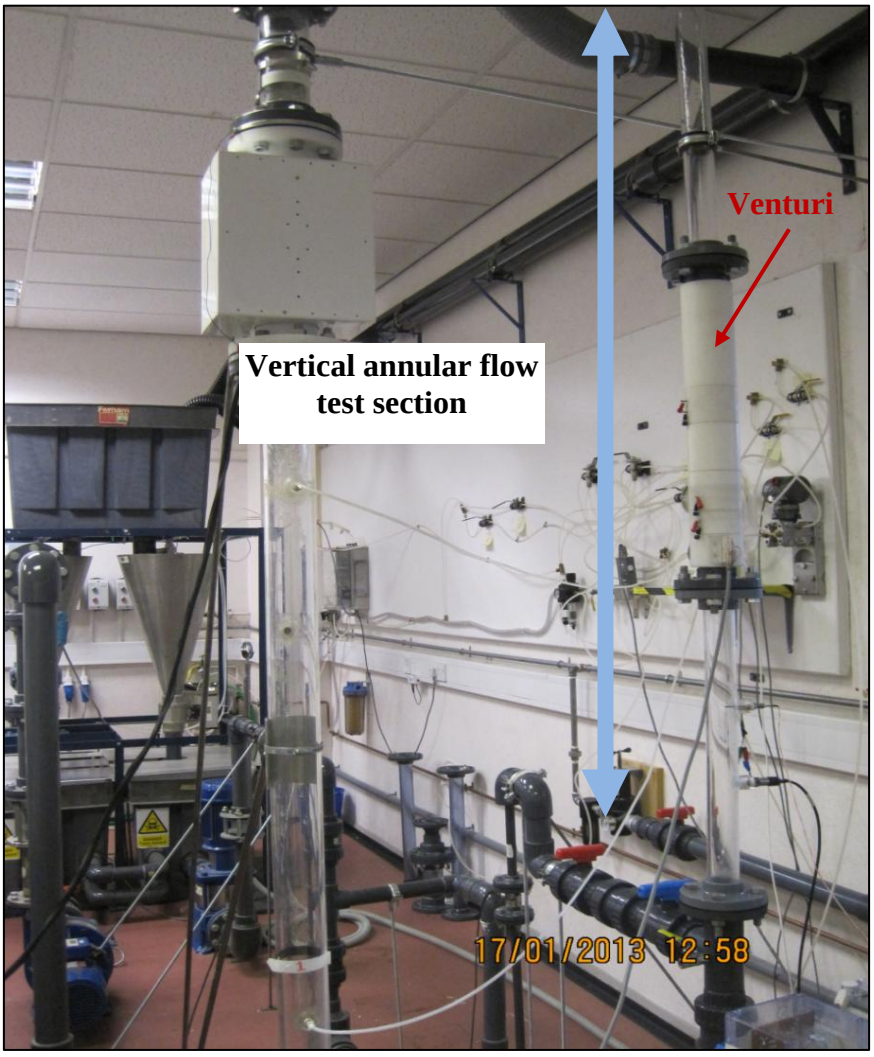

Figure 6-1 The gas-water two phase flow loop at the University of Huddersfield. The Venturi with conductance sensors is shown mounted in the test section.

6.1.1 Annular gas-water two phase flow configuration

In order to carry out the measurements using the Venturi with conductance ring sensors at the inlet and throat in annular flow, a vertical annular two phase flow configuration was established in the flow loop test section. A schematic diagram of the vertical annular two phase flow rig is shown in Figure 6-2. With reference to Figure 6-2, water was pumped from the water tank into the vertical test section through a turbine flow meter using a centrifugal pump.

The turbine flow meter was used to provide a reference measurement of the water volumetric flow rate $Q_{w,ref}$ in the rage of $0.472\ \mathrm{m^3/hr}$ up to $2.994\ \mathrm{m^3/hr}$ corresponding to water superficial velocities U_{ws} in the range of $0.066\ (\mathrm{m/s})$ up to $0.423\ (\mathrm{m/s})$.

Air was pumped using a "side channel blower", RT-1900 (see Section 6.2.1), into the vertical test section through a variable area flow meter (see Section 6.2.2) to give reference measurement of the gas flow rate in the range $50\ \mathrm{m^3/hr}$ up to $155\ \mathrm{m^3/hr}$ corresponding to gas superficial velocities U_{gs} in the range of $7.073\ (\mathrm{m/s})$ up to $21.927\ (\mathrm{m/s})$. The reference gas volumetric flow rate was denoted $Q_{g,ref}$. The sum of the reference gas and water volumetric flow rates gives the reference mixture volumetric flow rate, $Q_{m,ref}$.

Predicted gas, water and mixture volumetric flow rates (Q_g , Q_w and Q_m respectively) were obtained using The Abbas (2010) [81] and the homogenous flow models (see Chapter 3) and the models of Murdock [10] and de Leeuw [15, 16] (described in Chapter 2) using the Venturi with conductance sensors. These results were compared with the reference gas, water and mixture volumetric flow rates $Q_{g,ref}$, $Q_{w,ref}$ and $Q_{m,ref}$ to analyse the error in the predicted flow rates (see Chapter 7). A Honeywell DP cell, STD-120 (see Section 6.2.4), was used to measure the differential pressure, $\Delta P_{TP,wg}$, between the inlet and the throat of the Venturi.

The other models [12], [14], [13] and [2] (described in Chapter 2) were used as well but the error in the predicted gas, water and mixture flow rates was more worst.

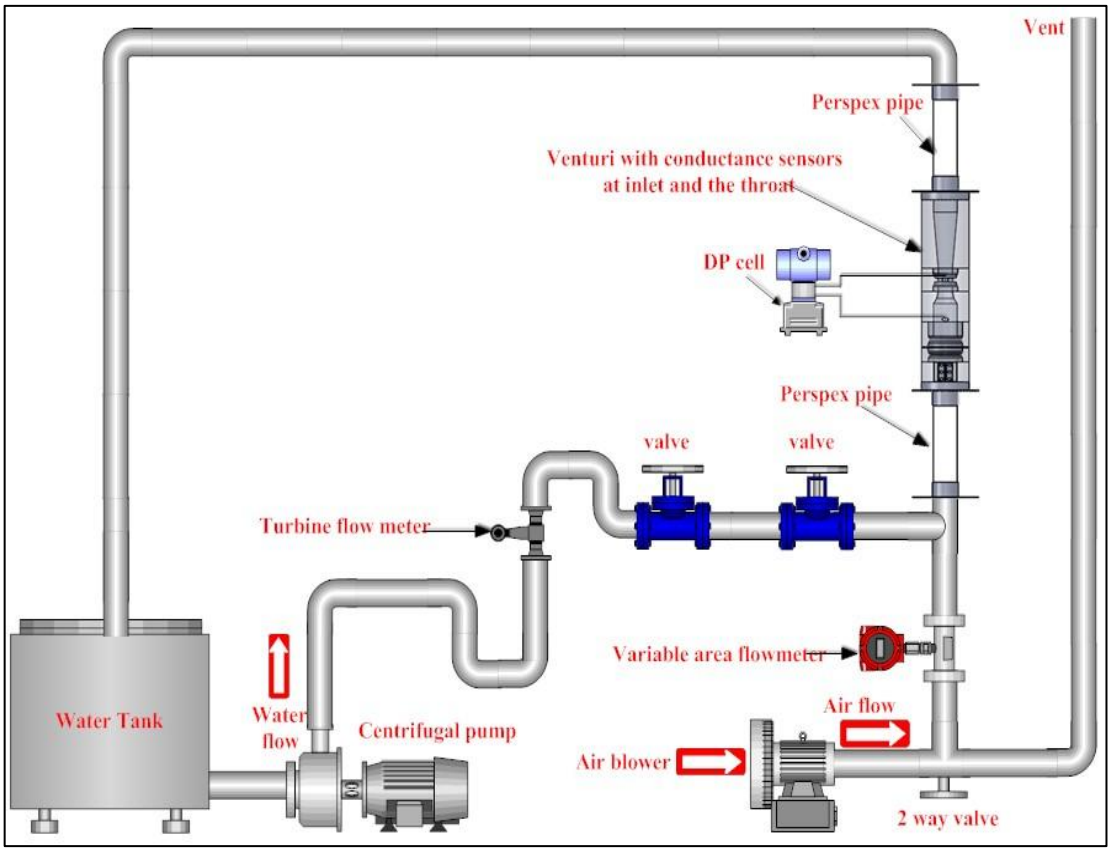

Figure 6-2: A schematic diagram of the vertical annular gas-water two phase flow loop at the University of Huddersfield.

The digital level sensor at the inlet of the Venturi was used to measure the film thickness $\tilde{\delta}$ of annular two phase flow in order to determine the water volume fraction $\alpha_{w,1}$ at the inlet of the Venturi using Equation (3.1). The two ring sensors A and B (electrodes 3, 4, 5 and 6) at the inlet of the Venturi were used to measure the liquid film velocity $U_{f,xc}$ of the annular two phase flow using a cross correlation technique. The ring sensor B at the inlet was used to measure the gas volume fraction α_1 at the inlet of the Venturi and used as an alternative technique to measure the film thickness δ provided that the water conductivity was already known. The alternative ring sensor, was used in conjunction with the digital level sensor to measure water conductivity. The ring sensor C (electrodes 1 and 2) at the throat of the Venturi was used to measure the gas volume fraction α_2 at the Venturi throat.

Once the gas volume fraction α_1 at the inlet, the gas volume fraction α_2 at the throat and the differential pressure $\Delta P_{TP,wg}$ across the Venturi are measured, the predicted gas and water volumetric flow rate in annular two phase flow can then be predicted using the models given in Chapter 3. A schematic diagram of the instrumentation systems together with the interfacing system is shown in Figure 6-3.

For the throat ring sensor C, one electrode of the ring sensor was connected to the excitation voltage (2 volt peak to peak) with the sine wave frequency (10 kHz). The other electrode was connected to the electrical conductance circuit of the throat (see Section 4.2.2) by which the gas volume fraction, α_2, could be obtained from the dc output voltages.

For ring sensor A at the inlet, one electrode was connected to the to the excitation voltage (2 volt peak to peak) with the sine wave frequency (10 kHz). The other electrode was connected to the electrical conductance circuit channel A at the Venturi inlet. For ring sensor B at the inlet one electrode was connected to the excitation voltage (2 volt peak to peak) with the sine wave frequency (10 kHz) and the other electrode was connected to the electrical conductance circuit channel B at the Venturi inlet (see section 4.2.1). With this configuration the film velocity $U_{f,xc}$ could be obtained by cross correlation from the dc output voltages from ring sensors A and B.

For the digital level sensor, the excitation electrode of the sensor was connected to the excitation voltage (2 volt peak to peak) with a 10 kHz sine wave frequency. The measurement electrodes of the sensor head were connected to the digital level sensor electrical conductance circuit (see Section 4.2.3) by which the liquid film thickness $\tilde{\delta}$ could be obtained.

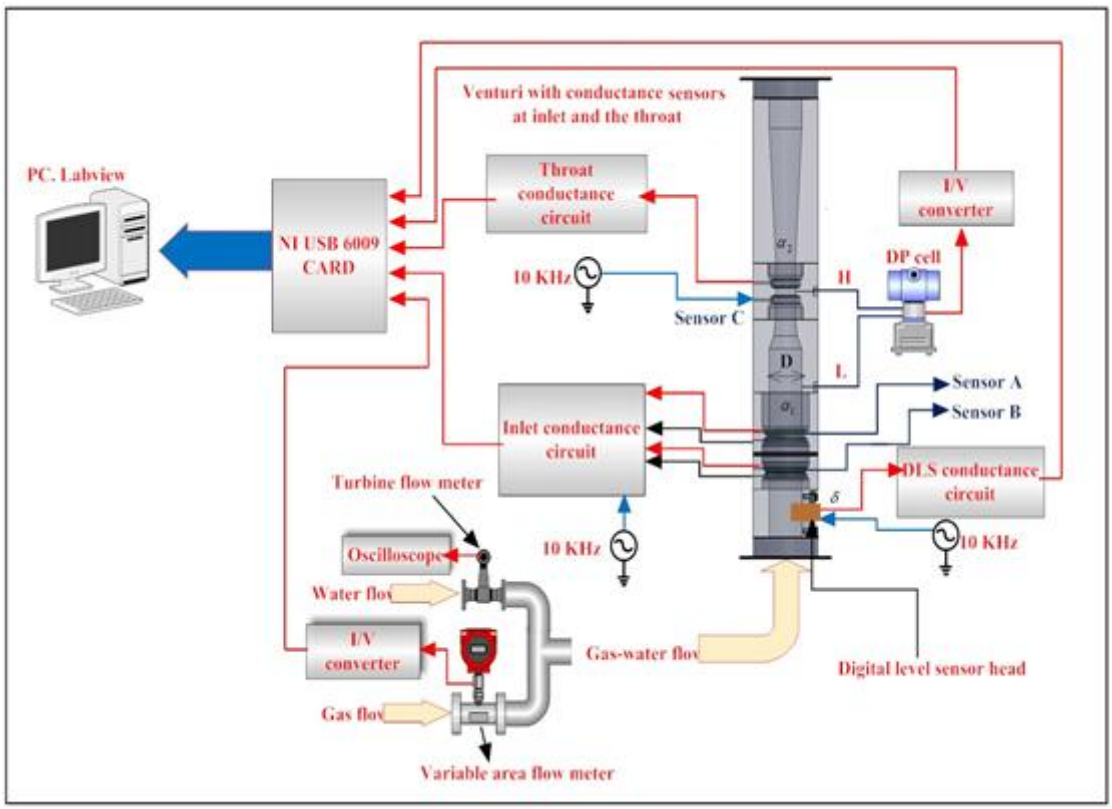

Figure 6-3: Schematic diagram of the instrumentation systems and the interfacing system

6.2 Reference measurement devices used on the gas-water two phase flow loop

As stated previously, the Venturi flow meter with conductance at the inlet and the throat represented the device under test used in vertical annular two phase flows. Additional instruments on the flow loop are described below.

6.2.1 Air supply

The air flow is supplied by the Airtec Air Systems Ltd RT-1900 side channel blower [85]. A side channel blower was used for the current study to give the necessary high gas flow rate in vertical annular gas-water two phase flows. A photo of the side channel blower (RT-1900) and its specification are shown in Figure 6-4. From Figure 6-4 it is clear that the gas flow rate Q_g provided by the side channel blower depends on the differential pressure ΔP.

A 2 way valve as shown in Figure 6-2, is needed because the air flow rate from the side channel blower is approximately constant and we could not vary the speed of the side channel blower. The only way we can adjust the air flow rate is by increasing or decreasing the amount of air flow through the vent using the 2 way valve.

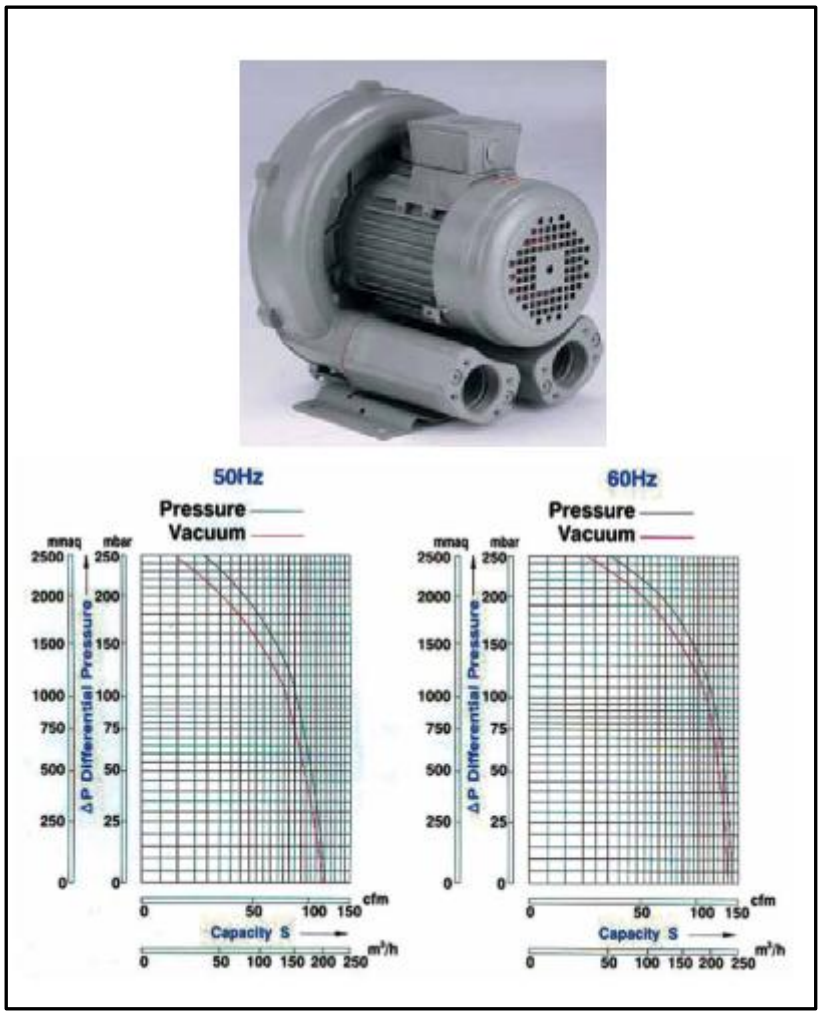

Figure 6-4: A photo of Airtec Air Systems Ltd RT-1900 side channel blower and its specification [85]

6.2.2 The Variable Area Flowmeter (VAF)

An "Able" variable area flowmetr (type 50PTnAAI75) was used to provide a reference measurement of the gas volumetric flow rate received from the side channel blower. The working of the variable area flowmeter is that the differential pressure remains constant and the air flow is measured by the position of a moving float in a

tube of varying cross-sectional area. For this flow meter, air passing inside the meter moves the profiled float to a position where the forces created by the flow are balanced by the weight of the float.

A photograph of the VAF is shown in Figure 6-5. The flow rate measured by the VAF can be read directly from the front display that was calibrated by the manufacturer to give the gas volumetric flow rate in a range of $30\ \mathrm{m}^3/\mathrm{hr}$ to $300\ \mathrm{m}^3/\mathrm{hr}$.

The VAF also gives an output from 4 to 20mA, with 4mA corresponding to the flow rate of approximately $30\ \mathrm{m}^3/\mathrm{hr}$ and 20mA corresponding approximately to $300\ \mathrm{m}^3/\mathrm{hr}$. A calibration procedure relating the 4 to 20mA output to the actual gas flow rate is given below. In order to interface this 4 to 20mA output to the NI USB 6009 data acquisition card, a current to voltage (I/V) converter was needed (refer to Figure 6-7). This converter converted the current output signal from the VAF (4-20 mA) into a dc output voltage (1-5V) to provide voltage signals for the NI USB 6009 data acquisition card to read. [A further current-to-voltage (I/V) converter circuits was used to convert the current output signals from the DP cell (4-20 mA) into dc output voltages (1-5V)].

The dc output voltage from the (I/V) convertor circuit of the VAF was calibrated against the analogue signal read from the gauge meter on the front display of the VAF for different values of the gas volumetric flow rates, the analogue display having previously been calibrated by the VAF manufacture.

The relationship between the dc output voltage V_{VAF} and the gas volumetric flow rate Q_g (read from the gauge meter of the front display) is shown in Figure 6-6. It can been seen from the Figure 6-6 that the output voltage V_{VAF} from VAF is upto 3.5 Volt dc and we did not calibrate upto 5 Volt dc corresponding approximately to $300\ \mathrm{m}^3/\mathrm{hr}$ this is because such high flow rates could not be achieved from the side channel blower (RT-1900).

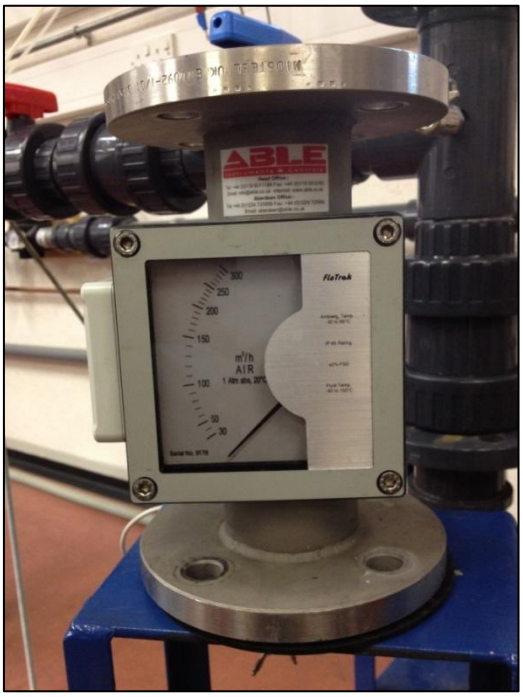

Figure 6-5: A photograph of the VAF

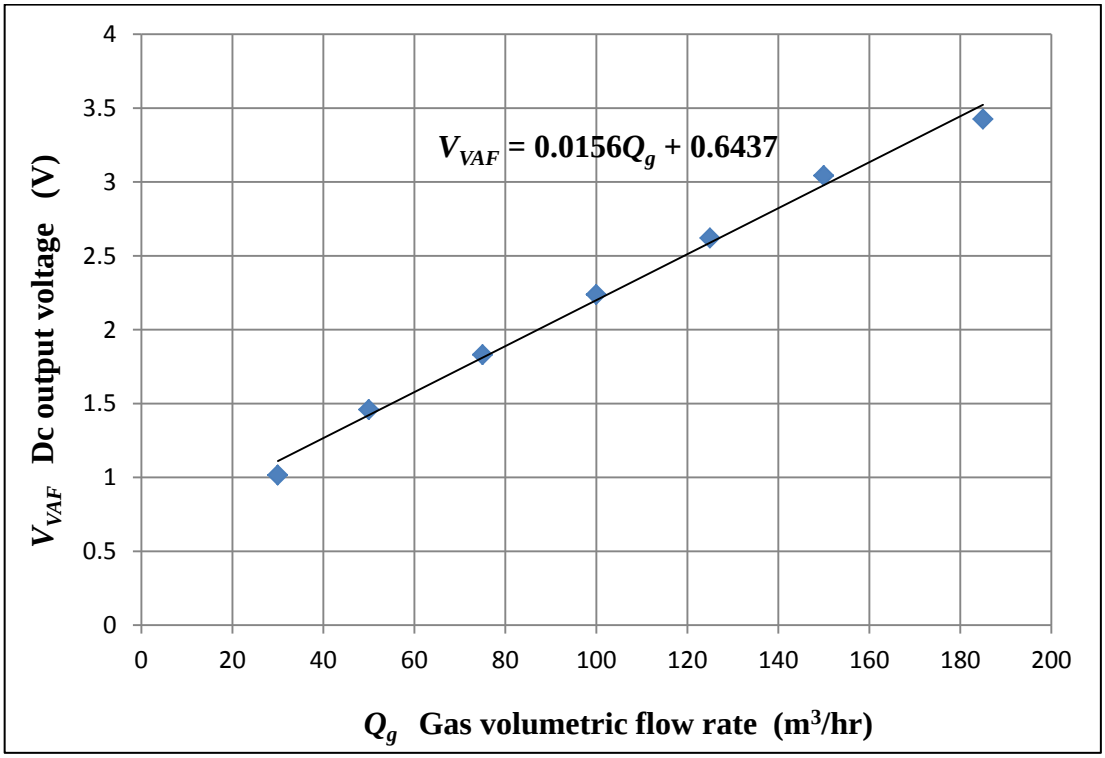

Figure 6-6: Output voltage V_{VAF} from VAF against gas volumetric flow rate Q_g

The quantitative relationship between the dc output voltage V_{VAF} and the gas volumetric flow rate Q_g through the VAF (refer to Figure 6-6) is given by:

$$Q_{g,ref} = \frac{V_{VAF} - 0.6437}{0.0156} \quad (\mathrm{m^3/h_r})$$

Equation 6.1

A current to voltage converter (I/V) (refer to Figure 6-7) was used to convert the VAF output signal (4-20 mA) to (1-5) dc V for the air flow meter range 30m^3/hr to 300m^3/hr. In this circuit the reference resistor (R_{ref} 1) is a 250 Ω ±1% high precision resistor with a low temperature coefficient. The voltage drops across this resistor is fed into two buffer amplifiers. The outputs results from the two buffers are connected to the input of a unity gain differential amplifier. The output voltage of the differential amplifier (output of the current to voltage convertor circuit) was connected to the NI USB 6009 data acquisition card.

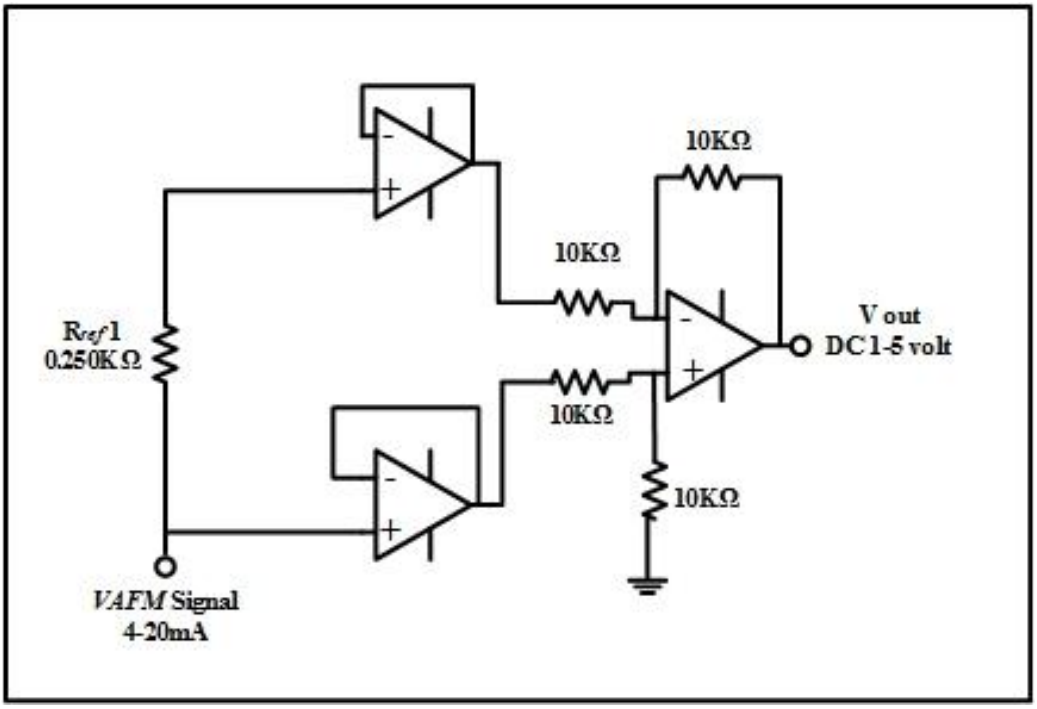

Figure 6-7: Schematic diagram of I/V converter circuit

6.2.3 Turbine flow meter

The turbine meter (type ABLE NT13) was installed in the water line of the flow loop as shown Figure 6.2 and was used to measure the reference water volumetric flow rate $Q_{w,ref}$ supplied to the test section by the centrifugal pump. Turbine flow meters provide measurements of the water volumetric flow rates by counting the rotation frequency of the turbine rotor. They are designed so that the rotation frequency f_q of the turbine is proportional to water flow rate over the specified operational range of the meter. Figure 6-8 shows a photograph of the turbine flow meter used in the present study.

The turbine flow meter used in annular flow was brand new and the calibration data supplied by the manufacturer was assumed to be accurate. The flow rate range provided by the manufacture of the turbine meter was from 0.48 m^3/hr to 4.8 m^3/hr. The relationship between the water volumetric flow rate Q_w and the measured frequency f_q of the output from the turbine flow meter, provided by the manufacturer's calibration data, is given by:

$$Q_w = \left(f_q * 3600/1141.943\right)/1000 \quad m^3/hr$$

Equation 6.2

where the constant 1141.943 (average pulses per litre) is called the meter factor, or k-factor, which is specified on the calibration certificate from the manufacture

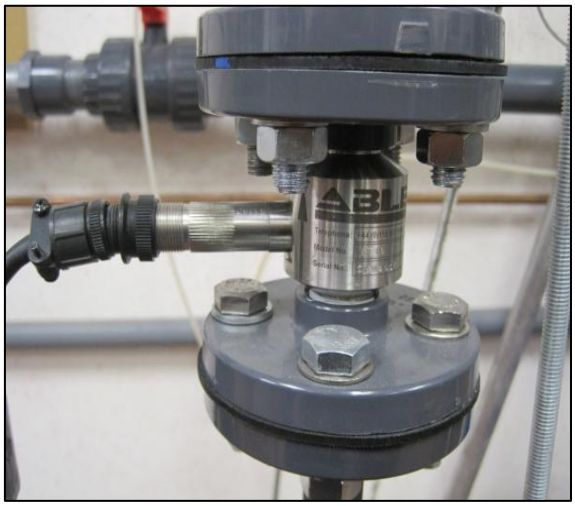

Figure 6-8: A photograph of a turbine flow meter

6.2.4 Differential pressure device

To measure the differential pressure between the inlet and the throat of the Venturi meter a differential pressure transducer was required as shown in Figure 6.2. The differential pressure transmitter installed in the flow loop and used in the current investigation was a Honeywell DP cell, STD120. It was required to calibrate this differential pressure transmitter. Figure 6-9 shows a photograph of the DP cell model used in the present study. A flushing system was used to guarantee that no air was present in the water filled measurement lines. The operating range of the DP cell sensor was 0 to 40 inches H_2O.

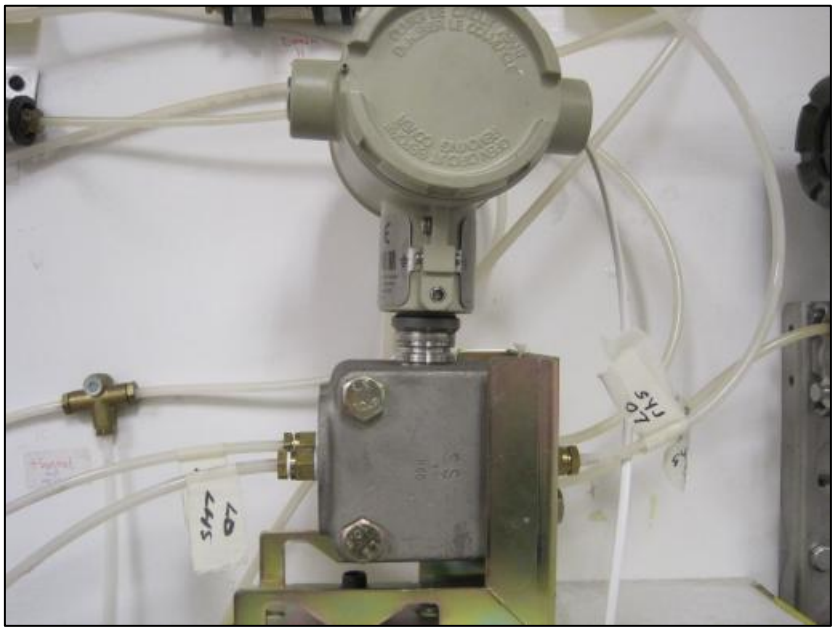

Figure 6-9: Photograph of the Honeywell differential pressure transmitter (DP cell)

Since the output from the DP cell sensor was a current (4-20 mA), a current-to-voltage (I/V) converter circuit identical to that shown in Figure 6.7 was used to convert the current output signal from the DP cell to a dc output voltage (1-5V), which could then be provided to the NI USB 6009 data acquisition device.

For this study, the DP cell sensor was calibrated with a pressure tapping separation distance of 1m in a long Perspex pipe. The output from DP cell (4-20mA) was connected to the (I/V) converter circuit. The calibration procedure was carried out in different stages by both increasing and decreasing the water level in the Perspex pipe and the output voltage from the (I/V) converter circuit (refer to Figure 6.7) was recorded for each stage. Figure 6-10 shows the calibration curve of the Honeywell DP cell, STD120 relating the dc output voltage from the I/V converter circuit to the applied differential pressure.

It can be seen from Figure 6-10 that by plotting the DC output voltage from the current-to-voltage (I/V) converter circuit on the y-axis and the differential pressure on the x-axis yields a perfect fit polynomial equation. This defines the dc output voltage

as a function of the differential pressure, from which the differential pressure can be determined directly from the equation in the chart. Note that in order to be used in the Venturi models given in chapters 2 and 3 of this thesis, the measured differential pressure ($\Delta P_{wg,meas}$ in Equation (3.13) and (3.18)) must be converted from "inches H_2O to Pascals".

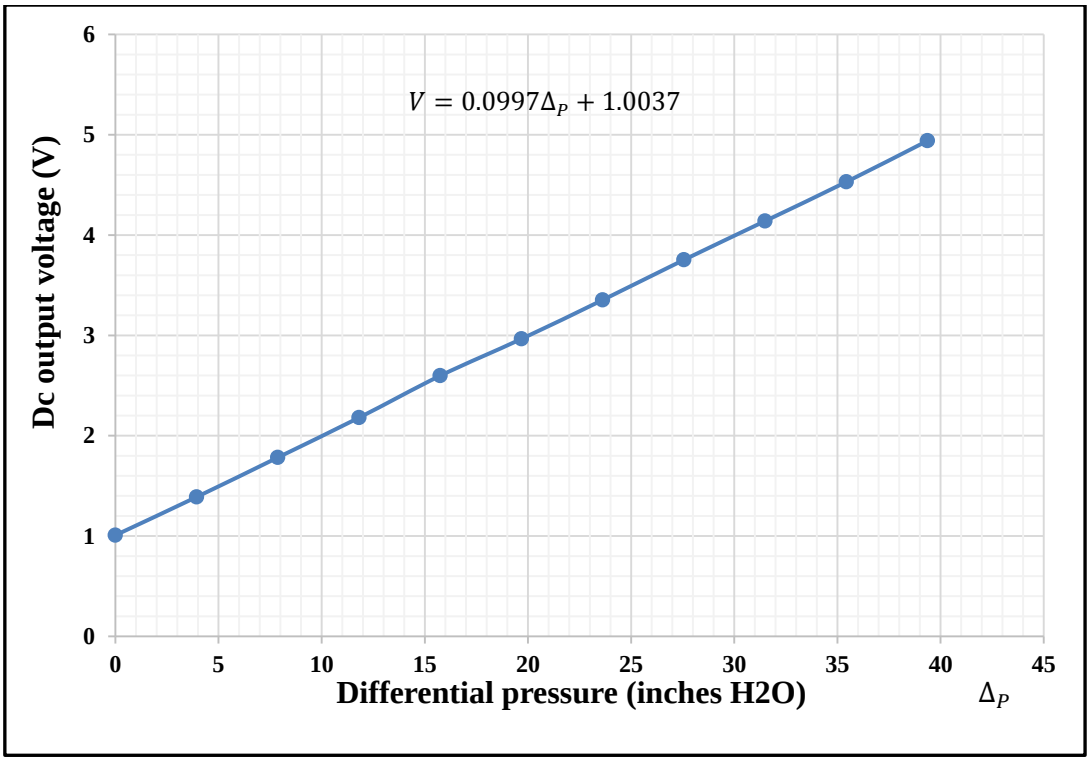

Figure 6-10: Calibration of the Honeywell DP cell SDT120

6.3 The change-over valve and flushing system

The Honeywell differential pressure transmitter used in the present study cannot read a differential pressure when the pressure at the 'high' input is smaller than the pressure at the 'low' input. In the annular two phase flow, the inlet and the throat of the Venturi meter are connected to the Honeywell DP cell, STD120, through water filled lines where the air-water two phase pressure drop across the Venturi meter could change its sign from positive to negative.

To avoid this problem a "change-over" valve system was used to ensure that the pressure applied to the high (+) side of the DP cell was always greater that the pressure applied to the low (-) side. From Figure 6-11 it should be noted that a flushing system, connected to a high pressure water supply, was used to remove any air bubbles between the Honeywell DP cell lines and the Venturi flow meter, including the water filled lines connected to the '+' and '-' inputs of the Honeywell DP cell. This is because air trapped in any of the pressure lines can cause faulty differential pressure measurements.

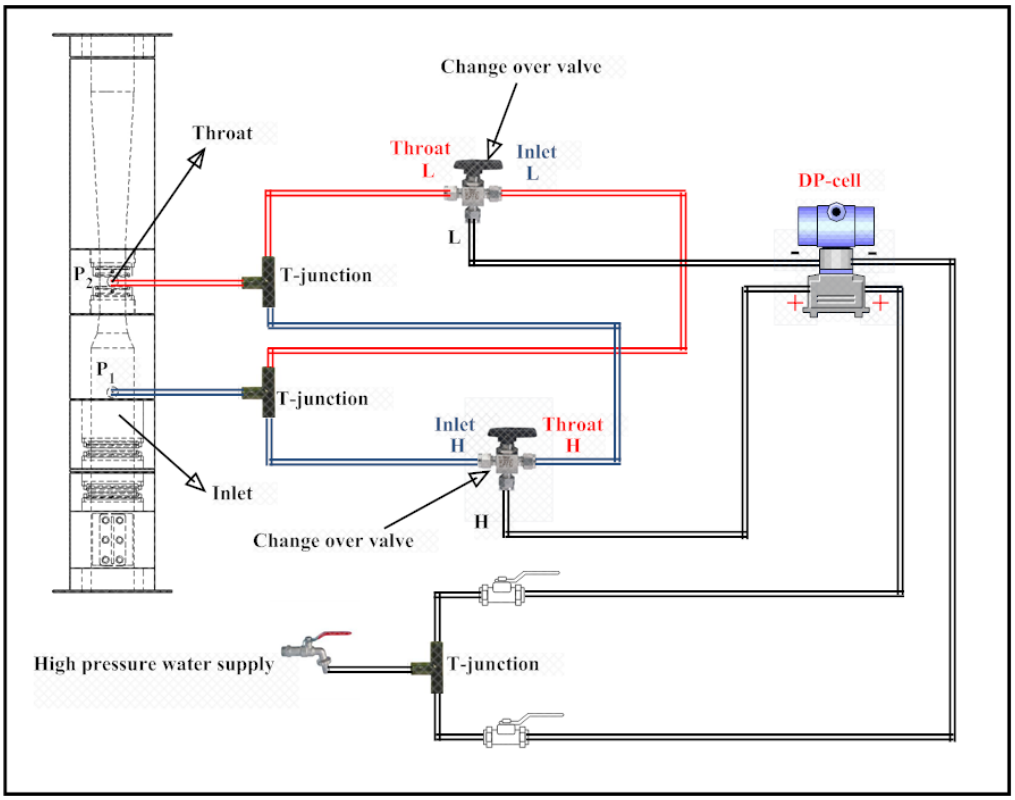

Figure 6-11: DP cell change-over valve and flushing system

6.4 Data Acquisition and Control

The measurement system used a NI USB 6009 data acquisition device to integrate the system measurements and to control the operation of the Venturi system. A Labview software program was created to read the input signals (from the throat conductance ring sensor, the digital level sensor, the inlet conductance ring sensors (channels A and B), the variable flow meter, the turbine flow meter and the differential pressure

sensor). Then the Labview software calculates the water film thickness in annular flow, the reference water and gas flow rates and the differential pressure online during the experiments. Then the Labview software saves all the collected and calculated data in an Excel file. The water an gas volumetric flow rates (e.g. from [81], [10] and [15, 16]) where calculated offline using an Excel spreadsheet.

6.4.1 National Instruments USB-6009 data acquisition (DAQ) device

During the test and measurement procedures it was necessary to collect the data directly and to be able to save them for later investigation. This was achieved by using a NI USB 6009 data acquisition device as shown in Figure 6.12.

Figure 6-12: Photograph of a NI USB 6009 data acquisition device

The NI USB 6009 device has several functions. It provides eight single-ended analogue input (AI) channels, two analogue output (AO) channels, 12 digital input/output (DIO) channels, and a 32-bit counter with a full-speed USB interface. For of the present work, the NI USB 6009 device used six channels for analogue input signals (AI0-AI5) which were controlled by using the Labview function DAQ MAX. These were for reading the analogue signals from the Venturi throat conductance ring sensor, the Venturi inlet conductance ring sensors (A and B), the DP cell sensor, the

air flowmeter and turbine flowmeter. It also has eight digital input channels which again can be controlled by using the Labview function DAQ MAX for reading the digital signals from the digital level sensor.

6.4.2 System interface

Data from the ring conductance sensors at the inlet and the throat of the Venturi, the differential pressure sensor (DP cell), the digital level sensor, the air flow meter and the turbine flow meter were acquired by a PC with a National Instrument NI USB 6009 DAQ card using a Labview program which also calculated the reference gas and water volumetric rates. Therefore six analogue signals, together with the digital signals from the digital level sensor, were interfaced to the PC via the NI USB 6009 data acquisition device (refer to Figure 6-13). The operation of the NI card was controlled using Labview software.

Data were collected simultaneously from the conductance sensors at the Venturi inlet and the throat, the DP cell sensor, the air flow meter and turbine flow meter at a sampling rate of 1 kHz. Each data collection was made one hundred times over a sixty second period and then averaged to reduce random errors. Once all necessary signals were received by the NI USB 6009 data acquisition card, Labview program was run and the required flow parameters recorded to determine the reference gas, water and mixture volumetric flow rates. Figure 6-14 shows the layout of the graphical interface programmed by the Labview software.

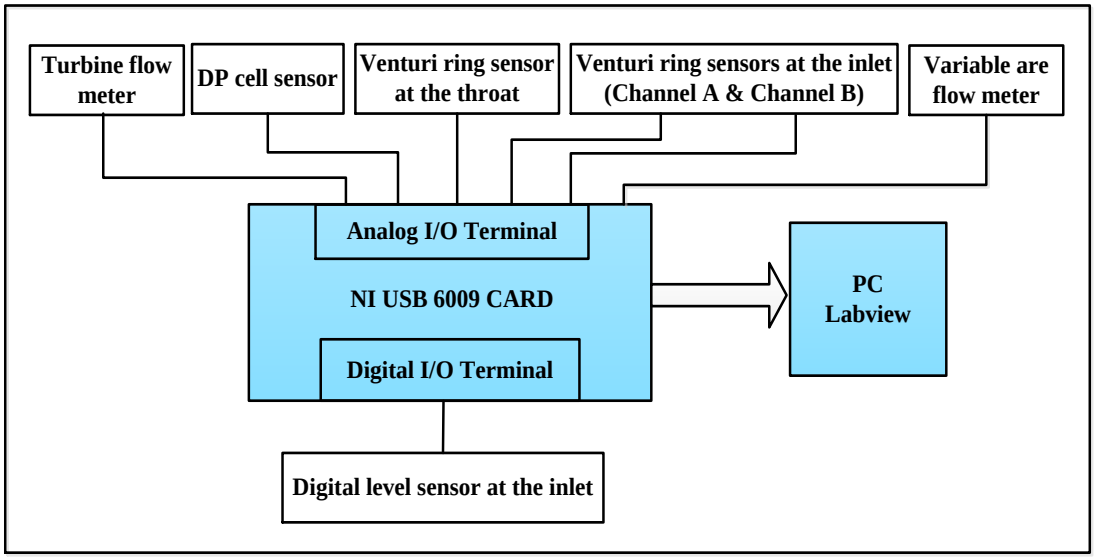

Figure 6-13: System interface and wiring diagram

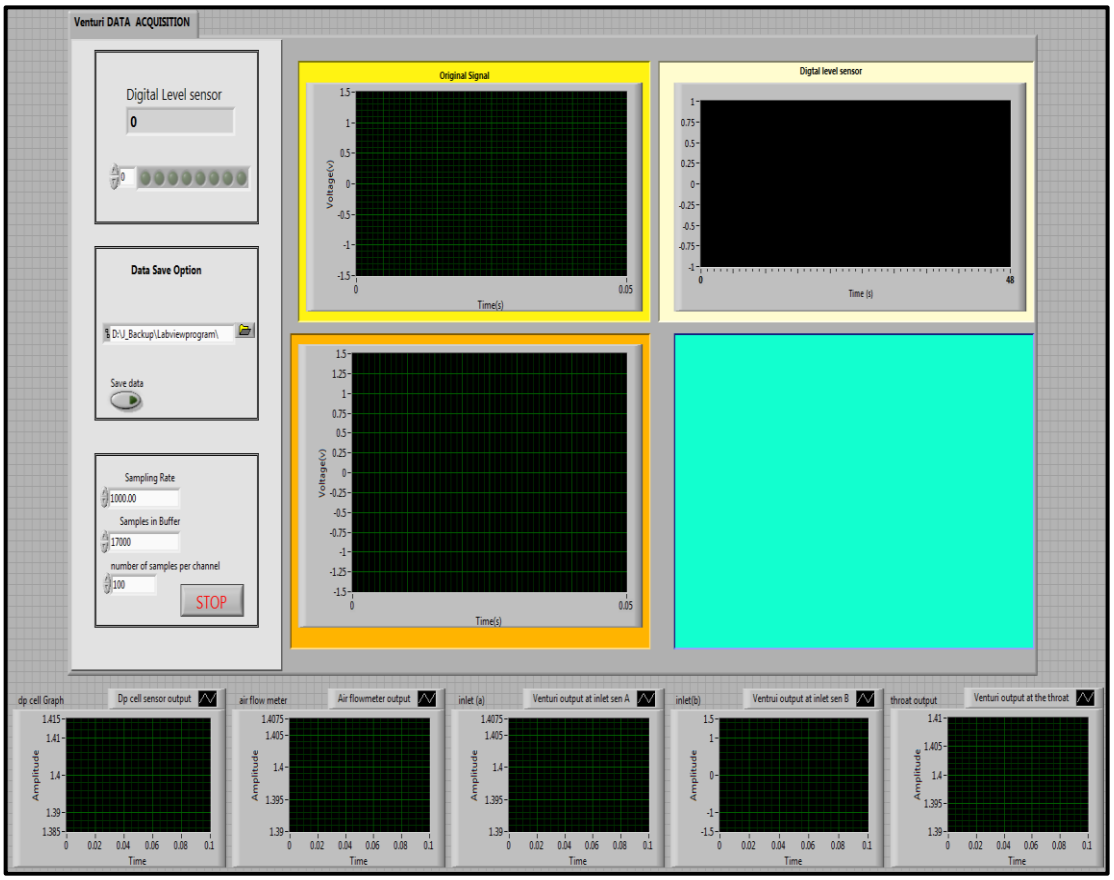

Figure 6-14 A general Labview layout of the system

6.5 Parameters and flow conditions of the experiment

All of the experimental procedures were performed in a vertical test section with Perspex pipes at the inlet and the outlet of the Venturi, in order to observe the annular flow regime during the experiments. The internal diameters of the Venturi inlet and outlet and the Perspex pipes were 50mm. The air and water were supplied at room temperature during all experiments.

The lowest water volumetric flow rate selected ($0.472 m^3/h$) provided an unbroken water film in the Venturi for all gas flow rates used in the experiment. If the water flow rate was too low the water film broke and resulted in flooding which was easy to see via the Perspex pipe. For each flow condition during the experiments, the following measurements were made:

- Digital level sensor to obtain the liquid film thickness $\tilde{\delta}$ (and hence the gas volume fraction α_1) at the Venturi inlet.
- Conductance ring sensors (A and B) at the Venturi inlet to determine the liquid film velocity $U_{f,xc}$ using a cross-correlation technique.
- Ring sensor B to obtain the film thickness δ (and hence the gas volume fraction α_1).
- Water conductivity always measured in the current investigation using a proprietary conductivity meter.
- Conductance ring sensor C at the throat to obtain the gas volume fraction α_2.
- DP cell sensor to obtain the differential pressure between inlet and the throat of the Venturi.
- The reference water and air volume flow rates using variable area flow meter and turbine flow meter.
- The atmospheric pressure using a barometer.

It should be mentioned again that the film thickness of the annular flow was measured by the ring sensor B and the digital level sensor at the inlet of the Venturi. Therefore the gas volume fraction $\alpha_1$and α_2 at inlet and the throat of the Venturi were obtained

using ring sensor B at the Venturi inlet and ring sensor C at the throat of the Venturi respectively.

The procedure used for all experimental flow condition runs is shown in the form of a flowchart (see Figure 6.15). As explained earlier in Chapter 4, the conductance ring sensors at the inlet and the throat of the Venturi were fully calibrated before starting the experimental measurements.

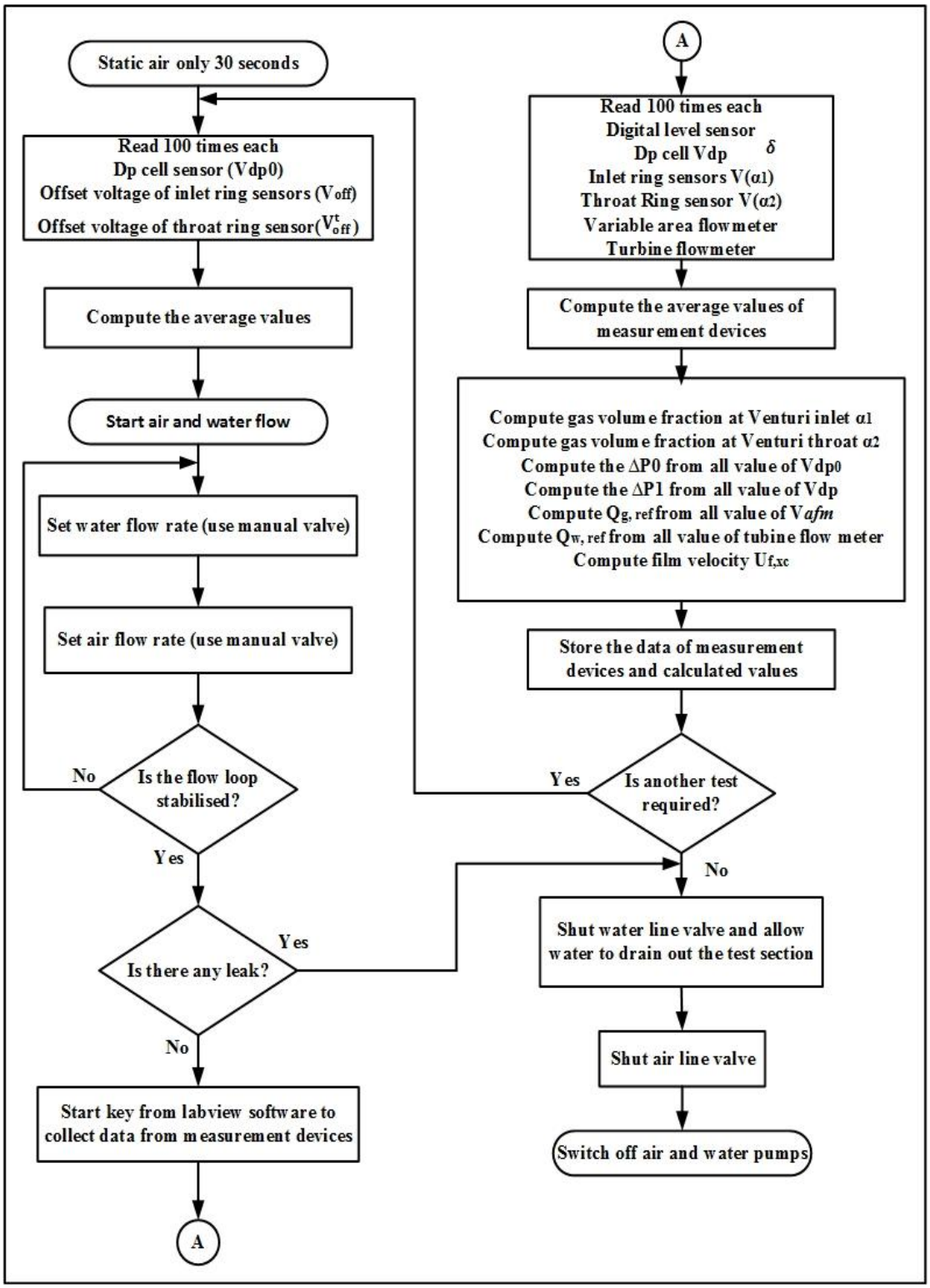

Figure 6-15: Flow chart of data collection procedure

Summary

To perform measurements on gas and water two phase flows using a Venturi with ring conductance sensors at the inlet and throat in an annular flow regime, several items of apparatus were necessary. The experiments were carried out by modifying a flow loop and equipment that was already available at the University of Huddersfield. As part of the present investigation, the water-gas two phase flow loop was further developed to enable vertical annular gas-water flows to be established. The Venturi with ring conductance sensors at inlet and throat represented the device under test while all other devices on the flow loop were reference and auxiliary devices. An explanation of the reference devices was presented in Section 6.2 and the data acquisition and control system was explained in Section 6.4.

Chapter 7 Experimental Results

Introduction

The Venturi meter with conductance sensors at inlet and throat was designed to measure the gas volume fraction at the inlet and the throat of the Venturi, the film thickness at the inlet and the film velocity in vertical annular gas-water two phase flow. The ring sensors A and B at the inlet of the Venturi were used to measure the film velocity $U_{f,xc}$ by cross correlation; ring sensor B was also used to measure the film thickness δ (and the gas volume fraction α_1) at the Venturi inlet; the ring sensor C at the throat was used to measure the gas volume fraction α_2 at the Venturi throat and the digital level sensor was used to measure the liquid film thickness $\tilde{\delta}$ (and the gas volume fraction α_1) at the inlet of the Venturi.

The reason for measuring the film thickness, the film velocity and the gas volume fraction at the inlet and the throat of the Venturi is to determine the gas mass flow rate and the gas and water flow rates in annular wet gas two phase flow.

The mathematical model of [81], and a homogenous model assuming no slip gas volume fraction (described in Chapter 3), were applied to determine the gas and water flow rates.

This chapter discusses the experimental results of vertical annular (wet gas) flow through the Venturi meter with conductance sensors. The error in the predicted gas and water flow rates, and the gas mass flow rate using the Equation(3.66) from [81] was larger than expected. Therefore, a homogenous model assuming no slip gas volume was used to determine the estimated gas and water flow rates, and gas mass flow rate in water-gas two phase flows.

7.1 Effect of the gas superficial velocities on film thickness at the inlet of the Venturi

As mentioned in Chapter 4, the digital level sensor head mounted on the inner surface of the Venturi flow meter was used to measure the film thickness at the inlet of the Venturi. In order to analyse as fully as possible the effect of the gas superficial velocities on the liquid film thickness as measured by the digital level sensor at the inlet of the Venturi in vertical annular water-gas flow, seventy different flow conditions were tested.

A summary of the flow sets is given in Table 7-1. Seven different sets of data were used to investigate the effect of gas superficial velocity on film thickness, with water flow rates from 0.0000436 m^3/s to 0.000393 m^3/s and the corresponding range of water superficial velocity U_{ws} from 0.022 m/s to 0.200 m/s, the air flow rates from 0.0166 m^3/s to 0.0416 m^3/s with corresponding range of gas superficial velocity U_{gs} from 8.48 m/s to 21.22 m/s. The mode of operation was to maintain the water superficial velocity constant while the gas superficial velocity was varied in each flow set.

A plot of film thickness $\tilde{\delta}$ vs U_{gs} is shown in Figure (7-1) for a variety of flow conditions with increasing gas superficial velocity at different water superficial velocities for all sets of data. It can be seen that, in general the liquid film thickness at the inlet of the Venturi decreases as the gas superficial velocity increases. Also it can be seen that the inlet film thicknesses at higher gas superficial velocity were similar for all sets of data. Results, in this study, showed that the digital level sensor (dls) was able to read maximum and minimum film thicknesses $\tilde{\delta}$ of 9.59 mm and 1.84 mm respectively.

Data set no.	Water superficial velocity U_{ws} (m/s)	Gas superficial velocity U_{gs} (m/s)
Flow set 1	0.022	8.48 to 21.22
Flow set 2	0.033	8.48 to 21.22
Flow set 3	0.044	8.48 to 21.22
Flow set 4	0.055	8.48 to 21.22
Flow set 5	0.111	8.48 to 21.22
Flow set 6	0.156	8.48 to 21.22
Flow set 7	0.200	8.48 to 21.22

Table 7-1: Flow conditions used to investigate effect of gas superficial velocity on liquid film thickness measured by the digital level sensor

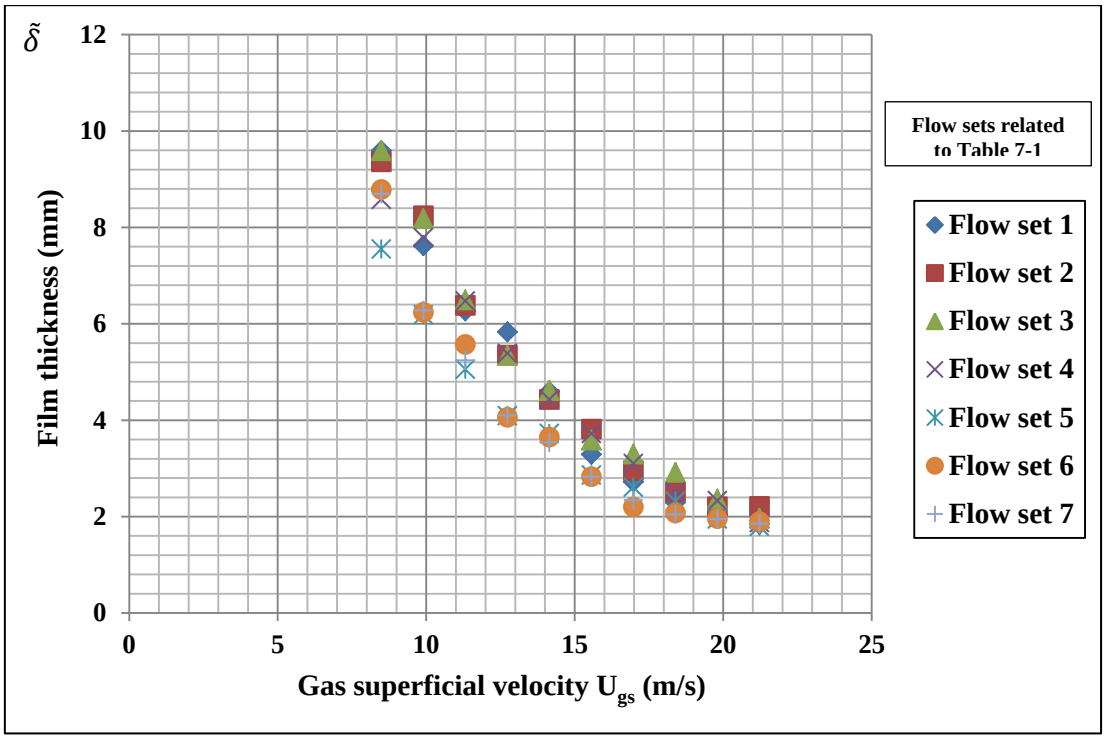

Figure 7-1: Effect of gas superficial velocity on liquid film thickness measured by the digital level sensor at the Ventuir inlet in annular flow

7.2 Effect of the water superficial velocities on film thickness at the inlet of the Venturi

In order to analyse as fully as possible the effect of the water superficial velocities on the liquid film thickness as measured by the digital level sensor, sixty three different flow conditions were tested. A summary of the flow conditions is given in Table 7-2. Seven different sets of data were used to investigate the effect of water superficial velocities on film thickness, with air flow rates from 0.025 m^3/s to 0.0416 m^3/s and water flow rates from 0.000131 m^3/s to 0.000830 m^3/s. The water superficial velocity U_{ws} ranged from 0.066 m/s to 0.423 m/s for all the seven different sets of data.

A plot of film thickness $\tilde{\delta}$ vs U_{ws} is shown in Figure 7-2 where it was found that the liquid film thickness increased with increasing water superficial velocity at different gas superficial velocities. At the minimum water superficial velocity the film thickness is much lower than it is at the maximum water superficial velocity. With further increases in water superficial velocity the liquid film collapses into the core of the annular flow resulting in the over flooding of the (unstable) system.

Data set no.	Gas superficial velocity U_{gs} (m/s)	Water superficial velocity U_{ws} (m/s)
Flow set 8	11.151 to 13.729	0.066 to 0.423
Flow set 9	9.813 to 14.793	0.066 to 0.423
Flow set 10	9.757 to 16.719	0.066 to 0.423
Flow set 11	10.504 to 17.726	0.066 to 0.423
Flow set 12	10.567 to 18.814	0.066 to 0.423
Flow set 13	10.697 to 18.809	0.066 to 0.423
Flow set 14	10.918 to 19.555	0.066 to 0.423

Table 7-2: Flow conditions used to investigate effect of water superficial velocity on liquid film thickness measured by the digital level sensor

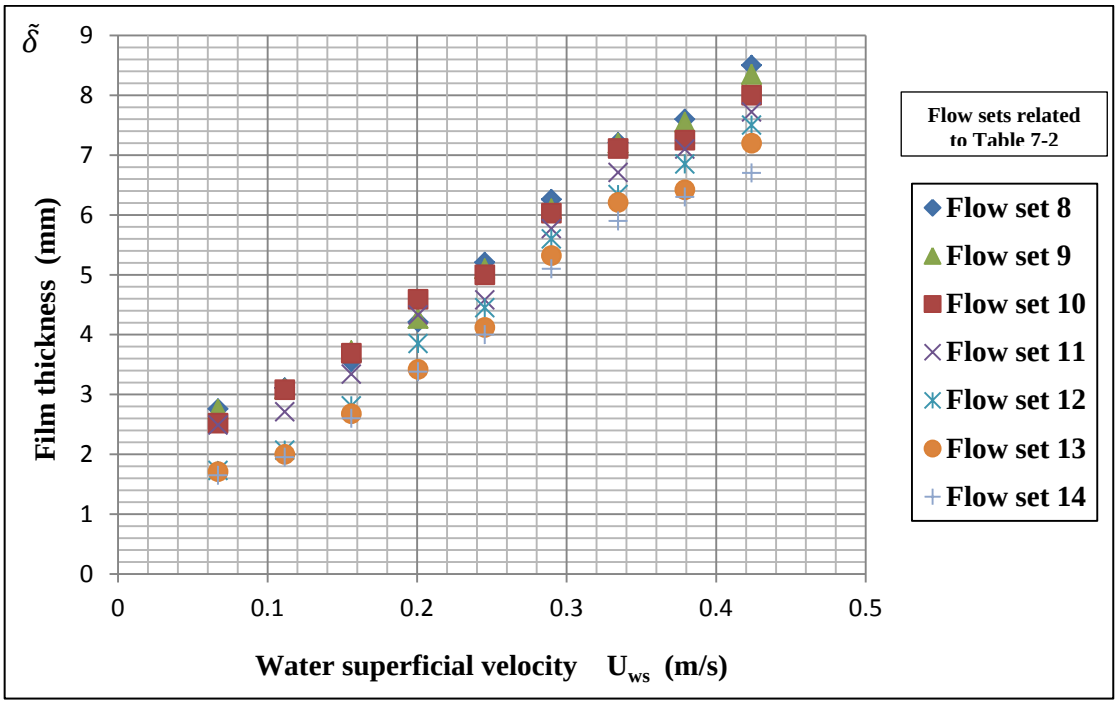

Figure 7-2: Effect of water superficial velocity on liquid film thickness measured by the digital level sensor in annular flow at the Ventuir inlet in annular flow

7.3 Flow conditions of vertical annular (wet gas) flows

Experiments were performed on a vertical annular wet gas (air-water) flow using the novel wet gas flow metering technique, which combines a Venturi with conductance sensors at the inlet and throat. Sixty three different flow conditions were tested with the water reference volumetric flow rate, $Q_{w,ref}$ in the range of 0.000131 m^3/s to 0.000831 m^3/s (0.472 m^3/hr to 2.994 m^3/hr). See Table 7-5 for the gas reference volumetric flow rate $Q_{g,ref}$.

Seven different sets of data were tested. The water flow rate range of data was kept the same while the range of gas flow rates was varied for the all sets of data. The summary of the flow conditions of all seven sets of data used for the experimental work is given in Table 7-3.

Data set no.	Gas superficial velocity U_{gs} (m/s)	Water superficial velocity U_{ws} (m/s)
Flow set 8	11.151 to 13.729	0.066 to 0.423
Flow set 9	9.813 to 14.793	0.066 to 0.423
Flow set 10	9.757 to 16.719	0.066 to 0.423
Flow set 11	10.504 to 17.726	0.066 to 0.423
Flow set 12	10.567 to 18.814	0.066 to 0.423
Flow set 13	10.697 to 18.809	0.066 to 0.423
Flow set 14	10.918 to 19.555	0.066 to 0.423

Table 7-3: Flow conditions of all sets of data in annular (wet gas) flow

$Q_{w,ref}$ (m^3/hr)	0.472	0.788	1.103	1.418	1.733	2.049	2.364	2.679	2.994
U_{ws} (m/s)	0.066	0.111	0.156	0.200	0.245	0.289	0.334	0.379	0.423

Table 7-4: Reference water flow rates and the corresponding water superficial velocities used throughout the experiments

Data set no.	Reference Gas flow rate $Q_{q,ref}$ (m^3/s)
Flow set 8	0.021 to 0.026
Flow set 9	0.006 to 0.029
Flow set 10	0.019 to 0.032
Flow set 11	0.020 to 0.034
Flow set 12	0.020 to 0.036
Flow set 13	0.021 to 0.036
Flow set 14	0.021 to 0.038

Table 7-5: Reference gas flow rates used throughout the experiments

The results presented in this chapter will show how the Venturi designed with conductance sensors at the inlet and throat can measure separate properties of two phase gas-water systems in vertical annular flow. These properties are the liquid film thickness δ at the Venturi inlet, liquid film velocity $U_{f,xc}$ at the Venturi inlet, the gas volume fraction α_1 at the inlet and the gas volume fraction α_2 at throat of the Venturi. Later in this chapter it will be explained how these measurement results are applied to the Abbas, de Leeuw, Murdock and homogenous models to determine gas and water flow rates.

7.4 Liquid film thickness measurement at the inlet of the Venturi

Two techniques were used to measure the film thickness at the inlet of the Venturi, namely:

- **Digital level sensor:** a digital level sensor circuit was used to measure the film thickness $\tilde{\delta}$ of the liquid at the Venturi inlet in order to determine the water volume fraction $\alpha_{w,1}$ at the inlet of the Venturi using Equation (3.1). $\tilde{\delta}$ is the symbol used to represent the film thickness measured using digital level sensor.

- **Ring sensor B:** two ring electrodes flush mounted with the inner surface of the Venturi inlet were used to measure the film thickness δ at the inlet of the Venturi. The water conductivity σ_w was measured by a conventional conductivity meter and Equation (3.7) could be used to determine the cell constant $\overline{K}(\alpha_1)$ for sensor B at the inlet, for a given flow condition. For this value of $\overline{K}(\alpha_1)$, the gas volume fraction α_1 at the inlet was obtained using Figure 5-5 and form this, the value of δ could be determined. δ is the symbol used to represent the film thickness measured using ring sensor B.

A comparison of the film thickness at the inlet of the Venturi measured by the digital level sensor and the ring sensor B at the inlet for five sets of data is shown in Figure 7-3. It can be seen that both techniques showed fair agreement. As shown in Figure 7-

3, the values of digital level sensor $\tilde{\delta}$ and ring sensor δ, (liquid film thickness) were close to each other.

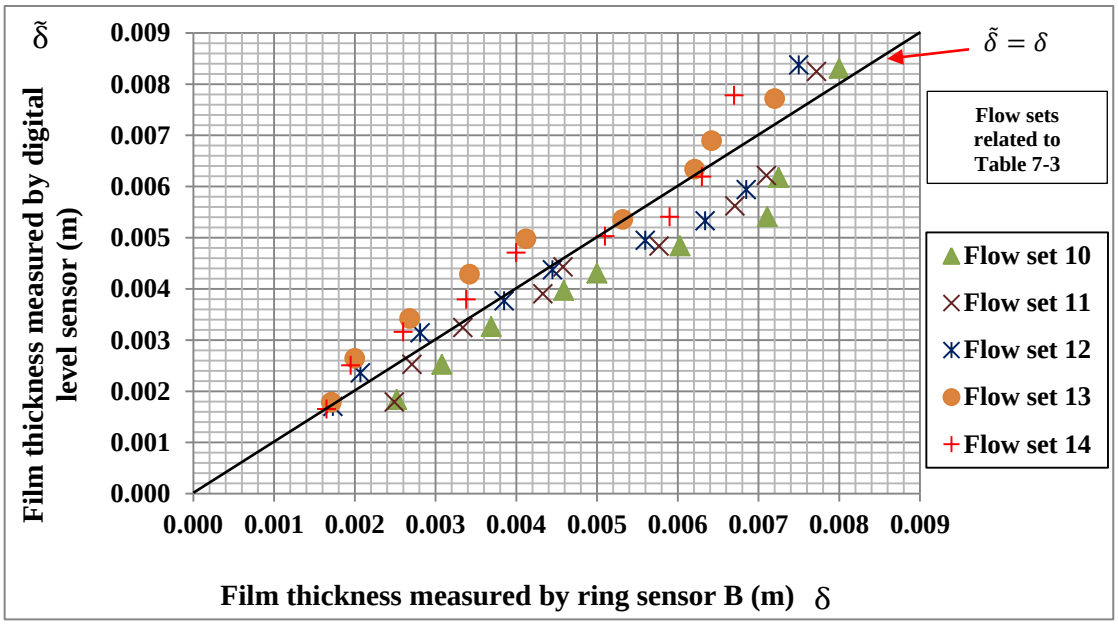

Figure 7-3: Comparison between the film thicknesses measured by digital level sensor $(\tilde{\delta})$ and ring sensor (δ) at Venturi inlet

7.5 Study of the gas volume fraction at the inlet and the throat of the Venturi in annular (wet gas) flows

To determine the gas and the water flow rates using the [81] (see Section (3.2)), homogenous (see Sections (3.3) and (3.4)), [10] (see Section (2.5.1)) and [15, 16] (see Section (2.2.5)) models, measurements of the gas volume fractions α_1 and α_2 at the inlet and the throat of the Venturi in annular (wet gas) flow must be obtained. To do this, a Venturi with conductance sensors at the inlet and the throat was designed and constructed (see Section 4.1). The ring sensor C (two electrodes) at the throat and the ring sensor B (two electrodes) at the inlet of the Venturi were used to measure the gas volume fractions α_1 and α_2 at the inlet and the throat of the Venturi. The digital level sensor measurement was used also to obtain the gas volume fraction α_1 at the Venturi inlet.

7.5.1 The gas volume fraction measurement at the inlet of the Venturi

To determine the gas and the water flow rates using Equations (3.42) and (3.2) respectively, measurements of the gas volume fractions α_1 (see Equations (3.8) and section 5.1) at the inlet of the Venturi in annular (wet gas) flow must be obtained. The ring sensor B at the Venturi inlet and the digital level sensor at the inlet of the Venturi were used to measure the gas volume fractions α_1 at the inlet of the Venturi. $\alpha_{1,rs}$ represent the gas volume fraction measured by the ring sensor and $\alpha_{1,dls}$ represent the gas volume fraction obtained by digital level sensor. Figure 7-4 shows a comparison between the gas volume fraction determined by the digital level sensor $\alpha_{1,dls}$ and that obtained by the ring sensor $\alpha_{1,rs}$ at the inlet of the Venturi.

It can be seen from Figure 7-4 that, in general, the gas volume fraction measured by ring sensor $\alpha_{1,rs}$ agrees approximately with that obtained by digital level sensor $\alpha_{1,dls}$ at the inlet of the Venturi. Also it can be seen from these figures that, the gas volume fraction $\alpha_{1,rs}$ measured using ring sensor B at the inlet of the Venturi was generally greater than the gas volume fraction $\alpha_{1,dls}$ measured by the digital level sensor at the Venturi inlet, perhaps the reason is that the digital level sensor intrusive into the film whereas the ring sensor dose not intrude on the film. Therefor the digital level sensor may affect the film thickness and reduces the film thickness around the digital level sensor. For this work the gas volume fraction measured by ring sensor B at the Venturi inlet was used to find the gas and water volumetric flow rates.

The gas volume fraction measurement results by ring sensor $\alpha_{1,rs}$ and digital level sensor $\alpha_{1,dls}$ from Figure 7-4 are in fair agreement except for flow sets 8 and 9, this may be due to the limitation in the air fan (side channel blower (RT-1900)), the side channel blower could not achieve a stable liquid film flow rate at all flow conditions. In other words, pulsations occurred in the liquid film causing additional differences between the results measured by the two techniques.

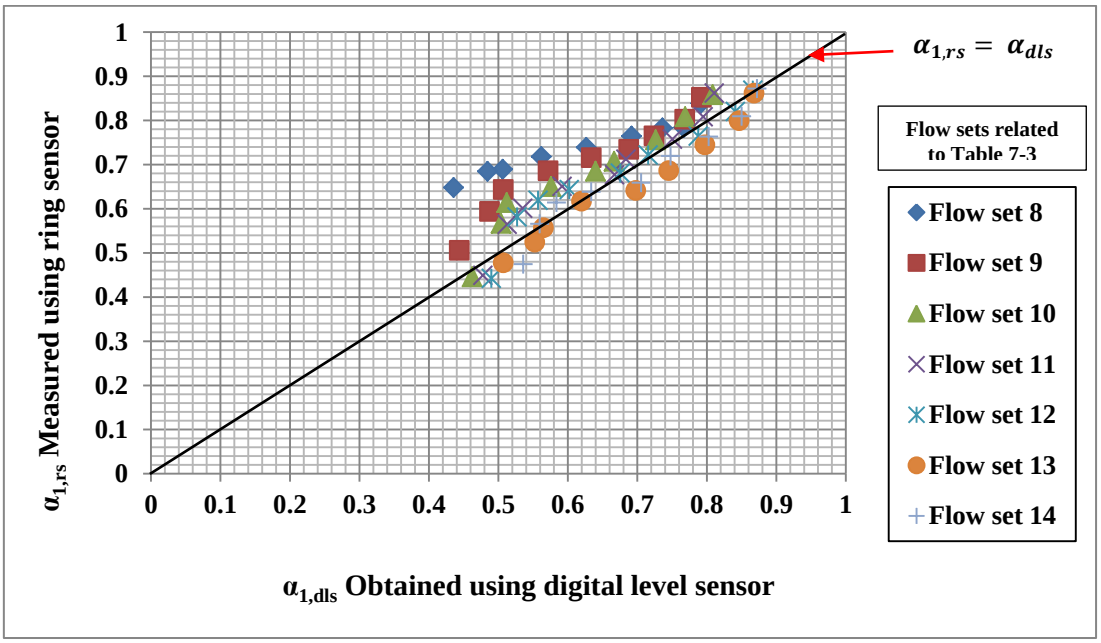

Figure 7-4: Gas volume fraction at Venturi inlet obtained using ring and digital level sensors $(\alpha_{1,rs}$ vs $\alpha_{1,dls})$

7.5.2 Comparison between the gas volume fraction at the throat and no-slip gas volume fraction in the homogenous model

Measurement of the gas volume fraction α_2 at the throat of the Venturi in annular gas-water flow must be obtained in order to determine the gas and water flow rate in annular wet gas flow. To do this, a ring sensor C at the throat was used to determine the gas volume fraction $\alpha_{2,rs}$ at the Venturi throat (see Section 5.1.3) using the water conductivity σ_w measured by a conventional conductivity meter (see Section 3.1.4). For the homogenous model, assuming no slip, the gas volume fraction α_{ns} was obtained using Equation (3.56).

Figures 7-5 show the comparison between gas volume fraction α_{ns} in the homogenous model, assuming no slip and the gas volume fraction $\alpha_{2,rs}$ as measured by ring sensor C at the Venturi throat (α_{ns} vs $\alpha_{2,rs}$) . It can be seen from the figure that, in general, the gas volume fraction $\alpha_{2,rs}$ measured at the throat of the Venturi was slightly less than the gas volume fraction α_{ns} for $\alpha_{ns} < 0.97$. For $\alpha_{ns} > 0.97$, α_{ns} and $\alpha_{2,rs}$ agree fairly well.

From the Figure 7-5, it can be seen that, in general, the gas volume fraction $\alpha_{2,rs}$ as measured by ring sensor C at the Venturi throat is in fair agreement with the gas volume fraction α_{ns} in the homogenous model, assuming no slip, for all of the flow conditions. This result suggests that an assumption of homogenous conditions at the Venturi throat is valid under the flow conditions investigated.

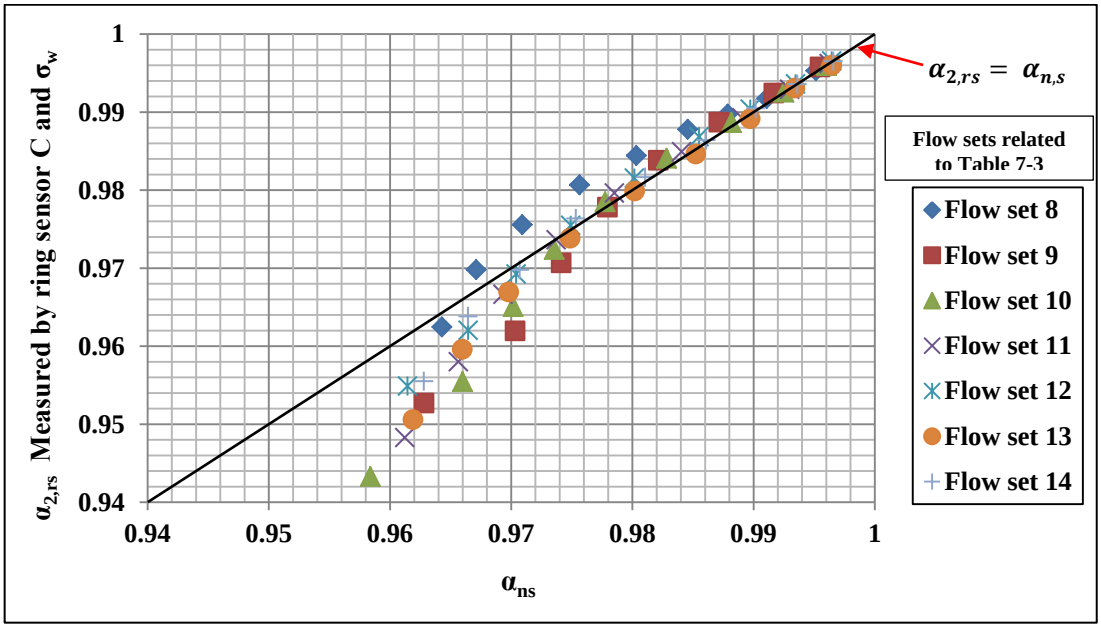

Figure 7-5: Comparison between the gas volume fraction $\alpha_{2,rs}$ and α_{ns}

7.5.3 Comparison between the gas volume fraction at the inlet and no-slip gas volume fraction in the homogenous model

Measurement of the gas volume fraction $\alpha_{1,rs}$ at the inlet of the Venturi in annular gas-water flow must be obtained in order to determine the gas and water flow rates in annular wet gas flow. To do this, a ring sensor B was used to determine the gas volume fraction $\alpha_{1,rs}$ at the Venturi inlet using water conductivity σ_w measured by a conventional conductivity meter. For the homogenous model, assuming no slip, the gas volume fraction α_{ns} was obtained using Equation (3.56).

A plot of α_{ns} vs $\alpha_{1,rs}$ is shown in Figure 7-6. It can be seen that, the gas volume fraction $\alpha_{1,rs}$ as measured by ring sensor B at the Venturi inlet is much less than the

gas volume fraction α_{ns} in the homogenous model, assuming no slip, for all of the flow conditions investigated.

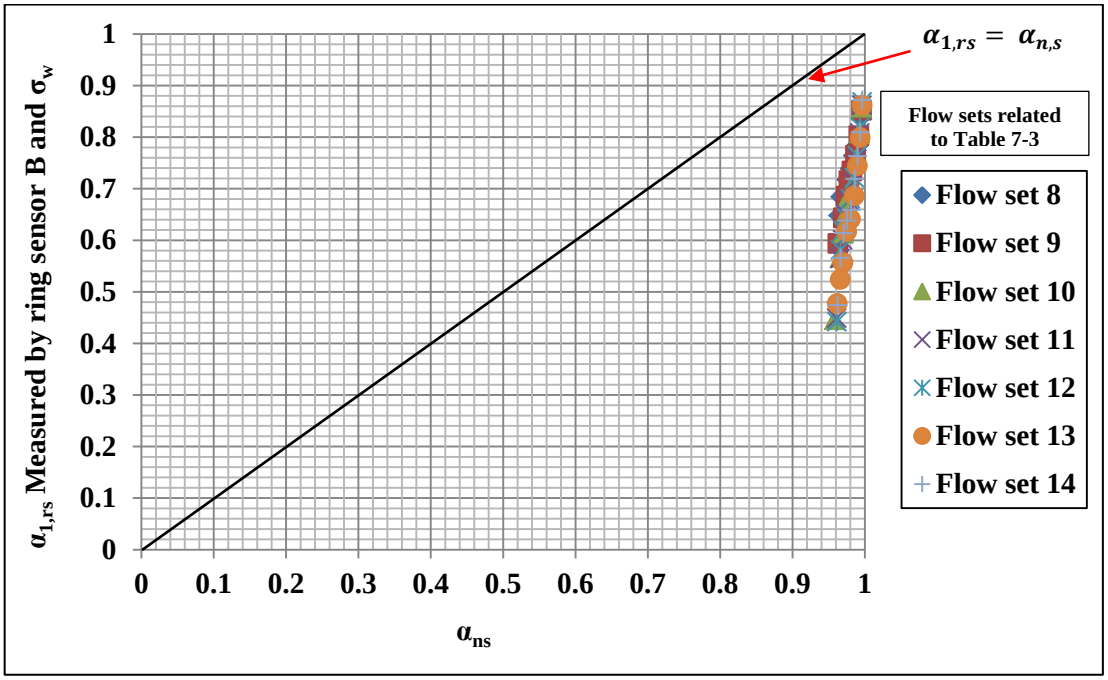

Figure 7-6: Comparison between the gas volume fraction $\alpha_{1,rs}$ and α_{ns}

7.5.4 Comparison between inlet gas volume fraction and the throat gas volume fraction

Measurement of the gas volume fraction at the inlet and at the throat of the Venturi in annular gas-water flow must be obtained in order to determine the gas and water flow rate in annular wet gas flow. To do this, a ring sensor B at the inlet of the Venturi was used to determine the gas volume fraction $\alpha_{1,rs}$ and a ring sensor C at the Venturi throat was used to determine the gas volume fraction $\alpha_{2,rs}$ using water conductivity σ_w measured by a conventional conductivity meter.

A plot of $\alpha_{1,rs}$ vs $\alpha_{2,rs}$ is shown in Figure 7-7. It can be seen that, in general, the gas volume fraction $\alpha_{1,rs}$ as measured by ring sensor B at the Venturi inlet is less than the throat gas volume fraction $\alpha_{2,rs}$, for all of the flow conditions investigated. This is due to the fact that the water film becomes relatively much thinner as the flow accelerates though the throat of the Venturi.

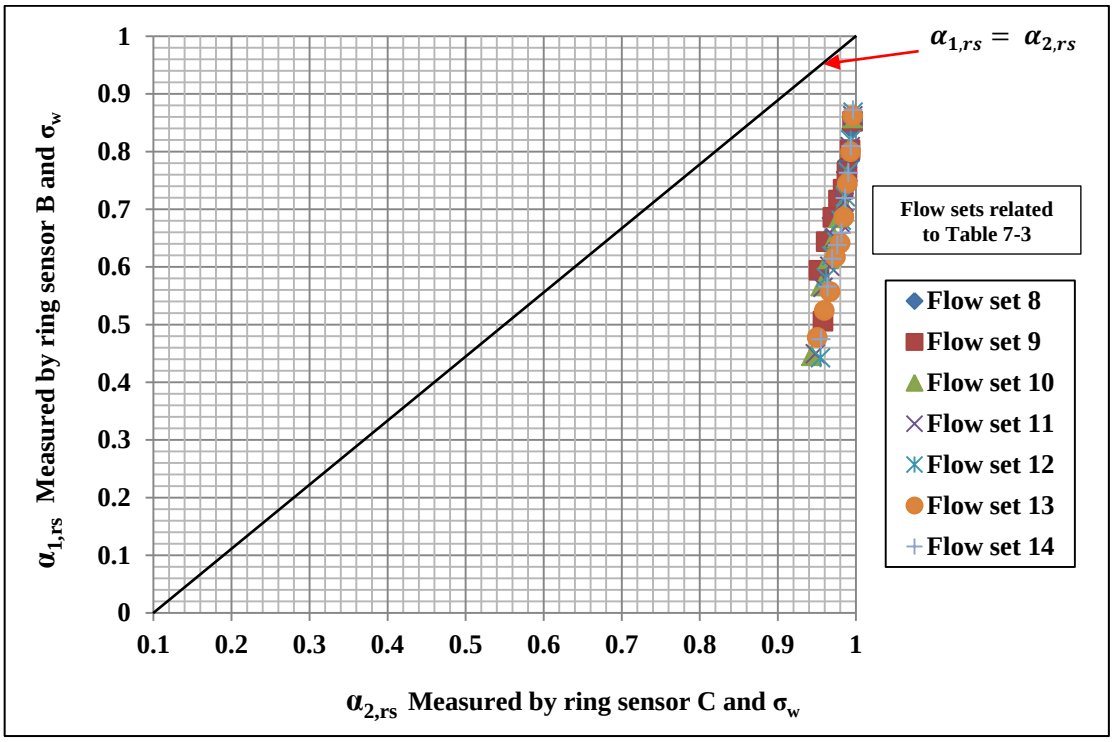

Figure 7-7: Comparison between the gas volume fraction $\alpha_{1,rs}$ and $\alpha_{2,rs}$

7.6 Cross-correlating the conductance upstream ring sensors A and B

The aim of acquiring signals from the two axially separated conductance ring sensors A and B at the inlet of the Venturi is to cross-correlate between the two sensors at a sampling frequency of 1 kHz over a sixty second sampling period to obtain the film velocity of the liquid in vertical annular wet gas flow. By cross-correlating the upstream ring sensors (A and B) signals, the water film velocity may be estimated. The separation between the two ring sensors A and B was 0.05 m. As an example, for the flow condition in which the water superficial velocity was $U_{w,s} = 0.0668$ m/s, the time taken for the liquid film to travel this distance was 0.0460 s (refer to Figure 7-8). Hence the velocity of the water film $U_{f,xc} = 0.05/0.0460 = 1.0869$ m/s. The reference volume flow rate of the water was measured $Q_{w,ref} = 0.000131$ m^3/s, where the reference water volumetric flow rate was measured directly from the turbine flow meter.

The predicted water flow rate from cross correlation can be obtained using the relationship:

$$Q_w = U_{f,xc}\, A_f$$

Equation 7.1

where Q_w is the water flow rate, $U_{f,xc}$ is the velocity of the water film and A_f is the cross-sectional area of the water film. The value of A_f is given by Equation (7.2).

$$A_f = \pi(2\delta R - \delta^2)$$

Equation 7.2

where δ is the film thickness measured by the ring sensor B at the Venturi inlet and R is the pipe internal radius (the radius of the Venturi inlet =25mm). Once the area of the water film A_f and the velocity of water film $U_{f,xc}$ were obtained, the water film volumetric flow rate Q_w predicted using cross correlation in annular wet gas flow can be determined using Equation (7.1).

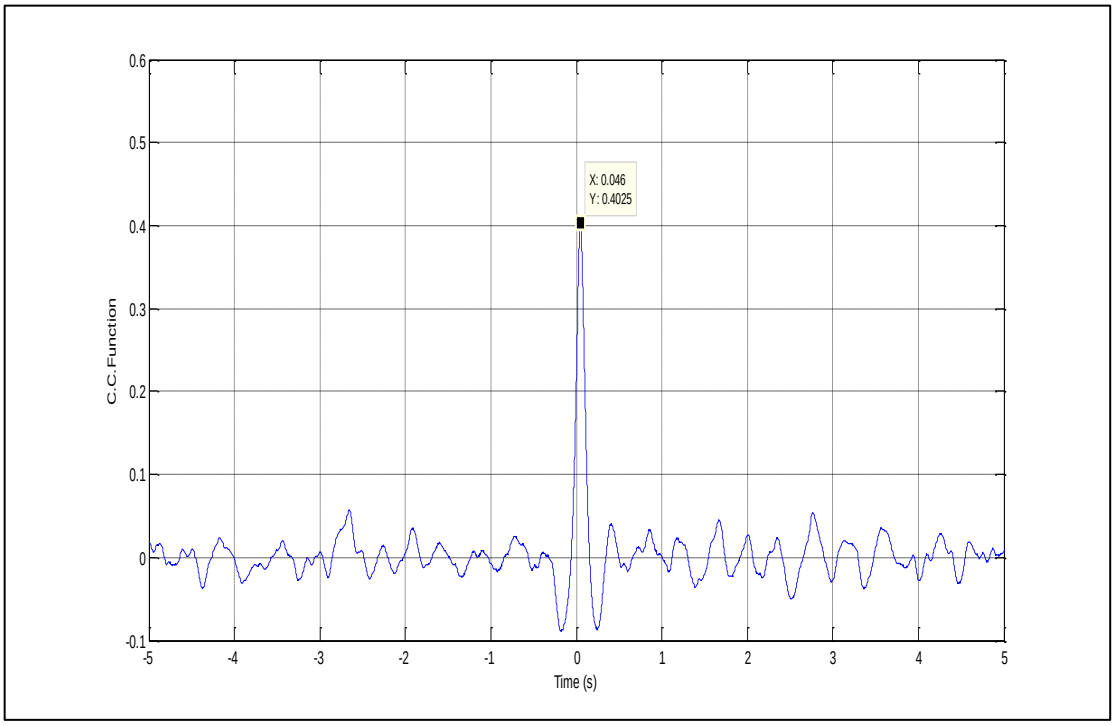

Figure 7-8: Correlogram of the two ring sensors signals at Venturi inlet, 1 kHz sampling rate

7.7 Measuring the water flow rate in annular gas-water two phase flows

To determine the water flow rate using Equation (7.1), measurements of the film thickness and liquid film velocity at the Venturi inlet in vertical annular (wet gas) flow were obtained. The gas volume fraction at the inlet of the Venturi $\alpha_{1,rs}$ was determined from ring sensor B and using water conductivity σ_w measured by a conventional conductivity meter to have a value of 155μScm^{-1}. The film thickness δ at the Venturi inlet was determined from $\alpha_{1,rs}$. The liquid film velocity $U_{f,xc}$ has been obtained by cross-correlation between the two ring sensors A and B at the Venturi inlet; hence, the water flow rate can be determined using Equation (7.1).

The results obtained in this investigation for the water flow rate using Equations (7.1) and (7.2) were compared to the reference water flow rate. The reason for this comparison is to see if the predicted water flow rate agrees with the reference flow rate as measured by the turbine flow meter for all flow conditions. It can been seen from Figure 7-9 that the water volumetric flow rate $Q_{w,rs}$ (determined using the film thickness δ measured by ring sensor B at the Venturi inlet) is significantly greater than the reference water volumetric flow rate $Q_{w,ref}$ (measured from the turbine flow meter):

$$Q_{w,rs} = U_{f,xc}\, A_f$$

Equation 7.3

where A_f is based upon the gas volume fraction $\alpha_{1,rs}$ measured by the ring sensor B at the Venturi inlet. We know from Figure 7.4 that the gas volume fraction $\alpha_{1,rs}$ measured by the ring sensor at the Venturi inlet is fairly accurate, therefore the liquid film velocity $U_{f,xc}$ obtained by cross-correlation between the two ring sensors A and B at the Venturi inlet must be much too high because the predicted water volumetric flow rate $Q_{w,rs}$ obtained using Equation (7.3) is much too high. The results obtained in this investigation for the water flow rate using Equation (7.3) will be investigated in detail (see Section 7.11) to determine the correct water flow rate.

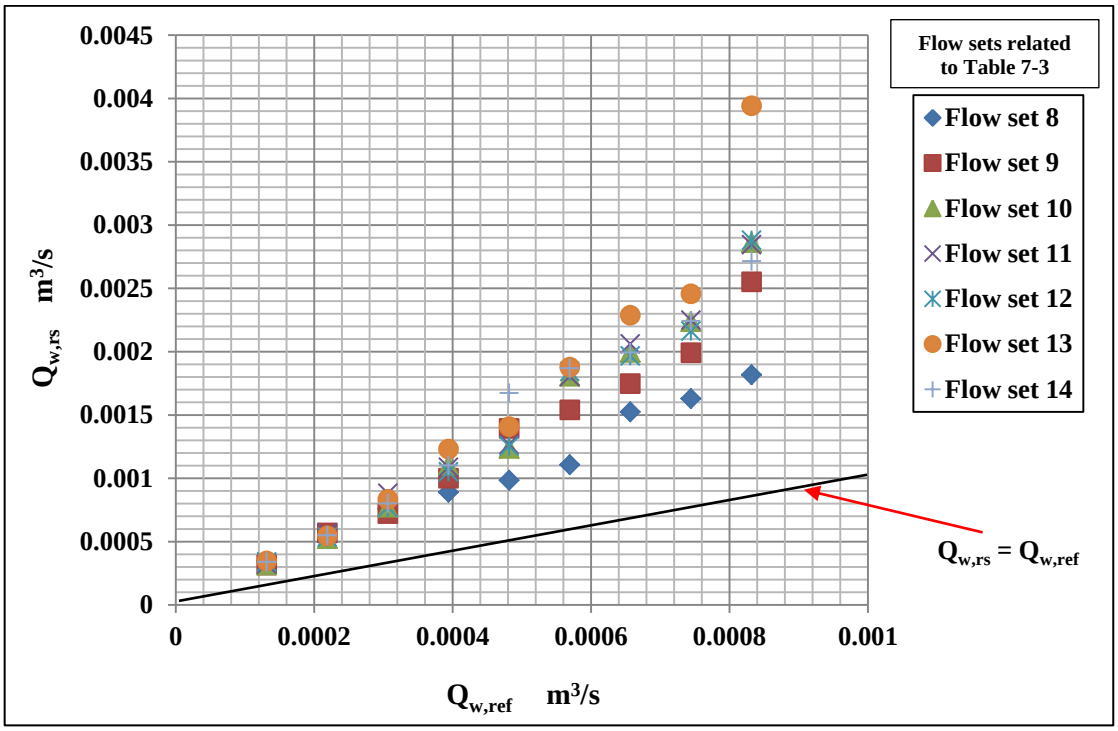

Figure 7-9: Comparison between obtained water flow rates and the reference water flow rates $Q_{w,rs}$ vs $Q_{w,ref}$

7.8 Abbas Model

7.8.1 Measuring the gas flow rate in vertical annular water-gas flow using the Abbas model [81]

The mathematical Abbas model of vertical annular (wet gas) flow through a Venturi meter (which depends on measurement of the gas volume fraction at the inlet and the throat of the Venturi as described in Section 3.2) was applied to determine the gas volumetric flow rate. To determine the gas volumetric flow rate using Equations (3.42) and (3.39) respectively, measurements of the gas volume fractions α_1 and α_2 at the inlet and the throat of the Venturi and measurement of the differential pressure between inlet and the throat of the Venturi must be obtained.

Ring sensor C at the throat of the Venturi was used to measure the gas volume fraction α_2; the film thickness measurement at the Venturi inlet using digital level

sensor enables the gas volume fraction α_1 at the inlet to be obtained from Equation (3.8).

A plot of Q_g vs $Q_{g,ref}$ (Figure 7-10) shows that the predicted gas volumetric flow rate determined by Equation (3.42) in the Abbas model does not agree with the reference gas flow rate measured by the air flow meter. It has been found that the Abbas model does not work well for the flow conditions investigated in this thesis. A summary of the different conditions between the current study and the Abbas work is given in Table 7-6.

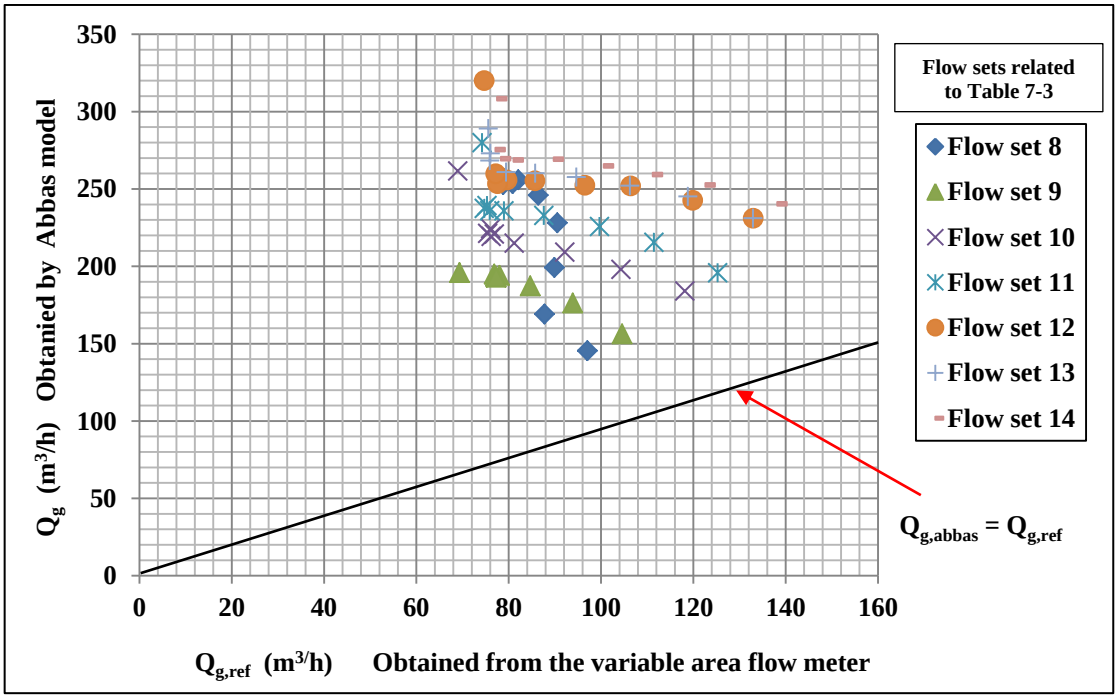

Figure 7-10: Comparison between the reference and obtained gas flow rates using Abbas model Q_g vs $Q_{g,ref}$

The error in the predicted gas volumetric flow rate, using the Abbas model, in vertical annular (wet gas) flows was larger than expected. This may be due to different flow conditions or pipe diameter or possibly the side channel blower which could not provide sufficient gas under all flow conditions causing a pulsation in the water film flow. Therefore, an alternative model (homogenous model) described in Section 3.3

was applied to determine the gas and water flow rates in vertical annular water-gas flow.

Difference	**Current work**	**Abbas work**
Water flow conditions	Water flow rates were varied	Water flow rates were kept constant
Gas flow conditions	Gas flow rates were varied	Gas flow rates were varied
Venturi inlet diameter	50mm	80mm
Venturi throat diameter	30mm	48mm
Gas superficial velocity U_{gs} (m/s)	Higher U_{gs} range *Flow set 8* 11.151 to 13.729 *Flow set 9* 9.813 to 14.793 *Flow set 10* 9.757 to 16.719 *Flow set 11* 10.504 to 17.726 *Flow set 12* 10.567 to 18.814 *Flow set 13* 10.697 to 18.809 *Flow set 14* 10.918 to 19.555	Lower U_{gs} range *Flow set* 1 6.919 to 8.566 *Flow set 2* 6.350 to 8.259 *Flow set 3* 6.837 to 8.323 *Flow set 4* 6.451 to 7.903
Water superficial velocity U_{ws} (m/s)	Higher U_{ws} range *Flow set 8* 0.066 to 0.423 *Flow set 9* 0.066 to 0.423 *Flow set 10* 0.066 to 0.423 *Flow set 11* 0.066 to 0.423 *Flow set 12* 0.066 to 0.423 *Flow set 13* 0.066 to 0.423 *Flow set 14* 0.066 to 0.423	Lower U_{ws} range *Flow set 1* 0.0104 *Flow set 2* 0.0163 *Flow set 3* 0.0153 *Flow set 4* 0.0123
Gas volume fraction at inlet and the throat of the Venturi	$\alpha_2 > \alpha_1$ The throat gas volume fraction is greater than inlet gas volume fraction	$\alpha_1 > \alpha_2$ The inlet gas volume fraction is greater than throat gas volume fraction

Table 7-6: Flow conditions of current work and Abbas work

7.9 Homogenous model

7.9.1 Measuring the homogenous mixture volumetric flow rate

The mathematical model of a homogenous gas-water two phase flow through the Venturi with conductance sensors at the inlet and throat (described in Section 3.3) was applied to see if better results could be obtained than from the Abbas model. To determine the homogenous mixture flow rate, the differential pressure ΔP_B (Equation (3.46)) and the homogenous mixture density ρ_m (Equation (3.47)) must be obtained in order that the homogenous mixture flow rate Q_m can be determined.

The gas volume fraction at the inlet and the throat of the Venturi (α_1 and α_2) measured from ring sensors B and C (refer to Figure 4-12) using water conductivity σ_w (measured by a conventional conductivity meter to be 155μScm-1) was used to determine the homogenous mixture density ρ_m using Equation (3.47), while the differential pressure ΔP_B was obtained from Equation (3.46). Once the mixture density and the differential pressure were obtained then the mathematical model described in Section 3.3 can be used to determine the homogenous mixture volumetric flow rate Q_m using Equation (3.53).

The results obtained in this investigation for the homogenous mixture volumetric flow rate $Q_{m,H}$ were compared with the reference homogenous mixture volumetric flow rate $Q_{m,ref}$ obtained by adding the reference water volumetric flow rate $Q_{w,ref}$ (obtained from the turbine flow meter described in Section 6.2.3) and the reference gas volumetric flow rate $Q_{g,ref}$ (obtained from the air flow meter described in Section 6.2.2) (see Equation 3.54).
The reason for this comparison was to see if the predicted mixture volumetric flow rate $Q_{m,H}$, defined by Equation (7.4), agreed with the reference homogenous mixture volumetric flow rate $Q_{m,ref}$, defined by Equation (3.54).

The predicted homogenous mixture flow rate $Q_{m,H}$ was obtained in by of using the gas volume fraction at inlet and the throat of the Venturi. ($\alpha_{1,rs}, \alpha_{2,rs}$) as measured by the conductance ring sensor and using the differential pressure ΔP_B defined in Equation (3.46) using the relationship:

$$Q_{m,H} = \left\{\frac{2\,\Delta P_B}{\rho_m}\right\}^{\frac{1}{2}} \frac{A_2}{\left[1 - \left(\frac{A_2}{A_1}\right)^2\right]^{\frac{1}{2}}}$$

Equation 7.4

where the homogenous mixture density is given by

$$\rho_m = \rho_w(1 - \bar{\alpha})$$

Equation 7.5

and where

$$\bar{\alpha} = \frac{\alpha_{1,rs} + \alpha_{2,rs}}{2}$$

Equation 7.6

The predicted gas flow rate $Q_{g,H}$ is obtained by:

$$Q_{g,H} = \bar{\alpha}\, Q_{m,H}$$

Equation 7.7

Plots of $Q_{m,H}$ vs $Q_{m,ref}$ and $Q_{g,H}$ vs $Q_{g,ref}$ are shown in Figures 7-11 and 7-12. It can been seen from the figures that the obtained homogenous mixture flow rate $Q_{m,H}$ and gas volumetric flow rate $Q_{g,H}$ are both significantly lower than their analogous reference values $Q_{m,ref}$ and $Q_{g,ref}$.

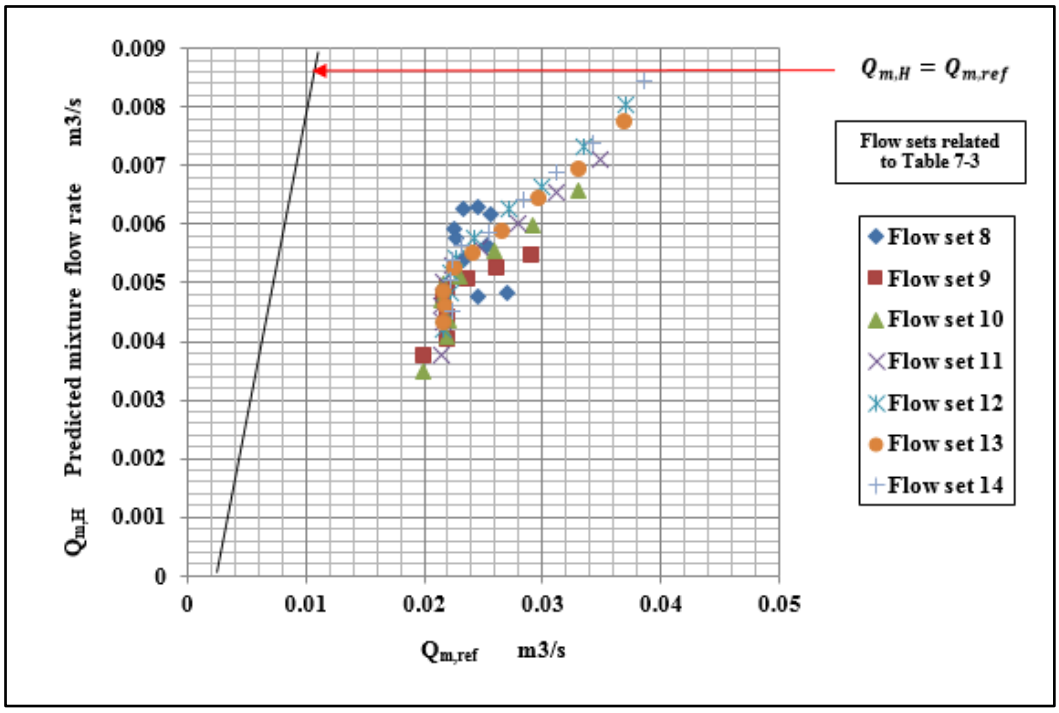

Figure 7-11: Comparison between the reference and predicted mixture flow rates using homogenous model $Q_{m,H}$ vs $Q_{m,ref}$

Based on $\rho_m = \rho_w(1-\bar{\alpha})$ and $\bar{\alpha} = \frac{\alpha_{1,rs}+\alpha_{2,rs}}{2}$

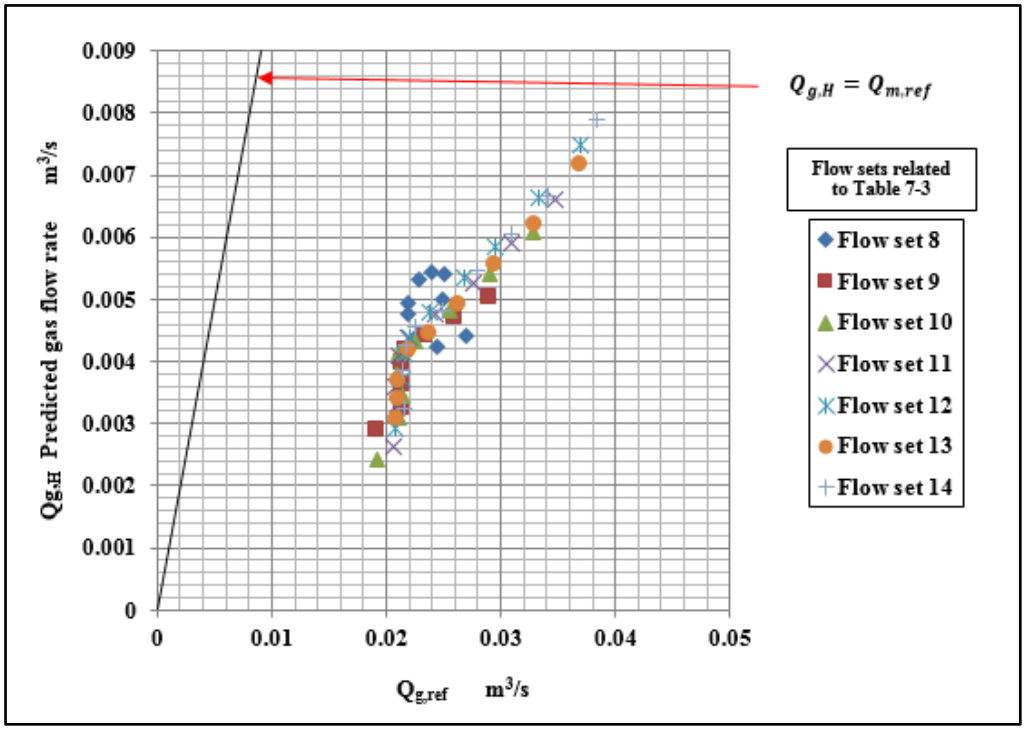

Figure 7-12: Comparison between the reference and obtained gas flow rates using homogenous model $Q_{g,H}$ vs $Q_{g,ref}$

Based on $\rho_m = \rho_w(1-\bar{\alpha})$ and $\bar{\alpha} = \frac{\alpha_{1,rs}+\alpha_{2,rs}}{2}$

The results of the predicted homogenous mixture volumetric flow rate $Q_{m,H}$ using the homogenous model in vertical annular (wet gas) flows were not in agreement with the reference homogenous mixture volumetric flow rate. Therefore, a new homogenous model, assuming a no slip gas volume fraction as described in Section 3.4 was applied to determine the gas and water flow rates in vertical annular water-gas flow (see Section 7.10). The difference between the two homogenous models is that the model in this Section (7.9) the mixture density ρ_m is based on the gas volume fraction at the inlet and the throat of the Venturi $(\alpha_{1,rs}, \alpha_{2,rs})$ (see Equations (3.47) and (3.48)) while for the no slip model in Section 7.10 the mixture density $\rho_{m,ns}$ is based on the gas volume fraction calculated from the reference gas flow rate and the reference water flow rate (see Equations (3.56) and (3.57)).

7.10 Homogenous model assuming no slip gas volume fraction

7.10.1 Measuring the homogenous mixture flow rate assuming no slip gas volume fraction

The mathematical model of homogenous assuming the no slip gas volume fraction described in Section 3.4 was applied to determine the homogenous mixture flow rate and the gas and water flow rates. Measurement of the gas volume fraction $\alpha_{2,rs}$ at the throat of the Venturi was obtained using water conductivity σ_w 155μScm^{-1} measured by a conventional conductivity meter. The differential pressure ignoring the hydrostatic head loss ΔP_H to find a better result for the homogenous mixture flow rate $Q_{m,ns}$ assuming no slip gas volume fraction between the inlet and the throat of the Venturi was also required. The differential pressure ΔP_B and the homogenous mixture density $\rho_{m,ns}$ must be obtained in order that the homogenous mixture flow rate $Q_{m,ns}$ can be determined assuming a no slip gas volume fraction. Since in this section, the hydrostatic head ΔP_H is ignored, ΔP_B is equal to $\Delta P_{TP,wg}$ (see Equation (3.46)).

To determine the mixture density, the no slip gas volume fraction α_{ns} must be obtained using Equation (3.56). Having obtained α_{ns}, then the mixture density $\rho_{m,ns}$ in the homogenous model can be determined using Equation (3.57). Note that to

determine the mixture density use either the gas volume fraction measured at the throat $\alpha_{2,rs}$ or the no slip gas volume fraction α_{ns} since both of these parameters are in reasonable agreement with each other (refer to Figure (7.5)). For this work we use the no slip gas volume fraction α_{ns} to determine the mixture density assuming no slip gas volume fraction. The homogenous mixture flow rate, assuming no slip, gas volume fraction is given by:

$$Q_{m,ns} = \left\{\frac{2\,\Delta P_B}{\rho_{m,ns}}\right\}^{\frac{1}{2}} \frac{A_2}{\left[1-\left(\frac{A_2}{A_1}\right)^2\right]^{\frac{1}{2}}}$$

Equation 7.8

Results were achieved in this investigation for the homogenous model assuming no slip gas volume fraction. The homogenous mixture volumetric flow rate $Q_{m,ns}$ results were compared with the reference homogenous mixture volumetric flow rate $Q_{m,ref}$ determined by adding the reference water volumetric flow rate $Q_{w,ref}$ (obtained from the turbine flow meter described in Section 6.2.3) and the reference gas volumetric flow rate $Q_{g,ref}$ (obtained from the air flow meter described in Section 6.2.2). The reason for this comparison was to see if the predicted homogenous volumetric flow rate, assuming no slip, gas volume fraction defined by Equation (7.8) agreed with the reference homogenous mixture volumetric flow rate defined by Equation (7.54).

A plot of $Q_{m,ns}$ vs $Q_{m,ref}$ is shown in Figure 7-13. It can been seen from Figure 7-13 that the homogenous mixture volumetric flow rate $Q_{m,ns}$, assuming the no slip gas volume fraction, is lower than the reference homogenous mixture volumetric flow rate $Q_{m,ref}$. This could arise from the differential pressure ΔP_B being too low or the mixture density $\rho_{m,ns}$ too high, but the homogenous mixture volumetric flow rate $Q_{m,ns}$ assuming no slip gas volume fraction is much better than the homogenous mixture flow rate $Q_{m,H}$ in Figure 7-11 when compared with the reference homogenous flow rate $Q_{m,ref}$.

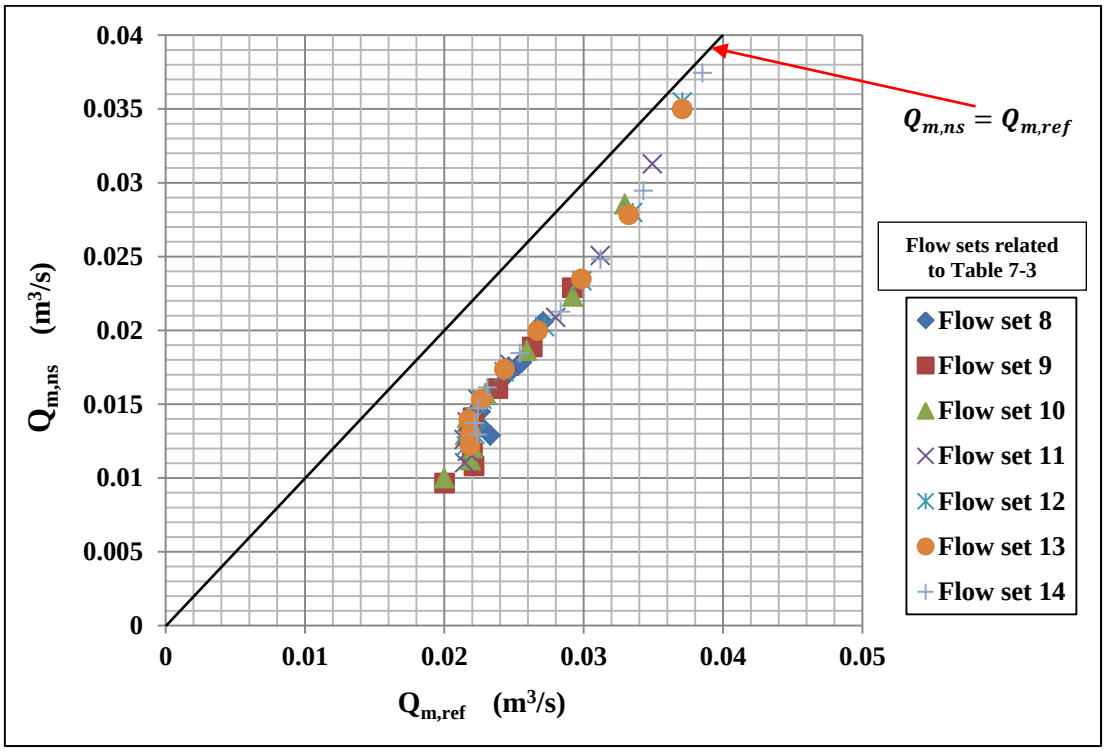

Figure 7-13: Comparison between the mixture homogenous flow rate assuming no slip and the reference mixture flow rate $Q_{m,ns}$ vs $Q_{m,ref}$

It can been seen by comparing the Figures 7-11 and 7-13 that the results of the homogenous mixture flow rate $Q_{m,H}$ obtained by Equation (7.4) are less than the results of homogenous mixture flow rate assuming no slip gas volume fraction $Q_{m,ns}$ obtained by Equation (7.8). From Figure 7-7 the gas volume fraction $\alpha_{1,rs}$ at the Venturi inlet is less than the gas volume fraction $\alpha_{2,rs}$ at the throat of the Venturi ($\alpha_{1,rs} < \alpha_{2,rs}$), from Figure 7-5 the gas volume fraction $\alpha_{2,rs}$ at the throat of the Venturi is in fair agreement with the no slip gas volume fraction α_{ns} $(\alpha_{2,rs} \cong \alpha_{ns})$.

Also from Figure 7-6 the gas volume fraction $\alpha_{1,rs}$ at the inlet of the Venturi is much less than the no slip gas volume fraction α_{ns} $(\alpha_{1,rs} << \alpha_{ns})$ and so the mean gas volume fraction $\bar{\alpha}$ in the converging section of the Venturi is less than the nonslip gas volume fraction α_{ns} $(\bar{\alpha} < \alpha_{ns})$ consequently the mixture density ρ_m is greater than the mixture density in the model which assume the no slip gas volume fraction $\rho_{m,ns}$ $(\rho_m > \rho_{m,ns})$. As a results, the predicted homogenous mixture volumetric flow rate

$Q_{m,H}$ obtained by Equation (7.4) (which also uses the hydrostatic head loss ΔP_H) is less than the predicted homogenous mixture volumetric flow rate assuming no slip gas volume fraction (and which ignores the hydrostatic head loss ΔP_H). In summary the data suggest that, for a given set of flow conditions, the reason why $Q_{m,\mathrm{H}}$ is lower than $Q_{m,ns}$ is because the mixture density ρ_m predicted by Equations (7.5) and (7.6) is too high. Conversely, the mixture density used to predicted $Q_{m,ns}$ (Equation (3.57)) is much lower, giving better agreement between $Q_{m,ns}$ and $Q_{m,ref}$.

[15, 16] and [10] models also were used to predict the gas flow rate, and the results obtained from these models were compared with the reference gas flow rate $Q_{g,ref}$ obtained from the variable area flow meter.

Plots of $Q_{g,de\ Leeuw}$ vs $Q_{g,ref}$ and $Q_{g,Murdock}$ vs $Q_{g,ref}$ are shown in Figures 7-14 and 7-15 respectively. The results from Figures 7-14 and 7-15 were compared with those of

The gas flow rate $Q_{g,ns}$ in homogenous model, assuming the no slip gas volume fraction (refer to Figure 7-17).

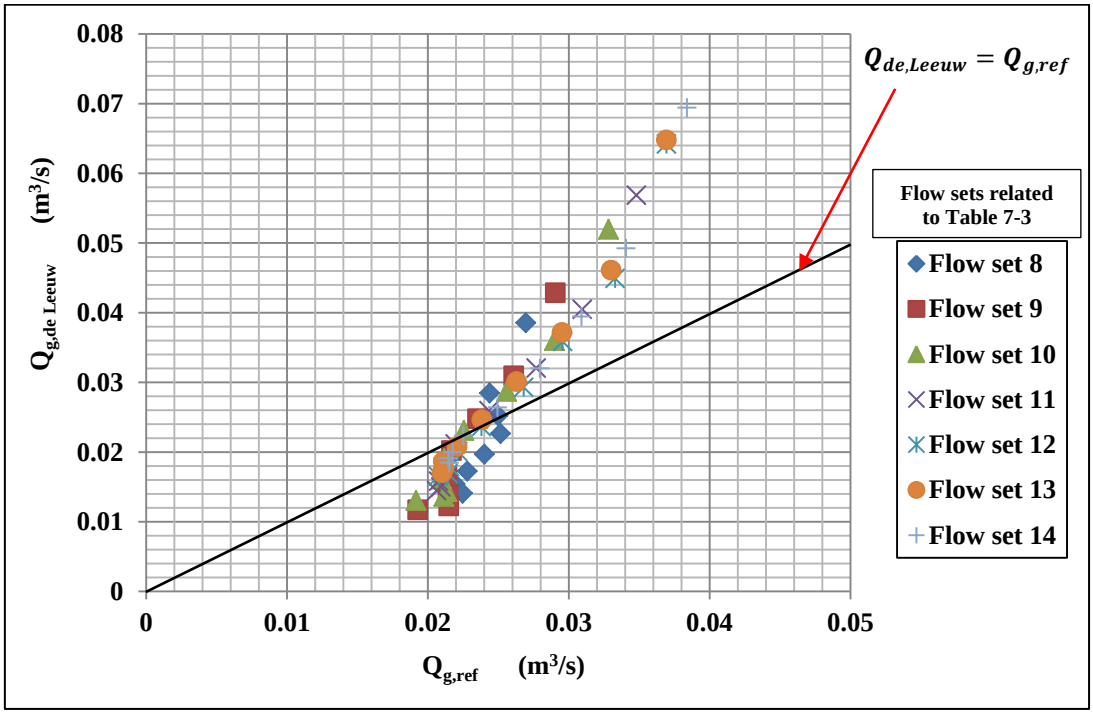

Figure 7-14: Comparison between $Q_{g,de\ Leeuw}$ and $Q_{g,ref}$

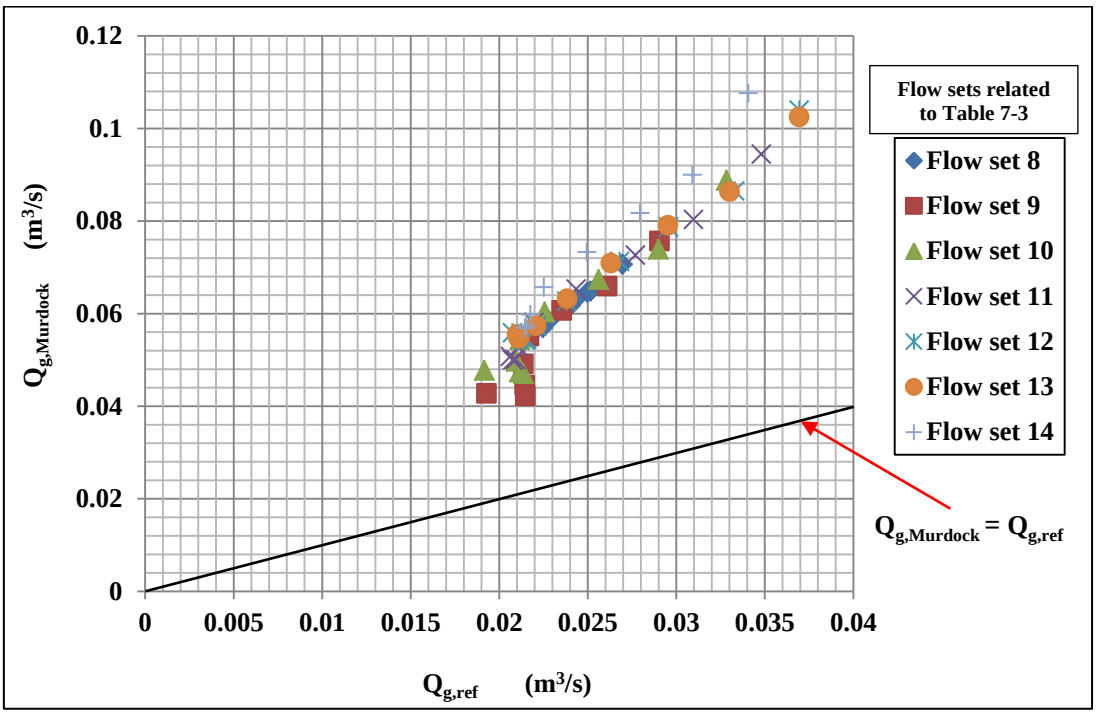

Figure 7-15: Comparison between Q_g obtained by Murdock model and $Q_{g,ref}$

The gas flow rate $Q_{g,ns}$ in homogenous model, assuming the no slip gas volume fraction (refer to Figure 7-17) is better than both the de Leeuw and Murdock models (refer to Figures 7-14 and 7-15). Also the Abbas model (refer to Figure 7-10) does not appear to be very useful, and the homogenous model based mean gas volume fraction $\bar{\alpha}$ defined by Equation (7.6) is not very useful (refer to Figures 7-11 and 7-12).

Predicted gas, water and mixture volumetric flow rates (Q_g , Q_w and Q_m respectively) were obtained using the other models (Chisholm, Lin, Smith & Leang and Steven) as well described in Chapter 2 but the error in the predicted flow rates more worst.

A plot of $Q_{w,ns}$ vs $Q_{w,ref}$ is shown in Figure 7-16. The values obtained for the water flow rate $Q_{w,ns}$ in the homogenous model, assuming the no slip gas volume fraction (which can be determined by using Equation (3.60)) are lower than the reference

water volumetric flow rate $Q_{w,ref}$ (measured from the turbine flow meter). This discrepancy increase with increasing $Q_{w,ref}$.

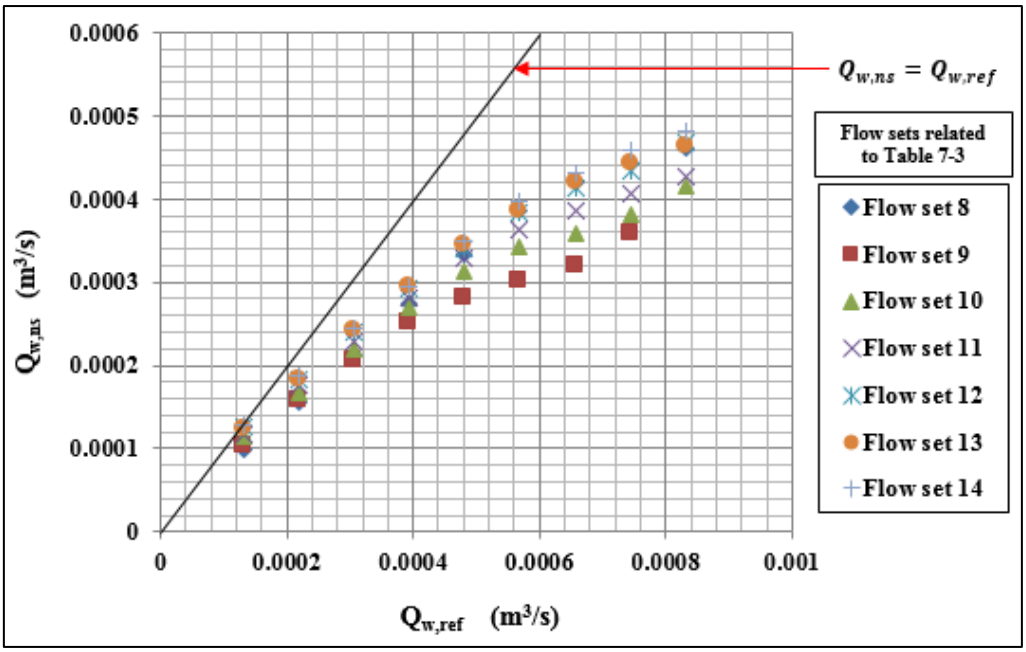

Figure 7-16: Comparison between $Q_{w,ns}$ vs $Q_{w,ref}$

A plot of $Q_{g,ns}$ vs $Q_{g,ref}$ is shown in Figure 7-17. The gas flow rate $Q_{g,ns}$ in the homogenous model, assuming no slip gas volume fraction, (determined by using Equation (3.59)) is lower than the reference gas volumetric flow rate $Q_{g,ref}$ (obtained from the air flow meter described in Section 6.2.2), as can be seen in Figure 7-17.

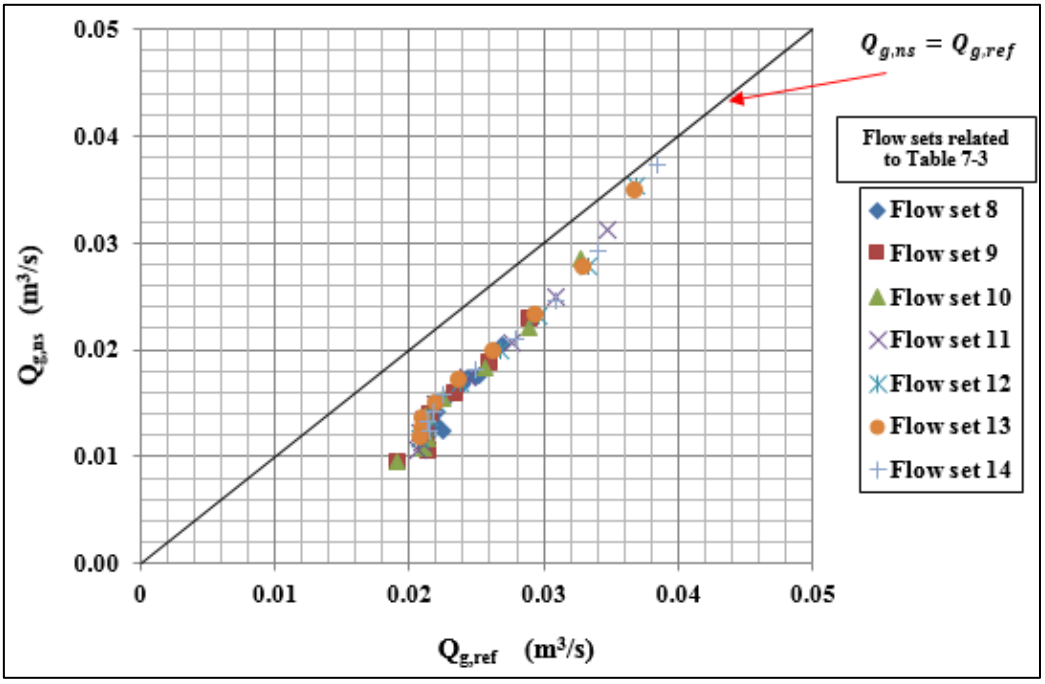

Figure 7-17: Comparison between $Q_{g,ref}$ vs $Q_{g,ns}$

7.10.2 Measuring water flow rate using homogenous, assuming no slip, gas volume fraction and cross-correlating

The above results in Figure 7-16 show that, the water flow rate $Q_{w,ns}$ is too low compared with the reference water volumetric flow rate $Q_{w,ref}$. The water flow rate $Q_{w,ns,xc}$ can also be predicted using the homogenous gas volume fraction, assuming no slip and the film velocity $U_{f,xc}$ obtained by the cross-correlation technique between two ring sensors A and B at the inlet of the Venturi, using the relationship:

$$Q_{w,ns,xc} = \pi R^2 U_{f,xc}(1 - \alpha_{ns})$$

Equation 7.9

A plot of $Q_{w,ns,xc}$ vs $Q_{w,ref}$ is shown in Figure 7-18. The water flow rate $Q_{w,ns,xc}$ determined from Equation (7.9), is far too low compared with the reference water volumetric flow rate $Q_{w,ref}$ (measured from the turbine flow meter) this is because even though the measured film velocity $U_{f,xc}$ is too high, the no slip gas volume fraction α_{ns} is far too large compared with the actual inlet gas volume fraction

making $(1-\alpha_{ns})$ far too low. This results in the very low values for $Q_{w,ns,xc}$ shown in Figure 7-18.

For a given set of flow conditions the water flow rate $Q_{w,ns,xc}$ is also much lower than the water flow rate $Q_{w,rs}$ (refer to Figure 7-9). This is because $Q_{w,rs}$ is calculated according to Equation (7.3) and the cross section area of the film A_f is based on $\alpha_{1,rs}$ because $\alpha_{1,rs}$ is much smaller than $\alpha_{1,ns}$ the film area A_f is much larger when it is based on $\alpha_{1,rs}$. This in turn leads to much larger values for $Q_{w,rs}$ than for $Q_{w,ns}$.

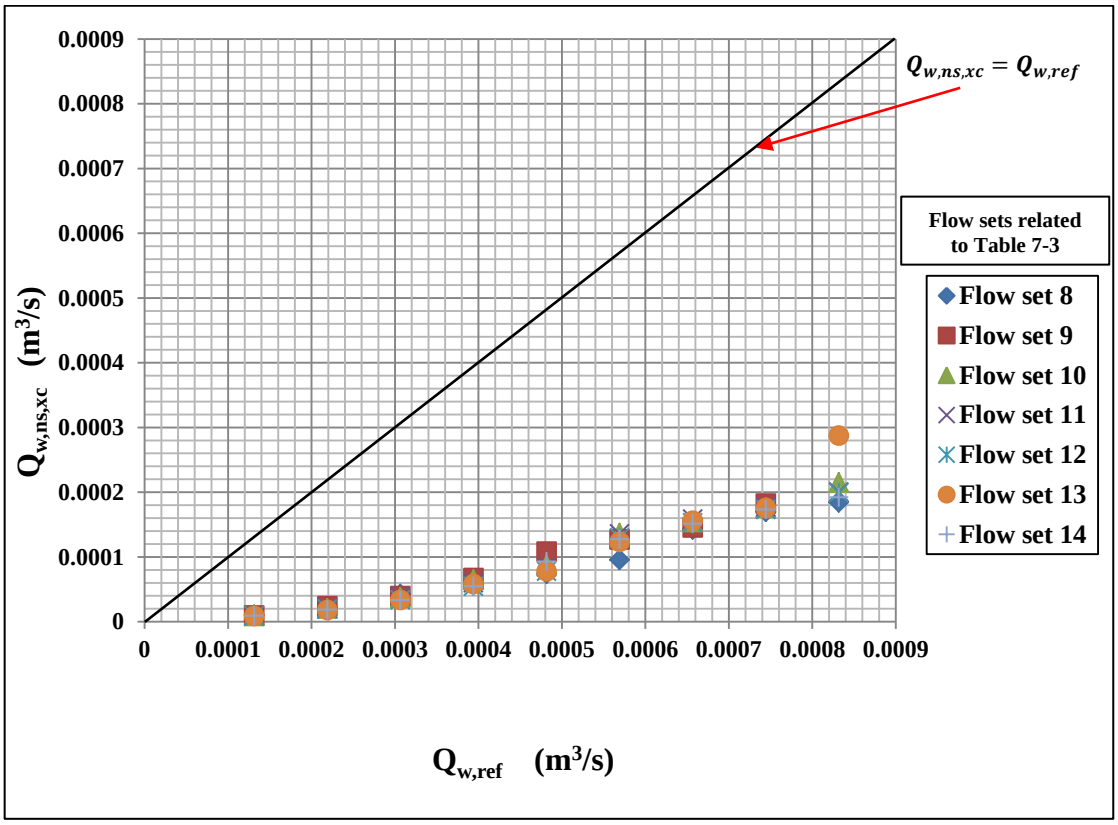

Figure 7-18: $Q_{w,ns,xc}$ vs $Q_{w,ref}$ reference water flow rate

Comparing the results between $Q_{w,ns,xc}$ vs $Q_{w,ref}$ (Figure 7-18) gives $Q_{w,ns,xc} < Q_{w,ref}$ and those between $Q_{w,rs}$ vs $Q_{w,ref}$ (refer to Figure 7-9) gives $Q_{w,rs} > Q_{w,ref}$. The reason why $Q_{w,rs}$ is greater than $Q_{w,ref}$ is because either the assumed gas volume fraction at the Venturi inlet $\alpha_{1,rs}$ is too small (and hence the water volume fraction is too large) or that the measured velocity of the liquid film $U_{f,xc}$ is too large.

The following work in Section 7.11 introduces "scaling factors" which can be used to correct the gas volume fraction $\alpha_{1,rs}$ at the Venturi inlet and the liquid film velocity $U_{f,xc}$ at the Venturi inlet in order to achieve the correct water volumetric flow rate using measurements from the Venturi with conductance sensors.

Note also that the accepted models of de Leeuw and Murdock, as well as Abbas model and the homogenous model described in this section, do not enable the gas flow rate in the flow conditions used in the present study to be accurately obtained. Accordingly an approach using scaling factors is also adopted in Section 7.12 in order to obtain the correct gas flow rate using measurements from the Venturi with conductance sensors

7.11 Scaling factors required to obtain the correct water flow rate

7.11.1 Scaling factor ɣ based on the assumption that the inlet gas volume fraction $\alpha_{1,rs}$ measured by the inlet ring senor is incorrect and the liquid film velocity $U_{f,xc}$ is correct

Using Equations (7.1) and (7.2) the correct inlet gas volume fraction $\hat{\alpha}_1$ is required, assuming the liquid film velocity $U_{f,xc}$ is correct, to give the correct water flow rate in annular wet gas flow. So for each flow condition the correct gas volume fraction $\hat{\alpha}_1$ may be assumed to be given by:

$$\hat{\alpha}_1 = \gamma\, \alpha_{1,rs}$$

Equation 7.10

where $\hat{\alpha}_1$ is the actual value of the inlet gas volume fraction required to give the correct value of the water flow rate $Q_{w,ref}$, ɣ is a scaling factor which must be multiplied by $\alpha_{1,rs}$ to give the actual value of the gas volume fraction at the Venturi inlet, assuming the measured film velocity is correct. The correct value of the water flow rate $Q_{w,ref}$ is then given by:

$$Q_{w,ref} = A_1(1 - \hat{\alpha}_1)U_{f,xc}$$

Equation 7.11

Combining Equations (7.10) and (7.11) gives:

$$Q_{w,ref} = A_1\left(1 - \gamma\, \alpha_{1,rs}\right)U_{f,xc}$$

Equation 7.12

The scaling factor ɣ can be expressed as:

$$\gamma = \frac{1}{\alpha_{1,rs}} - \frac{Q_{w,ref}}{U_{f,xc}\, A_1\, \alpha_{1,rs}}$$

Equation 7.13

A plot of ɣ vs $Q_{w,ref}$ is shown in Figure 7-19.

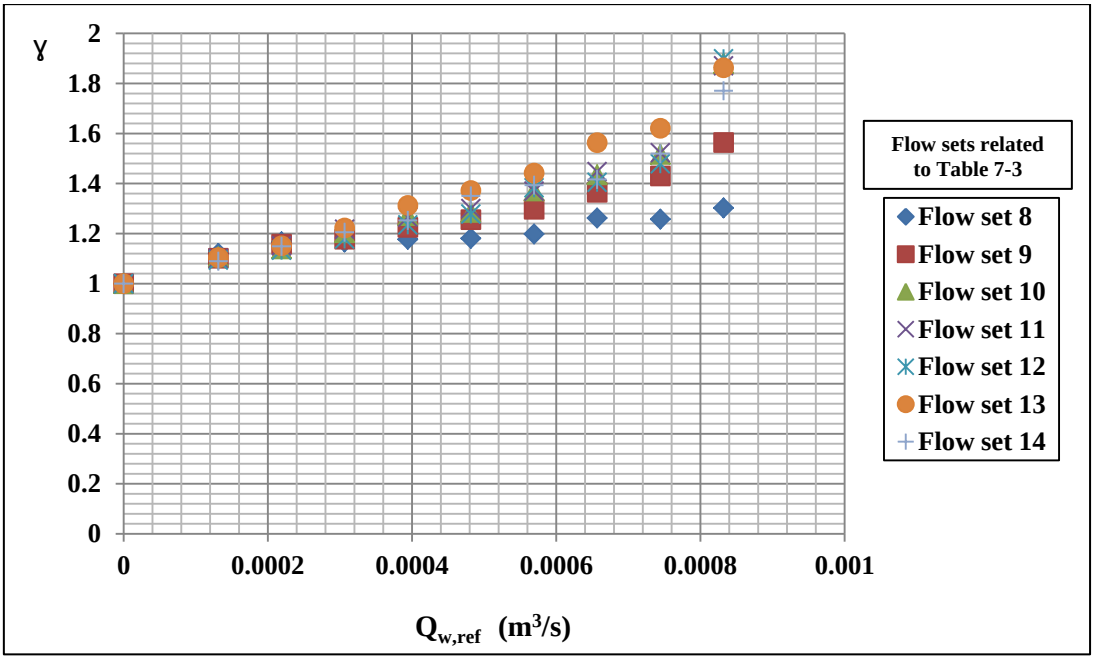

Figure 7-19: ɣ vs $Q_{w,ref}$ reference water flow rate

A plot of $\gamma\alpha_{1,rs}$ vs α_{dls} is shown in Figure 7-20.

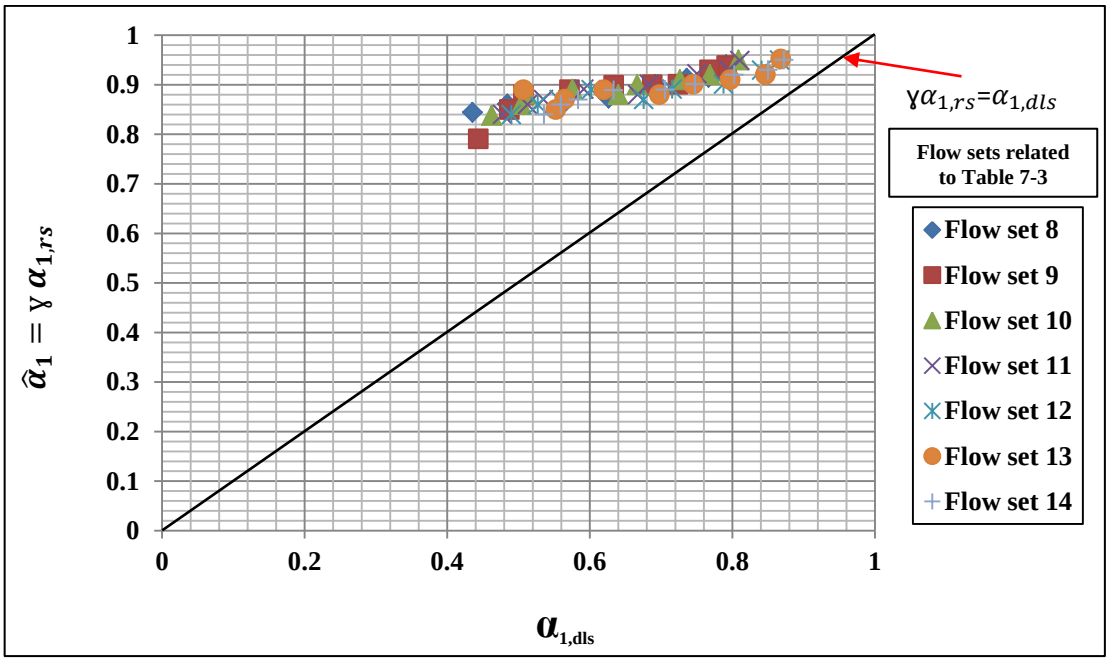

Figure 7-20: $(\gamma\,\alpha_{1,rs})$ vs (α_{dls})

From comparing the results for inlet gas volume fraction measured using ring sensor B $(\alpha_{1,rs})$ and digital level sensor $(\alpha_{1,dls})$ shown in Figure 7-4 it can be seen that the gas volume fraction measured using ring sensor B at the inlet of the Venturi is probably fairly accurate therefore implying the inlet liquid film velocity $U_{f,xc}$ is incorrect. Also the Figure 7-20 shows a huge discrepancy between $(\gamma\, \alpha_{1,rs})$ and $(\alpha_{1,dls})$ therefore implying that the scaling factor γ multiplied by $\alpha_{1,rs}$ dose not give the correct inlet gas volume fraction $\hat{\alpha}_1$. This further implies that the liquid film velocity $U_{f,xc}$ measured by cross correlation at inlet of the Venturi is incorrect.

7.11.2 Scaling factor Ψ based on the assumption that the measured gas volume fraction $\alpha_{1,rs}$ is correct and the film velocity $U_{f,xc}$ is incorrect

If it is assumed that the measured film velocity $U_{f,xc}$ using the cross correlation technique is incorrect and, assuming the gas volume fraction at the inlet $\alpha_{1,rs}$ measured by the ring sensor is correct, then, for each flow condition, the correct film velocity $\widehat{U}_{f,xc}$ is given by the relationship:

$$\widehat{U}_{f,xc} = \Psi U_{f,xc}$$

Equation 7.14

where Ψ is a scaling factor by which the measured inlet liquid film velocity $U_{f,xc}$ must be multiplied to give the correct film velocity.

[Note: - $\widehat{U}_{f,xc}$ is the correct film velocity and $U_{f,xc}$ is the measured film velocity obtained by cross correlation between the two ring sensors at the Venturi inlet.] Assuming the gas volume fraction $\alpha_{1,rs}$ measured by the ring sensor B is correct, then

$$Q_{w,ref} = A_1(1 - \alpha_{1,rs}\,\gamma)U_{f,xc}$$

Equation 7.15

and

$$Q_{w,ref} = A_1(1 - \alpha_{1,rs})\widehat{U}_{f,xc}$$

Equation 7.16

By rearranging Equations (7.14), (7.15) and (7.16)

$$(1-\alpha_{1,rs}\gamma)U_{f,xc} = (1-\alpha_{1,rs})\Psi U_{f,xc}$$

Equation 7.17

$$\Psi = \frac{1-\alpha_{1,rs}\,\gamma}{1-\alpha_{1,rs}}$$

Equation 7.18

A plot of ɣ vs $Q_{g,ref}$ is shown in Figure 7-21. The values of ɣ vary from 1 to 1.89 as the reference gas flow rate reduces from 0.038 m^3/s to 0.02 m^3/s. It is likely that at low gas flow rate $Q_{g,ref}$, the actual film speed $\widehat{U}_{f,xc}$ is much lower than the velocity of the water film measured using a cross correlation technique at the inlet of the Venturi.

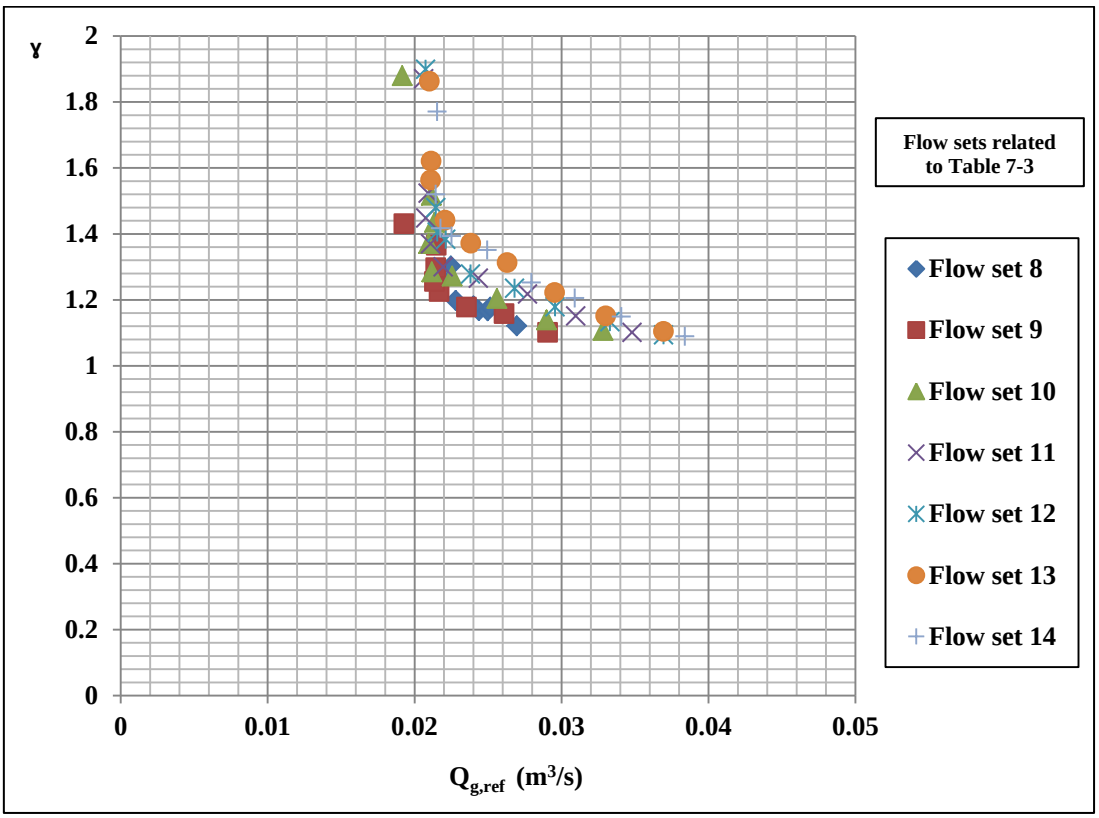

Figure 7-21: ɣ vs $Q_{g,ref}$ reference gas flow rate

Using Figure 7-21 and Equation (7.18) a plot of Ψ vs $Q_{g,ref}$ is shown in Figure 7-22. Ψ varies from 0.2 to 0.5 but clusters around a value of 0.35 suggesting that liquid film

velocity $U_{f,xc}$ measured by cross correlation technique at the inlet of the Venturi is an overestimate of the fair film velocity by about a factor 3.

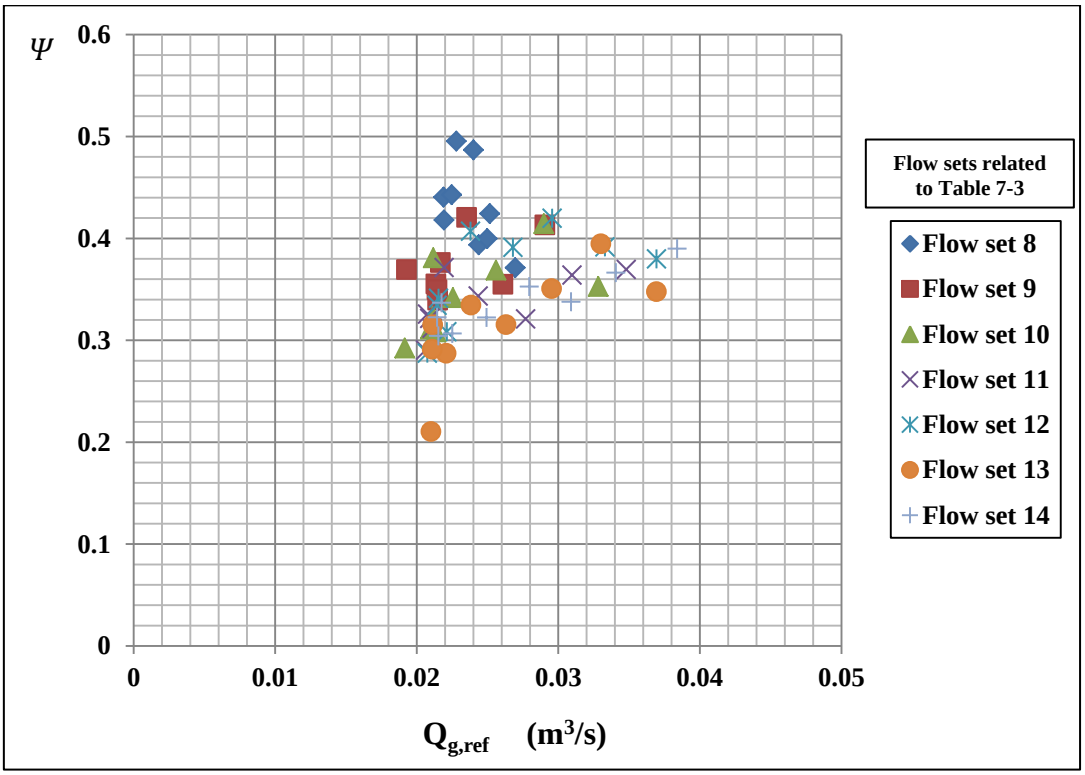

Figure 7-22 Ψ vs $Q_{g,ref}$ reference gas flow rate

It was stated earlier that the incorrect high water flow rate measurements in Figure 7-9 arise because either the gas volume fraction measured using ring sensor $\alpha_{1,rs}$ at the inlet of the Venturi is too low or the film velocity measured using a cross correlation technique $U_{f,xc}$ is too large. Since we have good agreement between the inlet gas volume fraction $\alpha_{1,rs}$ measured suing ring sensor B and the gas volume fraction $\alpha_{1,dls}$ at the inlet of the Venturi measured using digital level sensor as showing in Figure 7-4, it is most likely that the measured liquid film velocity $U_{f,xc}$ at the Venturi inlet is too high.

It is likely that fast moving waves on the surface of water film at the Venturi inlet is the reason why the measured liquid film velocity $U_{f,xc}$ is to high, meaning that the waves on the surface of the water film are traveling faster than the water film. It is

likely that the cross correlation technique preferentially measures the velocity of these waves rather than the velocity of the water film, at the Venturi inlet.

7.11.3 The effect of Entrainment

The entrainment fraction E in annular flow is defined as the fraction of the total liquid flowing in the form of droplets through the central gas core, and can be used to provide a better estimate of Ψ to give the correct film velocity $\widehat{U}_{f,xc}$. To do this, entrainment fraction data is used from [21] . The entrainment fraction E is given by:

$$E = \frac{Q_{w,c}}{Q_{w,ref}}$$

Equation 7.19

$$Q_{w,c} = E Q_{w,ref}$$

Equation 7.20

where $Q_{w,c}$ is the water droplet volumetric flow rate in the gas core and $Q_{w,ref}$ the reference water volumetric flow rate measured by the turbine flow meter. The water film volumetric flow rate Q_w is given by:

$$Q_w = Q_{w,ref} - Q_{w,c}$$

Equation 7.21

By combining Equations (7.20) and (7.21)

$$Q_w = Q_{w,ref} - E\ Q_{w,ref}$$

Equation 7.22

$$Q_w = Q_{w,ref}\ (1 - E\ )$$

Equation 7.23

$$Q_w = \left(1 - \alpha_{1,rs}\right) A_1 \widetilde{\Psi} U_{f,xc}$$

Equation 7.24

By arranging Equations (7.23) and (7.24)

$$Q_{w,ref}\ (1 - E\ ) = \left(1 - \alpha_{1,rs}\right) A_1 \widetilde{\Psi} U_{f,xc}$$

Equation 7.25

So, a better estimate of Ψ is given by:

$$\widetilde{\Psi} = \frac{Q_{w,ref}\ (1 - E\ )}{\left(1 - \alpha_{1,rs}\right) A_1 U_{f,xc}}$$

Equation 7.26

Using values of E from [21] Equation (7.26) can be used with the obtained data to determine the best estimate of $\widetilde{\Psi}$ for the sixty three flow conditions tested. Figures 7-23 and 7-24 shows $\widetilde{\Psi}$ vs $Q_{g,ref}$ and $\widetilde{\Psi}$ vs $Q_{w,ref}$ respectively. Comparing the Figure 7-22 and Figure 7-23 shows the effect of taking the entrainment fraction into account is small. i.e. $\widetilde{\Psi} \simeq \Psi$.

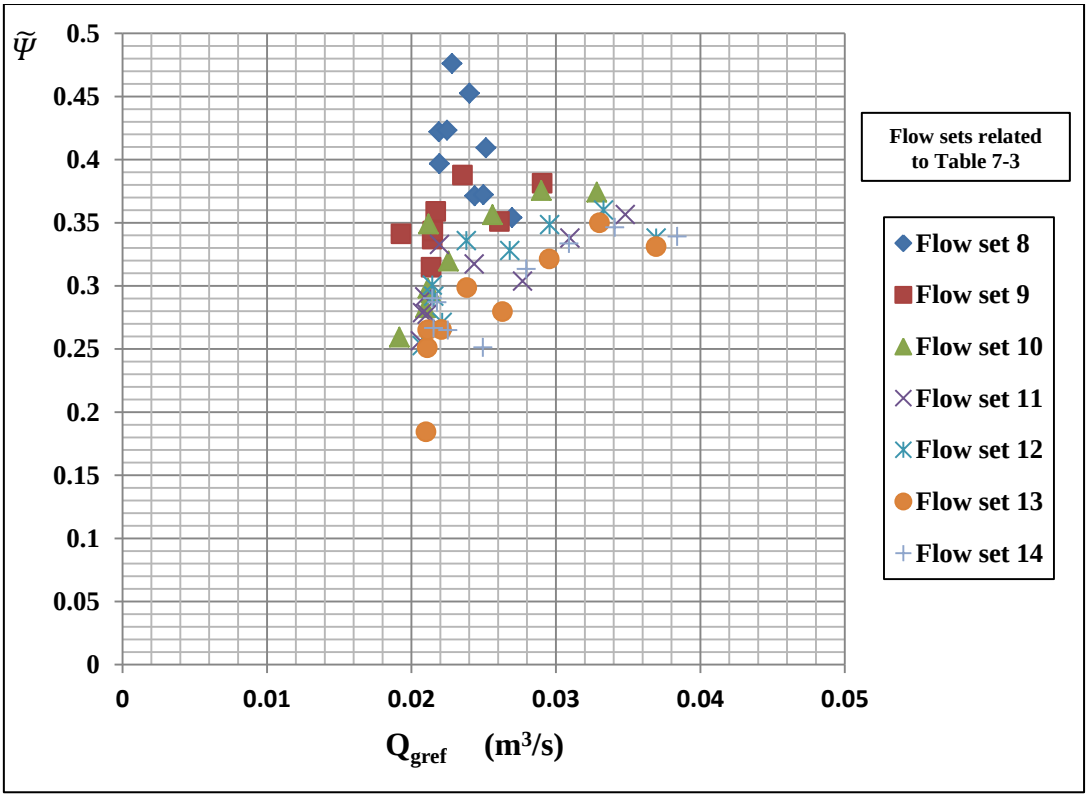

Figure 7-23: $\widetilde{\Psi}$ vs $Q_{g,ref}$ reference gas flow rate

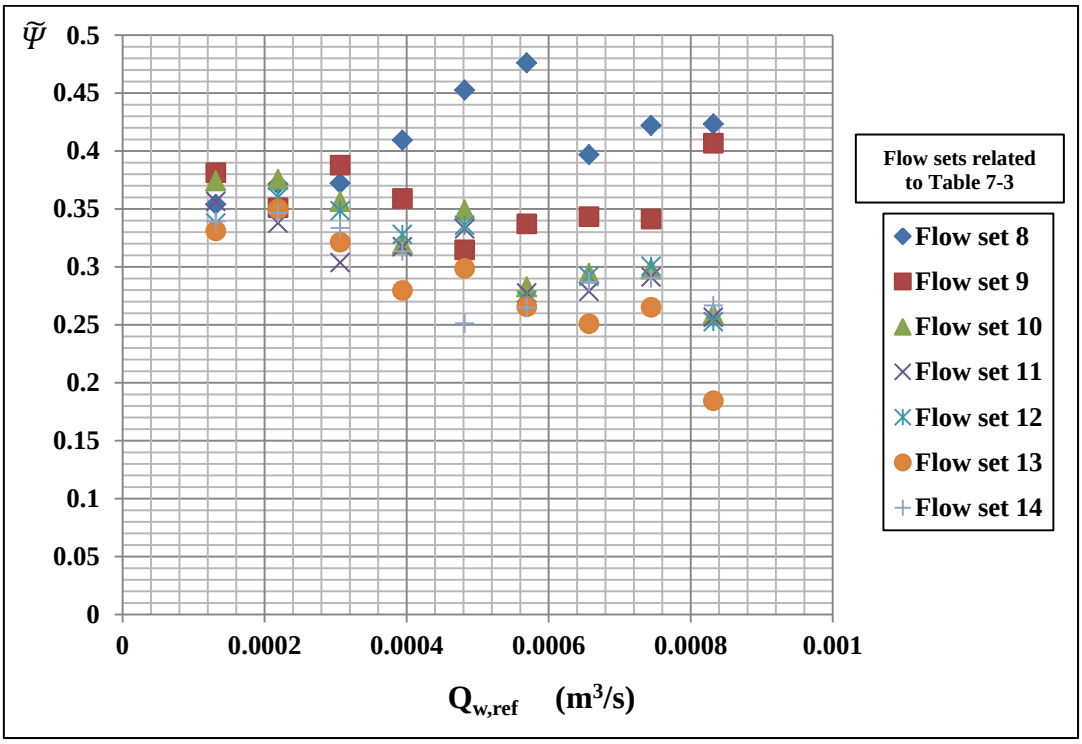

Figure 7-24: $\tilde{\Psi}$ vs $Q_{w,ref}$ reference water flow rate

7.12 Scaling factors required to obtain the correct gas flow rate using the homogenous model, and assuming no slip gas volume fraction

The following analysis was used to determine the correct gas flow rate. The correct gas volume fraction $\hat{\alpha}_2$ at the throat of the Venturi is required to give the correct gas flow rate in annular wet gas flow using a homogenous model. In this section the scaling factor $\tilde{\emptyset}$ is defined to enable the corrected gas volume fraction $\hat{\alpha}_2$ to be related to the measured gas volume fraction $\alpha_{2,rs}$ at the Venturi throat as follows:

$$\hat{\alpha}_2 = \tilde{\emptyset}\, \alpha_{2,rs}$$

Equation 7.27

The corrected gas volume fraction $\hat{\alpha}_2$ is such that the calculated gas volumetric flow rate $Q_{g,\tilde{\emptyset}}$ is equal to the reference gas volumetric flow rate $Q_{g,ref}$ where the corrected gas flow rate $Q_{g,\tilde{\emptyset}}$ is given by:

$$Q_{g,\tilde{\emptyset}} = \left(\tilde{\emptyset}\, \alpha_{2,rs}\right) Q_{m,\tilde{\emptyset}}$$

Equation 7.28

where

$$Q_{m,\tilde{\emptyset}} = \left\{\frac{2\,\Delta P_{TP,wg}}{\rho_{m,\tilde{\emptyset}}}\right\}^{\frac{1}{2}} \frac{A_2}{\left[1-\left(\frac{A_2}{A_1}\right)^2\right]^{\frac{1}{2}}}$$

Equation 7.29

and where the mixture density is given by:

$$\rho_{m,\tilde{\emptyset}} = \rho_w(1-\hat{\alpha}_2)$$

Equation 7.30

And so

$$\rho_{m,\tilde{\emptyset}} = \rho_w\left(1-\tilde{\emptyset}\,\alpha_{2,rs}\right)$$

Equation 7.31

Equations (7.28) and (7.29) can be used with the obtained data to determine the correct gas flow rates respectively for the sixty three flow conditions tested.

Figure 7-25 shows $\tilde{\emptyset}$ vs $Q_{g,ref}$. The values of $\tilde{\emptyset}$ increase from 1 to 1.045 over all flow conditions as the reference gas flow rate reduces from 0.038 m^3/s to 0.02 m^3/s.

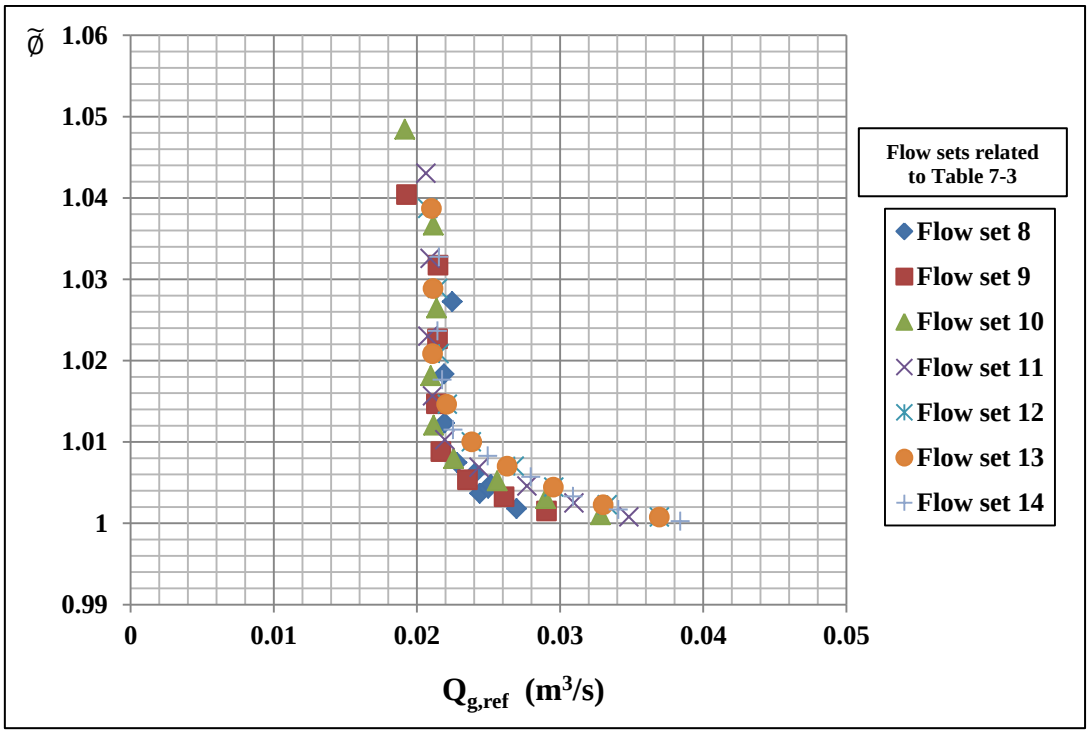

Figure 7-25: $\tilde{\emptyset}$ vs $Q_{g,ref}$ reference gas flow rate

A plot of $\tilde{\emptyset}$ vs $Q_{m,ref}$ is shown in Figure 7-26.

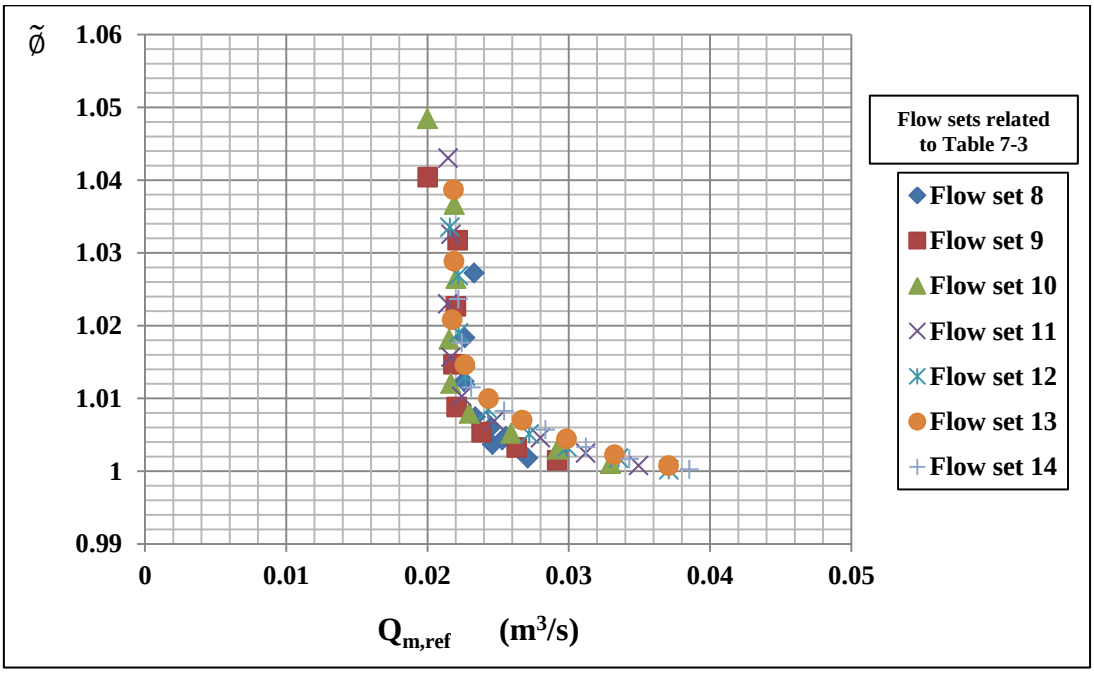

Figure 7-26: $\tilde{\emptyset}$ vs $Q_{m,ref}$ reference mixture flow rate

[Note that with reference to Figure 7-7 we can infer that the correct gas volume fraction $\hat{\alpha}_2$ at the throat of the Venturi is greater than the correct gas volume fraction $\hat{\alpha}_1$ at the inlet of the Venturi in vertical annular (wet gas) flows]. From the current investigation, we find that the homogenous flow model enables us to obtain a good estimate of the gas flow rate based on the gas volume fraction $\alpha_{2,rs}$ at the throat not at the inlet. Therefore measurement of the gas volume fraction $\alpha_{2,rs}$ at the throat of the Venturi is necessary, as the homogenous flow model also based on mixture density $\rho_{m,\tilde{\emptyset}}$ at the throat.

From the above results, the homogenous model, combined with the scaling factor $\tilde{\emptyset}$ is the best model investigated so far, yielding better results for the gas flow rate in vertical annular (wet gas) flow than any of the previous models (Abbas model, de Leeuw and Murdock models) cited in Sections (7.8) and (7.9). By applying the appropriate value of the scaling factor $\tilde{\emptyset}$ (Figures 7-25 and 7-26), which for all of the flow conditions investigated in this thesis has a value between 1 and about 1.05, to the

gas volume fraction $\alpha_{2,\mathrm{rs}}$ measured by a ring conductance sensor at the Venturi throat we obtain the mixture density $\rho_{m,\tilde{\emptyset}}$ using Equation (7.31). By using this value of $\rho_{m,\tilde{\emptyset}}$ with the measured two phase pressure drop $\Delta P_{TP,wg}$ and the homogenous model given in Equation (7.29) an estimate of the mixture volumetric flow rate $Q_{m,\tilde{\emptyset}}$ is made. From this value of $Q_{m,\tilde{\emptyset}}$ the gas volumetric flow rate $Q_{g,\tilde{\emptyset}}$ is obtained using Equation (7.28). Provided that the correct value of $\tilde{\emptyset}$ is used for the prevailing flow conditions this value of $Q_{g,\tilde{\emptyset}}$ will be equal to the true gas volumetric flow rate $Q_{g,ref}$.

Provided the gas volume fraction $\alpha_{2,\mathrm{rs}}$ is measured then, even if $\tilde{\emptyset}$ (the symbol on the vertical axis of figure 7-25) is not used, the gas volumetric flow rate can be measured from the two phase pressure drop to an accuracy of +/- 2.5% of reading for the flow conditions investigated. If the correct value of $\tilde{\emptyset}$ is used (from figure 7-25) for the prevailing flow conditions then the gas volumetric flow rate should be measurable to an accuracy of better than +/-1%, for the flow conditions investigated.

Summary

A novel Venturi meter with conductance sensors at the inlet and throat was used to measure gas volume fraction at inlet and the throat, film thickness of the liquid and the liquid film velocity at the Venturi inlet in vertical annular gas-water two phase flows.

The [81] model and the homogenous model described in chapter 3 were used to determine the gas mass flow rate and gas and water volumetric flow rates in vertical annular two phase flows. Seven flow conditions were investigated.

Two techniques were used to measure the liquid film thickness at inlet of the Venturi, namely a digital level sensor and ring sensor; the gas volume fraction α_1 at the inlet was measured by the ring sensor B and a digital level sensor, while the gas volume fraction α_2 at the throat of the Venturi was measured using ring sensor C and digital level sensor. It was found that, in general, the gas volume fraction α_1 measured by the ring sensor is in agreement with the gas volume fraction measured by the digital level sensor. Also, the gas volume fraction α_2 at the throat measured by ring sensor C agrees fairly well with α_{ns}, the no slip gas volume fraction obtained from Equation (3.56).

The error in the predicted gas volumetric flow rate using the Abbas model, by applying the collected data to Equation (3.42) and the volumetric water flow rate determined using Equation (7.3), was larger than expected. This may be due to pulsations in the water film which cause an unsteady water film flow rate or from the different flow conditions between the current work and that of the Abbas work.

An alternative model (homogenous model) was applied to the collected data. It was found that the homogenous model, assuming no slip, results were better than the Abbas model, de Leeuw and Murdock models, so that the gas and water volumetric flow rates using the Venturi meter with conductance sensors could be successfully estimated.

By applying a scaling factor $\widetilde{\Psi}$ to the film velocity measured using cross correlation at the Venturi inlet, and combining this with the gas volume fraction $\alpha_{1,rs}$ measured at the Venturi inlet, a good estimate of the volumetric flow rate is obtained.

By applying a scaling factor $\widetilde{\emptyset}$ to the gas volume fraction $\alpha_{2,rs}$ measured at the Venturi throat an estimate $\rho_{m,\widetilde{\emptyset}}$ of the gas-water mixture density can be made. From $\rho_{m,\widetilde{\emptyset}}$ and the measured pressure drop $\Delta P_{TP,wg}$ between the inlet and the throat of the Venturi a homogenous model Equation (7.29) is used to predict $Q_{m,\widetilde{\emptyset}}$ the mixture volumetric flow rate. From $Q_{m,\widetilde{\emptyset}}$, $\alpha_{2,rs}$ and $\widetilde{\emptyset}$ an estimate of the gas volumetric flow rate $Q_{g,\widetilde{\emptyset}}$ is made using Equation (7.28). If the correct value of $\widetilde{\emptyset}$ is used for the prevailing flow conditions then $Q_{g,\widetilde{\emptyset}}$ is equal to the true gas flow rate $Q_{g,ref}$.

Chapter 8 Conclusions and Future Work

The completion of this research study has produced a number of different contributions to knowledge. These contributions are the outcome of the various conclusions drawn from this study.

8.1 Conclusions

The aim of this research program was to design a novel wet gas flow metering technique which combines a Venturi tube with ring conductance sensors placed at the inlet and throat, which is capable of measuring the gas and water flow rates in vertical annular gas-water two phase flow. The measurement of the gas volume fraction at the inlet and the throat of the Venturi (α_1 and α_2), the film thickness δ, and the film velocity $U_{f,xc}$, has been undertaken to estimate the gas and water flow rates in vertical annular flow using Equations (3.42) and (3.2).

A Venturi with ring conductance sensors at the inlet and throat has been designed and built to enable gas volume fraction measurements to be made in vertical gas-water flow. The conductance Venturi flow meter consists of two upstream ring sensors (A and B ring sensors) flush mounted with the inner surface of the inlet section, a ring sensor C flush mounted with the inner surface of the throat section and a digital level sensor head mounted on the inner surface of the inlet section. This allowed the measurement of the gas volume fraction at the inlet and the throat of the Venturi meter, the liquid film velocity and the liquid film thickness at the Venturi inlet in a vertical annular gas-water two phase flow.

A flow loop has been designed and constructed to establish and investigate vertical annular two phase flows under different known flow conditions. A side channel blower was used to give the necessary high air flow in these vertical annular gas-water two phase flows. A variable area flowmeter was used to provide a reference measurement of the gas volumetric flow rate $Q_{g,ref}$. A turbine flow meter was used

to measure the reference water volumetric flow rate $Q_{w,ref}$ in the annular flow supplied by the centrifugal pump. A differential pressure cell was used to measure the differential pressure between the inlet and the throat of the Venturi flow meter.

A new device, the digital level sensor, has been built that is capable of measuring the film thickness when the liquid film is electrically conducting at the Venturi inlet. One of the ring sensors at the inlet may also be used as an alternative technique to measure the liquid thickness at the inlet. The film thickness increases with increasing liquid flow rate or decreasing gas flow rate at all the flow conditions. The two upstream ring sensors (A and B ring sensors) are capable of measuring the liquid film velocity using cross-correlation.

The data obtained from the digital level sensor at the Venturi inlet were used to investigate effect of gas and water superficial velocity on liquid film thickness. The experimental results showed that at constant water superficial velocity the liquid film thickness at the inlet of the Venturi decreases as the gas superficial velocity increases while the liquid film thickness increased with increasing water superficial velocity at different gas superficial velocities, see Sections 7.1 and 7.2.

In addition, a comparison of the measurements obtained for the liquid film thickness at the inlet of the Venturi in vertical annular (wet gas) flows using the digital level sensor and ring sensor, showed that both sets of results are in agreement, see Section 7.4.

The experimental results for the gas volume fraction α_1 measured at the inlet of the Venturi using the digital level sensor and ring sensor B also showed approximate agreement in this region, see Section 7.5.1.

The experimental results for the measurement of the gas volume fraction α_2 at the throat of the Venturi in annular gas-water flow, showed that the gas volume fraction α_2 as measured by the ring conductance sensor at the Venturi throat is in reasonable agreement with the gas volume fraction α_{ns} assuming no slip, for all flow conditions, see Section 7.5.2.

The data obtained from the Venturi with conductance sensors at the inlet and throat (i.e. the volume fraction at the inlet and throat, film thickness at the inlet, liquid film velocity) were used to determine the gas mass flow rate and the gas and water flow rate in annular wet gas two phase flow.

Experimental results were obtained for the predicted water flow rate in annular gas-water two phase flows based on the inlet gas volume fraction $\alpha_{1,rs}$ using a ring conductance sensor and the film velocity $U_{f,xc}$ obtained by cross correlating the output from the two ring conductance sensors at the Venturi inlet (Equation (7.3)). These results showed an error in the predicted water volumetric flow rate, which was greater than the reference water volumetric flow rate (measured from the turbine flow meter). This error could arise from the measured gas volume fraction $\alpha_{1,rs}$ being too low or the film velocity $U_{f,xc}$ being too large, see Section 7.7. Therefore, the error in the predicted water volumetric flow rate was investigated to find the correct water flow rate by first assuming the measured gas volume fraction $\alpha_{1,rs}$ is too low and the film velocity is correct and then by assuming the gas volume fraction is correct and the film velocity $U_{f,xc}$ is too large.

It was found that, if a scaling factor ɣ is applied to $\alpha_{1,rs}$ to give the correct water volumetric flow rate then ɣ $\alpha_{1,rs}$ is much lower than $\alpha_{1,dls}$ measured by the digital level sensor, whereas $\alpha_{1,rs}$ and $\alpha_{1,dls}$ are if fair agreement (Figure 7-4). It was therefore concluded that $\alpha_{1,rs}$ is approximately correct and that $U_{f,xc}$ was too large. Consequently a scaling factor $\widetilde{\Psi}$ was applied to $U_{f,xc}$ in order to achieve the correct water flow rate. Since the values of $\widetilde{\Psi}$ were centred around 0.35, this implies that the cross correlation technique overestimates the true film velocity by a factor of about 3. This overestimation is probably due to the cross correlation technique preferentially measuring the velocity of waves on the surface of the film.

The experimental results for the gas and gas mass flow rate in vertical annular water-gas flow using the [81] Equation (3.66) showed that the predicted gas volumetric flow using the Abbas model did not agree with the reference gas flow rate measured by the air flow meter. It has been found that the Abbas model does not work well in all flow

conditions, see Section 7.8.1. Also [10] and models [15, 16] (Figures 7.14 and 7.15) showing that they also do not accurately predicted the gas flow rate. Therefore, an alternative model (the homogenous model) was tested to determine the gas and water flow rates flow rate in vertical annular water-gas flow using the Venturi with conductance sensors described in Chapter 4.

The results of the predicted homogenous mixture volumetric flow rate Q_m using the homogenous model and using a mixture density based on $\alpha_{1,rs}$ and $\alpha_{2,rs}$ were not in agreement with the reference homogenous mixture volumetric flow rate, see Section 7.9. Therefore, a homogenous model, assuming a no slip gas volume fraction as described in Section 3.4, was applied to determine the gas and water flow rates in vertical annular water-gas flow.

The results of the homogenous model, assuming no slip gas volume fraction, showed that the homogenous mixture volumetric flow rate $Q_{m,ns}$ is lower than the reference homogenous mixture volumetric flow rate $Q_{m,ref}$. This could arise from the differential pressure ΔP_B being too low or from the mixture density based on α_{ns} being too high, but the homogenous no slip gas volume fraction $Q_{m,ns}$ result is much better than the homogenous flow rate Q_m when compared with the reference homogenous flow rate $Q_{m,ref}$, see Section 7.10.1.

The gas volumetric flow rate using a homogenous model was investigated further in an attempt to predict the correct gas flow rate. A scaling factor $\widetilde{\emptyset}$ was applied to the measured gas volume fraction $\alpha_{2,rs}$ at the Venturi throat in order to obtain the mixture density $\rho_{m,\widetilde{\emptyset}}$. Using the mixture density $\rho_{m,\widetilde{\emptyset}}$ with the measured pressure drop and a homogenous Venturi model, the correct gas flow rate is predicted, which agrees with the reference gas flow rate. [It should be noted that $\widetilde{\emptyset}$ only varied in the range 1 to 1.05 for the flow condition investigated and so $\alpha_{2,rs}$ is always within 5% of the correct value of gas volume fraction at the throat]. It is believed that measurement of $\alpha_{2,rs}$, in conjunction with use of the scaling factor $\widetilde{\emptyset}$ appropriate to the prevailing flow conditions to predict Q_g, represent a novel and major contribution to the field of multiphase flow measurement.

Provided the gas volume fraction at the through tot the Venturi $\alpha_{2,\mathrm{rs}}$ is measured then, even if $\widetilde{\emptyset}$ (the symbol on the vertical axis of figure 7-25) is not used, the gas volumetric flow rate Q_g, can be measured from the two phase pressure drop to an accuracy of +/- 2.5% of reading for all the flow conditions investigated. If the correct value of $\widetilde{\emptyset}$ is used (from figure 7-25) for the prevailing flow conditions then the gas volumetric flow rate Q_g should be measurable to an accuracy of better than +/-1%, for all the flow conditions investigated.

8.2 Present contribution

- The design of a new experimental loop to establish two phase annular flow.
- The design of a Venturi meter with conductance sensors at the inlet and throat that is capable of measuring the gas volume fraction at the throat of the Venturi. The Venturi has been tested successfully for vertical upward flows.
- Development of conductance electronic circuits used to measure the gas volume fraction at inlet and the throat of the Venturi, film thickness and the film velocity at the Venturi inlet.
- Testing of the Venturi in annular two phase flows.
- Introduction of novel scaling factors $\widetilde{\Psi}$ and $\widetilde{\emptyset}$ enabling correction of $\alpha_{2,rs}$ and $U_{f,xc}$ there by enabling prediction of the correct gas and liquid flow rates in annular two phase flow.

8.3 Recommendations for Future Work

Based on the present research, the following recommendations can be made:

- The Venturi should be made in transparent material (Plexiglas) to allow visual observations of the annular flow. These could help in order to gather information on the liquid film, e.g., liquid distribution, film thickness and wave height.

- Future work could preformed to improve the digital level sensor to measure the film thickness at the throat of the Venturi, with improved accuracy.

- Investigation as to why the Abbas model did not appear to correctly predict the gas and water flow rates in the flows investigated.

- Extend the range of flow conditions to investigate the range of applicability of the scaling factors $\widetilde{\Psi}$ and $\widetilde{\emptyset}$ developed during the current work.

References

1. Mehdizadeh, P., *State of the art multiphase flow metering.* 2002 **API 2002-100094 report** (API 2002-100094 report).
2. Steven, R.N., *Wet gas metering with a horizontally mounted Venturi meter.* Flow Measurement and Instrumentation, 2002. **12**(5): p. 361-372.
3. Justo, H.R., *Low differential pressure and multiphase flow measurements by means of differential pressure devices*. 2004, Texas A&M University.
4. Lawrence, P.A., *Wet gas measurement.* Vol. 1. 2009. 163-178
5. Falcone, G., et al., *Multiphase flow metering: Current trends and future developments.* JPT, Journal of Petroleum Technology, 2002. **54**(4): p. 77-84.
6. Fukano, T. and T. Furukawa, *Prediction of the effects of liquid viscosity on interfacial shear stress and frictional pressure drop in vertical upward gas–liquid annular flow.* International Journal of Multiphase Flow, 1998. **24**(4): p. 587-603.
7. Keshock, E.G. and C.S. Lin, *Two-phase annular flow in helical coil flow channels in a reduced gravity environment.* NASA Conference Publication, 1996(3338): p. 115-120.
8. Lockhart, R.W. and R.C. Martinelli, *Proposed correlation of data for isothermal two-phase, two-component flow in pipes.* Chemical Engineering Progress, 1949. **45**(1): p. 39--48.
9. Corneliussen, S., et al., *Handbook of multiphase flow metering.* Norwegian Society for Oil and Gas Measurement (NFOGM), Revision, 2005. **2**.
10. Murdock, J.W., *Two-Phase Flow Measurement With Orifices.* Journal of Fluids Engineering, 1962. **84**(4): p. 419-432.
11. Chisholm, D., *Flow of incompressible two-phase mixtures through sharp-edged orifices.* ARCHIVE: Journal of Mechanical Engineering Science 1959-1982 (vols 1-23), 1967. **9**(1): p. 72-78.
12. Chisholm, D., *Research note: two-phase flow through sharp-edged orifices.* ARCHIVE: Journal of Mechanical Engineering Science 1959-1982 (vols 1-23), 1977. **19**(3): p. 128-130.
13. Smith, R.V. and J.T. Leang, *Evaluations of Correlations for Two-Phase Flowmeters Three Current–One New.* Journal of Engineering for Power, 1975. **97**(4): p. 589.
14. Lin, Z.H., *Two-phase flow measurements with sharp-edged orifices.* International Journal of Multiphase Flow, 1982. **8**(6): p. 683-693.
15. de Leeuw, R., *Wet Gas Flow Measurement by Means of a Venturi Meter and a Tracer Technique,*. North Sea Flow Measurement Workshop, Norway, Shell Expro., Scotland:, 1994.
16. de Leeuw, R., *Liquid correction of Venturi meter readings in wet gas flow.* North Sea Flow Measurement Workshop, Norway, Shell Expro., The Netherlands, 1997.
17. van Maanen, H.R.E., *Cost Reduction for Wet-Gas Measurement using Tracer-Venturi Combination.* Proceeding of the workshop Practical Development in Gas Flow Metering, East Kilbride, Scotland, 1999: p. paper 2.

18. Jamieson, A.W., *High-performance multiphase metering: A personal perspective.* Measurement and Control, 2000. **33**(3): p. 73-77.
19. Xu, Y., et al., *Non separation two phase flow measurement of natural gas condensate.* Natural Gas Industry, 2011. **31**(4): p. 103-108.
20. Scheers, L., et al., *Multiphase Flow Metering Per Well . Can it be Justified? .* 20th North Sea FlowMeasurement Workshop, St. Andrews, Scotland., 2002.
21. Al-Yarubi, Q., *Phase flow rate measurements of annular flows in Ph.D thesis.* 2010, Huddersfield University.
22. Erik, M., *Handbook of Multiphase Metering*, ed. R. 2. 2005 Norwegian Society of Oil and Gas Measurement
23. Asali, J.C., T.J. Hanratty, and P. Andreussi, *Interfacial drag and film height for vertical annular flow.* AIChE Journal, 1985. **31**(6): p. 895-902.
24. Azzopardi, B. and P. Whalley. *Artificial waves in annular two-phase flow*. in *ASME Winter Annual Meeting, Chicago, Published in Basic Mechanisms in Two-Phase Flow and Heat-Transfer (ASME)*. 1980.
25. de Sampaio, P.A.B., J.L.H. Faccini, and J. Su, *Modelling of stratified gas–liquid two-phase flow in horizontal circular pipes.* International Journal of Heat and Mass Transfer, 2008. **51**(11): p. 2752-2761.
26. Oddie, G., et al., *Experimental study of two and three phase flows in large diameter inclined pipes.* International Journal of Multiphase Flow, 2003. **29**(4): p. 527-558.
27. Tan, C., F. Dong, and M. Wu, *Identification of gas/liquid two-phase flow regime through ERT-based measurement and feature extraction.* Flow Measurement and Instrumentation, 2007. **18**(5): p. 255-261.
28. Xu, L.J. and L.A. Xu, *Gas/liquid two-phase flow regime identification by ultrasonic tomography.* Flow Measurement and Instrumentation, 1998. **8**(3): p. 145-155.
29. Revellin, R. and J.R. Thome, *A theoretical model for the prediction of the critical heat flux in heated microchannels.* International Journal of Heat and Mass Transfer, 2008. **51**(5): p. 1216-1225.
30. Saitoh, S., H. Daiguji, and E. Hihara, *Correlation for boiling heat transfer of R-134a in horizontal tubes including effect of tube diameter.* International Journal of Heat and Mass Transfer, 2007. **50**(25): p. 5215-5225.
31. Ariyadasa, U., *An Investigation of Film Thickness and Pressure in Upward and Downward Annular Two-Phase Flow*, in *Department of Mechanical Eng*. 2002, University of Saskatchewan: University of Saskatchewan.
32. Clark, W.W., *Liquid film thickness measurement.* Multiphase Science and Technology, 2002. **14**(1): p. 1-74.
33. Wada, S., H. Kikura, and M. Aritomi, *Pattern recognition and signal processing of ultrasonic echo signal on two-phase flow.* Flow Measurement and Instrumentation, 2006. **17**(4): p. 207-224.
34. Lu, Q., N.V. Suryanarayana, and C. Christodoulu, *Film thickness measurement with an ultrasonic transducer.* Experimental Thermal and Fluid Science, 1993. **7**(4): p. 354-361.
35. Steinbrenner, J.E., et al., *Measurement and modeling of liquid film thickness evolution in stratified two-phase microchannel flows.* Applied Thermal Engineering, 2007. **27**(10): p. 1722-1727.

36. Dallman, J.C., *INVESTIGATION OF SEPARATED FLOW MODEL IN ANNULAR GAS-LIQUID TWO-PHASE FLOWS*. 1978, University of Illinois at Urbana-Champaign.
37. Laurinat, J.E. and T.J. Hanratty, *STUDIES OF THE EFFECTS OF PIPE SIZE ON HORIZONTAL ANNULAR TWO-PHASE FLOWS*. 1982, Department of Chemical Engineering, University of Illinois at Urbana-Champaign
38. Sekoguchi, K., et al., *AIR-WATER ANNULAR TWO-PHASE FLOW IN A HORIZONTAL TUBE - 1. CIRCUMFERENTIAL DISTRIBUTION OF FILM THICKNESSES.* Bulletin of the JSME, 1982. **25**(208): p. 1559-1566.
39. Fukano, T. and A. Ousaka, *Prediction of the circumferential distribution of film thickness in horizontal and near-horizontal gas-liquid annular flows.* Int.J.Multiphase Flow. **15**(3): p. 403-419.
40. Coney, J.E.R., E.A.M. El-Shafei, and C.G.W. Sheppard, *A dual laser beam method for wavy film thickness measurement.* Optics and Lasers in Engineering, 1989. **11**(1): p. 1-14.
41. Fukano, T., *Measurement of time varying thickness of liquid film flowing with high speed gas flow by a constant electric current method (CECM).* Nuclear Engineering and Design, 1998. **184**(2): p. 363-377.
42. Ozgu, M.R., J.C. Chen, and N. Eberhardt, *A capacitance method for measurement of film thickness in two-phase flow.* Review of Scientific Instruments, 1973. **79**(12): p. 1714-1716.
43. Thorncroft, G.E. and J.F. Klausner, *A capacitance sensor for two-phase liquid film thickness measurements in a square duct.* Journal of Fluids Engineering, Transactions of the ASME, 1997. **119**(1): p. 164-169.
44. Olsen, H.O., *Theoretical and experimental investigation of impedance void meters*. 1967, Institutt for Atomenergi, Kjeller (Norway).
45. Spigt, C.L., *On the hydraulic characteristics of a boiling water channel with natural circulation*. 1966, Technische Hogeschool.
46. Hasan, A.H.A.M. and G.P. Lucas, *Experimental and theoretical study of the gas–water two phase flow through a conductance multiphase Venturi meter in vertical annular (wet gas) flow.* Nuclear Engineering and Design, 2011. **241**(6): p. 1998-2005.
47. Fossa, M., *Design and performance of a conductance probe for measuring the liquid fraction in two-phase gas-liquid flows.* Flow Measurement and Instrumentation, 1998. **9**(2): p. 103-109.
48. Shi, Y., F. Dong, and C. Tan. *Conductance probe for the measurement of liquid volume fraction and axial velocity in gas-liquid two phase flow*. in *Electronic Measurement & Instruments, 2009. ICEMI'09. 9th International Conference*. 2009. IEEE.
49. Lina, Y. and L. Yingwei. *On Conductance Probe Measurement Model for Measuring Oil-Water Annular Flow*. in *Information Science and Engineering (ICISE), 2009 1st International Conference*. 2009. IEEE.
50. Fan, S. and T. Yan, *Two-Phase Air-Water Slug Flow Measurement in Horizontal Pipe Using Conductance Probes and Neural Network.* IEEE Transactions on Instrumentation and Measurement, 2014. **63**(2): p. 456-466.
51. Hammer, E.A. and G.A. Johansen, *Measurement Principles in Multiphase Metering- Their Benefits and Limitations.* The Future of Multiphase Metering, London, UK: IBC UK Conference Limited,, 1998.

52. Maxwell, J.C., *A treatise on electricity and magnetism*. Vol. 1. 1954, Oxford: Clarendon press.
53. Cho, K.-H., S. Kim, and Y.-J. Lee, *A fast EIT image reconstruction method for the two-phase flow visualization.* International Communications in Heat and Mass Transfer, 1999. **26**(5): p. 637-646.
54. Schmitz, D. and D. Mewes, *Tomographic imaging of transient multiphase flow in bubble columns.* Chemical Engineering Journal, 2000. **77**(1): p. 99-104.
55. Thorn, R., G.A. Johansen, and B.T. Hjertaker, *Three-phase flow measurement in the petroleum industry.* Measurement Science and Technology, 2013. **24**(1): p. 012003.
56. Thorn, R., G.A. Johansen, and E.A. Hammer, *Recent developments in three-phase flow measurement.* Measurement Science and Technology, 1997. **8**(7): p. 691-701.
57. Hammer, E.A., J. Tollefsen, and K. Olsvik, *Capacitance transducers for non-intrusive measurement of water in crude oil.* Flow Measurement and Instrumentation, 1989. **1**(1): p. 51-58.
58. Dyakowski, T., *Process tomography applied to multi-phase flow measurement.* Measurement Science and Technology, 1996. **7**(3): p. 343-353.
59. George, D.L., et al., *Validation of electrical-impedance tomography for measurements of material distribution in two-phase flows.* International Journal of Multiphase Flow, 2000. **26**(4): p. 549-581.
60. Marashdeh, Q., et al., *Electrical Capacitance Tomography − A Perspective.* Industrial & Engineering Chemistry Research, 2008. **47**(10): p. 3708-3719.
61. Ismail, I., et al., *Tomography for multi-phase flow measurement in the oil industry.* Flow Measurement and Instrumentation, 2005. **16**(2): p. 145-155.
62. Abouelwafa, M.S.A. and E.J.M. Kendall, *The measurement of component ratios in multiphase systems using alpha -ray attenuation.* Journal of Physics E: Scientific Instruments, 1980. **13**(3): p. 341-345.
63. Petrick, M. and B.S. Swanson, *Radiation Attenuation Method of Measuring Density of a Two-Phase Fluid.* Review of Scientific Instruments, 1958. **39**(12): p. 1079-1085.
64. Lucas, G.P., *The Measurement of Two-Phase Flow Parameters in Vertical and Deviated Flows (Vertical Flows)in Ph.D thesis*. 1987, University of Manchester, Institute of Science and Technology.
65. Xie, D., G. Liang, and F. Wang. *Analysis on dynamic differential pressures of multi-loop flowmeter for the measurement of gas-liquid two-phase flow*. 2007.
66. Olsen, A.B., *Framo Subsea Multiphase Flow Meter System*, in *Multiphase meters their subsea application*. 1993, Multiphase meters their subsea application Seminar: London. p. 3.
67. Herringe, R.A., *Slurry flow metering by pressure differential devices.* International Journal of Multiphase Flow, 1977. **3**(3): p. 285-298.
68. Boyer, C. and H. Lemonnier, *Design of a flow metering process for two-phase dispersed flows.* International Journal of Multiphase Flow, 1996. **22**(4): p. 713-732.
69. Hasan, A. and G. Lucas. *Modelling and Measurement of the Gas Flow Rate in Vertical Annular Gas-Water Flow Using a 'Conductance Multiphase Venturi meter'*. What Where When Multi-dimensional Advances for Industrial Process Monitoring, Leeds, UK: University of Leeds, 2009.

70. Blaney, S., *Gamma radiation methods for clamp-on multiphase flow metering*. 2008, (Dissertation/Thesis), Cranfield University
71. Beck, M. S., & Plaskowski, A. (1987). *Cross correlation flowmeters: their design and application.* Bristol: Hilger.
72. Zheng, G.-B., et al., *Gas–liquid two phase flow measurement method based on combination instrument of turbine flowmeter and conductance sensor.* International Journal of Multiphase Flow, 2008. **34**(11): p. 1031-1047.
73. Crabtree, M.A., *Industrial flow measurement in Master thesis*. 2009, Huddersfield Universirt
74. Achilli, A. and M. Greco, *Two-phase flow measurement for SPES3 facility: spool piece mathematical correlations.* 2010.
75. Rouhani, Z., *MEASURING TECHNIQUES.* VON KARMAN INSTITUTE FOR FLUID DYNAMICS, p.13-1974.
76. Aya, I., *Model to calculate mass flow rate and other quantities of two-phase flow in a pipe with a densitometer, a drag disk, and a turbine meter.* 1975(ORNL-TM--4759): p. 57.
77. Turnage, K.G. and C.E. Davis, *Advanced spool piece development*. 1979: Presented at the 7th Water Reactor Safety Research Information Meeting, Gaithersburg, Maryland,.
78. Foussat, A.J.M. and J.-P. Hulin, *VERTICAL LIQUID-LIQUID AND LIQUID-GAS TWO-PHASE FLOW MEASUREMENTS WITH A VORTEX FLOW METER.* 1984. 651-676.
79. Lynnworth, L.C. and Y. Liu, *Ultrasonic flowmeters: Half-century progress report, 1955–2005.* Ultrasonics, 2006. **44**: p. e1371-e1378.
80. Ltd, T.S. *NEL*. February 22, 2015]; Available from: http://www.tuvnel.com/.
81. Hasan, A., *Multiphase Flow Rate Measurement Using a Novel Conductance Venturi Meter: Experimental and Theoretical Study In Different Flow Regimes in Ph.D thesis*. 2010, Huddersfield University.
82. Horowitz, P. and W. Hill, *The art of electronics*. 1989, Cambridge: Cambridge University Press.
83. Coney, M.W.E., *The theory and application of conductance probes for the measurement of liquid film thickness in two-phase flow.* Journal of Physics E: Scientific Instruments, 1973. **6**(9): p. 903-911.
84. Musbah, A. and G. Lucas, *Experimental and theoretical study of annular flow using a venturi with conductance sensors*. 2012, University of Huddersfield.
85. Airtec Air Systems Ltd. *Side Channel Blowers*. 2010 February 27, 2015]; Available from: http://www.airtecairsystems.ltd.uk/sidechannelblowers.html.